Doctoral Thesis

"Synthesis of Diethyl Carbonate from Carbon Dioxide: Optimization of the Esterification Reaction of CO_2 and Ethanol by utilization of Pervaporation and alternative Catalyst Carriers"

A thesis for the degree of
Doctor technicae
786 730

submitted at
"Technische Universität Wien", Faculty of Mechanical and Industrial Engineering
by

Kouessan AZIABA
Mat.Nr.: 01125202

under the supervision of

Univ.Prof. Dipl.-Ing. Dr.techn. **Michael Harasek**
Technische Universität Wien, Institute of Chemical, Environmental and Bioscience Engineering, Vienna, Austria

and co-supervision of

Dipl.-Ing. Dr.techn. **Christian Jordan**
Technische Universität Wien, Institute of Chemical, Environmental and Bioscience Engineering, Vienna, Austria

reviewed by:

Univ.Prof.in Dr.in **Maria Cruz Sanchez Sanchez**
Technische Universität Wien, Institute of Chemical, Environmental and Bioscience Engineering, Vienna, Austria

and:

Univ.Prof. Dipl.-Ing. Dr.techn. **Christoph Pfeifer**
University of Natural Resources and Life Sciences, Institute of Chemical and Energy Engineering, Vienna, Austria

Vienna, 2025

Affidavit

I, Kouessan Aziaba, declare in lieu of an oath

1. that I am the sole author of this doctoral thesis. I performed the associated research by myself, using only literature cited in this volume. I have not used any source or tool than those referenced.
2. that I have not prior to this date submitted this thesis as any examination in Austria or abroad.
3. that going to press of this thesis needs the confirmation of the examination committee.

Vienna, January 2025

Kouessan Aziaba

Acknowledgment

As this doctoral program is coming to a conclusion, these moments provide excellent opportunities to reilluminate the path that was passed and also who was walking side-by-side with me.

I would like to express my deep gratitude to Michael Harasek for his role as my supervisor. His guidance and trust in my abilities allowed me to grow with the challenges I faced throughout the past years. I thank him for his outstanding efforts in my professional and personal development.

Christian Jordan played a huge role as my co-supervisor. These few sentences cannot pay justice to the vast value he contributed to my development. I am truly grateful for the vivid discussions that we had. It was these that brought up countless ideas to solve issue after issue and overcome the present limits. I thank him for his unwavering commitment to my development.

Throughout my time, I was entrusted with a row of projects. Each of them was incredibly exciting and gave me the opportunity to grow professionally. I would genuinely like to express my gratitude to Magdalena Teufner-Kabas and Florian Kabas. Their inventiveness and tireless dedication kept my contribution to the projects on the right path.

I really enjoyed the time at the office with my colleagues. The fact that we have been simply thrown together but still worked so well is especially valuable to me. Since words would not pay justice to what I would like to say, let me at least write this:
I thank you for every single lunch break you forced me to have because I would forget the time and end up eating at 4 pm.

I also genuinely thank Professor Sanchez and Professor Pfeifer for agreeing to review my thesis and being part of the scientific committee.

My friends deserve so much gratitude for the support they provided me throughout many years. In some cases, even two decades now. I am looking forward to the next time.

My family shall receive my greatest gratitude. None of this would have been possible without them. Their faith in me and my abilities always gave me the power to achieve. This will never change.

Akpé nami...

Abstract

The emission of greenhouse gases into the atmosphere, including the resulting challenges, has motivated research and industry to provide a large bandwidth of new ideas to reduce CO_2 emissions. Technologies that selectively separate and use CO_2 (CCU) are considered sustainable approaches to energy transition. Among these, especially the direct synthesis of diethyl carbonate from CO_2 and ethanol (EtOH) is considered to have a high potential to be involved in a more sustainable future in the chemical industry. Diethyl carbonate is intensely used within the pharmaceutical industry, in the production of batteries, and generally as a solvent for multiple applications. The current production opportunities for diethyl carbonate (DEC) rely on toxic processes. The direct synthesis enables bypassing this issue. However, it also comes with several obstacles.

The DEC yield of the esterification reaction of EtOH and CO_2 does not yet meet the demands for a feasible production on an industrial scale. Only a few catalysts that show high performances have been observed. Unfortunately, their excellent abrasive properties pose a threat to equipment for industrial use. Modified carriers bearing catalytic active compounds have been applied within the direct synthesis reaction. The productivity of some carriers ranks in the performance class of commercial options. Nevertheless, the overall yields remain insufficient.

Following the law of le Chatelier, the presence of both products should slow down the reaction. In contrast, water was associated with being significantly adverse to the progress of the reaction, and low yields were observed. Current solutions propose chemical dehydrating agents to remove the drawback of the water present. Nevertheless, further energy-intensive steps for product purification would become a necessity.

The dehydration of the reactive mixture for DEC synthesis was investigated with a selection of membranes using pervaporation. The selectivities were comparably high while observing a moderate flux. A scale-up of the dehydration performance of the membrane that was coupled to the DEC synthesis reaction was simulated. A self-developed and published membrane model was used, which is suitable for gas permeation and pervaporation applications. The enrichment of DEC could thus be significantly increased. Scaling and optimization of the process can hence be substantially simplified.

This work observed a correlation between strongly dissociating acids and diethyl carbonate decomposition, which indicates why the simultaneous presence of water and CO_2 may be a drawback for the direct synthesis of DEC. The developments and discoveries from this work were utilized in a pilot membrane reactor.

Kurzfassung

Die Emission von Treibhausgasen in die Atmosphäre und die daraus resultierenden Herausforderungen für Forschung und Industrie, brachte in den letzten Jahren eine große Bandbreite an neuen Ideen zur Reduktion der CO_2 Emissionen hervor. Darunter werden die selektive Abscheidung und Nutzung (CCU) von CO_2 als besonders zielführende Technologien angesehen, welche einen wesentlichen Beitrag zur Energiewende leisten könnten. Der direkten Synthese von Diethylcarbonat aus CO_2 und Ethanol wird als einer der bereits erwähnten CCU Technologien ein besonders hohes Potential zugeschrieben Teile der chemischen Industrie nachhaltiger zu gestalten. Diethylcarbonat wird derzeit intensiv als Lösungsmittel und im Rahmen pharmazeutischer Herstellungsverfahren, in der Batterieherstellung und als Lösungsmittel eingesetzt. Die derzeitigen Synthesemöglichkeiten von Diethylcarbonat basieren auf toxischen Verfahren. Die direkte Synthese umgeht die Nachteile der etablierten Produktionsrouten, wobei auch hier einige Nachteile bekannt sind.

Die DEC Ausbeute aus der Versesterungsreaktion von EtOH und CO_2 entspricht noch nicht den Anforderungen um im industriellen Maßstab konkurrenzfähig zu sein. Die wenigen Katalysatoren, die eine vielversprechende Leistungsfähigkeit zeigen, bergen aufgrund ihrer abrasiven Eigenschaft ein relevantes Risiko für Anlagenteile und Eqipment. Modifizierte Träger wurden ersatzweise im Rahmen der direkten DEC Synthese eingesetzt. Die beobachteten Ergebnisse reihen sich in die Leistungsklasse von kommerziell verfügbaren Katalysatoren ein. Dennoch sind die erzielten Ausbeuten als unzureichend anzusehen.

Obwohl nach dem Gesetz von Le Chatelier die Anwesenheit beider Produkte die Reaktionsgeschwindigkeit verlangsamen müsste, ist die Anwesenheit von Wasser als besonders nachteilig für den Verlauf der Reaktion beschrieben worden. Die gleichzeitige Präsenz von CO_2 und Wasser könnte dabei maßgeblich sein. Der Einsatz chemischer Wasserfänger wurde vielfach als eine Option beschrieben, die Verlangsamung der Reaktion zu beschränken. Daraus ergibt sich aber die Notwendigkeit einer meist energieaufwändigen Stofftrennung.

Diese Arbeit greift auf die Nutzung einer Membran im Rahmen von Pervaporation zur dehydrierung des Reaktionsgemisches auf. Dabei konnten besonders hohe Selektivitäten bei moderatem transmembranen Fluss beobachtet. Eine Skalierung der Membran in kombination mit der DEC Synthese wurde im Rahmen von Prozesssimulation berechnet und ausgewertet. Dabei kam ein selbstentwickeltes und veröffentlichtes Membranmodel zum Einsatz, welches sich sowohl für Gaspermeations- und Pervaporationsanwendungen eignet. Die Anreicherung von DEC könnte somit deutlich gesteigert werden. Die Entdeckungen dieser Arbeit konnten im Rahmen eines Pilotmembranreaktors verwertet werden.

Contents

List of appended publications

Journal Publication I
Stability of Diethyl Carbonate in the Presence of Acidic and Basic Solvents
K. Aziaba, F.M. Možina, M. Teufner–Kabas, F. Kabas, C. Jordan, and M. Harasek
Chemical Engineering Transactions, vol. 105, pp. 163–168, Nov. 2023
doi:10.3303/CET23105028.

Author's Contribution: The author contributed to the design, execution, and analysis of the experiments in coordination with the co–authors. The evaluation of the degradation grades and the writing of the paper was carried out in intensive cooperation with the second author.

Journal Publication II
Dehydration by Pervaporation of an Organic Solution for the Direct Synthesis of Diethyl Carbonate
K. Aziaba, M. Annerl, G. Greilinger, M. Teufner–Kabas, F. Kabas, C. Jordan, and M. Harasek
Separations, vol. 11(10), no. 289, Oct. 2024
doi:10.3390/separations11100289

Author's Contribution: The author contributed to the assembly of the equipment and conceptualization, design, execution, and assessment of the experiments. The extended evaluation regarding the applicability of the membranes was based on the work of the second and third authors of the study. The writing was carried out by the author and the second author.

Journal Publication III
Design of a Gas Permeation and Pervaporation Membrane Model for an Open Source Process Simulation Tool
K. Aziaba, C. Jordan, B. Haddadi, and M. Harasek
Membranes, vol. 12(12), no. 1186, Nov. 2022
doi:10.3390/membranes12121186

Author's Contribution: The author planned, designed, developed, tested, and validated the model with the assistance of the co–authors. The paper has been written by the author and revised by the co–authors.

Journal Publication IV
High Purity Hydrogen from Liquid NH_3 – Proposal and Evaluation of a Process Chain
K. Aziaba, B.D. Weiss, V. Illyes, C. Jordan, M. Haider, and M. Harasek
Chemical Engineering Transactions, vol. 96, pp. 169–174, Nov. 2022
doi:10.3303/CET2296029

Author's Contribution: The author and all co–authors have contributed to conceptualizing the paper. The author has researched, designed, and simulated the separation of the decompositions off–gas. The writing process was equally shared between the author and the second and third authors and supervised by the other authors.

Austrian Patent
Process for the Preparation of Organic Carbonates [pending]
Original title: Verfahren zur Herstellung organische Carbonate
G. Greilinger, C. Jordan, F. Kabas, K. Aziaba, M. Genov, M. Teufner–Kabas, and M. Harasek
Patent number: AT527086A1

Author's Contribution: The author contributed to preliminary obtained findings on which this patent is developed. Further, the author contributed to the design, construction, commission, and operation of the system resulting from this patent.

List of supervised and co-supervised theses

The following bachelor– and master theses have been supervised or co–supervised by the author:

Master theses:

Gerhard Greilinger:	Construction of a membrane pervaporation unit for the dehydration of an organic reaction mixture
Marco Annerl:	Improvement of diethyl carbonate synthesis from CO_2 and ethanol by pervaporation
Florian Wallisch:	Bau eines Prototyp–Membranreaktors zur Herstellung von Diethylcarbonat
Peter Glatzl:	Aufbau eines CCU–Prozesses zur Bestimmung des Nachhaltigkeitspotentials der Kohlensäureester–Herstellung

Bachelor theses:

Florian Možina:	CO_2 as raw material for chemical industry – Characterization of miscibility and chemical stability of Diethyl carbonate
Durra Chiban:	Synthesis of diethyl carbonate using experimental catalysts
Laura Ballmann:	Ceroxid–Katalysatoren in der DEC–Synthese – Chemisch analytische Untersuchungen & Kreislaufprozess

List of Figures

List of Tables

List of Abbreviations

Å	ångström
AC	activated carbon
ATR	attenuated total reflectance
BMED	bipolar membrane electrodialysis
CAE	carbonic acid ester
cat	catalyst
CC	carbon capture
CCS	carbon capture and storage
CCU	carbon capture and utilization
CCUS	carbon capture and storage/utilization
COC	cyclic organic linear carbonate
Eq.	equation
FSC	fixed–site–carrier
GC–FID	gas chromatography – flame ionization detector
FTIR	Fourier transform infrared spectroscopy
GHG	greenhouse gas
GPU	gas permeance unit
KFT	Karl Fischer titration
MS	molecular sieve
OC	organic carbonate
PCC	post–combustion capture
PEO	polyethylene oxide
perm	permeate
PLS	partial least squares
PSA	pressure swing adsorption
Ref	reference
SINTEF	The Foundation for Industrial and Technical Research
TRL	technology readiness level
UN	United Nations
$\mathbf{V_{R}}_i$	Reactor experiment i
XRD	X-ray diffraction
XRF	X-ray fluorescence

Parameters and Symbols:

A	area
$Comp$	number of compartments in membrane model
$\dot{J}_{total}$	total flux
$\dot{J}_i$	flux of compound i
K_{eq}	equilibrium constant
M_i	molar mass of compound i
N	total molar feed flow
N_{eff}	effective molar flow in active membrane model compartment
P	pressure
P^0	ambient pressure
$P_{carrier}$	performance per mass of carrier
P_{cat}	performance per mass of catalyst
P_F	feed pressure
Q_i	permeance of compound i
Q_{all}	list of all permeances
R	universal gas constant
T	temperature
V	volume
Y_i	yield of compound i
c_i	concentration of compound i
d_{if}	inner diameters of fiber
l_f	length per fiber
$m_{carrier}$	mass of the carrier
m_{cat}	mass of the catalyst
m_i	mass of compound i
$m_{i,0}$	mass of compound i at the beginning of an experiment
m_{total}	total mass
n_F	molar flow of feed
n_{fib}	number of fibers
n_i	molar mass of compound i
n_p	molar flow of permeate
$p_{xF,i}$	partial pressure of compound i in feed
$p_{yi,i}$	partial pressure of compound i in permeate
p_p	permeate pressure
$q_{i,0}$	initially estimated molar flow per compartment
$q_{i,p}$	molar flux of compound i per compartment
$q_{i,r}$	total molar flux per compartment
$q_{t,p}$	molar retentate flow of compound i per compartment
$q_{t,r}$	total molar retentate flow per compartment
w_i	weight fraction of compound i
$w_{c,i}$	weight fraction of compound i in circulate
$w_{p,i}$	weight fraction of compound i in permeate
x_i	molar fraction of compound i
$x_{F,i}$	molar fraction in feed of compound i
x_r	molar fraction in retentate
$x_{r,i}$	molar fraction in retentate of compound i

y_i	molar fraction of compound i
$\Delta_r Cp_m$	change in specific heat of a reaction
$\Delta_r G_m^0$	standard Gibbs free enthalpy of reaction
$\Delta_r H_m^0$	standard enthalpy of reaction
$\Delta_r S_m^0$	standard entropy of reaction
Δn	change in the number of moles in chemical reaction
Δp_i	partial pressure difference of compound i
Δt	duration
α	ideal selectivity
α_i	pressure ratio
$\alpha_{i/j}$	ideal selectivity for compound i over compound j
λ	wavelength
θ_i	stage cut of compound i
$\wedge$	logical conjunction
$\vee$	logical disjunction

Elements and Molecules:

2CP	2–cyanopyridine
Al	aluminium
Al_2O_3	aluminium(III) oxide
CaC_2	calcium carbide
CaO	calcium oxide
CeO_2	cerium(IV) oxide
CH_2Cl_2	dichloromethane
CH_2O	formaldehyde
CH_4	methane
CO	carbon monoxide
CO_2	carbon dioxide
Cu	copper
DEC	diethyl carbonate
DEP	2,2–diethoxypropane
DMC	dimethyl carbonate
DME	dimethyl ether
DPC	dipropyl carbonate
EC	ethylene carbonate
EtI	ethyl iodide
EtOH	ethanol
Fe_2O_3	iron(III) oxide
H_2	hydrogen
H_2O	water
H_2SO_2	sulfuric acid
H_3O^+	hydronium
H_3PO_4	phosphoric acid
HCl	hydrochloric acid
HF	hydrofluoric acid
Hg	mercury
K_2CO_3	potassium carbonate
KOH	potassium hydroxide
MeOH	methanol
MTBE	methyl *tert*-butyl ether
N_2	nitrogen
Na_2CO_3	sodium carbonate
NH_3	ammonia
NaCl	sodium chloride
NaOH	sodium hydroxide
Ni	nickel
NO	nitrogen monoxide
NO_x	nitrogen oxides
O_2	oxygen
PBT	polybutylene terephthalate
PEM	proton-exchange membrane
PEO	polyethylene oxide
PI	polyimide
PSF	polysulfone
Pt	platinum
PVAm	polyvinylamine
SiO_2	silica
SO_2	sulfur dioxide
SO_x	sulfur oxides
TiO_2	titanium dioxide
TOC	total organic carbon
Zn	zinc
ZrO_2	zirconium dioxide

CHAPTER 1

Motivation

The greenhouse gas effect of carbon dioxide (CO_2) has been reported already back in the year 1857 [1]. The potential harm to the climate and the biosphere that the effects of greenhouse gas emissions could cause has been proposed in the 1950s [2, 3]. As of today, it can be stated that the increasing amount of adverse weather incidents can be linked to the effects of increased anthropogenic greenhouse gas emissions into the atmosphere [4]. Multiple poly–lateral agreements, such as the Paris Agreement in 2015 [5] or the UN Climate Action Summit [6], have been made to limit greenhouse gas emissions. As a major contributor to GHG emissions, the industry is in demand to revise multiple processes and routines towards more sustainable methods [7]. An interesting approach to reducing CO_2 emissions is carbon capture and storage (CCS). CCS is a terminology that combines technologies that store CO_2 captured from industrial and non–industrial sources in intended containers. Even though this technology is considered highly interesting, it comes with serious drawbacks since suitable storage spaces are challenging to find. Projects for CO_2 storage in depleted fossil fuel reservoirs or underground water bodies have been reported [8]. Both faced challenges like leakages or risks of injection–induced seismicity [9, 10]. Other CCS technologies have also been investigated, such as converting CO_2 to solid carbon or fixation into metal oxides, forming carbonates. Some approaches are considered promising alternatives to storing CO_2 in its native gaseous form [11]. Alongside the storage of CO_2, carbon capture utilization (CCU) applications are also gaining increasing awareness. Instead of storing CO_2, CCU applications search for a favorable condition in which CO_2 would be handled as an educt within a chemical reaction to form a product that could be reused. [12] This approach could substitute fossil sources while maintaining a part of the currently available infrastructure and consequently pursuing the net zero emission goals posed by the Green Deal of the European Union [13]. Furthermore, GHG emissions from industrial processes could also be drastically reduced if CO_2 and other GHGs were separated from various processes' off–gasses [14].

CCS and CCU technologies require separation technologies to recover carbon as hydro-

carbons or as CO_2 from various sources (e.g., combustion, fermentation, biomass, cement plants, power plants, air, etc.) [15]. Among multiple possibilities, membrane separation technologies have been considered as an emerging technology in the last decades, with significant advantages in comparably lower operating costs and complexity. Furthermore, membranes may be engineered to separate non–desired components from mixtures, which will be addressed in this thesis.

The chemical industry's interest in switching from conventional production processes and the use of classic building block compounds for syntheses to newer sustainable methods is steadily increasing. For example, the shift in mobility away from fossil combustion engines towards electric vehicles is a topic of great scientific [16], economic [17, 18] and political [19, 20] relevance. Last but not least, suitable electrolytes and solvents are essential for producing battery electric vehicles. Organic carbonates are often used for this purpose. The production of these is predominantly still based on toxic chemicals [21].

One promising CCU application is the direct synthesis of organic carbonates from alcohol and CO_2. Major challenges in establishing a process based on a reaction between alcohol and CO_2 are the unfavorable thermodynamics, the presence of water, and the necessity of developing suitable catalysts. [21]

Since the development and operation of processes are very time–consuming and comparably expensive, simulations have been extensively carried out to estimate the feasibility, results, and most relevant influences within the mentioned CCU applications.

1.1 Target of this work

This research aims to valorize CO_2 provided by industry by contributing findings on an alternative organic carbonate synthesis process based on comparably more sustainable methods than the current standard. To accomplish this objective the following tasks have been seen as crucial for achieving the target:

- Validating the current state of research in direct synthesis of diethyl carbonate by conducting the esterification reaction of EtOH and CO_2 with a commercial catalyst, proving that the reported characteristics in literature have been reproduced. This shall be carried out in both configurations, with and without applying a chemical dehydrating agent.

- Research on materials catalyzing the direct synthesis substituting commercial CeO_2 while achieving competitive or better productivities. CeO_2 is commonly used as a polishing agent [22]. Thus, any parts in contact with the suspension of CeO_2 and the reaction mixture formed are at risk of being damaged. Therefore, the actual catalytic component applied must be changed or immobilized. The result of this research must be benchmarked in comparison to commercial options and evaluated for the use of an entire process chain.

- The availability of a membrane to dehydrate the reaction mixture, of which water formed during the process massively decreases the progress of the reaction [21], shall be investigated, tested, and evaluated for its eligibility for process integration.
- These findings shall be implemented into a digital equivalent as a simulation. Since the availability of free models for open–source process simulation tools is limited, the modeling of necessary unit operations such as gas permeation, pervaporation, and a membrane reactor has to be contemplated.
- It should be investigated whether all the points mentioned above enable the creation of an overall process. For this purpose, the findings above shall be considered within the design, conceptualization, assembly, and operation of a pilot reactor capable of producing DEC.

CHAPTER 2

State–of–the–art – CCU in industrial processes

The primary emphasis will be on the opportunities for CO_2 usage. More in–depth information on the separation of carbon dioxide is given in section 2.1.

The use of carbon dioxide as a feedstock has been discussed in research, at least since the middle of the 20th century – initially for the production of dry ice [23]. The non–reactive and stable molecular nature of CO_2 makes it rather challenging to plan and operate economically feasible processes based on CO_2 [12]. Nevertheless, recent years have come with a rising trend of research on the use of CO_2, resulting in promising technologies that may be divided into carbon capture and storage (CCS) and carbon capture and utilization (CCU). Both are preceded by the separation of CO_2 from various sources. CCS technologies aim for a long–lasting effect of CO_2 retention where CO_2 shall react and form a stable compound like in mineralization, where inorganic carbonates are formed from minerals and CO_2 [15]. Another example of CCS applications is the CO_2 sequestration in reservoirs. CCU technologies include CO_2 as a renewable carbon source for the synthesis of downstream products, which serve as temporary CO_2 emission sinks. [12] The current (year 2023) global energy–related CO_2 emissions have grown to a record of 37.4 Gt of CO_2/year [24]. Currently operated CO_2 capture projects processed between 230 and 280 Mt of CO_2/year, mainly being used for urea production (57 %), enhanced oil recovery (34 %), food industry–related applications (6 %), and others [25].

The extension of CCU and CCS (CCUS)technologies is being highly considered for many decarbonization strategies. The substantial rise in current publications reflects the considerable potential of CCUS applications.

Even though many technologies behind CCUS applications have already been initially proposed in the past century, the interest in CCUS applications has risen since 2010,

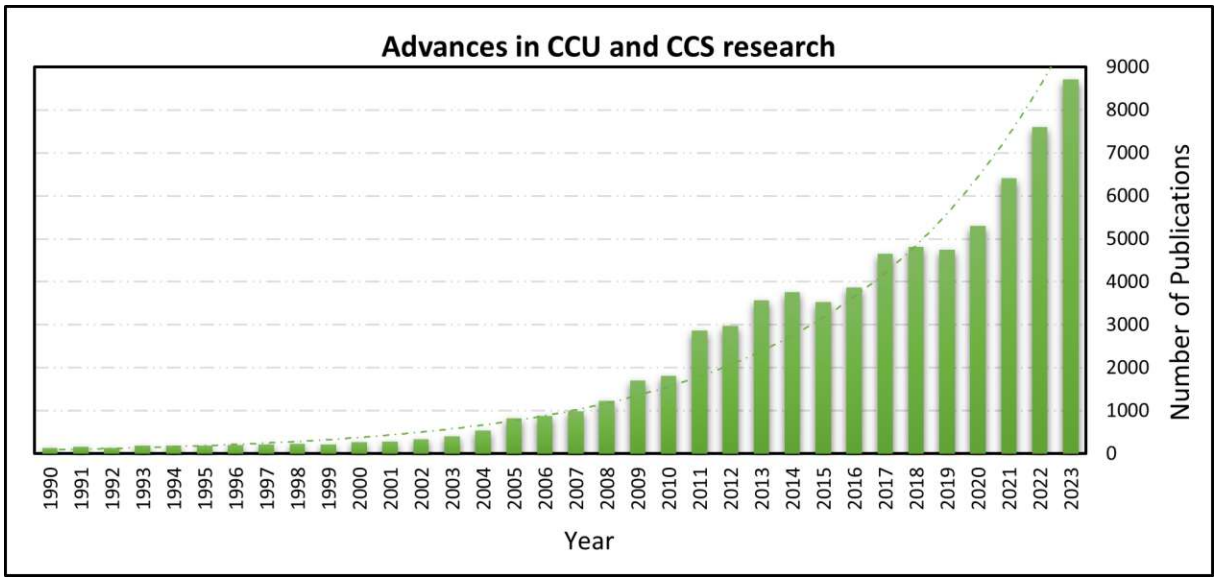

Figure 1: Records in number of publications on CCUS since 1990 [26]

according to Figure 1. Especially the 2020s seem to have a rather boosting impact on the research of CCU and CCS technologies.

A classification of CCU technologies into smaller groups has been proposed by Zhang et al., as illustrated in Figure 2 [27].

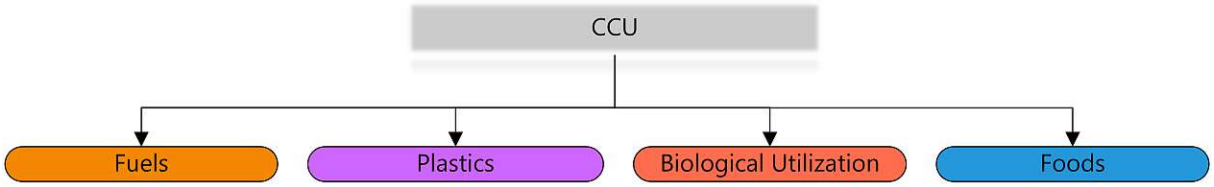

Figure 2: Classification of CCU technologies (adapted from [15])

Thus, the pathways in which CO_2 is used as a feedstock are diverse. A large variety of applications proposed are currently being developed further to produce chemicals and fuels (e.g., methane (CH_4) [28], methanol (MeOH) [29], formic acid [30], urea [31], cyclic carbonates [32] and other hydrocarbons [33]) from CO_2. Manufacturing plastics from CO_2–like polyols [34] and polyoxymethylene dimethyl ethers [35] decreases petrochemical consumption while simultaneously carrying out temporary CO_2 fixation.

Biological utilization through algae cultivation [36] and biofuel production is an intensively studied subject today [37]. Wang et al. have discussed the opportunities in catalyzing the hydrogenation reactions of CO_2 to produce industrially widely demanded compounds such as methanol, carbon monoxide, methane, formic acid, and many more substances. Primary emphasis was placed on the performance of the researched metal–based catalysts on which these reactions heavily rely. [38]

The solar–driven production of CO from CO_2 has been explored in the work of Agliuzza

et al., in which the application of electrochemical CO_2 reduction is reviewed. Coupling photovoltaic with electrolysis leads to promising results while releasing no additional CO_2 into the atmosphere. The lack of suitable energy storage technologies has been mentioned as an adverse aspect of this method. [39]

Ihsanullah et al. have discussed the CO_2 consumption by rejected brine simultaneously reducing its salinity as a potentially relevant CCU process [40]. Reactions of brine samples with ammonia and CO_2 reducing 90 % of the CO_2 concentration in a CH_4 – CO_2 mixture were observed by Dindi et al. while sodium bicarbonate was formed [41]. However, this process requires ammonia, which is produced by the Haber–Bosch process from nitrogen (N_2) and hydrogen (H_2), which is currently produced with energy–intensive and CO_2–emitting processes itself. Wang et al. have presented a comparative assessment of conventional ammonia (NH_3) production in comparison to NH_3 synthesis coupled with carbon capture technologies [42]. Bipolar membrane electrodialysis (BMED) has been recently discussed by Khoiruddin et al., being considered an effective measure to reduce the CO_2 levels in seawater and simultaneous decalcification. Sodium carbonate (Na_2CO_3) is an industrially relevant side product yielded with BMED. Future advances are expected in membrane fouling drawbacks [43].

The synthesis of dimethyl ether (DME) from CO_2 was discussed in the review of Catizzone et al., which revealed that DME is a potential circular hydrogen carrier. Although a wide range of possible applications are already described today, the direct hydrogenation of CO_2 into DME is a significant issue that needs to be overcome. Even though a couple of catalysts for this purpose have been named, further advances in the design of the catalyst are desired [44].

CO_2 is currently being used within the food and beverage industry today. Wang et al. discuss how CO_2 is utilized as an agent for multiple purposes, e.g., the extraction of bioactive compounds (essential oils, phenolic compounds, lipids) from foods. [45]

In conclusion, CCU technologies are currently discussed intensively as solutions for issues related to GHGs. Although some drawbacks are currently present, some of the mentioned technologies are expected to become sufficiently competitive or surpass conventional technologies as time passes [46].

2.1 Carbon Capture Technologies

The capture of carbon precedes the utilization or storage of carbon. Carbon compounds other than CO_2, not classified as greenhouse gases, only enter the atmosphere when they are degraded into CO_2. Although there are also major efforts to develop more sustainable circular economies for other carbon compounds, this work relates to the use of CO_2 and, thus, its capture from process streams in its gaseous form.

The oxy–fuel method uses pure oxygen instead of air for combustion and recirculated flue gas, controlling and limiting the temperature. Chilling of the flue gas leads to separating gaseous water and CO_2. An air separation unit (ASU) based on a cryogenic system pro-

vides O_2, accounting for significant energy consumption for the cooling and compressing units [14]. Further information on oxy-fuel combustion and forms of applications have been described by Carrasco–Molando et al. [47].

Technologies removing CO_2 from fossil sources before combustion are described as pre–combustion capture. Gasifiers are usually applied to convert fuel to syngas (H_2 & CO). Subsequently, CO_2 is separated from the syngas, relying on pressure swing adsorption or stripping, which is considered costly and complex [48]. Ramzan et al. have described more details on carbon capture with pre–combustion [49].

Opposing pre–combustion capture, post–combustion Capture (PCC) is centered around separating flue gas components after the combustion process with air. The literature proposes various capturing processes for PCC technologies [50–52]. PCC is currently regarded as the most mature and widely applied toolset of technologies, even capable of being used in other technologies such as biogas upgrading or direct air capture (DAC). An overview of the technologies available in the industry and the literature on PCC is illustrated in Figure 3.[53]

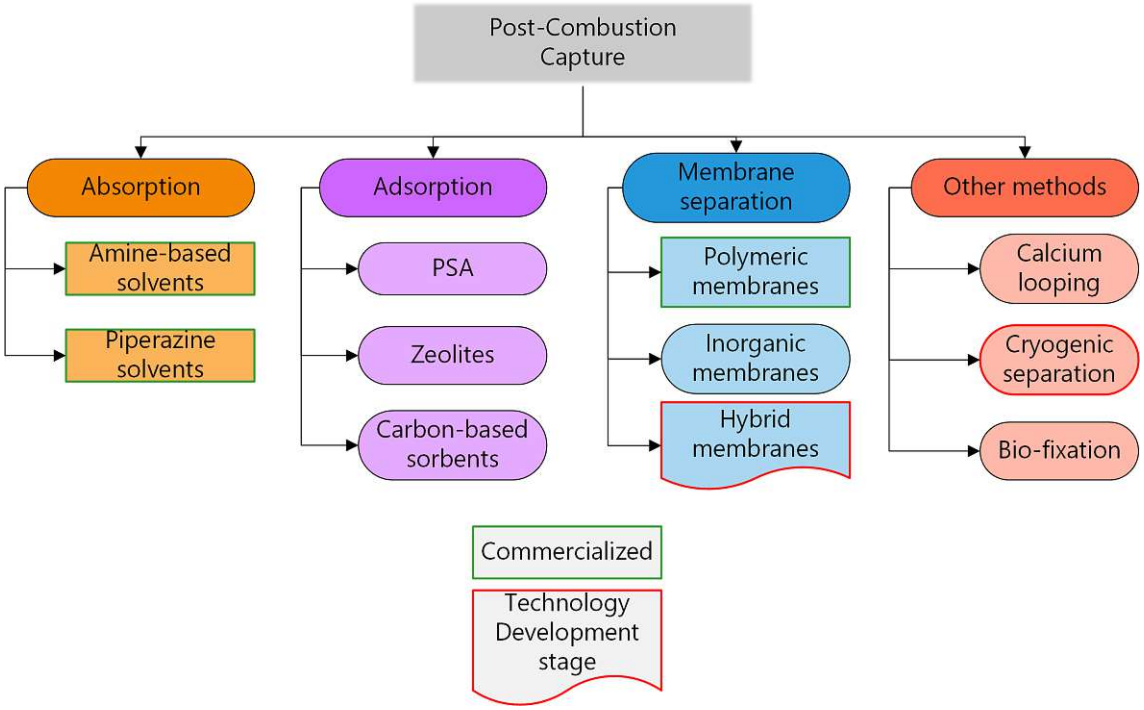

Figure 3: Overview of post–combustion capture technologies (adapted from [50])

Absorption relies on physical or chemical mechanisms to separate CO_2 from flue gas and incorporate it into the bulk of liquid solvents. Absorptive techniques include amine–based methods, the application of piperazine as a solvent, alkali absorption, and the Kerr–McGee/ AGG Lummus Crest or Fluor Econamine FG Plus process [50, 51]. An in–depth description of absorption–based PCC, including recent advances, has been reviewed by Peu et al. [54]

Table 1: Advantages and drawbacks of currently in literature discussed PCC technologies

Advantages	Disadvantages	Ref
Amine–based solvents		
high recovery rates (80 – 95 %) > 95 % of solvent regenerated Large scale application High CO_2 purity (> 98 %)	Solvent degradation High energy demand Corrosive environment Amine losses due to evaporation Toxicity of solvents	[50, 56]
Adsorption		
Regeneration of Adsorbents High recovery rate Long term use	High energy demand Presence of SO_x and NO_x problematic	[50]
Membrane separation		
Non–complex maintenance High recovery rates Lower capital cost Low energy consumption Fast development due to modular setup Comparably facile design and scale–up	Aging Comparably weaker stability at high temperatures Water causes swelling of the membrane Comparably limited purity of CO_2 O_2 and SO_2 may pass with CO_2	[50, 57]

Due to physical forces of attraction, the attachment of gases and impurities on surfaces of specific carriers are assigned to adsorption–based PCC. PSA, Temperature Swing Adsorption (TSA), Vacuum Swing Adsorption (VSA), and Electrical Swing Adsorption (ESA) rely on solids (e.g., activated carbon (AC), zeolites, and metal–organic frameworks). The performance of some adsorptive materials is enhanced by impregnation with chemically active compounds [50, 51]. Raganati et al. have published a comprehensive review of adsorptive methods for carbon capture, which includes a detailed comparison of various adsorbing solids. [55]

Membranes are currently a key issue in PCC. A more detailed description can be found in the following section. [50–52]
The advantages and drawbacks of selected PCC methods observed in the literature are presented in Table 1.

Both Adsorption and amine–based methods lead to high purities of CO_2. However, high energy consumption must be taken into account. The regeneration of amine–based solvents is possible, nevertheless, a gradual degradation is inevitable. Another drawback is the toxicity of the solvents used. Adsorption processes exhibit large operational lifespans but are prone to problems due to SO_x and NO_x impurities, which must be removed from the flue gas in advance. Amine–based PCC is a well–known technology that is available commercially. The operation of membranes in PCC has not yet been fully commercialized on an industrial scale (see Table 1). Still, they exhibit considerable potential for sustainable PCC applications due to their comparably facile maintenance, low energy demand,

and high possible recovery rates.

2.2 Membrane technology in Post carbon capture

Membrane technology in the context of PCC primarily considers flue–gas cleaning. Therefore, an overview of the membrane material types currently in literature for CO_2–selective gas permeation is illustrated in Figure 4.

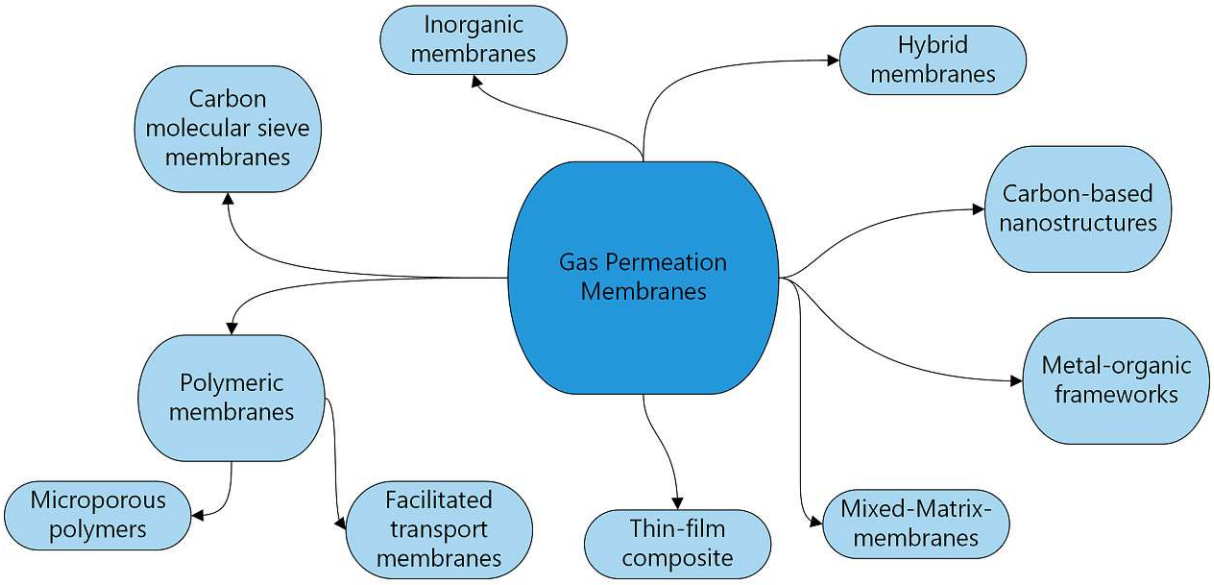

Figure 4: Overview of available membrane materials for PCC (adapted from [58])

Various membrane material types are available for CO_2 separation from gaseous mixtures and flue gas. Advances in research have resulted in the development of further hybrid and subcategories of membranes, which have previously been just divided into polymeric or inorganic membranes. [58]

Most current gas permeation applications are operated with polymeric or polymer–based membranes. The Polaris membrane, a polymer flat–sheet membrane, is distributed by MTR - "*Membrane Technology & Research*" and is one of the few commercially available CO_2–selective membranes. Depending on the flue gas properties, a recovery rate of 90 % for CO_2 while maintaining a high flux (1000 GPU) was reported, delivering CO_2 concentrations as high as 95 %, driven by a vacuum pump. The Polaris membrane has been reported to be used on multiple occasions for PCC applications and is considered one of the most promising opportunities [59, 60]. Further developments of the Polaris membranes, which aim for a 2 – 3 times higher flux for CO_2, are currently being tested [61–63].

Helmholtz–Zentrum Hereon has used a PEO–based polymer to design the PolyActive flat–sheet membrane module. Few applications have been made public using this membrane for PCC purposes. Brinkmann et al. [64] have characterized the performance of flue gas from biomass and coal–fired processes. Despite the low feed concentration of CO_2

Table 2: Overview of selected gas permeation membranes for PCC

Membrane	T [°C]	P_F [bara]	p_p [bara]	Q_{CO_2} [GPU]	α_{CO_2/N_2}	Material	Recovery rate [%]	Ref
Prism PA1020	20 – 60	1.8 – 3	ambient	361	37	PSF	80 – 85	[68]
Polaris	< 38	1.5	0.11	1000	50	polymeric	90	[59]
PolyActive	30 – 90	< 3	0.05 – 0.2	1480	45	PEO–PBT	43 – 80	[64, 65]
SINTEF	40 – 45	1.013	0.1 – 0.2	222	< 300	PVAm–FSC	30 – 90	[66, 67]
UBE – UMS–A5	< 60	1.8 – 7	1.013	21.7	45	PI	< 30	[68, 69]

(9 %), the membrane operation enriched the permeate concentration of CO_2 above 45 %. As with the SINTEF and Polaris membrane, a vacuum pump ensured the driving force, allowing feed pressures close to ambient pressure. Applying a second stage increased the permeate purity above 95 % of CO_2. However, less than 43 % of CO_2 was recovered from the flue gas. [65]

Facilitated transport membranes are carrier–bearing hybrid membranes that can interact reversibly with one or more specific components, introducing an extra transport mechanism. This supports the target compound's movement, while the other compounds' movement through the membrane relies solely on the solution–diffusion mechanism.[58]

A polymer–based facilitated transport flat–sheet membrane utilizing fixed–site carriers was developed by SINTEF – "*Stiftelsen for industriell og teknisk forskning*" (english translation: "*The Foundation for Industrial and Technical Research*") in cooperation with NTNU – "*Norges teknisk-naturvitenskapelige universitet*" (english name: "*Norwegian University of Science and Technology*") and intended to separate CO_2 from flue gas. [66, 67] Permeate purities of up to 75 % of CO_2 have been reported on flue gas fed up to 12 % CO_2. A two–stage application increased the purity to 99.5 %, with recovery rates exceeding 90 % for CO_2. A vacuum creates The driving force by reducing the pressure on the permeate side to 0.1 – 0.2 bar. The endurance towards impurities (e.g., SO_2, NO_x, O_2, humidity, and dust) was described as good as the feed concentration of NO_x and SO_2 remained comparably low [66, 67].

Table 2 shows a selection of membranes applied in gas separation applications. All listed membranes are polymeric or polymer–based membranes of diverse performance. The Polaris and PolyActive membranes have been tested and operated in an exhaust gas environment with promising results. On the other hand, the Prism PA1020 is mainly considered for natural gas purification but could be attractive for flue gas separation in a subsequential step.

The Robeson plot can be considered helpful for selecting suitable membranes for flue gas separation. The Robeson plot for CO_2/N_2 gas pair separation is portrayed in Figure 5.

It includes a graphic illustration of the relation between the permeability of CO_2 and the ideal selectivity of CO_2 over N_2 for a significantly large amount of membranes. Each symbol represents either a specific membrane material or a the selective layer of a membrane. Conventional membranes are usually either highly selective or have an exceptionally high flux for the more permeable component, but not both. This results in an upper bound

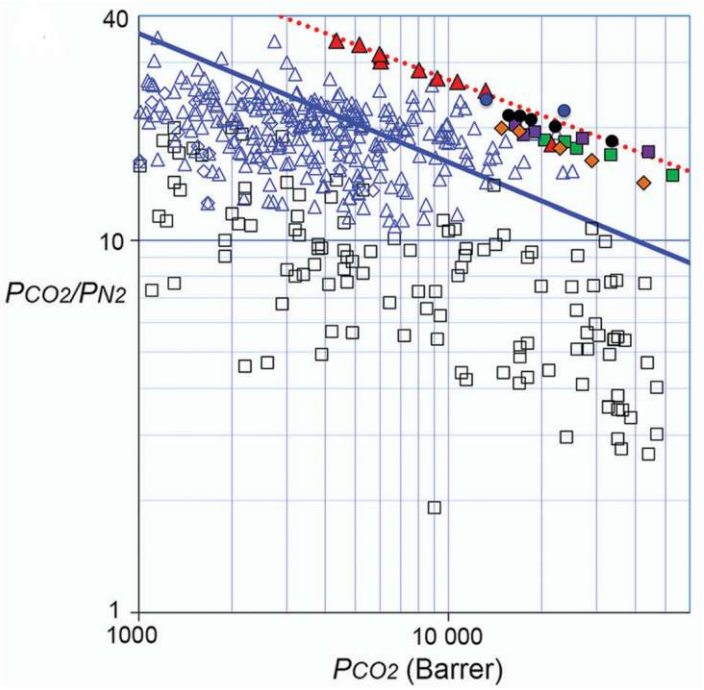

Figure 5: Robeson plot for CO_2/N_2 gas pairs (assumption 25 °C and 1.013 bar) [70]

as a function of the permeability and selectivity, displayed as a straight blue line. The research in novel membranes has resulted in better–performing membranes shifting the upper bound (dotted red line) [70, 71]. Since flue gas from fossil fuel combustion consists mainly of N_2 [72, 73], the separation properties of the membranes with respect to N_2 were mentioned. However, to evaluate the performance of membranes, other factors such as the selectivity of other flue gas components, material behavior in humid conditions, durability and other factors must also be considered. An extensive overview of further membranes for post–combustion currently being researched has been provided by Liu et al. [74]
Due to the relevance to this work, a selection of pervaporation membranes for dehydration of organic solutions has been published in **[Journal Publication II]**.

2.3 Organic carbonates

This work focuses on diethyl carbonate (DEC) and its synthesis based on CO_2, which will be discussed in more detail in subsection 2.3.1.

A delve into organic carbonate production from CO_2 is gaining more attention [75]. Organic carbonates (OCs), also called carbonic acid esters (CAE), form a group of compounds consisting of a carbonyl group flanked by two alkoxy/aryloxy groups that do not necessarily require to be identical. The formulae illustrated in Figure 6 represent some possible chemical structures. [40]

OCs are commonly attributed to low toxicity, low vapor pressure, and fair biodegradability as aprotic polar solvents for esters, cellulose ethers, and polymers [76]. They are

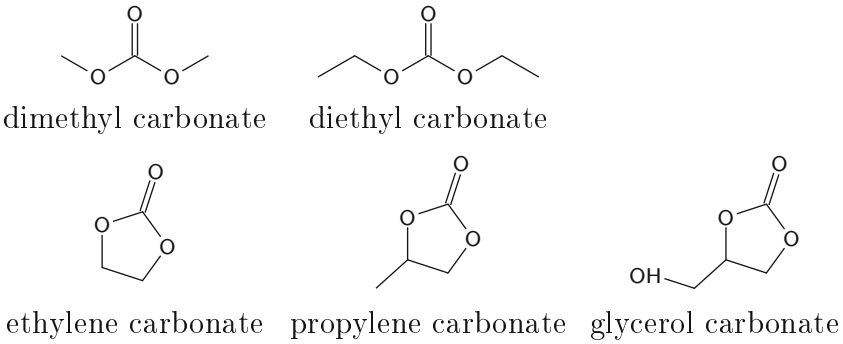

Figure 6: Structural formulae of various organic carbonates (adapted from [16])

found in highly diverse applications in both industry and scientific laboratories [77, 78]. Dimethyl carbonate (DMC) is an essential and versatile chemical in the polymer– and pharmaceutical industry [79]. The pharmaceutical industry uses DMC as an intermediate for medicines and veterinary drugs [80], while other industrial branches apply DMC to produce adhesives [81, 82]. The high oxygen content makes it a good additive for fuel, reducing the emission of soot particles and substituting methyl *tert*–butyl ether (MTBE), which is already banned in some countries [83]. Its solvating capabilities as a nonaqueous electrolyte resulted in DMC's application as an electrolyte in batteries, increasing their lifespan [84]. Dipropyl carbonate (DPC) shares many fields of application with DMC, such as its use as a solvent and electrolyte additive in lithium–ion batteries and as an intermediate for pharmaceuticals. It is also used to produce pesticides, polycarbonates, and urethane [85]. Cyclic organic carbonates (COCs), sometimes just cyclic carbonates, serve similar purposes as linear OCs (e.g., industrial lubricants, solvents, electrolytes for batteries, and intermediates for polycarbonates) [86]. COCs seem to find increasing application as a building block for polymer synthesis [87, 88]

OCs are traditionally produced from phosgenation of alcohol in the presence of pyridine as an acid acceptor and dichloromethane. The specific OC formed depends on the alcohol used in the synthesis. The interest in methods other than phosgenation kept rising due to phosgene's corrosive and toxic nature [89, 90]. The reaction equation for OC synthesis from phosgene and alcohol is available in equation (Eq.) 1 [76].

(1)

phosgene alcohol organic carbonate hydrogen chloride

Oxidative carbonylation is a comparably younger approach to producing organic carbonates from alcohols using CO and O_2. This method comes with relatively high requirements for the catalyst. The presence of CO and the resulting toxicity is another drawbacks of its industrial usage [91, 92]. The diphenyl carbonate synthesis from phenol's oxidative carbonylation is available in Eq. 2 [91].

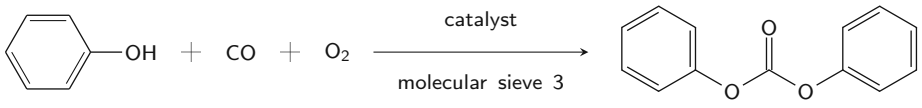

(2)

Substituting phosgene with urea led to an alternative method to produce OCs. The ammonia formed within the reaction could be reused to regenerate urea [16, 93]. However, this requires an efficient dehydration of ammonia carbamate, which is formed as an intermediate product [94]. The "International Agency for Research on Cancer" has classified ethyl carbamate as cancerogenic [95, 96]. The reaction equation for the alcoholysis of urea to form OCs is available in Eq. 3 [93].

(3)

This route's adverse effect lies in the formation of isocyanates as a byproduct [97].

COCs are currently produced from CO_2 and epoxides, which are already considered as comparably less toxic and more sustainable than the other methods for OC synthesis that have already been mentioned since the reaction already uses CO_2 as a feed. The reaction of CO_2 and cyclic carbonates forming COCs is available in Eq. 4 [98].

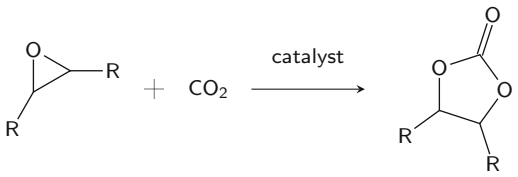

(4)

2.3.1 Diethyl carbonate

The versatile opportunities for DEC processing in industrial applications lead to significant importance for this work's research in sustainable DEC production. DEC is a linear organic carbonate classified as an important raw material for syntheses in the chemical industry. It shares the major properties of other organic carbonates, a biodegradable compound of low toxicity that is used to produce pharmaceuticals, pesticides, lithium–ion batteries, dyes, fertilizers, and more. A more detailed consideration of DEC's toxicity in comparison to other common solvents can be found in the work of Tobiszewski et al. [99]

Including the synthesis options described in 2.3, the current literature provides the following possibilities mentioned in Eqs. 5 - 12

- phosgenation of ethanol [100] (see also Eq. 1):

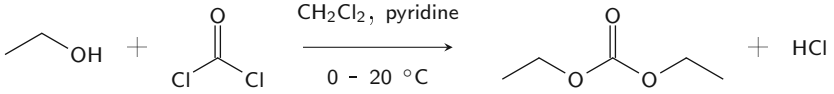

(5)

- oxidative carbonylation of ethanol [21, 101] (see also Eq. 2):

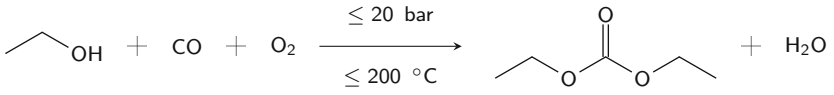

(6)

- alcoholysis of urea [102, 103]:

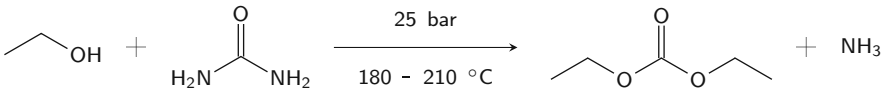

(7)

- direct synthesis from CO_2:

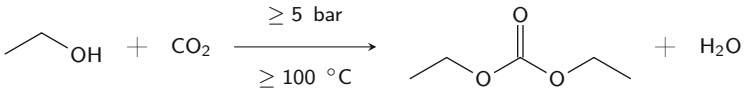

(8)

- transesterification:
  - from DMC [104, 105]:

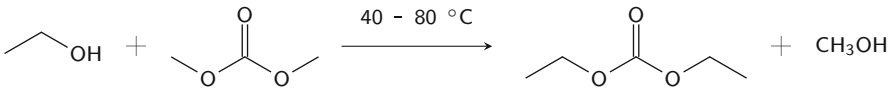

(9)

  - from EC [106, 107]:

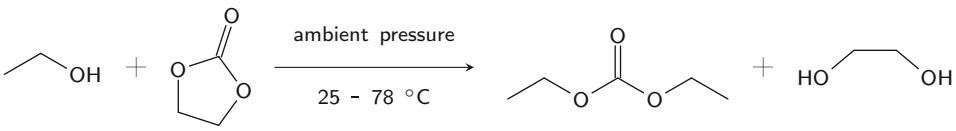

(10)

- from ethyl nitrite [108]:

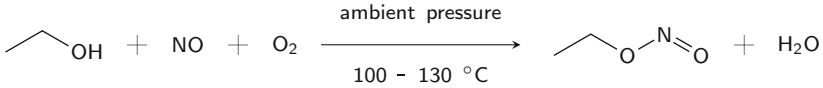

(11a)

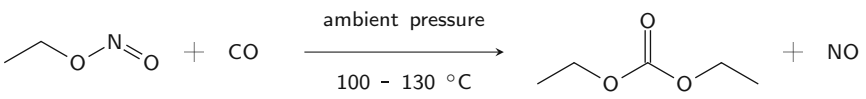

(11b)

Table 3: Thermodynamic data for different synthesis reactions for DEC

Reaction	Reactant	$\Delta_r H_m^0$ [kJ/mol]	$\Delta_r S_m^0$ [J/(mol×K)]	$\Delta_r Cp_m$ [a] [J/(mol×K)]	$\Delta_r G_m^0$ [kJ/mol]	Ref
Eq. 7	Urea	102.02	258.57	–35.40	24.93	[110]
Eq. 8	CO_2	–18.61	–166.21	24.34 [b]	30.95	
Eq. 9	DMC	4.24	–4.57	–22.00	5.60	
Eq. 10	EC	2.20	8.29	18.26	–0.27	
Eq. 6	$CO + O_2$	–91.33	–250.39	17.63	–16.68	[111, 112]
DMC Synthesis	CO_2	–24.26	–162.41	46.343	24.16	[113]

[a] assumption that C_p remains constant
[b] reference [114]

- from diethyl oxalate [109]:

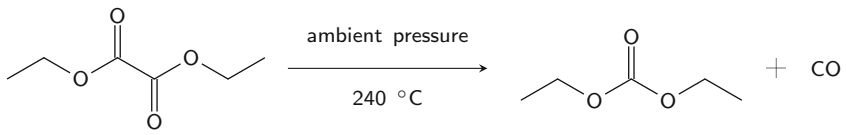

(12)

The review by Shukla et al. gives good insight into the various synthesis routes available in literature. [21] It remains to be mentioned that it can be assumed that phosgenation is the predominantly applied synthesis method [16]. In contrast, the others are applied on a smaller scale or are still to be developed to market maturity. The alcoholysis of urea is considered to be a promising option. The opportunity to recover urea from the ammonia formed as a product via a conversion with CO_2 was discussed positively. Ethyl nitrite may be used to produce DEC at comparably low temperatures and pressures. A byproduct of these reactions is diethyl oxalate, which can also be used to produce DEC [108, 109].

2.3.2 Direct synthesis of DEC

The potential for large–scale industrial production of DEC from ethanol and CO_2 (see Eq. 8) is considered exceptionally high and can be classified as a CCU process. Nevertheless, utilizing CO_2 as the feed for DEC synthesis comes with a row of challenges. As already mentioned at the beginning of Chapter 2, CO_2 is a very stable compound that must be brought into a reactive state in the event of direct synthesis. The thermodynamic data of several reactions affiliated with DEC synthesis have been listed in Table 3.

Leino et al. investigated the thermodynamic equilibrium by calculating the free Gibbs energy using the Kirchhoff law (Eq. 12) and the Gibbs–Helmholtz equation (Eq. 14) [110, 115].

$$\left(\frac{\delta \Delta_r H_m}{\delta T}\right)_p = \Delta_r C_{p,m} \tag{13}$$

$$\left(\frac{\delta \Delta_r G_m / T}{\delta T}\right)_p = -\frac{\Delta_r H_m}{T^2} \tag{14}$$

$$\Delta_r G_m = \frac{T \Delta G_{298.15\ K}}{298.15} - (\Delta_r H_{298.15\ K} - \Delta_r C_{p,m} \times 298.15) \times \\ \times \left(\frac{1}{T} - \frac{1}{298.15}\right) T - \Delta_r C_{p,m} T \ln\left(\frac{T}{298.15}\right) \tag{15}$$

Eq. 15, derived from the integrated forms of Eq. 13 and 14, shows the quasi–linear trends of the free Gibbs energies of chosen DEC synthesis reaction routes depending on temperature, as illustrated in Figure 7.

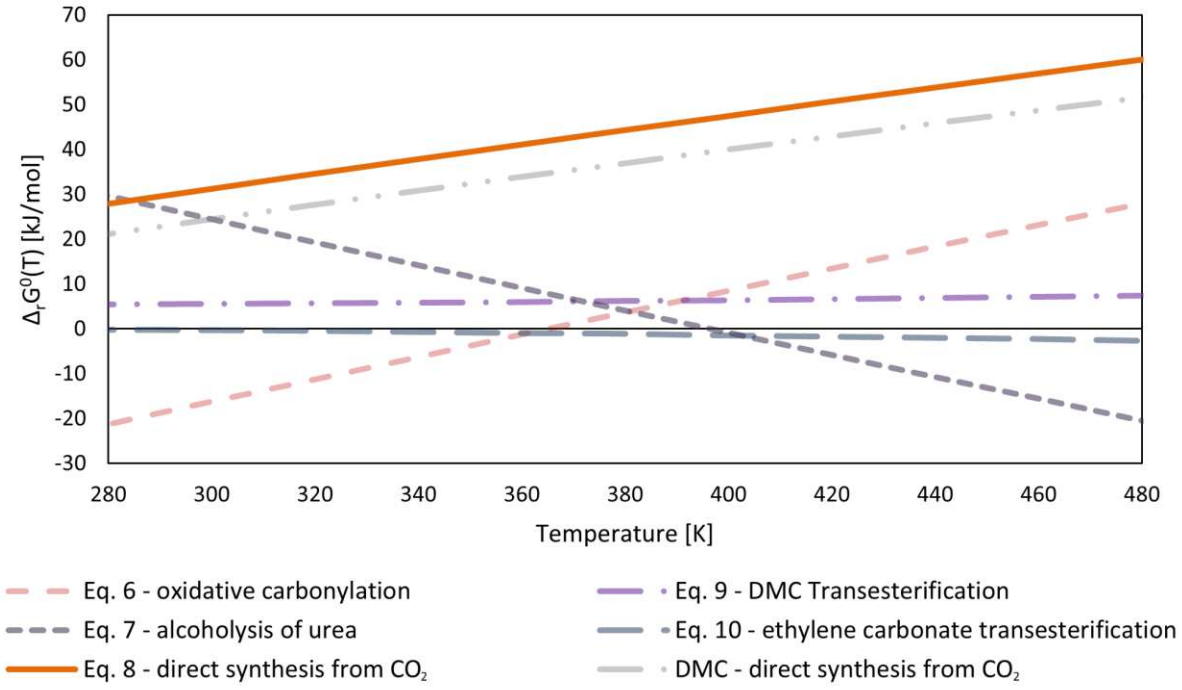

Figure 7: Gibbs energies of DEC yielding reactions depending on Temperature (calculated from [110–113, 115])

Thus, Leino et al.'s work showed that the direct synthesis of DEC is an endergonic reaction whose thermodynamic limitation becomes increasingly adverse with increasing temperature. Comparing the direct synthesis of DEC, only the alcoholysis of urea has a higher $\Delta_r G_m$, which becomes exergonic at just under 400 K. The oxidative carbonylation of EtOH is the only reaction that would run off spontaneously at room temperature. Three out of five reactions have a rising $\Delta_r G_m$ indicating the adverse influence of temperature on the thermodynamic limitation. The transesterification of ethylene carbonate to DEC seems like an arguable alternative since it seems to have an exergonic nature that is even

stronger with rising temperatures. However, it is an endothermic reaction. Even though the direct synthesis of DMC does not necessarily occur for DEC synthesis, it has been included for comparative reasons. The behavior of the reaction is very similar to the direct synthesis of DEC but with a slightly negative offset, proving the comparatively less endergonic nature.

Following the example of Shukla et al., the influence of pressure on $\Delta_r G_m$ can be expressed as in Eq. 16 [110].

$$\Delta_r G_m\left(T,P\right) = \Delta_r G_m\left(T,P^0\right) + \Delta n RT \ln\left(\frac{P}{P^0}\right) \tag{16}$$

A spontaneous reaction requires extremely high pressures ($P > 7.25 \times 10^5 MPa$ at 100 °C), which are not economically feasible on a large scale [115]. The equilibrium constant K_{eq} can be determined from the free Gibbs energy of the reaction or the law of mass action as described in Eq. 17.

$$K_{eq} = e^{-\left(\frac{\Delta_r G_m(T,P)}{RT}\right)} = \frac{c_{DEC} \times c_{H_2O}}{{c_{EtOH}}^2 \times c_{CO_2}} \tag{17}$$

The literature reports very low equilibrium constants $\left(K_{eq,\ 353K} = 1.89 \times 10^{-7}\right)$ which even decreases with rising temperature, proving that the reacting compounds are favored over the yielded ones. [115]

Buchmann et al. have investigated the influence of reaction temperature on the DEC yield by conducting experiments between 80 – 170 °C at 40 bar using a cerium-based catalyst [116]. It was observed that the major limiting factor is the kinetic aspect of the reaction as long as the temperature is kept lower than 140 °C. An increase in DEC yield was achieved despite the endergonic nature of the reaction ($\Delta G_{298\ K} = 30.95\ kJ/mol$; $\Delta G_{413\ K} = 49.58\ kJ/mol$). This result particularly emphasizes the importance of the catalyst in overcoming kinetic drawbacks.

The development of new types of catalysts is a central point of current research, which is currently focused on the performance of metal oxides within the esterification reaction of EtOH and CO_2. An example of the mechanism for DEC synthesis was investigated by Arbeláez et al. using a bimetallic Cu–Ni catalyst and is illustrated in Figure 8 [117].

The initial step is described as the attachment of EtOH to the catalyst, whereby a proton is split off. Simultaneously, the C–atom and one of the O–atoms of CO_2 are both attached to the catalyst surface, breaking up one of the earlier C–O double bonds and ultimately activating CO_2. It can be assumed that higher pressure plays a significant role in the attachment of CO_2 to the catalyst's active sites. Following this, the O–atom within the CH_3CH_2O–Cu/Ni group may attach to the C–atom of the CO_2–Cu/Ni species forming (CH_3CH_2O–Cu/Ni)CO– Cu/Ni. Another CH_3CH_2O–Cu/Ni group attaches to the earlier formed intermediate, resulting in DEC and a recovered catalyst, including water as a byproduct [117].

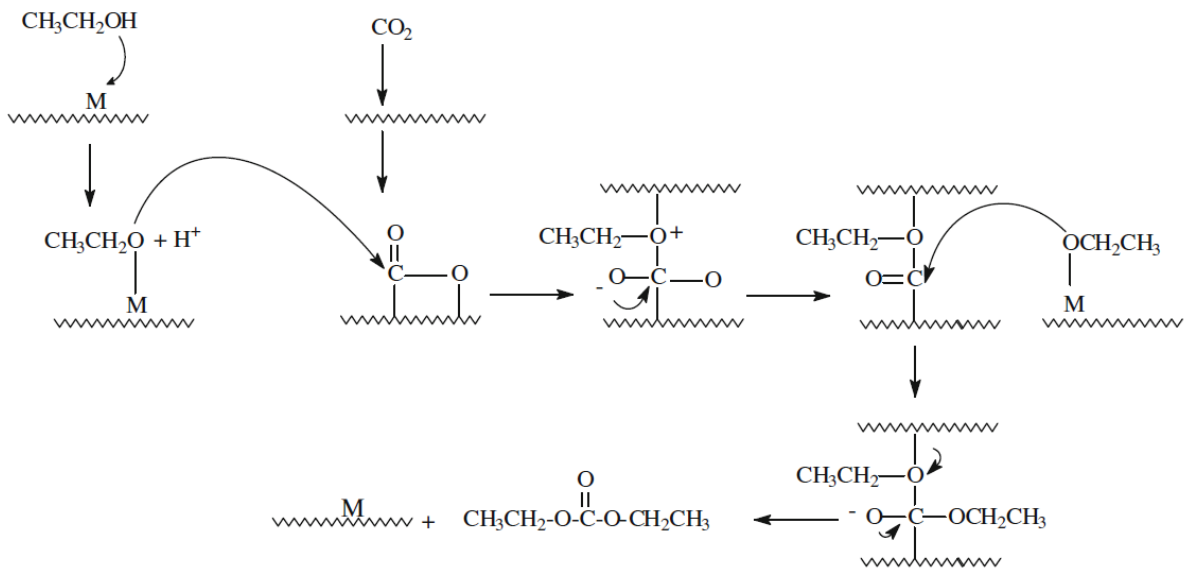

Figure 8: Reaction mechanism for direct Synthesis on a Cu–Ni/AC Catalyst [117]

Various catalysts have been studied and reported in the literature on the direct synthesis of DEC using CO_2 and EtOH. An overview of some is listed in Table 4.

CeO_2 is commercially available and has been used multiple times with comparably good results. However, the necessity of tiny CeO_2 nanoparticles results in a problematic applicability in a fixed bed. Further, its application as a polishing agent is challenging for refinery equipment. Other metal oxides like ZrO_2, Fe_2O_3, and others are also listed. Their application delivered comparably poor results but enormously improved by modifying carriers (molecular sieves, CaO, and CaC_2) with ZrO_2 and Fe_2O_3 [123]. At present, the catalyst performances reported in the literature are relatively different. Comparably low productivities as the work of Décultôt et al. with 0.01458 mmol/g_{cat}h (T = 110 °C, P = 36 bar) [128] have been reported using CeO_2, while another study used $Ce_{0.07}Zr_{0.93}O_2$ and achieved productivities as large as 0.28 mmol/g_{cat}h (T = 140 °C, P = 80 bar) [126]. The highest catalytic performance observed in the literature with no mentioning of a dehydrating agent within a one-pot synthesis was reported by Yoshida et al. by achieving a productivity of 4.5 mmol/g_{cat}h CeO_2 (V = 70 mL, T = 170 °C, 200 mmol EtOH, 200 mmol CO_2) [118].

A further important aspect of direct synthesis is the presence of the byproduct H_2O, which almost completely stops the reaction. This observation led to various approaches to remove the water formed to shift the reaction equilibrium towards the product side. [121] 2–cyanopyridine (2CP), also referred to as 2–pyridinecarbonitrile, was successfully used by Giram et al. to boost the DEC yield from 0.23 mol% to 45 mol% over a Ce–based catalyst [121]. Honda et al. achieved a catalytic productivity of 1.12 mmol/g_{cat}h using CeO_2 and 2CP at 50 bar and 120 °C, yielding 91 % DEC [129]. Other dehydrating agents include benzonitrile, acetonitrile, butylene oxide, acetals, ketals, and inorganic materials like zeolites [124] or molecular sieves [130]. The application of 2,2–diethoxypropane (DEP) as a dehydrating agent was studied in the work of Chang et al. [131]. Using faujasite (H–FAU) to enhance hydrolysis of DEP strongly increases the productivity of the catalyst up to 44 mmol/g_{cat}h (T = 120 °C, P = 50 bar) [131]. Membranes have also been

Table 4: Overview of selected catalysts used for direct synthesis of DEC in literature

Catalyst	T_r [°C]	P_F [bara]	yield	dehydrating agent	Ref
CeO_2	150	40	45 %	butylene oxide	[118–121]
Cu–Ni/Activated carbon	90	13	<2.7 %	n.a.	[117]
Cu–Ni/ZrO_2	90	13	2.7 %	none	[122]
Fe_2O_3	160	30	0.43 %	none	[123]
ZrO_2	160	30	0.89 %	none	[123]
$(ZrO_2)_1$–$(Fe_2O_3)_1$	160	30	1.95 %	none	[123]
$(ZrO_2)_1$–$(Fe_2O_3)_1$/3Å	160	30	7.55 %	none	[123]
$(ZrO_2)_1$–$(Fe_2O_3)_1$/CaO	160	30	12.3 %	none	[123]
$(ZrO_2)_1$–$(Fe_2O_3)_1$/CaO–CaC_2	160	30	31.2 %	none	[123]
$(ZrO_2)_1$–$(Fe_2O_3)_1$/3Å–CaO–CaC_2	160	30	46.1 %	none	[123]
$Ce_{0.8}Zr_{0.2}O_2$	140	140	0.7 %	none	[124]
$Ce_{0.9}Al_{0.1}O_{2-\delta}$	150	50	8.3 %	2CP	[121]
$Ce_{0.9}Cu_{0.1}O_{2-\delta}$	150	50	15 %	2CP	[121]
$Ce_{0.9}Ni_{0.1}O_{2-\delta}$	150	50	23.7 %	2CP	[121]
$Ce_{0.9}Zr_{0.1}O_{2-\delta}$	150	50	9.3 %	2CP	[121]
$Ce_{0.9}Zn_{0.1}O_{2-\delta}$	150	50	23.8 %	2CP	[121]
CeO_2–SiO_2	180	45	0.0009 %	1,2–epoxybutane	[126]
CeO_2–Al_2O_3	180	45	0.0006 %	1,2–epoxybutane	[125]
CeO_2–TiO_2	180	45	0.0003 %	1,2–epoxybutane	[125]
$Ce_{0.07}Zr_{0.93}O_2$	140	80	0.002 %	none	[126]
EtI/K_2CO_3	110	80	46 %	Yes	[127]

applied to dehydrate the mixture. However, the high pressure and CO_2 content resulted in comparably poor dehydration performance [119].

Alongside using a water trap, the reactor configuration also appears to have a significant influence. In particular, continuously operated reactors appear to have a decisive impact on the conversions of the experiments carried out, as the kinetic rate still appear to be comparatively high when the reactants initially come into contact [123]. O'Neill et al. reported very high productivities of 644 mmol/g_{cat}h for DEC synthesis at 200 bar and a temperature of 140 °C using a continuous flow reactor. A batch setup without using a dehydrating agent reached the equilibrium conversion of 0.29 % after 3 hours with a measured initial reaction rate of 21.7 mmol/h that rapidly slowed down subsequently [132].

This work will compare the catalytic performance of modified carriers (see 3.1.4) for direct synthesis of DEC to the work of Décultôt et al. [128] and Honda et al. [129] since the experimental configurations match these works the most closely.

2.4 Modeling and Simulations

Modeling and simulations have taken an essential position in the design and optimization of processes. They rely on mathematical equations involving linear, non–linear, and differential equations of heat and mass balances to imitate and predict a real–world process's behavior, which commonly demands a high amount of effort and is costly to operate. Their contribution to cost–effectiveness and yield maximization is achieved by the assessment of simulating diverse operating conditions (feed composition, pressure, temperature, flow rate, etc.) of processes. [133] As of today, modeling and simulations are regarded as irreplaceable in efforts to analyze, scale up, and optimize processes for commercialization. [134]

A fair number of process simulators are available today. Although, in some cases, they have been developed for specific purposes, many are used today for the development of CCU processes.

Chuquin-Vasco et al. have proposed a MeOH production process based on CO_2 hydrogenation using DWSIM. The initial objective of designing a neural network capable of predicting the MeOH output was achieved. [135] Another study relying on DWSIM was carried out by Varandas et al., in which the influence of pressure and temperature on the thermodynamic equilibrium was investigated. The CAPE–OPEN to CAPE–OPEN simulator (COCO simulator) was used as a supportive instance. [136]

Otto and Kempka used Cantera and the GRI-Mech 3.0 mechanism to predict the behavior of the Boudouard equilibrium, water-gas reaction, and the methanation reaction, with results that were reasonably close to those of experimental trials. [137]

Vorrias et al. have simulated the absorption of CO_2 in the Calcium looping in order to propose an optimized coal–fired power plant. ASPEN Plus was used in addition to IPSE Pro and concluded that the loss in net electric efficiency was significantly high. [138]

Tan et al. have applied process simulation to identify the most significant thermo-physical properties in each intermediate step of CCS technologies (capture, conditioning, transport, and storage) [139].

A DMC/MeOH azeotropic mixture separation was simulated using an Aspen Plus simulation by Wei et al. [140], optimizing the heat integration of a triple-column process.

A solid oxide fuel cell (SOFC) was simulated to obtain more information on the mass/heat transfer and electrochemical reactions based on the finite volume method in a computational fluid dynamics model (CFD). Specific information on a temperature range to avoid a successful methanation reaction, CO consumption, and influence of process parameters (operating potential, inlet gas composition) has been obtained [141].

Zachopoulos and Heracleous used AspenPlus for thermodynamic analysis of methanol synthesis based on the Gibbs minimization varying zeolite volume as a water trap, feed composition, temperature, and pressure. The simulation results revealed extensive poten-

tial improvement opportunities, ultimately almost tripling the yield for methanol [142]. Further application–oriented utilization of process simulation tools like the modeling of dry reforming [143], algae growth in photoautotrophic and photo–mixotrophic environments [144], the direct synthesis of DMC from CO_2 [145] and many more [146] are available in the literature.

This work will incorporate methods for creating new models for process simulation and methods that utilize existing and newly developed models to simulate real applications.

CHAPTER 3

Methodology

In this work, experimental and simulative methods were applied to optimize CO_2 conversion and product purification. The descriptions presented in this chapter shall extend the already presented elaborations in the publications and give a better understanding of the research presented in Chapter 4.

3.1 Experimental Methods

The most crucial reaction parameters of the direct synthesis of DEC from CO_2 and EtOH were investigated using an undisclosed catalyst.

3.1.1 Stability

Significant parts of the methods mentioned in this subsection have been described in more detail in **[Journal Publication I]**. The effect of a selection of acids (HCl, H_2SO_4, H_3PO_4, formic acid, acetic acid) and bases (NaOH, KOH, Na_2CO_3) on the chemical stability of diethyl carbonate (DEC) was investigated in experiments conducted in round–bottom flasks. Cerium oxide (CeO_2) was chosen as a possible catalyst for DEC degradation. Each test was carried out with 3 ml of DEC mixed with 1:1 volume ratio solutions of using 0.5 moles the previously mentioned compounds solved in water. The duration of the experiments was mainly 24 hours and was exceptionally extended to 72 hours. Eventually occurring two–phase systems were separated and subsequently analyzed. DEC and EtOH concentrations were measured with a FID–equipped gas chromatograph (GC–FID), as outlined in Section 3.1.6. Evaporation losses of DEC were considered negligible due to DEC's high boiling point. The experimental plan is illustrated as a tree structure in Figure 9.

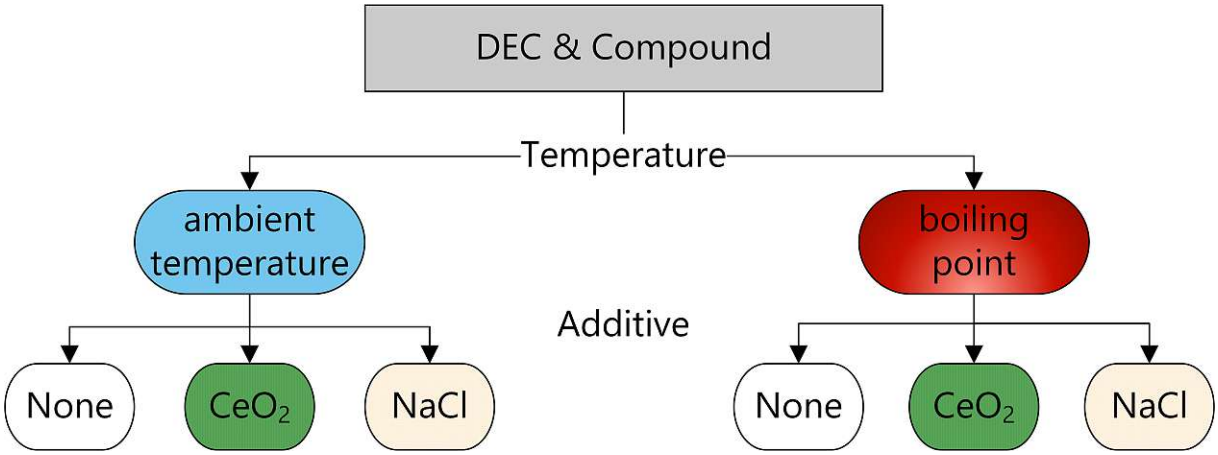

Figure 9: Tree structure diagram for the illustration of the experimental plan of DEC decomposition

For each substance, a set of experiments were carried out at ambient pressure, varying in temperature, the usage of 0.125 g CeO_2, and the usage of sodium chloride (NaCl). NaCl was dissolved in the aqueous phase, reaching a concentration of 250 g/L. The insoluble catalyst was separated from the mixture with a filter prior to analysis. Three samples were taken after experiments as a consequence of the formation of a two–phase product. The samples were taken one each from the organic, the aqueous, and one sample of the mixture of the phases.

DEC degradation has been calculated according to Eq. 18.

$$Degradation\ [\%] = \frac{m_{DEC,0} - m_{DEC}}{m_{DEC,0}} \times 100 \tag{18}$$

The theoretical EtOH formation was calculated according to Eq. 19.

$$m_{EtOH_{theoretical}} = 2 \times \frac{m_{DEC,0} - m_{DEC}}{M_{DEC}} \times M_{EtOH} \tag{19}$$

The results of these experiments have been published in **[Journal Publication I]**.

3.1.2 Miscibility

The miscibility of the ternary system of DEC (99.9 %, Carl Roth), EtOH (99.9 % Chem Lab), and water was investigated using clear point and cloud point determination. The experiments were carried out at ambient pressure and a temperature of 23 °C. Two experiments were performed to gain data for the miscibility gap. Either 41 ml water or 26 ml DEC was used as the starting substance for the experiments. The first set of experiments started with water as the first compound within the beaker. DEC was added utilizing a burette until the cloud point was reached, which marked a specific composition on the binodal/spinodal miscibility gap of the binary water/DEC system. The data for

the ternary system was obtained by increasing the excess of DEC to the initial water sample exceeding the cloud point and subsequently adding ethanol until the clear point was reached. The procedure was repeated with DEC as the starting compound, adding water to reach the cloud point. A magnetic stirrer has homogenized all solutions throughout all experiments. The development of full equilibrium was assumed to take no longer than 10 minutes. Parafilm was used to cover the beaker to avoid vaporization. The phases were assessed independently by GC–FID detecting DEC and EtOH. The water content was calculated from DEC and EtOH content. The tie–lines were determined from the detected mass of the two phases.

3.1.3 Diethyl carbonate synthesis experiments

The experiments were conducted in a pressurized 1 L stirred reactor system from Parr instruments equipped with a 4848 controller and a heating mantle. The system was extended with a 1/8–inch Swagelok pipe and a low–flow metering valve as a sampling unit. A scheme of the experimental setup is portrayed in Figure 10.

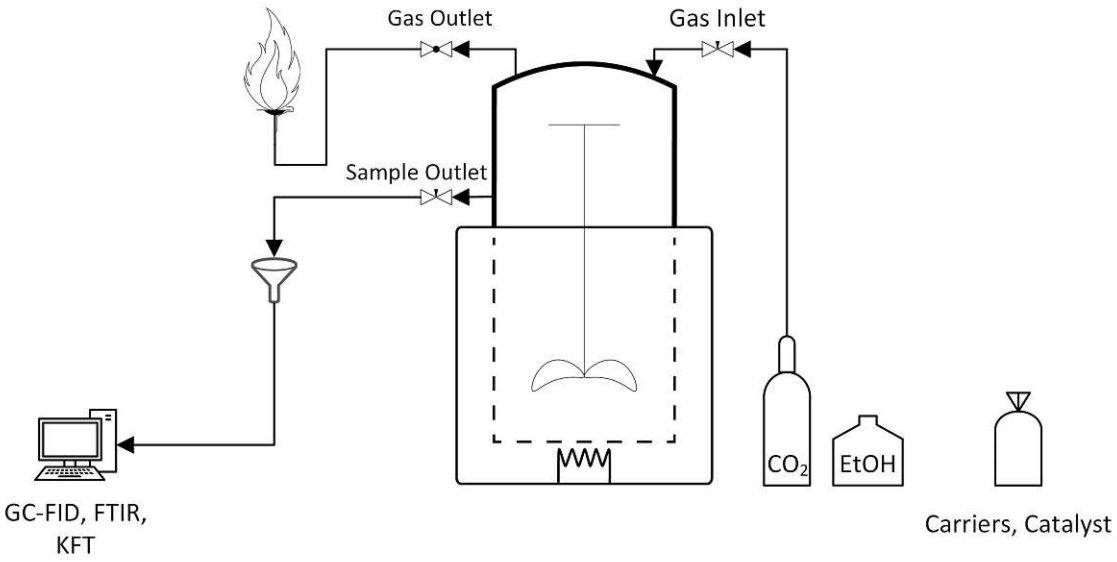

Figure 10: Scheme of the 1 L pressurized Parr Instruments reactor system

EtOH (99.9 %, denatured with toluene, Australco), 2CP (99 %, Sigma Aldrich), modified catalytic active carriers, and other catalysts are submitted comparably simply by opening and removing the bottom part of the steel vessel of which the reactor mainly consists. The modified carriers have been supplied by TU Wien and kleinkraft OG whereas the production process is non–disclosed. The catalytic active component is CeO_2 based. The single input connector in use was connected to a pressurized CO_2 bottle.

The feedstock, excluding CO_2, was submitted to the reactor. Since 2CP is delivered in a solid state, it was either briefly stored in a water bath of 50 °C or lightly poked into little fragments and subsequently added to the reactor. The reactor is sealed in the following and checked for leakages by filling in CO_2 up to 10 bar and releasing the gas phase three

times. This test also serves as an additional step to remove traces of air in the reactor before reaching higher temperatures. Following this, the reactor was heated up to 120 °C. Subsequently, CO_2 was submitted to the reactor, increasing the pressure until the target pressure of the experiment (see Chapter 4). The experiments were carried out with various durations. Samples were taken during and after the experiment, cooling down to 35 °C and depressurizing the equipment.

The experimental plan has been set up in four groups. Commercial CeO_2 ($<$ 25 nm, Sigma Aldrich) varying the presence of the dehydrating agent 2CP and the EtOH feed mass has been used initially to verify the equipment's suitability in reproducing the direct synthesis described in subsection 2.3.2. The second series of tests involved modified carriers deployed in the reactor as catalysts to assess their productivity using 2CP. The variation of feed ethanol content, temperature, and pressure shall give insight into the influence of these parameters on the catalyst's productivity in the reaction carried out. The data obtained shall enable a comparison of the customized carriers' catalytic activity and general eligibility to commercial CeO_2. The third series of experiments was carried out with chosen modified carriers, waiving the use of a dehydrating agent. The last part of the experimental trial was carried out by reusing already deployed carried to observe their decline in activity depending on their usage. The experiments were generally carried out at 120 °C and on an absolute pressure of 40 bar. The feed mass of EtOH, 2CP, and the mass of the carriers/catalyst were parameters that have been varied. More information on the substance quantities used are available in the Tables close to the results (Tables 6 - 9) in section 4.1.

The yield of the reactions was calculated according to Eq. 20. The obtained sample mass of DEC was referenced to the feed mass of EtOH.

$$Y_{DEC} = \frac{n_{DEC}}{0.5 \times n_{EtOH}} \tag{20}$$

The carrier's catalytic productivity related to the carrier mass $P_{carrier}$ and the catalyst's mass P_{cat} on the carriers were calculated according to Eq. 21.

$$P_{carrier} = \frac{m_{total} \times c_{DEC}}{m_{carrier} \times \Delta t}, \qquad P_{cat} = \frac{m_{total} \times c_{DEC}}{m_{cat} \times \Delta t} \tag{21}$$

3.1.4 Pervaporation setup

Mixtures of various concentrations consisting of deionized EtOH, DEC, and water were prepared for experiments. Approximately 1 L of the prepared mixtures were introduced into the feed tank and pumped through a hot water bath to reach the aimed operating temperature. The water bath heated another tube enclosing the membrane module. More details on the methods for the experiments (e.g., applied membranes, parameters of experiments) have been published in **[Journal Publication II]**.

The system was pressurized by introducing CO_2 on the feed side. The permeate side of the system was operated with a continuous sweep gas flow of nitrogen (N_2) at ambient

pressure. The permeate was collected in two steps by condensation using a Liebig cooler with a collection flask and, subsequently, a salted ice–water mixture reaching temperatures between −15 °C and −20 °C. In cases of low permeate flow, the Liebig condenser was bypassed. The volumetric flow of the circulating mixture was operated between 1.5 –1.7 L/min. The feed side of the equipment was operated in a closed circle. Thus, the retentate of a cycle is the feed of the subsequent cycle. An illustration of the pervaporation equipment is portrayed in Figure 11.

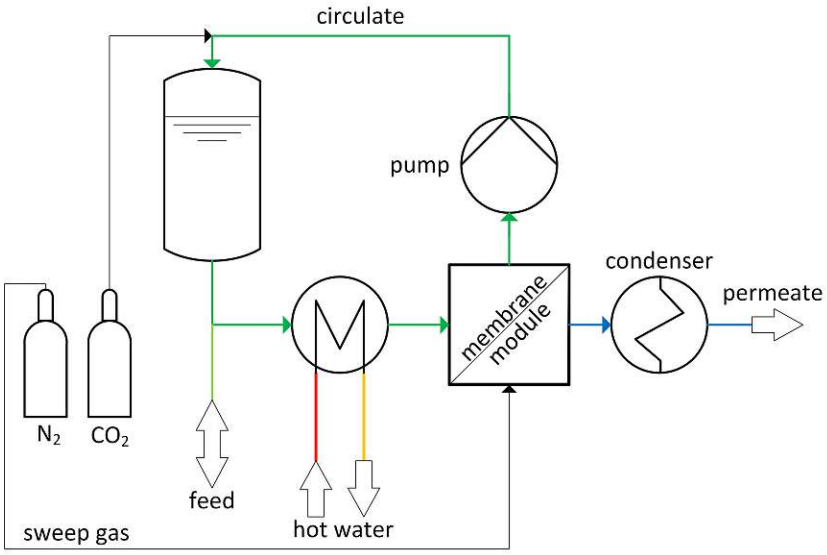

Figure 11: Schematic illustration of the pervaporation setup

The system was flushed with EtOH to remove contaminants prior to each test. Each experiment's feed was running through the system for > 30 min to establish homogenization, including the remaining dead volumes, stable temperatures, and pressure. The ideal selectivity α for water over EtOH was calculated according to Eq. 22.

$$\alpha_{H_2O/EtOH} = \frac{w_{H_2O_{perm}}/w_{EtOH_{perm}}}{w_{H_2O_{feed}}/w_{EtOH_{feed}}} \tag{22}$$

The flow passing through the membrane can be either calculated by using the solution–diffusion–model **[Journal Publication II, Journal Publication III]** or calculated from the mass m_{total} yielded per time Δt and membrane surface area $A = 0.00565\ m^2$. The flux $\dot{J}$ was calculated according to Eq. 23.

$$\dot{J}_{total} = \frac{m_{total}}{A \times \Delta t}, \qquad \dot{J}_i = \frac{m_{total} \times w_i}{A \times \Delta t} \tag{23}$$

As the relation of the mass flow of the permeating compound depending on the partial pressure difference Δp_i the permeance Q_i for each compound is calculated as in Eq. 24.

Table 5: GC–FID method parameters

Parameters	Value	Unit
Carrier gas	Helium	–
Pressure carrier gas	64.6	kPa
Total flow carrier gas	405.9	mL/min
Column flow carrier gas	7.9	mL/min
Linear velocity carrier gas	45.8	cm/s
Purge flow	3.0	mL/min
Injection volume	1.0	μL
Temperature Injector	180.0	$°C$
Split ratio	50.0	–
Temperature detector	280.0	$°C$
Helium flow	30.0	mL/min
Hydrogen flow	40.0	mL/min
Air flow	400.0	mL
column start temp	30	$°C$

$$Q_i = \frac{\dot{J}_i}{\Delta p_i} = \frac{m_{total} \times w_i}{A \times \Delta t \times \Delta p_i} \tag{24}$$

The membranes have been operated with a sweep gas to keep the permeating compounds' partial pressure very low. Thus, It was assumed that the partial pressure on the permeate side was negligible and therefore $\Delta p_i \approx p_{i,F}$.

3.1.5 Analytics

GC–FID

The feed, retentate, and permeate samples acquired in the experiments of **[Journal Publication II]**, the products of decomposing DEC in the experiments of **[Journal Publication I]** and the products from the DEC synthesis experiments in subsection 4.1.1 and in **[Patent]** have been analyzed using a gas chromatograph (Shimadzu GC-2010, Kyōto, Japan) with a flame ionization detector (GC–FID) equipped with a Shimadzu AOC–5000 autosampler and a Restek RTX volatiles capillary column (60 m length, 0.53 mm inner diameter, film thickness 2 µm, Bad Homburg v. d. Höhe, Germany). The compositions of the samples were assessed using standards mainly consisting of EtOH, DEC, and water in differing concentrations. Further standards also included 2CP. The general settings and method of measurement are provided in Table 5 and Figure 12.

The sample measured in Figure 12 was obtained from the experiment V_{R12} (see 4.1.1). The peaks occurring on the chromatogram are clearly separated, making the retention times of all compounds recognizable. Toluene, dioxane, and picolinamide/2CP were observed alongside the predominant EtOH peak. EtOH was obtained denatured with toluene, resulting in its presence in the chromatogram. Dioxane was used to rinse the syringe

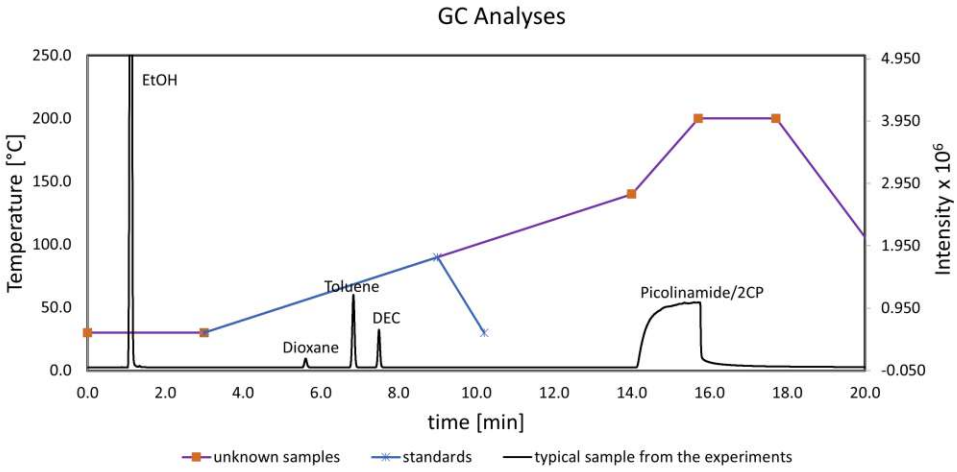

Figure 12: Temperature ramps and peak identification for a GC–FID measurement for an exemplary sample (source-file read with OpenChrom)

between the measurements, causing traces to be detected in the results.

Fourier–transform infrared spectroscopy – Attenuated total reflectance

A Vertex 70 (Bruker) was used to obtain Infrared spectra (FTIR–ATR) which were assessed with partial least squares (PLS) modeling to obtain qualitative and quantitative results. FTIR–ATR was used to characterize samples from the membrane experiments **[Journal Publication II]** and the synthesis of DEC **[Patent]**.

Karl–Fischer Titration

The quantitative analyses of water were carried out using an Eco KF Titrator (Metrohm) for Karl Fischer titration (KFT). The samples analyzed were taken from the experiments for **[Journal Publication II, Patent]**. The injection volume of the sample varied between 25 – 1000 µL.

3.2 Process simulation

Mass and energy balances are inevitable in obtaining expressive information about the whole process. Therefore, plant designs were mainly modeled using DWSIM (V6.0.0 – V8.8.1) as a process simulator **[Journal Publication III, Patent]**. Aspen Plus was sporadically used for comparisons and for the remaining simulations. Both DWSIM and Aspen Plus are sequential simulators solving steady–state calculation. Aspen Plus is an established, widely used software with a known scope of performance. DWSIM is commonly described as software with similar functionality as an open–source alternative. It provides a toolset to create models and calculations and to increase the flexibility of already available models. [147] The model library was extended by a custom membrane

model **[Journal Publication III]**, of which the development is elaborated in more detail in section 3.3.

3.2.1 Direct DEC synthesis

Substance–specific values have been included from ChemSep by DWSIM. The direct synthesis reaction (Eq. 8) was modeled at 120 °C and 40 bar with an equilibrium reactor using $K_{eq} = 2.698 \times 10^{-5}$ (calculated from the thermodynamic data in Table 3) as the equilibrium constant and a Gibbs reactor. The separation of the product was based on a custom membrane model in DWSIM **[Journal Publication II, Journal Publication III]**. The flowsheet of the DEC synthesis process is portrayed in Figure 13.

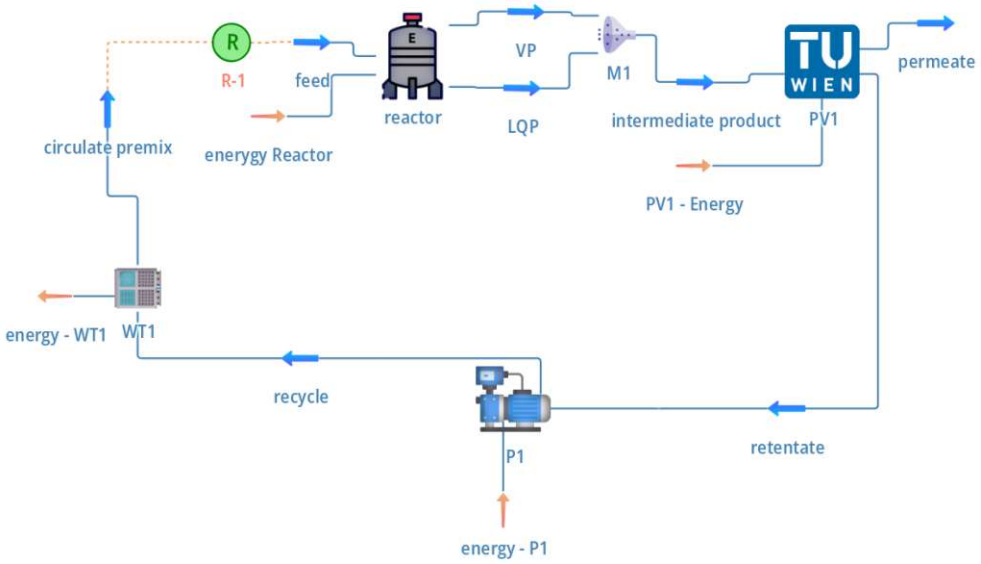

Figure 13: Flowsheet of DWSIM simulation for DEC synthesis

1 mol of CO_2 and 2 mol EtOH are each introduced to the flowsheet on the feed stream at 120 °C and 40 bar and lead into the reactor. After the reaction, the initial separated gaseous and liquid product streams are accumulated by the mixer M1 and fed into the pervaporation membrane model PV1. The membrane is simulated in co–current flow mode and operated using a permeate pressure of $p_p = 2000\ Pa$ on the permeate side. The permeance of water $Q_{H_2O} = 1.675 \times 10^{-9}\ \frac{mol}{Pa \times m^2 \times s}$ and the ideal selectivity of water over EtOH have $\alpha_{H_2O/EtOH} = 3800$ have been taken from experimentally assessed results for the ZEBREX ZX0 membrane **[Journal Publication II]**. The permeance of EtOH $Q_{EtOH} = 4.408 \times 10^{-13}\ \frac{mol}{Pa \times m^2 \times s}$ has been calculated according to Eq. 25.

$$\frac{Q_i}{Q_j} = \alpha_{i/j} \tag{25}$$

Since neither CO_2 nor DEC have been detected in the permeate stream in the ZEBREX ZX0 membrane experiments **[Journal Publication II]**, the permeances of both compounds

have been set to $Q_{CO_2} = Q_{DEC} = 4.4 \times 10^{-20} \frac{mol}{Pa \times m^2 \times s}$ to model a flux which is practically zero. The permeate leaves the flowsheet in the following.

The retentate stream of the membrane runs through a Pump P1 and subsequently a heat exchanger WT1 in which the pressure and temperature are adjusted back to 120 °C and 40 bar. The recycled stream ("circulate premix") is reintroduced as the feed stream for the reactor by running through a recycle block.

3.2.2 Ammonia decomposition

The simulation of ammonia decomposition was carried out as a case study to increase insight into the potential of ammonia used as an energy storage material. The products of a complete ammonia decomposition consist of H_2 and N_2. Membrane technology could be a highly efficient method to purify H_2 to elevated purities, thus providing opportunities for subsequent processes. The membrane model, which was developed in **[Journal Publication III]**, has been used to predict the flow and quality of the output that could be achieved. This study thus represents a further application of the algorithm. The flowsheet of the membrane separation in DWSIM is portrayed in Figure 14.

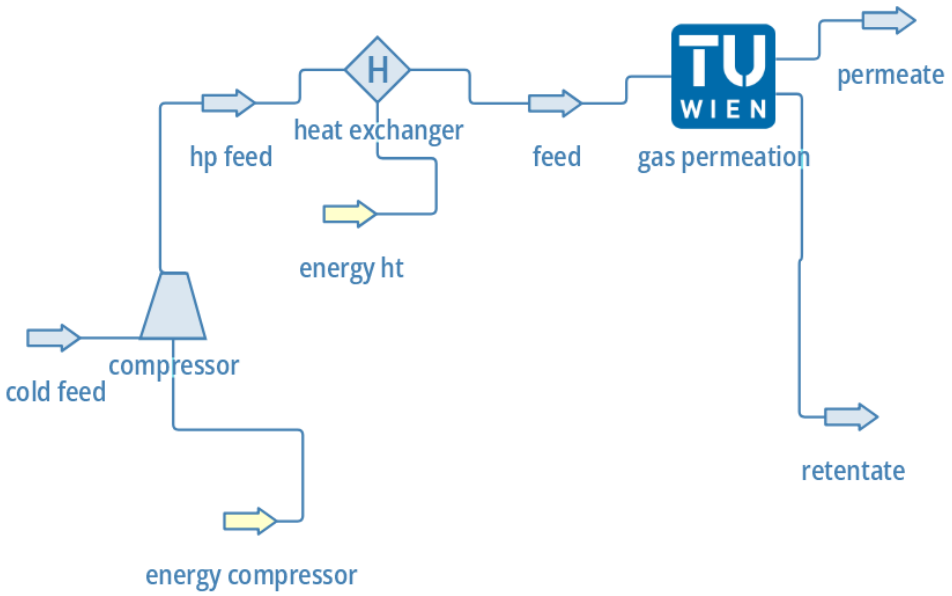

Figure 14: DWSIM flowsheet of Membrane separation for NH_3 decomposition downstream processing **[Journal Publication IV]**

The downstream processing of the NH_3 decomposition was simulated in DWSIM with the Matrimid 5218 membrane data ($Q_{H_2} = 2.618 \times 10^{-8}; Q_{N_2} = 3.156 \times 10^{-11}$; $[Q] = \frac{mol}{Pa \times m^2 \times s}$) [148]. After an initial compression step, the feed gaseous mixture is cooled down to the operation conditions of 23 °C and 11 bar. The permeate pressure was set to 1.013 bar. This separation operation represents a dedicated case study for the use of the membrane model developed in **[Journal Publication II]** according to the published test cases.

3.3 Membrane Modeling

The custom DWSIM membrane model **[Journal Publication III]** was created using Visual Studio Enterprise 2022. The target framework used was ".NET Framework 4.6.2". The membrane model was designed based on the solution diffusion model based on Eq. 26.

$$\dot{J}_i = y_i n_p = AQ\left(x_r P_F - y_i p_p\right) \tag{26}$$

The model is capable of simulating gas permeation and pervaporation applications. Both can be calculated in either co–current (Eq. 27) or counter current (Eq. 28) flow configuration.

$$y_i = \frac{Q_i x_{F,i} \alpha_i \sum_{j\neq i}^{k} y_j}{\sum_{j\neq i}^{k} Q_j \left(x_{F,j}\alpha_j - y_j\right) + Q_i \sum_{j\neq i}^{k} y_j} \tag{27}$$

$$y_i = \frac{Q_i x_{r,i} \alpha_i \sum_{j\neq i}^{k} y_j}{\sum_{j\neq i}^{k} Q_j \left(x_{r,j}\alpha_j - y_j\right) + Q_i \sum_{j\neq i}^{k} y_j} \tag{28}$$

Both flow configurations of the membrane model are illustrated in Figure 15.

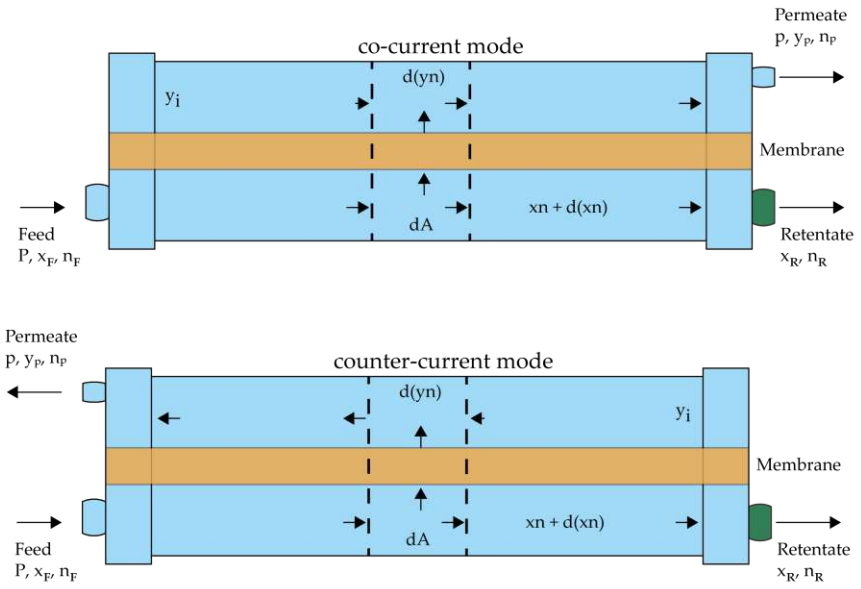

Figure 15: Schematic representation of co–current and counter–current cross–section **[Journal Publication III]**

In order to simplify the code fragments, each term (see Eq. 29 and Eq. 30) was substituted with in the variables $A\,[i]$,$B\,[i]$, and $C\,[i]$ using $x_{F,i}$ for co–current or $x_{r,i}$ counter–current flow mode.

$$A\left[i\right] = Q_i x_{F/r,i} \alpha_i \sum_{j=i}^{k} y_j, \qquad B\left[i\right] = \sum_{j=i}^{k} Q_j \left(x_{F/r,i} \alpha_i - y_j\right), \qquad C\left[i\right] = Q_i \sum_{j=i}^{k} y_j \tag{29}$$

$$y_i = \frac{A\left[i\right]}{B\left[i\right] + C\left[i\right]} \tag{30}$$

The model was designed to store values as properties within the model itself while DWSIM uses it. These properties represent values, e.g., p, l_f, d_{if}, n_{fib}, Q, Q_{all} and more. These properties can be called by each other and the solver in the following. A schematic network of the properties used is illustrated in Figure 16.

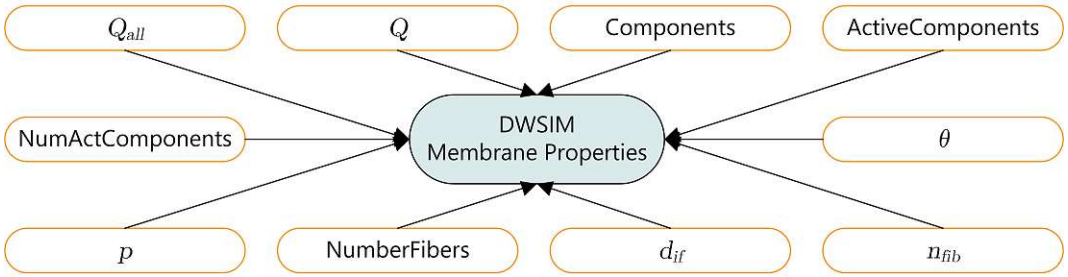

Figure 16: Selected parameters for the calculation of the membrane separation **[Journal Publication III]**

Object-oriented programming allows access to the implemented properties throughout the code, enabling a modular design. The iterative algorithm containing the calculation routine for each compartment has been described in Figure 17. The solving routine is initiated by calculating the stage cut θ_i from the inlet flow N_{eff_i}, permeances Q_i, and the mean logarithmic partial pressure difference (see Eq. 31) for each compound. The total area A is divided by the number of stages Comp to model each compartment individually. Eq. 32 refers to the calculation of the individual fluxes $q_{i,p}$ of each compound, which are summed up to obtain the total transmembrane flux $q_{t,p}$ using Eq. 33. The molar composition of the transmembrane flux y_p is obtained by dividing the flux of each single compound by the total flux (see Eq. 34). The remaining feed flow is calculated using Eq. 35 and leaves the compartment as the retentate $q_{i,r}$ and becomes the new inlet flow N_{eff_i} for the following compartment. The total retentate flow $q_{i,r}$ is calculated (see Eq. 36) and used to calculate the molar fraction of the retentate $x_{r,i}$ (see Eq. 37) in each iteration step. The partial pressures $p_{x_F,i}$ of the feed flow for the next compartment is calculated using the law of Dalton (Eq. 38). Eq. 39 is used to calculate the error from the currently calculated flux $q_{i,p}$ the calculated flux from the previous step $q_{i,0}$. The error must stay below 10^{-4} to break the while-loop. If this condition remains unmet, the same compartment will be recalculated with the new values until it converges.

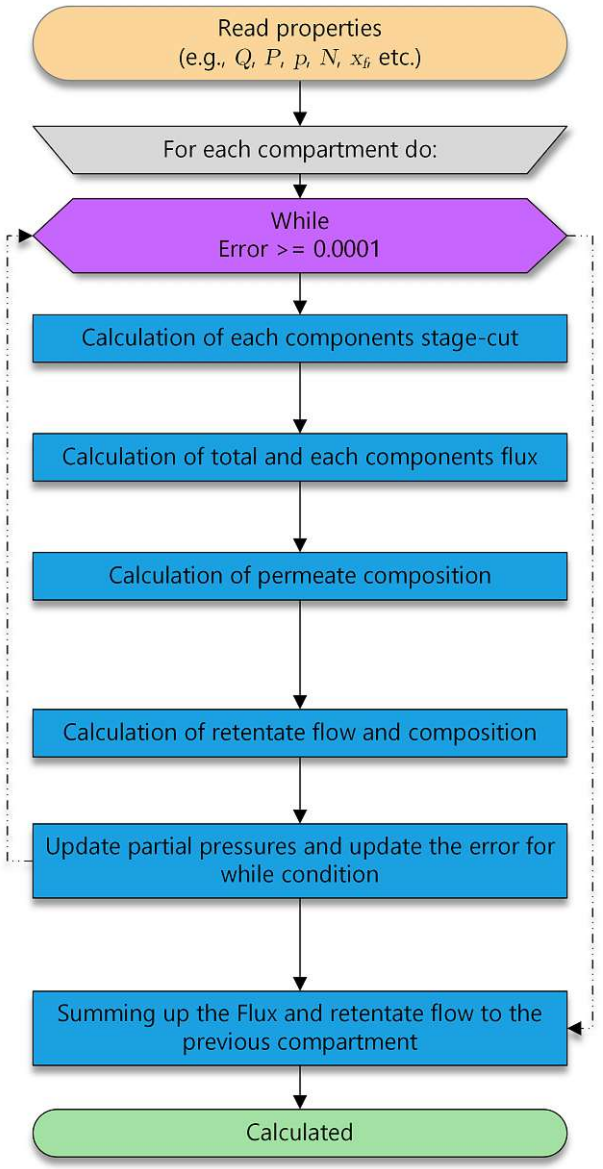

$$\theta_i = Q_i \times \frac{A}{Comp} \times \frac{\overline{(p_{x_F,i} - p_{y_i,i})}}{N_{eff_i}} \quad (31)$$

$$q_{i,p} = \theta_i \times N_{eff_i} \quad (32)$$

$$q_{t,p} = \sum_{i}^{n} q_{i,p} \quad (33)$$

$$y_p = \frac{q_{i,p}}{q_{t,p}} \quad (34)$$

$$q_{i,r} = N_{eff_i} - q_{i,p} \quad (35)$$

$$q_{t,r} = \sum_{i}^{n} q_{i,r} \quad (36)$$

$$x_{r,i} = \frac{q_{i,r}}{q_{t,r}} \quad (37)$$

$$p_{x_F,i} = P_F \times x_{r,i} \quad (38)$$

$$error = |q_{i,p} - q_{i,0}| \quad (39)$$

Figure 17: Sequence of calculation routine for the membrane model **[Journal Publication III]**

CHAPTER 4

Results

4.1 Miscibility of DEC

The thermodynamic equilibrium at atmospheric pressure and ambient temperature was assessed by the cloud–point method. The tie–lines and binodal curve are presented in Figure 18.

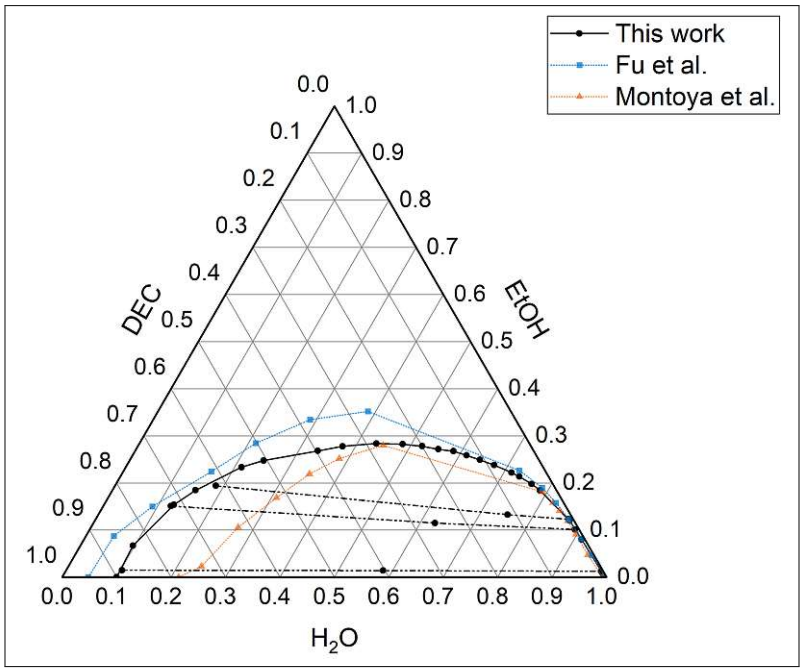

Figure 18: Experimental binodal curves and tie–lines of ternary liquid–liquid equilibria of DEC, water, and EtOH mixtures at 23 °C (Montoya et al. [149] and this work) and 25 °C Fu et al. [150] (Experiments partially carried out by Florian Možina)

The most apparent development observed is the miscibility gap between DEC and H_2O. Following this, DEC/H_2O mixtures are two–phase systems for most mixing ratios. Adding EtOH leads to the formation of a homogeneous phase. In direct synthesis starting from EtOH and CO_2, the system is single–phase and far from a two–phase mixture. Therefore, it cannot be relied on for product separation. Selective removal of water or DEC is inevitable to boost the reaction speed. These findings were essential for the design of the studies of section 4.2 and **[Journal Publication I, Journal Publication II]**

4.2 Synthesis of DEC

Reaction conditions and productivity of the catalysts for direct DEC synthesis reported in the literature vary. Therefore, a side–by–side comparison of experiments using chosen mixing ratios of EtOH/CO_2/CeO_2 shall give insight into the behavior of the reaction. The parameters for the reactions V_{R1} – V_{R8} are covered in Table 6. The experiments applied with commercial CeO_2 have used the stirrer within the reactor to homogenize the reactive mixture. V_{R2} is the only exception that did not apply the stirrer to obtain some information on the significance of the stirrer.

Table 6: CeO_2 as catalyst on 120 °C temperature and a total pressure of 40 bar

Experiment	EtOH Feed [g]	2CP Feed [g]	CeO_2 mass [g]	Stirring speed [rpm]
V_{R1}	45.39	50.02	3.35	780
V_{R2}	200.73	52.61	3.37	0
V_{R3}	400.76	47.51	3.35	700
V_{R4}[a]	408.71	44.81	3.56	700
V_{R5}	392.38	47.86	1.73	700
V_{R6}[b]	200.00	0.00	3.21	440
V_{R7}	50.00	0.00	3.31	400
V_{R8}[c]	196.00	0.00	3.14	400

[a] carried out with 10 bar
[b] carried out with 80 °C
[c] carried out with 150 °C

Figure 19 portrays the levels of DEC yield achieved for the reactions V_{R1} – V_{R5}, which have been carried out using 2CP as a dehydrating agent. A clearly rising trend in the DEC yield of all experiments is displayed. V_{R1}, V_{R2}, and V_{R3} give the impression of an advantage in lower ethanol feeds in comparison for the reaction. More than 10 mol% of DEC was yielded by feeding 46 g of EtOH on 40 bar at 120 °C while increasing the EtOH feed by over 400 % to 200 g yielded just above 4 mol% within the same time. Another increase of the EtOH feed up to 400 g still reached a yield of 2 mol%. A reduction of the pressure down to 10 bar (V_{R4}) significantly decreased the yield from the synthesis to just above 1 mol% within the same timeframe of 140 minutes. Interestingly, the yield of using just half of the catalysts amount V_{R5} closely matched the trend of the reaction carried

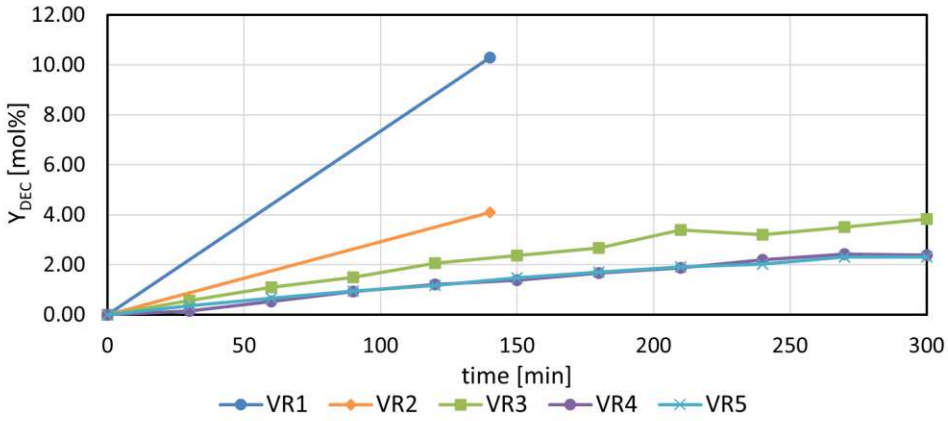

Figure 19: Comparison of direct synthesis experiments of V_{R1} – V_{R5} with 2CP as dehydrating agent

out at low pressure.

However, the productivity of the catalyst used is highly decisive for the assessment of the experiments. The comparably better performance using disproportionally high feed EtOH contents suggests a lower local concentration of the product molecules in a close neighborhood to the catalyst, resulting in a slower decay of the catalytic performance.

A major factor is the catalytic performance of the modified carriers. Depending on the carrier type and preparation, the yield of DEC shall be assessed in the following way by determining the hourly formation rate of DEC within the reactor experiment. Figure 20 portrays a comparison of the productivity of CeO_2 in the reactor experiments V_{R1} – V_{R8}.

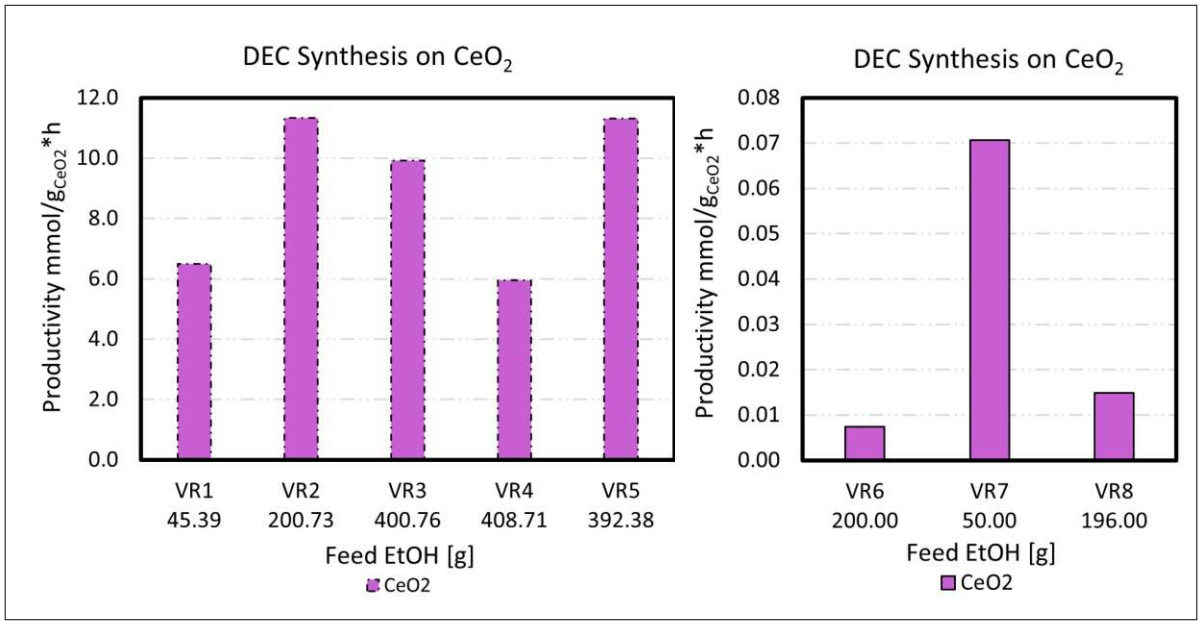

Figure 20: Comparison of different direct synthesis experiments over CeO_2 using different EtOH feed volumes with 2CP (left) and without 2CP (right)

Table 7: Experiments with modified carriers as catalysts on 120 °C and 40 bar using 2CP

Experiment	Carrier	EtOH Feed [g]	2CP Feed [g]	catalyst mass [g]	carrier mass [g]
V_{R9}	Clay	82.50	45.00	2.42	50.00
V_{R10}	Raschig Rings	51.00	50.00	0.07	50.00
V_{R11}	MS 3 Å	60.41	44.05	0.84	52.31
V_{R12}	MS 4 Å	65.00	45.95	2.96	52.55
V_{R13}	MS 5 Å	50.08	44.63	1.71	53.30
V_{R14}	MS 10 Å	50.00	50.00	3.68	43.60

Adding the catalyst's productivity to the assessment of the reaction slightly alters the observations made. The productivity of CeO_2 with 2CP was moderate with > 6 mmol/g_{cat}h. Increasing the dilution ratio to reach a feed EtOH mass of 200 g drives the catalyst's productivity high and delivers the strongest productivity observed (11.33 mmol/g_{cat}h). Another increase of the EtOH in the feed seemingly cannot compete with V_{R2}'s catalyst's performance. However, V_{R5} shows a productivity that is considerably comparable to V_{R2}. The seemingly equivalent performance of the low pressure experiment (V_{R4}) and V_{R5} seems to rely on the strong productivity of the catalyst which is almost twice as strong in V_{R5}. Removing the water trap 2CP from the system caused a dramatic drop even below 1 % of the catalyst's productivity, while a reaction temperature of 120 °C delivered the best performance (0.07 mmol/g_{cat}h).

The catalytic performances of the experiments were observed to be considerably competitive in comparison to the values reported in the literature while using 2CP. Despite the drop in catalytic performance on renouncement of 2CP usage, the productivity of CeO_2 is still within the range of reported results (0.01458 - 4.5 mmol/g_{cat}h, [118, 126, 128]) in the literature. Still, it surpasses the closest referenced case in subsection 2.3.2.

The performance of commercial CeO_2 has been compared to catalyst-bearing modified carriers. Table 7 gives an overview of the experiments and the quantities of substances used as feed carried out with modified carriers. None of the experiments carried out using the alternative carriers have applied the stirrer within the reactor. Preliminary results have shown that the mechanical stability of the carriers was occasionally insufficient.

The comparison of commercial CeO_2, clay, Raschig Rings, and molecular sieves of various pore sizes (3 Å, 4 Å, 5 Å, and 10 Å) is portrayed (V_{R1} and V_{R9} – V_{R14}) in Figure 21 and Figure 22.

The 5 Å molecular sieve is the only carrier able to surpass the DEC yield achieved using commercial CeO_2. The reaction's yield rises with the surface area of the molecular sieve as the 3 Å MS starts with a yield of 1.5 mol%, proceeding over the 4 Å MS with a yield of 2.3 mol% and reaching the maximum with the 5 Å MS at 6.1 mol%. In contrast to the just described rise according to the inner pore size, the yield using modified 10 Å MS drops to 0.2 mol%. The yields using clay or Raschig rings do not surpass 1 mol%.

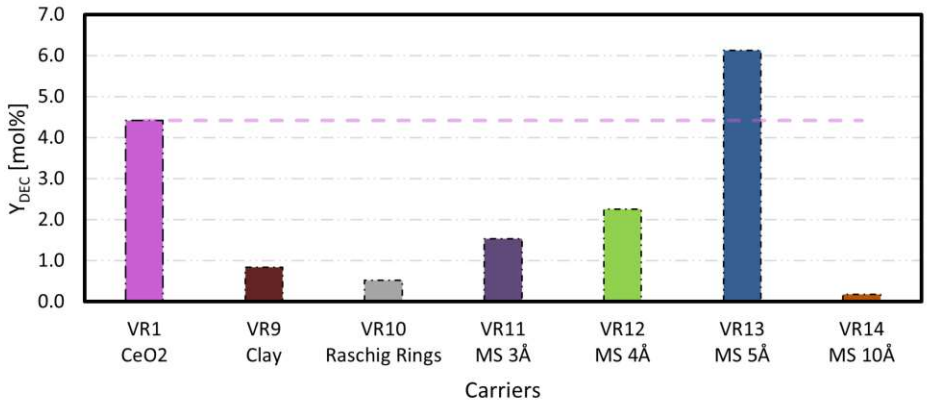

Figure 21: Comparison of experiments using modified carriers bearing a catalyst on DEC yield per hour with 2CP usage as a water trap (yield of V_{R1} as dashed purple line)

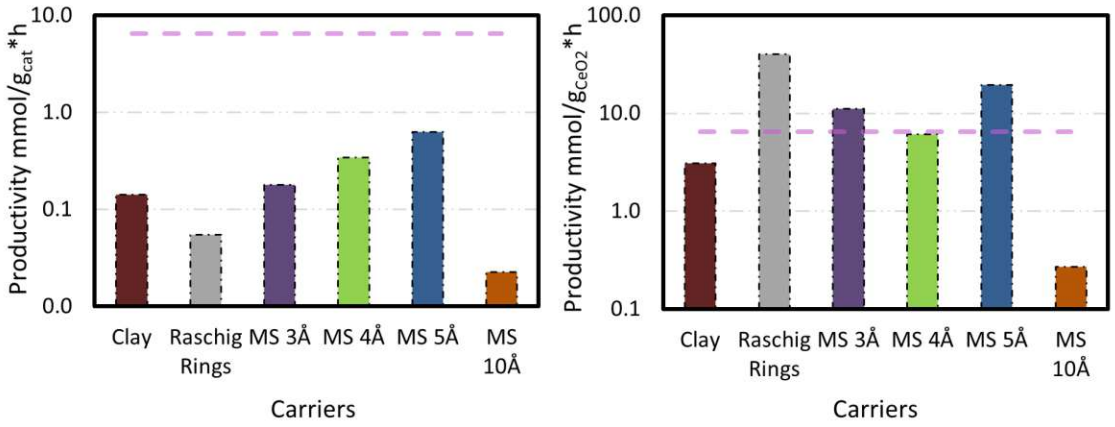

Figure 22: Comparison of productivity (mmol/gcarrier left; mmol/gcat right) of modified carriers bearing a catalyst with 2CP usage as a water trap (productivity of V_{R1} as dashed purple line)

As for the experiments using commercial CeO_2, the catalyst's productivity gives (see Figure 20) more insight into the reaction system's performance. Referring to the hourly formation of DEC, the mass of the carrier used draws a seemingly distinct relation of commercial CeO_2 performing at least 10–times stronger than 5 Å and subsequently more than every other carrier tested. Considering the catalytic inactivity of the carriers themselves, the productivity could be practically referenced to the mass of catalytically active compound on the carrier. This (see Figure 22, right) shifts the productivities of all carriers, excluding the 10 Å MS significantly closer to each other. In contrast to the yield achieved in the experiments, the modified Raschig rings show the highest productivity, up to 40 mmol/g_{cat}h. This suggests that the actual performance of the reaction using this catalyst may be slowed down due to possibly insufficient catalyst loads on the surface. The exact reason for this behavior, however, remains unknown. The residual molecular sieves reach or surpass the productivity of commercial CeO_2. The order of the productivity of the MS seems quite deceitful since the productivity of the 3 Å (11.14 mmol/g_{cat}h) surpasses the 4 Å (6.08 mmol/g_{cat}h) with the 5 Å MS (19.48 mmol/g_{cat}h) forming the

Table 8: Experiments with modified carriers as catalysts at 120 °C without using a dehydrating agent

Experiment	Carrier	Pressure [bar]	EtOH Feed [g]	catalyst mass [g]	carrier mass [g]
V_{R15}	MS 4 Å	40	70.00	2.59	50.00
V_{R16}	MS 4 Å	40	70.15	1.55[a]	50.00
V_{R17}	MS 4 Å	40	100.00	0.13	50.00
V_{R18}	MS 4 Å	10	70.70	2.00	50.00
V_{R19}	MS 4 Å	10	70.15	1.55[a]	50.00
V_{R20}	MS 5 Å	40	70.29	2.52	50.00
V_{R21}	MS 5 Å	40	72.50	2.78	50.00
V_{R22}	MS 5 Å	40	70.82	2.78	50.00
V_{R23}	MS 5 Å	10	70.82	2.78	50.00

[a] mass of catalyst was taken from average catalyst mass for specific carrier

top. Alongside the yield, the productivity must also meet the minimal requirements of a potentially promising output. The comparatively good performance of the molecular sieves could be due to their hygroscopic nature. This would additionally remove water molecules from the bulk. Nevertheless, the catalyst supports the reacting compounds on its surface. However, the exact location and size of the catalyst's particles are unknown. The catalyst's particle may be large enough to be immobilized in the outer path to the pores while the water molecules incorporate the pore's cavities.

Despite the large productivity, Raschig rings have not shown the yield necessary. Clay and 10 Å MS performed comparably insufficiently on any perspective investigated, and 3 Å has proven to be a promising carrier. However, the focus of the reactor experiments (V_{R15} – V_{R27}) was set on the 4 Å and 5 Å MS.

The catalytic performance of the modified carriers has been further investigated with the experiments listed in Table 8 without the availability of a dehydrating agent to enhance the conversion.

A comparison of the results of the experiments V_{R15} – V_{R23} has been portrayed in Figure 23. Waiving the use of a dehydrating agent causes a drop in DEC formation for all carriers used similarly to commercial CeO_R. When comparing the yields and productivities, it was observed that the performance of the reactions reached (4 Å MS) or exceeded (5 Å MS) the reference performance of commercial CeO_2 (V_{R1}), particularly in the experiments at 40 bar. The average productivities were within the same range, but the 5 Å MS yielded up to about 0.44 % of DEC. As expected, the DEC yields achieved at 10 bar are lower than those at 40 bar. However, the higher yield using a 4 Å MS compared to a 5 Å MS is unanticipated. Thus, this series of experiments also indicates the adverse influence on the reactions' progress.

No satisfactory explanation in the literature proves that water, in particular, is slowing down the direct synthesis reaction. Nevertheless, this is regularly assumed since remov-

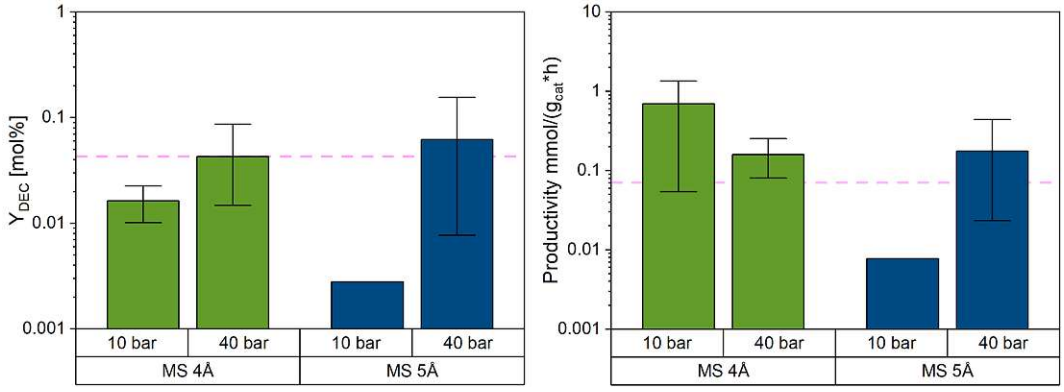

Figure 23: Comparison of yield per hour (left) and productivity (right) of modified carriers bearing a catalyst without water trap usage (Experiments V_{R15} – V_{R22}, data of V_{R1} as dashed purple line)

ing DEC from the reaction mixture was never reported to be an equivalently enhancing approach. Further, the observations in **[Journal Publication I]** regarding the reverse reaction using water and DEC to yield EtOH and CO_2 are noticeable as the composition of the mixture appears to be converging very slowly to the equilibrium. The decomposition of DEC was observed as a slow process (see **[Journal Publication I]**), seemingly demanding 24 hours for the decomposition of 13 wt% of DEC, even though an initial rapid decay would have to be expected. This could be related to the liquid-liquid equilibrium of DEC and water, which has a large miscibility gap resulting in limited availability of the reaction partners within each respective phase and the interface of the phases. This may cause a delayed acceleration of the reaction with increasing ethanol concentration since DEC and EtOH form a single phase if enough EtOH is available. The work of Raiguel et al. brought up another hypothesis that may explain the specific necessity of water removal, in which H_3O^+ is assumed to be the actual species to catalyze the decomposition of DEC [151] while being in contact with acids. With the presence of a sufficient number of water molecules, the hydration reaction of CO_2 may occur as well alongside the esterification reaction of EtOH and CO_2. The consequence would be a simultaneous formation of H_3O^+, which could offer a H^+ to each ethyl group, causing them to split off and form EtOH. This process could only be prevented if no available water molecules were present and would cause dehydration to have a more positive effect.

A single sample of 4 Å and 5 Å MS each have been recovered from the experiments and reused after drying at > 400 °C under atmospheric pressure. The reaction test data under which the modified carriers were reused are listed in Table 9, and the results are portrayed in Figure 24.

Both samples initially performed slightly under average. However, the 4 Å MS almost doubled its yield up to 0.04 % and productivity on its second use and maintained the performance on its third use. The share of catalyst on the carrier does not change from experimental iteration, but the regeneration of the MS may have removed residing compounds within the pores of the MS. In contrast, the 5 Å MS starts with a comparably good yield (0.03 %) but decreases drastically with each application, indicating an actual loss of catalytic active components from the MS.

Table 9: Experiments reusing modified carriers on 120 °C and 40 bar without a dehydrating agent

Experiment	Carrier	Usages [-]	EtOH Feed [g]	catalyst mass [g]	carrier mass [g]
V_{R17}	MS 4 Å	1	100.00		50
V_{R24}	MS 4 Å	2	70.72	0.13	50
V_{R25}	MS 4 Å	3	70.00		50
V_{R22}	MS 5 Å	1	70.82		50
V_{R26}	MS 5 Å	2	71.00	2.87	50
V_{R27}	MS 5 Å	3	74.00		50

In aggregate, 4 Å and 5 Å MS show a large potential as a catalyst carrier reaching competitive yields and productivities. 4 Å MS have demonstrated better stability, which has not been found using 5 Å MS. An adjustment of the regeneration process could possibly prevent the performance degradation. On the other hand, 5 Å MS have shown significantly better performances than commercial CeO_2. Using 2CP as a dehydration agent increases the productivity by 30 times for 4 Å MS and 97 times for 5 Å MS on average being highly competitive with commercial options. Instead of 2CP usage, membrane technology would be highly eligible for keeping the water concentration low, as observed in **[Journal Publication II]**, without the drawback of coping with picolineamide as another side product.

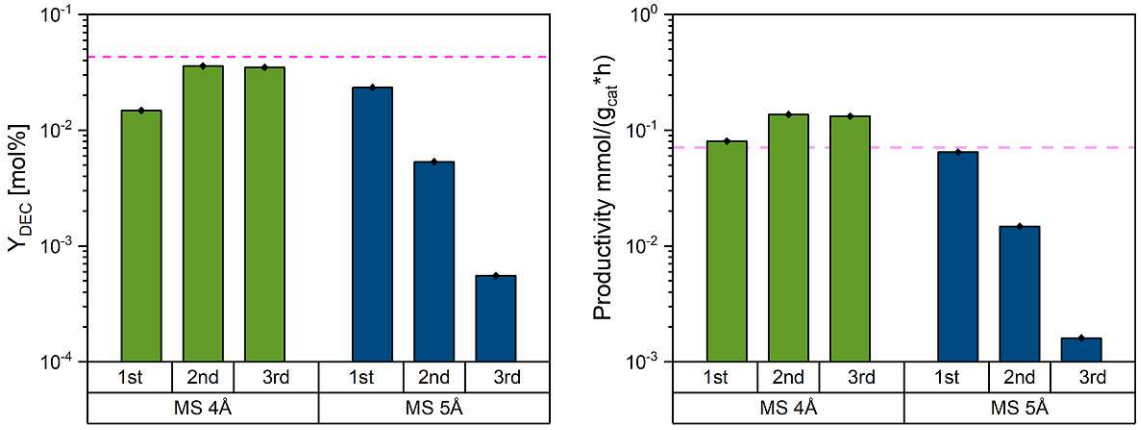

Figure 24: Comparison of yield per hour (left) and productivity (right) of modified carriers on multiple usage without water trap usage

4.3 Product removal

Among the various methods available to dehydrate the reaction mixture, pervaporation has been considered a promising approach. **[Journal Publication II]** tested and evaluated several membranes for usage in the DEC production process presented in **[patent]**. As mentioned in section 2.2 several polymeric and an inorganic ceramic membrane have

Table 10: Results of membrane pervaporation experiments in **[Journal Publication II]**

Membrane	w_{c,H_2O} $[wt\%]$	w_{p,H_2O} $[wt\%]$	α $[-]$	Q_{H_2O} $[mol/Pa \times m^2 \times h]$
ZEBREX™ ZX0	0.98	> 94.5	3080 – 200000	$< 6.03 \times 10^{-6}$
PERVAP™ 4155–80	1.01	~ 12.0	11 – 17	$< 1.80 \times 10^{-5}$
PERVAP™ 4100	0.94	4.7 – 5.1	5 – 6	$< 4.52 \times 10^{-6}$
PERVAP™ 4101	1.08	73.9	120 – 180	2.19×10^{-6}

been used to dehydrate ternary DEC/water/EtOH mixtures occurring during direct synthesis from EtOH and CO_2. The results of multiple experiments using 1 % DEC and water each and the rest of EtOH are available in Table 10.

The results show a good separation performance of the inorganic membrane based on water flux and purity, so dehydration during the reaction is conceivable.

Since low quantities of water already slow down the reaction, membrane performance in very low water concentrations is of high interest. **[Journal Publication II]** gives insight into the dehydration performance using an initial feed water content of 0.7 wt%, as illustrated in Figure 25.

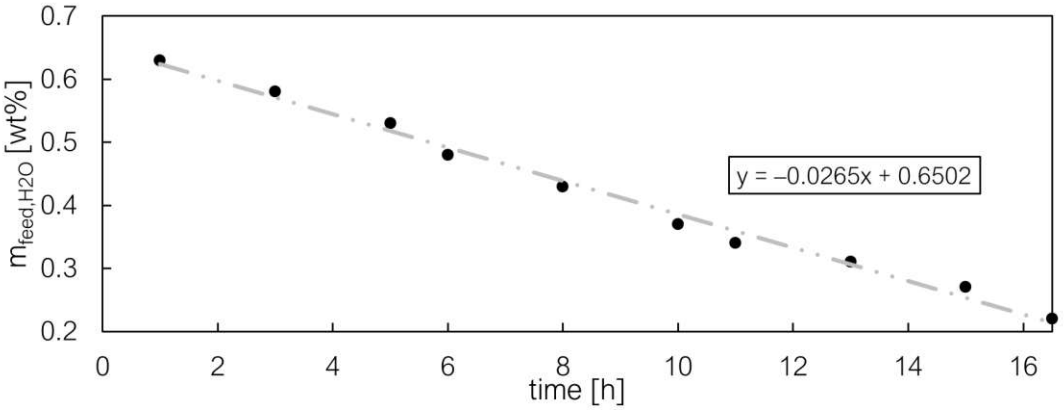

Figure 25: Water concentration of circulating feed of an exemplary experiment in **[Journal Publication II]**

The continuously decreasing water content in the feed shows that the membrane is capable of reducing the water concentration at very low levels. A closer look on the flux reveals a slowed-down dehydration. Nevertheless, increasing the surface area or the other parameters, such as sweep gas flow rate, would counteract the apparent deceleration. Membrane dehydration is possible as long as the water molecule mobility is given. The purity of the permeate was observed to decrease with lowering feed water content. However, the permeate's average purity in this experiment was observed to be 99.02 wt%. Other findings of **[Journal Publication II]** include that no significant alterifications on dehydration performance were observed despite using 9 wt% DEC feed content and, further, increasing the operating pressure resulted in a better performance without observing any traces of

CO_2 in the permeate. The design of the separation procedure should consider that low DEC degradation has been observed in **[Journal Publication I]** using CeO_2 while boiling water and DEC. This effect was visibly lower without the presence of CeO_2 and has not been observed at all in **[Journal Publication II]**. Nevertheless, DEC degradation due to adverse membrane material selection may be possible and must be ruled out. An effective dehydration would effectively prevent hydrolysis of DEC. However, this requires further research on how low the water concentration can reach by using pervaporation. These key findings have been considered in **[Patent]** and the manufacturing process of the pilot reactor.

4.4 Process simulation

The simulation of the process chain based on the data obtained from section 4.1 and **[Journal Publication II]** shall give insight into the production capabilities of the process chain. The results of the simulations are illustrated in Figure 26.

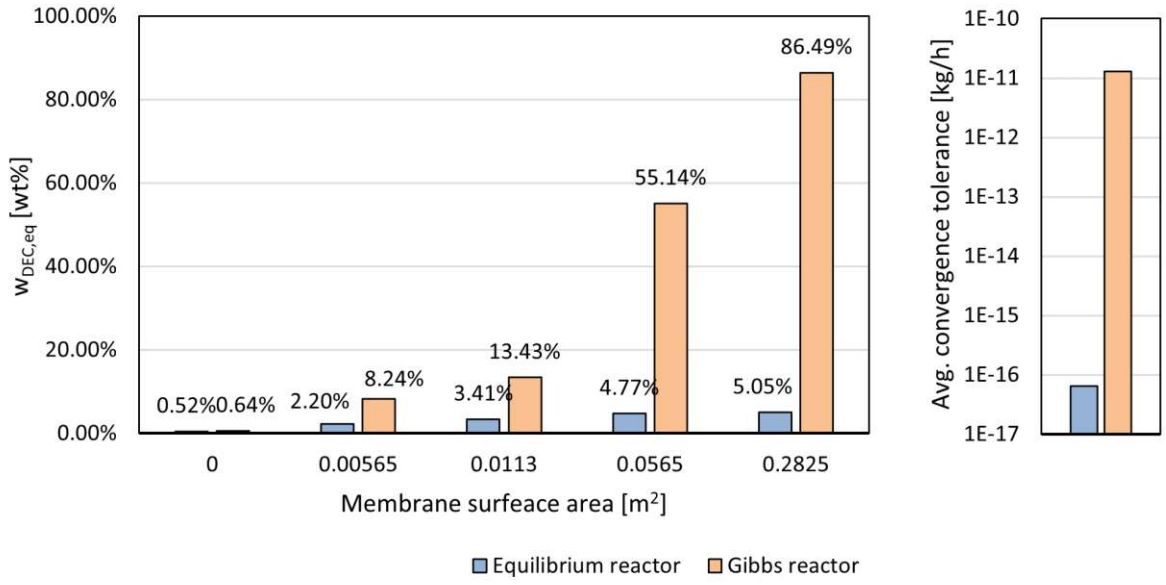

Figure 26: Simulated equilibrium concentrations of DEC in DWSIM simulating none, one, two, 10, and 50 ZX0 Membranes with either the Gibbs or the Equilibrium reactor

The equilibrium concentration of DEC $w_{DEC,eq}$ within the circulating mixture only reaches close to 0.5 wt % in both scenarios. This proves that the stored thermodynamic data is relatively close to each other. Simulating the use of one ZX0 Membrane already increases w_{DEC} by at least the 4–fold using the Equilibrium reactor and more than 12–fold for the Gibbs reactor. Thus, both models show a drastic increase in w_{DEC}. Simulations containing recycle streams are usually run iteratively and converge, neglecting a specific error under which the overall demands are still met. Even though the converging tolerance for water of the equilibrium reactor was already as low as $1.6 \times 10^{-11} kg/h$, low but significant changes in w_{DEC} have been observed increasing the concentration and decreasing the overall error in the cycle. The Gibbs reactor shows a low error tolerance of $6.4 \times 10^{-17} kg/h$ in

comparison to the equilibrium reactors error tolerance. Since this iterative approach was significantly more time-consuming for the Equilibrium reactor, the convergence condition was concluded earlier. The equilibrium reactor simulating the direct synthesis with the pervaporation using the 10–fold of the ZX0 membrane surface area doubles w_{DEC}. Further increases still increase w_{DEC}, with a low incline, which would already be significantly more DEC formed than in the literature (see subsection 2.3.2). The results delivered by the Gibbs reactor are massively enhanced by including the ZX0 membrane in the simulation. Increasing the surface up to the 50–fold ZX0 surface area of 0.28 m^2 even shifts the equilibrium of the system up to a DEC concentration w_{DEC} of over 86 wt%. More information on the shifted the equilibrium is obtained, by including the information of the residual water content in the circulating mixture, which is illustrated in Figure 27.

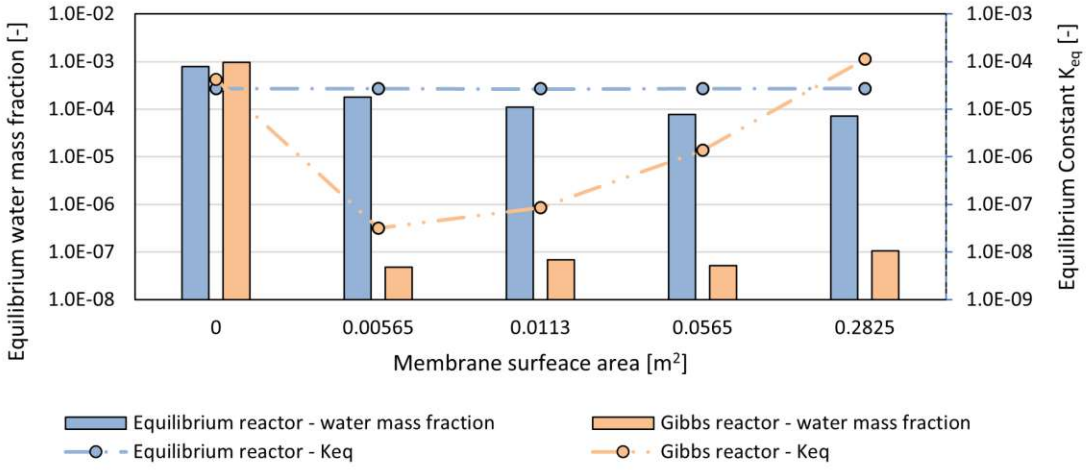

Figure 27: Simulated equilibrium mass fractions of water in Gibbs and Equilibrium reactor

The equilibrium water concentration in the reactor should decrease, which also resembles using the equilibrium reactor. The Gibbs reactor does not follow the expected trend, limiting the significance of the overall Gibbs reactor results. The calculated K_{eq} equilibrium constants of the direct synthesis of EtOH and CO_2 from the results match the used equilibrium constant (see subsection 3.2.1). The equilibrium constants K_{eq} calculated from the composition in the Gibbs reactor differ due to the extremely low water concentration observed. The relatively strong deviation of K_{eq} indicates that the actual water concentration would be higher than the one observed in the calculation to achieve the concentrations returned by the simulation. Thus, the membrane model effectively simulates a reduced water content, shifting the equilibrium towards higher DEC- and lower water concentrations. However, a more effective convergence calculation would result in slightly higher concentrations of DEC. The DEC concentrations observed from the Gibbs reactor seem too high to be valid in comparison. However, they still provide information on how low the water concentration needs to be driven to boost the reaction to achieve the observed DEC concentrations, which can be adjusted by membrane size.

CHAPTER 5

Summary of publications

5.1 Journal Publications

5.1.1 Journal Publication I

Title: Stability of Diethyl Carbonate in the Presence of Acidic and Basic Solvents [152]

This study explores the applicability of DEC by exposure to acidic and basic solvents. The chemical stability of DEC towards decomposition has been experimentally investigated under various temperatures and additives. The reagents used have been in contact at ambient temperatures up to the boiling point. The composition obtained subsequently was analytically assessed to detect decomposition products.

The experiments have shown the possible decomposition of DEC to EtOH and CO_2 in the presence of specific conditions. Degradation at ambient conditions does not follow tendencies and was generally comparably low (mostly < 10 %). Nonetheless, the degradation process accelerates significantly at higher temperatures, especially in the presence of bases. The influence of catalysts requires further investigation since its effect did not follow specific trends. Reduced base–catalyzed decomposition was found in the presence of sodium chloride (NaCl), counteracting previously observed elevated levels of DEC degradation.

5.1.2 Journal Publication II

Dehydration by Pervaporation of an Organic Solution for the Direct Synthesis of Diethyl Carbonate [153]

Dehydration of Ternary mixtures consisting of DEC, water, and ethanol has been investigated experimentally by a pervaporation setup. The presence of water was confirmed as a significant obstacle to the direct synthesis of DEC from EtOH and CO_2. Challenges in membrane separation have been reported in this context regarding membrane stability close to DEC synthesis temperatures, pressures, and swelling caused by CO_2. Pressurization was achieved by feeding CO_2 to the ternary system and extending the system to a quaternary system. A partial least squares model was written to enable a quick assessment of product compositions using FTIR–ATR measurements.

Three polymeric flat–sheet (PERVAP^{TM} 4100, 4101, and 4155–88) and one tubular ceramic (ZEBREX ZX0) membrane have been operated on various temperatures, feed compositions, and pressures to obtain separation characteristics of the membranes chosen. The PERVAP^{TM} 4155–88 and 4100 have shown the highest overall fluxes. However, the largest losses of DEC and EtOH have been recorded, resulting in their unsuitability for dehydration due to low selectivity ($\alpha < 18$). The PERVAP^{TM} 4101 demonstrated improved selectivity ($\alpha > 120$), but the DEC and EtOH losses remained too significant for an effective initial dehydration. Nevertheless, the PERVAP^{TM} 4101 membrane could possibly be considered for subsequent purification operations, though more research would be necessary for specific applications.

The tubular ZEBREX ZX0 ceramic membrane has shown the best overall dehydration capabilities with very high selectivities ($\alpha > 3800$, sometimes $\alpha > 10{,}000$), achieving permeate qualities of 98 wt % for water. Parameters like temperature, pressure, and sweep gas flow rate clearly influenced the membrane performance, while no significant influence resulting from increasing DEC concentrations has been observed. Increasing the temperature towards DEC synthesis conditions and a higher sweep gas velocity could increase water flux. No CO_2 was detected in the permeate while circulating feed remained saturated on CO_2. The tested ceramic membrane was a viable option to dehydrate the reaction mixture occurring during direct DEC synthesis from EtOH and CO_2. PLS modeling has shown excellent characteristics for product assessment.

5.1.3 Journal Publication III

Design of a Gas Permeation and Pervaporation Membrane Model for an Open Source Process Simulation Tool [154]

This study focuses on creating a gas permeation and pervaporation membrane model for open–source simulation tools to widen access to membrane operation simulations. The well-recognized solution–diffusion mechanism, widely used for gas permeation and pervaporation calculations, has been fostered into a modular, object–oriented model. This model has been realized for the open–source tool DWSIM and offers extensive customization and options for simulation accuracy enhancement.

The model interacts consistently with DWSIM, allowing operators to modify multiple membrane parameters for the flux and retentate calculation. Validation was conducted by comparing experimental data and simulations available in the literature throughout various test cases for gas permeation and pervaporation scenarios.

The results show close overlaps with experiments with deviations typically lower than 1 %, exposing the significance of its input parameters (e.g., feed composition, pressure, membrane area) on separation characteristics. The created tool supports detailed analyses for academic and industrial applications, including gas permeation (see **[Journal Publication IV]**) or pervaporation membrane separation simulations. Providing the open–source code shall encourage more extensive adjustments by the community, even increasing the accuracy of the desired specific field of application.

5.1.4 Journal Publication IV

High Purity Hydrogen from Liquid NH_3 – Proposal and Evaluation of a Process Chain [155]

A process chain to produce high–purity hydrogen by liquid endothermic ammonia decomposition has been presented in this study. The decomposition of ammonia followed by hydrogen purification incorporates reaction kinetics for the catalytic decomposition of ammonia-based catalysts such as Ni–Pt/Al_2O_3. Heat integration calculations have been carried out to improve energy efficiency. The purification of H_2 in the process chain has been proposed based on simulations using DWSIM and the membrane code proposed in **[Journal Publication III]**.

The separation of the product, mainly consisting of H_2 and N_2, is proposed by membrane technology using a polyimide membrane. Following this, H_2 purity levels up to 99.3 mol% are possible. However, despite the use of high–conversion reactors, NH_3 residues occur, which would require additional absorptive or adsorptive methods to drive the NH_3 concentration below 1 ppm. Additional pressure swing adsorption separation is suggested to achieve even higher qualities meeting proton-exchange membrane fuel–cells requirements.

5.2 Austrian Patent

Original title: *Verfahren zur Herstellung organischer Carbonate* [156] [pending]
Translated title: Process for organic carbonate synthesis

The invention describes a process for organic carbonate synthesis and separation. In particular, the catalytic direct organic carbonate (OC) synthesis from the corresponding alcohol and carbon dioxide, wherein water formed during the catalytic reaction is separated off via at least one inorganic membrane, is presented.

The patent details a membrane reactor built at least consisting of a reaction chamber equipped with an immobilized catalyst enabling the endergonic reaction. The catalyst, including at least metals, metal–oxides, salts, or an alloy of Cu and Ni as components, has been immobilized with a non–disclosed process on the surface structure of various solid porous carriers (e.g., activated carbon, molecular sieves, Raschig Rings, glass wool and clay,). Dehydration occurs locally close to the formation of DEC molecules, enabling a quick water separation. The piping system enables a continuous operation, pressurizing and saturating the circulating feed with CO_2 while simultaneously using CO_2 as sweep gas transporting permeating H_2O.

CHAPTER 6

Conclusion

This work regards multiple relevant aspects of the direct synthesis of DEC from CO_2 and EtOH. In addition, some DEC properties that are relevant for industrial use have also been investigated.

To optimize the direct synthesis of DEC from CO_2 and EtOH, a trial of experiments was carried out using a catalyst supported on modified carriers. The carriers involved included molecular sieves with different pore sizes, clay, and Raschig Rings. The DEC yields and the catalytic productivities observed in the experiments, which have been predominantly carried out at 120 °C and a total pressure of 40 bar, have been compared to experiments with commercial CeO_2.

It was found that the catalytic performance of modified clay, 10 Å molecular sieves, and Raschig Rings was insufficient. Conversely, the yields while applying molecular sieves with moderate pore sizes (4 Å, 5 Å) and the dehydrating agent 2CP have been observed to be between 2 - and 6 wt%. The performance of commercial CeO_2 applying comparable settings has been observed to be in between the mentioned range. A rise in DEC yield has been observed by using modified 3 Å, 4 Å, and 5 Å molecular sieves, with 5 Å showing the best yield and productivity. 10 Å molecular sieves break this trend by demonstrating an insufficient performance. A proposal for a solution to the obstacles connected with the mobility of the catalyst could be the use of the modified carriers applied in this work. However, further research should be carried out to maximize the catalytic performance's yield, productivity, and consistency.

Waiving the dehydration agent resulted in a massive drop in productivity in all experiments. Repetitions in the use of modified molecular sieves demonstrate a consistent activity of the 4 Å molecular sieves. In comparison, the 5 Å molecular sieves' catalytic performance declines from use to use.

The performance of modified 4 Å and 5 Å molecular sieves was still comparable to commercial alternatives in DEC formation. However, the water content fluctuated and did not correspond to the stoichiometric ratio of DEC/H_2O. The strongly hygroscopic nature of the molecular sieve may cause a share of the water molecules to adhere on the inner surface of the pores, resulting in a non-availability of the bulk of the mixture itself. This would cause a shift in water concentration, which is measured. Other materials with high porosity could be another suitable alternative. The removal of the dehydrating agent had by far the most significant impact on the productivity of every catalyst and carrier applied.

The removal of water to improve the DEC yield is inevitable. Dehydration of the reaction mixture consisting of DEC/water/EtOH/CO_2 was assessed using a pervaporation setup, which was operated with a sweep gas. Four membranes have been tested for eligibility for this purpose by introducing mixtures of DEC/water/EtOH into a circulating process equipped with a membrane module. The separative properties of the membranes have been investigated at various temperatures, pressures, and sweep gas flow rates. Since the pressurization was applied and maintained by introducing pressurized CO_2, this system also provides information about its usability in the reactive mixture for direct DEC synthesis.

The ZX0 membrane showed the best overall performance among the tested options. The selectivity α for water over EtOH mostly exceeded 10.000 with very good permeate purities ($>$ 98 wt%). Temperature, pressure, and sweep gas flow rate have been observed to be greatly influential parameters. Thus, there is a potential for optimizing the membrane's separation performance. Additional research into the parameters mentioned would be necessary. The influence of pressure has been identified to be the lowest among the parameters.

Heating the membrane with a water bath limits the maximum temperature used to just under 100 °C. However, the ZX0 membrane can be operated beyond this temperature, which would be closer to the usual DEC synthesis temperatures. While thermal stability was anticipated, an excellent resistance towards stability issues caused by CO_2 presence was also observed. No CO_2 has been detected in the permeate stream. As a result, the ZX0 membrane can be considered practically impermeable to CO_2.

A simulation of the synthesis reaction coupled with a variety of pervaporation scalings was carried out with DWSIM using the permeances obtained from the pervaporation experiments. The calculations based on the use of just one ZX0 membrane resulted in an increase of the yield of up to 400%.

The model was based on the solution-diffusion model. Its predictive capability was validated with gas permeation and pervaporation applications from the literature. As an open-source software, DWSIM allows its modification. Thus, an implementation of the membrane model was possible without restrictions. Other process simulators could rely upon or adapt the code if an implementation of customized calculation routines is possible.

Further membranes were used in the pervaporation experiments. Nevertheless, their performance was insufficient in comparison to the ceramic ZX0 membrane. The PERVAP™

Membrane has shown a selectivity ($\alpha > 120$), which may be relevant for a consecutive purification step of the permeate. High losses of DEC and EtOH have been observed while using polymeric membranes, which is considered particularly adverse.

DEC is already in use for a bandwidth of applications. However, only limited research on its specific chemical stability is available. Experiments on the decomposition of DEC by exposing it to water, and various acidic and basic compounds have been carried out under various conditions. The degradation of DEC has been observed at ambient and elevated temperatures in different forms. Lower degradation is manifested by applying ambient temperature. None of the reagents used caused a decomposition of DEC, which exceeded 20 wt%. However, the decomposition was increased by raising the temperature. This resulted in a total degradation of DEC while using basic reagents.

The base-catalyzed hydrolysis of DEC seems to be stronger than acid-catalyzed hydrolysis. Generally, a strong decomposition of DEC was assigned to the reagents with an exceptionally high acidity and alkalinity. The presence of water and dissolved CO_2 at high pressures forms H_3O^+ ions, which could ultimately react with DEC and cause its decomposition.

Using CeO_2 as a catalyst did not result in clear trends. Thus, a causal relation between acidity and alkalinity and the decomposition of DEC while using CeO_2 was not identified. More experiments with intermediate temperature steps could provide more information on the influence of CeO_2. A reduced degradation was observed by adding NaCl. This effect was more prominent at elevated temperatures.

Operating the same experiments in a pressurized device could extend the informative value of the same experiments since losses of EtOH or other volatiles could be avoided.

The mentioned findings have been cast into the efforts to design a pilot reactor, especially including the findings of the reaction and pervaporation experiments. The operation of the pilot membrane reactor exhibits a high potential to prove the concept introduced in its design and contribute to more sustainable production of DEC.

Bibliography

[1] E. Foote, "Circumstances affecting the heat of the sun's rays," *Am. J. Sci. Arts*, vol. 22, no. 66, pp. 383–384, 1856.

[2] G. S. Callendar, "Can carbon dioxide influence climate?" *Weather*, vol. 4, no. 10, pp. 310–314, 1949, _eprint: https://onlinelibrary.wiley.com/doi/pdf/10.1002/j.1477-8696.1949.tb00952.x, ISSN: 1477-8696. DOI: 10.1002/j.1477-8696.1949.tb00952.x. Accessed: Aug. 27, 2024.

[3] G. N. Plass, "Carbon dioxide and climate," *Scientific American*, vol. 201, no. 1, pp. 41–47, 1959, Publisher: Scientific American, a division of Nature America, Inc., ISSN: 0036-8733. Accessed: Aug. 27, 2024.

[4] Intergovernmental Panel On Climate Change (Ipcc), "Climate change 2022 – impacts, adaptation and vulnerability: Working group II contribution to the sixth assessment report of the intergovernmental panel on climate change," Cambridge University Press, Jun. 22, 2023. DOI: 10.1017/9781009325844. Accessed: Aug. 27, 2024. [Online]. Available: https://www.cambridge.org/core/product/identifier/9781009325844/type/book.

[5] UNFCCC. "Historic paris agreement on climate change: 195 nations set path to keep temperature rise well below 2 degrees celsius | UNFCCC," Accessed: Aug. 27, 2024. [Online]. Available: https://unfccc.int/news/finale-cop21.

[6] United Nations. "Report - climate action summit 2019 | department of economic and social affairs," Accessed: Aug. 27, 2024. [Online]. Available: https://sdgs.un.org/documents/report-climate-action-summit-2019-32820.

[7] T. Ahmad and D. Zhang, "A critical review of comparative global historical energy consumption and future demand: The story told so far," *Energy Reports*, vol. 6, pp. 1973–1991, Nov. 1, 2020, ISSN: 2352-4847. DOI: 10.1016/j.egyr.2020.07.020.

[8] X. Zhou *et al.*, "Review of carbon dioxide utilization and sequestration in depleted oil reservoirs," *Renewable and Sustainable Energy Reviews*, vol. 202, p. 114646, Sep. 1, 2024, ISSN: 1364-0321. DOI: 10.1016/j.rser.2024.114646.

[9] D. Ko, G. Yoo, S.-T. Yun, and H. Chung, "Impacts of CO_2 leakage on plants and microorganisms: A review of results from CO_2 release experiments and storage sites," *Greenhouse Gases: Science and Technology*, vol. 6, no. 3, pp. 319–338, Jun. 2016, ISSN: 2152-3878, 2152-3878. DOI: 10.1002/ghg.1593.

[10] M. D. Aminu, S. A. Nabavi, C. A. Rochelle, and V. Manovic, "A review of developments in carbon dioxide storage," *Applied Energy*, vol. 208, pp. 1389–1419, Dec. 15, 2017, ISSN: 0306-2619. DOI: 10.1016/j.apenergy.2017.09.015.

[11] M. Seyyedi and C. Consoli, "From gas to stone: In-situ carbon mineralisation as a permanent CO_2 removal solution," *International Journal of Greenhouse Gas Control*, vol. 137, p. 104 217, Sep. 2024, ISSN: 17505836. DOI: 10.1016/j.ijggc.2024.104217.

[12] P. R. Ellis, M. J. Hayes, N. Macleod, S. J. Schuyten, C. L. Tway, and C. M. Zalitis, "Carbon conversion: Opportunities in chemical productions," in *Surface Process, Transportation, and Storage*, Elsevier, 2023, pp. 479–524, ISBN: 978-0-12-823891-2. DOI: 10.1016/B978-0-12-823891-2.00006-5. Accessed: Aug. 26, 2024.

[13] *The european green deal*, in collab. with E. Comission, 2019. Accessed: Nov. 23, 2024. [Online]. Available: https://eur-lex.europa.eu/legal-content/EN/TXT/?uri=CELEX:52019DC0640.

[14] O. A. Ibigbami, O. D. Onilearo, and R. O. Akinyeye, "Post-combustion capture and other carbon capture and sequestration (CCS) technologies: A review," *Environmental Quality Management*, vol. 34, no. 1, e22180, Sep. 1, 2024, Publisher: John Wiley & Sons, Ltd, ISSN: 1520-6483. DOI: 10.1002/TQEM.22180. Accessed: Jul. 23, 2024.

[15] U.S. Department of Energy, Secretary of Energy Advisory Board (SEAB), "CO_2 utilization and negative emissions technologies."[Online]. Available: https://www.energy.gov/sites/prod/files/2016/12/f34/SEAB-CO2-TaskForce-FINAL-with%20transmittal%20ltr.pdf.

[16] B. Schäffner, F. Schäffner, S. P. Verevkin, and A. Börner, "Organic carbonates as solvents in synthesis and catalysis," *Chemical Reviews*, vol. 110, no. 8, pp. 4554–4581, Aug. 11, 2010, ISSN: 0009-2665, 1520-6890. DOI: 10.1021/cr900393d.

[17] Justice.gov. "Volkswagen to spend up to $14.7 billion to settle allegations of cheating emissions tests and deceiving customers on 2.0 liter diesel vehicles | united states department of justice," Office of Public Affairs, Accessed: Dec. 9, 2024. [Online]. Available: https://www.justice.gov/opa/pr/volkswagen-spend-147-billion-settle-allegations-cheating-emissions-tests-and-deceiving.

[18] J. of the Court (Grand Chamber), *IR v volkswagen AG*, Jul. 14, 2022. Accessed: Dec. 9, 2024. [Online]. Available: https://eur-lex.europa.eu/legal-content/EN/TXT/?uri=CELEX%5C%3A62020CJ0134.

[19] L. Elliott, "Biden announces 100 % tariff on chinese-made electric vehicles," *The Guardian*, May 14, 2024, ISSN: 0261-3077. Accessed: Dec. 9, 2024. [Online]. Available: https://www.theguardian.com/business/article/2024/may/14/joe-biden-tariff-chinese-made-electric-vehicles.

[20] L. O'Carroll, "EU leaders back extra chinese EV tariffs despite split vote," *The Guardian*, Oct. 4, 2024, ISSN: 0261-3077. Accessed: Dec. 9, 2024. [Online]. Available: https://www.theguardian.com/business/2024/oct/04/eu-chinese-ev-tariffs-split-vote-germany-car-firms.

[21] K. Shukla and V. C. Srivastava, "Diethyl carbonate: Critical review of synthesis routes, catalysts used and engineering aspects," *RSC Advances*, vol. 6, no. 39, pp. 32 624–32 645, 2016, ISSN: 2046-2069. DOI: 10.1039/C6RA02518H. Accessed: Aug. 8, 2024.

[22] W. Ye, Z. Baoguo, W. Pengfei, L. Min, C. Dexing, and X. Wenhao, "Improving the dispersion stability and chemical mechanical polishing performance of CeO_2 slurries," *ECS Journal of Solid State Science and Technology*, vol. 12, no. 4, p. 044 004, Apr. 1, 2023, ISSN: 2162-8769, 2162-8777. DOI: 10.1149/2162-8777/accaa5.

[23] H. E. Howe and F. J. V. Antwerpen, "Utilization of industrial wastes," *Industrial & Engineering Chemistry*, vol. 31, no. 11, pp. 1323–1330, Nov. 1939, ISSN: 0019-7866, 1541-5724. DOI: 10.1021/ie50359a005. Accessed: Aug. 26, 2024.

[24] IEA, "IEA - executive summary – CO_2 emissions in 2023 – analysis." Accessed: Aug. 26, 2024. [Online]. Available: https://www.iea.org/reports/co2-emissions-in-2023/executive-summary.

[25] IEA, "IEA - putting CO_2 to use – analysis," Sep. 25, 2019. Accessed: Aug. 26, 2024. [Online]. Available: https://www.iea.org/reports/putting-co2-to-use.

[26] "Scopus - analyze search results | signed in," Scopus, Accessed: Sep. 6, 2024. [Online]. Available: https://www.scopus.com/term/analyzer.uri?sort=plf-f&src=s&sid=8e07c99b6823aa1f7b517e8119b37724&sot=a&sdt=a&sl=283&s=%28TITLE-ABS-KEY%28carbon%29+AND+TITLE-ABS-KEY%28ccu%29+OR+TITLE-ABS-KEY%28carbon+AND+capture+AND+utilization%29+OR+TITLE-ABS-KEY%28carbon+AND+capture+AND+utilisation%29+OR+TITLE-ABS-KEY%28ccs%29+OR+TITLE-ABS-KEY%28carbon+AND+capture+AND+storage%29+OR+TITLE-ABS-KEY%28carbon+AND+capture%29+OR+TITLE-ABS-KEY%28ccus%29%29&origin=resultslist&count=10&analyzeResults=Analyze+results.

[27] Z. Zhang *et al.*, "Recent advances in carbon dioxide utilization," *Renewable and Sustainable Energy Reviews*, vol. 125, p. 109 799, Jun. 2020, ISSN: 13640321. DOI: 10.1016/j.rser.2020.109799.

[28] G. Reiter and J. Lindorfer, "Global warming potential of hydrogen and methane production from renewable electricity via power-to-gas technology," *The International Journal of Life Cycle Assessment*, vol. 20, no. 4, pp. 477–489, Apr. 2015, ISSN: 0948-3349, 1614-7502. DOI: 10.1007/s11367-015-0848-0.

[29] A. Peppas, S. Kottaridis, C. Politi, and P. M. Angelopoulos, "Carbon capture utilisation and storage in extractive industries for methanol production," *Eng*, vol. 4, no. 1, pp. 480–506, Mar. 2023, Number: 1 Publisher: Multidisciplinary Digital Publishing Institute, ISSN: 2673-4117. DOI: 10.3390/eng4010029.

[30] M. Pérez-Fortes, J. C. Schöneberger, A. Boulamanti, G. Harrison, and E. Tzimas, "Formic acid synthesis using CO_2 as raw material: Techno-economic and environmental evaluation and market potential," *International Journal of Hydrogen Energy*, vol. 41, no. 37, pp. 16 444–16 462, Oct. 2016, ISSN: 03603199. DOI: 10.1016/j.ijhydene.2016.05.199.

[31] E. Koohestanian, J. Sadeghi, D. Mohebbi-Kalhori, F. Shahraki, and A. Samimi, "A novel process for CO_2 capture from the flue gases to produce urea and ammonia," *Energy*, vol. 144, pp. 279–285, Feb. 1, 2018, ISSN: 0360-5442. DOI: 10.1016/j.energy.2017.12.034.

[32] Y. Ye, Y. Qu, and J. Sun, "Functionalized mesoporous SiO_2 materials for CO_2 capture and catalytic conversion to cyclic carbonates," *Catalysis Reviews*, vol. 66, no. 5, pp. 2153–2208, Nov. 25, 2024, Publisher: Taylor & Francis _eprint: https://doi.org/10.1080/0161
ISSN: 0161-4940. DOI: 10.1080/01614940.2023.2202528.

[33] Y. H. Choi *et al.*, "Carbon dioxide fischer-tropsch synthesis: A new path to carbon-neutral fuels," *Applied Catalysis B: Environmental*, vol. 202, pp. 605–610, Mar. 1, 2017, ISSN: 0926-3373. DOI: 10.1016/j.apcatb.2016.09.072.

[34] C. Fernández-Dacosta *et al.*, "Prospective techno-economic and environmental assessment of carbon capture at a refinery and CO_2 utilisation in polyol synthesis," *Journal of CO2 Utilization*, vol. 21, pp. 405–422, Oct. 2017, ISSN: 22129820. DOI: 10.1016/j.jcou.2017.08.005.

[35] M. Held, Y. Tönges, D. Pélerin, M. Härtl, G. Wachtmeister, and J. Burger, "On the energetic efficiency of producing polyoxymethylene dimethyl ethers from CO_2 using electrical energy," *Energy & Environmental Science*, vol. 12, no. 3, pp. 1019–1034, 2019, ISSN: 1754-5692, 1754-5706. DOI: 10.1039/C8EE02849D.

[36] R. Sen and S. Mukherjee, "Recent advances in microalgal carbon capture and utilization (bio-CCU) process vis-à-vis conventional carbon capture and storage (CCS) technologies," ISSN: 1064-3389.

[37] P. Nawkarkar, A. Ganesan, and S. Kumar, "Chapter 32 - carbon dioxide capture for biofuel production," in *Handbook of Biofuels*, S. Sahay, Ed., Academic Press, Jan. 1, 2022, pp. 605–619, ISBN: 978-0-12-822810-4. DOI: 10.1016/B978-0-12-822810-4.00032-4.

[38] W. Wang, S. Wang, X. Ma, and J. Gong, "Recent advances in catalytic hydrogenation of carbon dioxide," *Chemical Society Reviews*, vol. 40, no. 7, p. 3703, 2011, ISSN: 0306-0012, 1460-4744. DOI: 10.1039/c1cs15008a. Accessed: Aug. 26, 2024.

[39] M. Agliuzza, A. Mezza, and A. Sacco, "Solar-driven integrated carbon capture and utilization: Coupling CO_2 electroreduction toward CO with capture or photovoltaic systems," *Applied Energy*, vol. 334, p. 120 649, Mar. 15, 2023, ISSN: 0306-2619. DOI: 10.1016/j.apenergy.2023.120649.

[40] I. Ihsanullah, M. Atieh, M. Sajid, and M. Nazal, "Desalination and environment: A critical analysis of impacts, mitigation strategies, and greener desalination technologies," *Science of the Total Environment*, vol. 780, 2021. DOI: 10.1016/j.scitotenv.2021.146585.

[41] A. Dindi, D. V. Quang, and M. R. M. Abu-Zahra, "Simultaneous carbon dioxide capture and utilization using thermal desalination reject brine," *Applied Energy*, vol. 154, pp. 298–308, Sep. 15, 2015, ISSN: 0306-2619. DOI: 10.1016/j.apenergy.2015.05.010. Accessed: Aug. 26, 2024.

[42] M. Wang *et al.*, "Can sustainable ammonia synthesis pathways compete with fossil-fuel based haber–bosch processes?" *Energy & Environmental Science*, vol. 14, no. 5, pp. 2535–2548, 2021, ISSN: 1754-5692, 1754-5706. DOI: 10.1039/D0EE03808C.

[43] K. Khoiruddin, I. G. Wenten, and U. W. R. Siagian, "Advancements in bipolar membrane electrodialysis techniques for carbon capture," *Langmuir*, vol. 40, no. 18, pp. 9362–9384, May 7, 2024, ISSN: 0743-7463, 1520-5827. DOI: 10.1021/acs.langmuir.3c03873. Accessed: Aug. 26, 2024.

[44] E. Catizzone, C. Freda, G. Braccio, F. Frusteri, and G. Bonura, "Dimethyl ether as circular hydrogen carrier: Catalytic aspects of hydrogenation/dehydrogenation steps," *Journal of Energy Chemistry*, vol. 58, pp. 55–77, Jul. 1, 2021, ISSN: 2095-4956. DOI: 10.1016/j.jechem.2020.09.040.

[45] W. Wang, L. Rao, X. Wu, Y. Wang, L. Zhao, and X. Liao, "Supercritical carbon dioxide applications in food processing," *Food Engineering Reviews*, vol. 13, no. 3, pp. 570–591, Sep. 2021, ISSN: 1866-7910, 1866-7929. DOI: 10.1007/s12393-020-09270-9.

[46] F. De La Cruz-Martínez, J. A. Castro-Osma, and A. Lara-Sánchez, "Catalytic synthesis of bio-sourced organic carbonates and sustainable hybrid materials from CO_2," in *Advances in Catalysis*, vol. 70, Elsevier, 2022, pp. 189–236, ISBN: 978-0-323-98935-0. DOI: 10.1016/bs.acat.2022.07.003.

[47] F. Carrasco-Maldonado, R. Spörl, K. Fleiger, V. Hoenig, J. Maier, and G. Scheffknecht, "Oxy-fuel combustion technology for cement production – state of the art research and technology development," *International Journal of Greenhouse Gas Control*, vol. 45, pp. 189–199, Feb. 1, 2016, ISSN: 1750-5836. DOI: 10.1016/j.ijggc.2015.12.014.

[48] A. Olabi *et al.*, "Assessment of the pre-combustion carbon capture contribution into sustainable development goals SDGs using novel indicators," *Renewable and Sustainable Energy Reviews*, vol. 153, p. 111 710, Jan. 2022, ISSN: 13640321. DOI: 10.1016/j.rser.2021.111710.

[49] N. Ramzan *et al.*, "Pre-combustion carbon dioxide capture: A thermo-economic comparison for dual-stage selexol process and combined sulfinol-selexol process," *International Journal of Energy Research*, vol. 46, no. 15, pp. 23 775–23 795, 2022, _eprint: https://onlinelibrary.wiley.com/doi/pdf/10.1002/er.8674, ISSN: 1099-114X. DOI: 10.1002/er.8674.

[50] A. Kamolov *et al.*, "Decarbonization of power and industrial sectors: The role of membrane processes," *Membranes*, vol. 13, no. 2, p. 130, Jan. 19, 2023, ISSN: 2077-0375. DOI: 10.3390/membranes13020130. Accessed: Aug. 8, 2024.

[51] C. Chao, Y. Deng, R. Dewil, J. Baeyens, and X. Fan, "Post-combustion carbon capture," *Renewable and Sustainable Energy Reviews*, vol. 138, p. 110 490, Mar. 1, 2021, Publisher: Pergamon, ISSN: 1364-0321. DOI: 10.1016/J.RSER.2020.110490. Accessed: Dec. 12, 2023.

[52] M. Wang, A. Lawal, P. Stephenson, J. Sidders, and C. Ramshaw, "Post-combustion CO_2 capture with chemical absorption: A state-of-the-art review," *Chemical Engineering Research and Design*, vol. 89, no. 9, pp. 1609–1624, Sep. 1, 2011, Publisher: Elsevier, ISSN: 0263-8762. DOI: 10.1016/J.CHERD.2010.11.005. Accessed: Dec. 12, 2023.

[53] C. Wu *et al.*, "A comprehensive review of carbon capture science and technologies," *Carbon Capture Science & Technology*, vol. 11, p. 100 178, Jun. 2024, ISSN: 27726568. DOI: 10.1016/j.ccst.2023.100178.

[54] S. D. Peu *et al.*, "A comprehensive review on recent advancements in absorption-based post combustion carbon capture technologies to obtain a sustainable energy sector with clean environment," *Sustainability*, vol. 15, no. 7, p. 5827, Mar. 27, 2023, ISSN: 2071-1050. DOI: 10.3390/su15075827.

[55] F. Raganati, F. Miccio, and P. Ammendola, "Adsorption of carbon dioxide for post-combustion capture: A review," *Energy & Fuels*, vol. 35, no. 16, pp. 12 845–12 868, Aug. 19, 2021, ISSN: 0887-0624, 1520-5029. DOI: 10.1021/acs.energyfuels.1c01618.

[56] Z. Ziobrowski and A. Rotkegel, "Comparison of CO2 separation efficiency from flue gases based on commonly used methods and materials," *Materials*, vol. 15, no. 2, 2022, ISBN: 4832231081, ISSN: 19961944. DOI: 10.3390/ma15020460.

[57] E. E. Okoro, R. Josephs, S. E. Sanni, and Y. Nchila, "Advances in the use of nanocomposite membranes for carbon capture operations," *International Journal of Chemical Engineering*, vol. 2021, 2021, ISSN: 16878078. DOI: 10.1155/2021/6666242.

[58] D. Chen *et al.*, "Boosting membranes for CO_2 capture toward industrial decarbonization," *Carbon Capture Science and Technology*, vol. 7, April 2023, Publisher: Elsevier Ltd, ISSN: 27726568. DOI: 10.1016/j.ccst.2023.100117.

[59] L. S. White, K. D. Amo, T. Wu, and T. C. Merkel, "Extended field trials of polaris sweep modules for carbon capture," *Journal of Membrane Science*, vol. 542, pp. 217–225, August 2017, Publisher: Elsevier B.V., ISSN: 18733123. DOI: 10.1016/j.memsci.2017.08.017.

[60] R. W. Baker, T. Merkel, and B. C. Freeman, "Large pilot testing of the MTR membrane post-combustion CO_2 capture process," *Membrane Technology and Research, Inc.*, p. 5, 2018.

[61] L. S. White, X. Wei, S. Pande, T. Wu, and T. C. Merkel, "Extended flue gas trials with a membrane-based pilot plant at a one-ton-per-day carbon capture rate," *Journal of Membrane Science*, vol. 496, pp. 48–57, 2015, Publisher: Elsevier, ISSN: 18733123. DOI: 10.1016/j.memsci.2015.08.003.

[62] X. He, D. Chen, Z. Liang, and F. Yang, "Insight and comparison of energy-efficient membrane processes for CO_2 capture from flue gases in power plant and energy-intensive industry," *Carbon Capture Science and Technology*, vol. 2, p. 100 020, October 2021 2022, Publisher: Elsevier Ltd, ISSN: 27726568. DOI: 10.1016/j.ccst.2021.100020.

[63] V. Batoon *et al.*, "Scale-up and testing of advanced polaris membrane CO_2 capture technology (DE-FE0031591)," Carbon Capture-2020 Integrated Review Webinar, 2020.

[64] T. Brinkmann *et al.*, "Development of CO_2 selective poly(ethylene oxide)-based membranes: From laboratory to pilot plant scale," *Engineering*, vol. 3, no. 4, pp. 485–493, 2017, Publisher: Elsevier LTD on behalf of Chinese Academy of Engineering and Higher Education Press Limited Company, ISSN: 20958099. DOI: 10.1016/J.ENG.2017.04.004.

[65] J. Pohlmann, M. Bram, K. Wilkner, and T. Brinkmann, "Pilot scale separation of CO_2 from power plant flue gases by membrane technology," *International Journal of Greenhouse Gas Control*, vol. 53, pp. 56–64, 2016, Publisher: Elsevier Ltd, ISSN: 17505836. DOI: 10.1016/j.ijggc.2016.07.033.

[66] M. Sandru, T. J. Kim, W. Capala, M. Huijbers, and M. B. Hägg, "Pilot scale testing of polymeric membranes for CO_2 capture from coal fired power plants," *Energy Procedia*, vol. 37, pp. 6473–6480, 2013, Publisher: Elsevier B.V., ISSN: 18766102. DOI: 10.1016/j.egypro.2013.06.577.

[67] S. Janakiram, A. Lindbråthen, L. Ansaloni, T. Peters, and L. Deng, "Two-stage membrane cascades for post-combustion CO_2 capture using facilitated transport membranes: Importance on sequence of membrane types," *International Journal of Greenhouse Gas Control*, vol. 119, p. 103 698, February 2022, Publisher: Elsevier Ltd, ISSN: 17505836. DOI: 10.1016/j.ijggc.2022.103698.

[68] A. Janusz-Cygan, J. Jaschik, A. Wojdyła, and M. Tańczyk, "The separative performance of modules with polymeric membranes for a hybrid adsorptive/membrane process of CO_2 capture from flue gas," *Membranes*, vol. 10, no. 11, pp. 1–18, 2020, ISSN: 20770375. DOI: 10.3390/membranes10110309.

[69] M. Jaschik, M. Tanczyk, A. Janusz-Cygan, A. Wojdyła, and K. Warmuzinski, "The separation of carbon dioxide from $CO_2/n_2/o_2$ mixtures using polyimide and polysulphone membranes," *Chemical and Process Engineering - Inzynieria Chemiczna i Procesowa*, vol. 39, no. 4, pp. 449–456, 2018, ISSN: 02086425. DOI: 10.24425/122962.

[70] B. Comesaña-Gándara *et al.*, "Redefining the robeson upper bounds for CO_2/CH_4 and CO_2/n_2 separations using a series of ultrapermeable benzotriptycene-based polymers of intrinsic microporosity," *Energy & Environmental Science*, vol. 12, no. 9, pp. 2733–2740, 2019, ISSN: 1754-5692, 1754-5706. DOI: 10.1039/C9EE01384A.

[71] L. M. Robeson, "Correlation of separation factor versus permeability for polymeric membranes," *Journal of Membrane Science*, vol. 62, no. 2, pp. 165–185, Oct. 1991, ISSN: 03767388. DOI: 10.1016/0376-7388(91)80060-J.

[72] F. Scala, A. Lancia, R. Nigro, and G. Volpicelli, "Spray-dry desulfurization of flue gas from heavy oil combustion," *Journal of the Air & Waste Management Association*, vol. 55, no. 1, pp. 20–29, Jan. 2005, ISSN: 1096-2247, 2162-2906. DOI: 10.1080/10473289.2005.10464604.

[73] P. Wattanaphan, T. Sema, R. Idem, Z. Liang, and P. Tontiwachwuthikul, "Effects of flue gas composition on carbon steel (1020) corrosion in MEA-based CO_2 capture process," *International Journal of Greenhouse Gas Control*, vol. 19, pp. 340–349, Nov. 2013, ISSN: 17505836. DOI: 10.1016/j.ijggc.2013.08.021.

[74] M. Liu, M. D. Nothling, S. Zhang, Q. Fu, and G. G. Qiao, "Thin film composite membranes for postcombustion carbon capture: Polymers and beyond," *Progress in Polymer Science*, vol. 126, p. 101 504, 2022, Publisher: Elsevier B.V., ISSN: 00796700. DOI: 10.1016/j.progpolymsci.2022.101504.

[75] L. Mendes, J. L. De Medeiros, R. M. B. Alves, and O. Q. F. Araújo, "Production of methanol and organic carbonates for chemical sequestration of CO_2 from an NGCC power plant," *Clean Technologies and Environmental Policy*, Jan. 24, 2014, ISSN: 1618-954X, 1618-9558. DOI: 10.1007/s10098-014-0712-0.

[76] T. Tabanelli, D. Bonincontro, S. Albonetti, and F. Cavani, "Conversion of CO_2 to valuable chemicals: Organic carbonate as green candidates for the replacement of noxious reactants," in *Studies in Surface Science and Catalysis*, vol. 178, Elsevier, 2019, pp. 125–144, ISBN: 978-0-444-64127-4. DOI: 10.1016/B978-0-444-64127-4.00007-0.

[77] H. Zhang, H.-B. Liu, and J.-M. Yue, "Organic carbonates from natural sources," *Chemical Reviews*, vol. 114, no. 1, pp. 883–898, Jan. 8, 2014, ISSN: 0009-2665, 1520-6890. DOI: 10.1021/cr300430e.

[78] B. Zou and C. Hu, "Halogen-free processes for organic carbonate synthesis from CO_2," *Current Opinion in Green and Sustainable Chemistry*, vol. 3, pp. 11–16, Feb. 2017, ISSN: 24522236. DOI: 10.1016/j.cogsc.2016.10.007.

[79] M. Zhang, M. Xiao, S. Wang, D. Han, Y. Lu, and Y. Meng, "Cerium oxide-based catalysts made by template-precipitation for the dimethyl carbonate synthesis from carbon dioxide and methanol," *Journal of Cleaner Production*, vol. 103, pp. 847–853, Sep. 2015, ISSN: 09596526. DOI: 10.1016/j.jclepro.2014.09.024. Accessed: Aug. 7, 2024.

[80] M. Zhang *et al.*, "Catalytic materials for direct synthesis of dimethyl carbonate (DMC) from CO_2," *Journal of Cleaner Production*, vol. 279, p. 123 344, Jan. 2021, ISSN: 09596526. DOI: 10.1016/j.jclepro.2020.123344. Accessed: Aug. 7, 2024.

[81] X. Xi, A. Pizzi, and L. Delmotte, "Isocyanate-free polyurethane coatings and adhesives from mono- and di-saccharides," *Polymers*, vol. 10, no. 4, p. 402, Apr. 2018, Number: 4 Publisher: Multidisciplinary Digital Publishing Institute, ISSN: 2073-4360. DOI: 10.3390/polym10040402.

[82] X. Xi *et al.*, "Non-isocyanate polyurethane adhesive from sucrose used for particleboard," *Wood Science and Technology*, vol. 53, no. 2, pp. 393–405, Mar. 1, 2019, ISSN: 1432-5225. DOI: 10.1007/s00226-019-01083-2.

[83] D. J. Faria, L. Moreira Dos Santos, F. L. Bernard, I. Selbacch Pinto, M. A. Carmona Da Motta Resende, and S. Einloft, "Dehydrating agent effect on the synthesis of dimethyl carbonate (DMC) directly from methanol and carbon dioxide," *RSC Advances*, vol. 10, no. 57, pp. 34 895–34 902, 2020, ISSN: 2046-2069. DOI: 10.1039/D0RA06034H. Accessed: Aug. 7, 2024.

[84] A. H. Tamboli, A. A. Chaugule, and H. Kim, "Catalytic developments in the direct dimethyl carbonate synthesis from carbon dioxide and methanol," *Chemical Engineering Journal*, vol. 323, pp. 530–544, Sep. 2017, ISSN: 13858947. DOI: 10.1016/j.cej.2017.04.112. Accessed: Aug. 7, 2024.

[85] M. Fan and P. Zhang, "Activated carbon supported k_2CO_3 catalysts for transesterification of dimethyl carbonate with propyl alcohol," *Energy & Fuels*, vol. 21, no. 2, pp. 633–635, Mar. 1, 2007, ISSN: 0887-0624, 1520-5029. DOI: 10.1021/ef060492m.

[86] N. Bragato and G. Fiorani, "Cyclic organic carbonates from furanics: Opportunities and challenges," *Current Opinion in Green and Sustainable Chemistry*, vol. 30, p. 100 479, Aug. 2021, ISSN: 24522236. DOI: 10.1016/j.cogsc.2021.100479.

[87] Y. Nakagawa, M. Honda, and K. Tomishige, "Direct synthesis of organic carbonates from CO_2 and alcohols using heterogeneous oxide catalysts," in *Green Carbon Dioxide*, G. Centi and S. Perathoner, Eds., 1st ed., Wiley, Feb. 28, 2014, pp. 119–148, ISBN: 978-1-118-59088-1 978-1-118-83192-2. DOI: 10.1002/9781118831922.ch5.

[88] E. Lopes, A. Ribeiro, and L. Martins, "New trends in the conversion of CO_2 to cyclic carbonates," *Catalysts*, vol. 10, no. 5, p. 479, Apr. 27, 2020, ISSN: 2073-4344. DOI: 10.3390/catal10050479.

[89] K. Shukla and V. C. Srivastava, "Synthesis of organic carbonates from alcoholysis of urea: A review," *Catalysis Reviews*, vol. 59, no. 1, pp. 1–43, Jan. 2, 2017, ISSN: 0161-4940, 1520-5703. DOI: 10.1080/01614940.2016.1263088.

[90] A.-A. G. Shaikh and S. Sivaram, "Organic carbonates," *Chemical Reviews*, vol. 96, no. 3, pp. 951–976, Jan. 1, 1996, Publisher: American Chemical Society, ISSN: 0009-2665. DOI: 10.1021/cr950067i.

[91] K.-i. Okuyama, J.-i. Sugiyama, R. Nagahata, M. Asai, M. Ueda, and K. Takeuchi, "Oxidative carbonylation of phenol to diphenyl carbonate catalyzed by pd–carbene complexes," *Journal of Molecular Catalysis A: Chemical*, vol. 203, no. 1, pp. 21–27, Sep. 2003, ISSN: 13811169. DOI: 10.1016/S1381-1169(03)00281-4.

[92] W. B. Kim, U. A. Joshi, and J. S. Lee, "Making polycarbonates without employing phosgene: An overview on catalytic chemistry of intermediate and precursor syntheses for polycarbonate," *Industrial & Engineering Chemistry Research*, vol. 43, no. 9, pp. 1897–1914, Apr. 1, 2004, ISSN: 0888-5885, 1520-5045. DOI: 10.1021/ie034004z.

[93] M. Aresta, A. Dibenedetto, and A. Angelini, "Catalysis for the valorization of exhaust carbon: From CO_2 to chemicals, materials, and fuels. technological use of CO_2," *Chemical Reviews*, vol. 114, no. 3, pp. 1709–1742, Feb. 12, 2014, ISSN: 0009-2665, 1520-6890. DOI: 10.1021/cr4002758.

[94] M. Polyakov *et al.*, "Synthesis of dimethyl carbonate from urea and methanol," *DGMK Tagungsbericht*, vol. 2012, pp. 203–209, Jan. 2012.

[95] R. Baan *et al.*, "Carcinogenicity of alcoholic beverages," *The Lancet Oncology*, vol. 8, no. 4, pp. 292–293, Apr. 2007, ISSN: 14702045. DOI: 10.1016/S1470-2045(07)70099-2.

[96] D. W. Lachenmeier *et al.*, "Cancer risk assessment of ethyl carbamate in alcoholic beverages from brazil with special consideration to the spirits cachaça and tiquira," *BMC Cancer*, vol. 10, no. 1, p. 266, Jun. 8, 2010, ISSN: 1471-2407. DOI: 10.1186/1471-2407-10-266.

[97] X. Xiaoding and J. A. Moulijn, "Mitigation of CO_2 by chemical conversion: Plausible chemical reactions and promising products," *Energy & Fuels*, vol. 10, no. 2, pp. 305–325, Mar. 20, 1996, ISSN: 0887-0624, 1520-5029. DOI: 10.1021/ef9501511.

[98] P. P. Pescarmona, "Cyclic carbonates synthesised from CO_2: Applications, challenges and recent research trends," *Current Opinion in Green and Sustainable Chemistry*, vol. 29, p. 100 457, Jun. 2021, ISSN: 24522236. DOI: 10.1016/j.cogsc.2021.100457.

[99] M. Tobiszewski, W. Zabrocka, and M. Bystrzanowska, "Diethyl carbonate as a green extraction solvent for chlorophenol determination with dispersive liquid–liquid microextraction," *Analytical Methods*, vol. 11, no. 6, pp. 844–850, 2019, ISSN: 1759-9660, 1759-9679. DOI: 10.1039/C8AY02683A. Accessed: Aug. 8, 2024.

[100] I. E. Maskat and F. Strain, "Preparation of carbonic acid esters," U.S. Patent 2379250A, Jun. 26, 1945.

[101] B. C. Dunn *et al.*, "Production of diethyl carbonate from ethanol and carbon monoxide over a heterogeneous catalyst," *Energy & Fuels*, vol. 16, no. 1, pp. 177–181, Jan. 1, 2002, Publisher: American Chemical Society, ISSN: 0887-0624. DOI: 10.1021/ef0101816.

[102] S. Xin, L. Wang, H. Li, K. Huang, and F. Li, "Synthesis of diethyl carbonate from urea and ethanol over lanthanum oxide as a heterogeneous basic catalyst," *Fuel Processing Technology*, vol. 126, pp. 453–459, Oct. 1, 2014, ISSN: 0378-3820. DOI: 10.1016/j.fuproc.2014.05.029.

[103] D. Wang, B. Yang, X. Zhai, and L. Zhou, "Synthesis of diethyl carbonate by catalytic alcoholysis of urea," *Fuel Processing Technology*, vol. 88, no. 8, pp. 807–812, Aug. 2007, ISSN: 03783820. DOI: 10.1016/j.fuproc.2007.04.003.

[104] I. Zielinska-Nadolska, K. Warmuzinski, and J. Richter, "Zeolite and other heterogeneous catalysts for the transesterification reaction of dimethyl carbonate with ethanol," *Catalysis Today*, vol. 114, no. 2, pp. 226–230, May 2006, ISSN: 09205861. DOI: 10.1016/j.cattod.2006.01.001.

[105] C. Murugan and H. Bajaj, "Synthesis of diethyl carbonate from dimethyl carbonate and ethanol using KF/al_2o_3 as an efficient solid base catalyst," *Fuel Processing Technology*, vol. 92, no. 1, pp. 77–82, Jan. 2011, ISSN: 03783820. DOI: 10.1016/j.fuproc.2010.08.023.

[106] P. Qiu, L. Wang, X. Jiang, and B. Yang, "Synthesis of diethyl carbonate by the combined process of transesterification with distillation," *Energy & Fuels*, vol. 26, no. 2, pp. 1254–1258, Feb. 16, 2012, ISSN: 0887-0624, 1520-5029. DOI: 10.1021/ef201732w.

[107] P. Qiu, B. Yang, C. Yi, and S. Qi, "Characterization of $KF/\gamma\text{-}al_2o_3$ catalyst for the synthesis of diethyl carbonate by transesterification of ethylene carbonate," *Catalysis Letters*, vol. 137, no. 3, pp. 232–238, Jul. 2010, ISSN: 1011-372X, 1572-879X. DOI: 10.1007/s10562-010-0354-8.

[108] X. Ma, M. Fan, and P. Zhang, "Study on the catalytic synthesis of diethyl carbonate from CO and ethyl nitrite over supported pd catalysts," *Catalysis Communications*, vol. 5, no. 12, pp. 765–770, Dec. 2004, ISSN: 15667367. DOI: 10.1016/j.catcom.2004.09.013.

[109] C. Hao, S. Wang, and X. Ma, "Gas phase decarbonylation of diethyl oxalate to diethyl carbonate over alkali-containing catalyst," *Journal of Molecular Catalysis A: Chemical*, vol. 306, no. 1, pp. 130–135, Jul. 2009, ISSN: 13811169. DOI: 10.1016/j.molcata.2009.02.038.

[110] K. Shukla and V. C. Srivastava, "Synthesis of diethyl carbonate from ethanol through different routes: A thermodynamic and comparative analysis," *The Canadian Journal of Chemical Engineering*, vol. 96, no. 1, pp. 414–420, Jan. 2018, ISSN: 0008-4034, 1939-019X. DOI: 10.1002/cjce.22896. Accessed: Aug. 8, 2024.

[111] N. O. o. D. a. Informatics, *NIST chemistry WebBook*, Publisher: National Institute of Standards and Technology. DOI: https://doi.org/10.18434/T4D303. Accessed: Nov. 25, 2024. [Online]. Available: https://webbook.nist.gov/chemistry/.

[112] "Cheméo," Cheméo, Accessed: Nov. 25, 2024. [Online]. Available: https://www.chemeo.com/.

[113] S. Pandey, V. C. Srivastava, and V. Kumar, "Comparative thermodynamic analysis of CO_2 based dimethyl carbonate synthesis routes," *The Canadian Journal of Chemical Engineering*, vol. 99, no. 2, pp. 467–478, Feb. 2021, ISSN: 0008-4034, 1939-019X. DOI: 10.1002/cjce.23893.

[114] F. Comelli, A. Bigi, D. Vitalini, and K. Rubini, "Densities, viscosities, refractive indices, and heat capacities of poly(ethylene glycol-*ran*-propylene glycol) + esters of carbonic acid at (293.15 and 313.15) k and at atmospheric pressure," *Journal of Chemical & Engineering Data*, vol. 55, no. 1, pp. 205–210, Jan. 14, 2010, ISSN: 0021-9568, 1520-5134. DOI: 10.1021/je900307z.

[115] E. Leino *et al.*, "Enhanced yields of diethyl carbonate via one-pot synthesis from ethanol, carbon dioxide and butylene oxide over cerium (IV) oxide," *Chemical Engineering Journal*, vol. 176-177, pp. 124–133, Dec. 2011, ISSN: 13858947. DOI: 10.1016/j.cej.2011.07.054.

[116] M. Buchmann, M. Lucas, and M. Rose, "Catalytic CO_2 esterification with ethanol for the production of diethyl carbonate using optimized CeO_2 as catalyst," *Catalysis Science & Technology*, vol. 11, no. 5, pp. 1940–1948, 2021, ISSN: 2044-4753, 2044-4761. DOI: 10.1039/D0CY01793K.

[117] O. Arbeláez, A. Orrego, F. Bustamante, and A. L. Villa, "Direct synthesis of diethyl carbonate from CO_2 and CH_3CH_2OH over cu-ni/AC catalyst," *Topics in Catalysis*, vol. 55, no. 7, pp. 668–672, Jul. 27, 2012, Publisher: Springer, ISSN: 10225528. DOI: 10.1007/S11244-012-9849-4/FIGURES/7. Accessed: Feb. 9, 2023.

[118] Y. Yoshida, Y. Arai, S. Kado, K. Kunimori, and K. Tomishige, "Direct synthesis of organic carbonates from the reaction of CO2 with methanol and ethanol over CeO2 catalysts," *Catalysis Today*, vol. 115, no. 1, pp. 95–101, Jun. 2006, ISSN: 09205861. DOI: 10.1016/j.cattod.2006.02.027.

[119] A. Dibenedetto, M. Aresta, A. Angelini, J. Ethiraj, and B. M. Aresta, "Synthesis, characterization, and use of nb^{V}/ce^{IV}-mixed oxides in the direct carboxylation of ethanol by using pervaporation membranes for water removal," ISBN: 0805443606. DOI: 10.1002/chem.201201561. Accessed: Apr. 5, 2024.

[120] E. Leino *et al.*, "Influence of the synthesis parameters on the physico-chemical and catalytic properties of cerium oxide for application in the synthesis of diethyl carbonate," *Materials Chemistry and Physics*, vol. 143, no. 1, pp. 65–75, Dec. 2013, ISSN: 02540584. DOI: 10.1016/j.matchemphys.2013.08.012.

[121] G. G. Giram, V. V. Bokade, and S. Darbha, "Direct synthesis of diethyl carbonate from ethanol and carbon dioxide over ceria catalysts," *New Journal of Chemistry*, vol. 42, no. 21, pp. 17 546–17 552, 2018, Publisher: Royal Society of Chemistry, ISSN: 1144-0546, 1369-9261. DOI: 10.1039/C8NJ04090G. Accessed: Aug. 7, 2024.

[122] O. Arbeláez, A. Orrego, F. Bustamante, and A. L. Villa, "Effect of acidity, basicity and ZrO_2 phases of cu–ni/ZrO_2 catalysts on the direct synthesis of diethyl carbonate from CO_2 and ethanol," *Catalysis Letters*, vol. 146, no. 4, pp. 725–733, Apr. 2016, ISSN: 1011-372X, 1572-879X. DOI: 10.1007/s10562-016-1699-4. Accessed: Aug. 8, 2024.

[123] M. Zhang, "Product yield increasing more than 20 times achieved by reducing water poisoning for direct diethyl carbonate synthesis," *Langmuir*, vol. 40, no. 6, pp. 3125–3132, Feb. 13, 2024, ISSN: 0743-7463, 1520-5827. DOI: 10.1021/acs.langmuir.3c03547. Accessed: Aug. 8, 2024.

[124] I. Prymak, V. N. Kalevaru, S. Wohlrab, and A. Martin, "Continuous synthesis of diethyl carbonate from ethanol and CO_2 over ce–zr–o catalysts," *Catalysis Science & Technology*, vol. 5, no. 4, pp. 2322–2331, 2015, ISSN: 2044-4753, 2044-4761. DOI: 10.1039/C4CY01400F. Accessed: Aug. 7, 2024.

[125] E. Leino *et al.*, "Synthesis and characterization of ceria-supported catalysts for carbon dioxide transformation to diethyl carbonate," *Catalysis Today*, vol. 306, pp. 128–137, May 2018, ISSN: 09205861. DOI: 10.1016/j.cattod.2017.01.016. Accessed: Aug. 7, 2024.

[126] W. Wang, S. Wang, X. Ma, and J. Gong, "Crystal structures, acid–base properties, and reactivities of $ce_xzr_{1-x}o_2$ catalysts," *Catalysis Today*, vol. 148, no. 3, pp. 323–328, Nov. 2009, ISSN: 09205861. DOI: 10.1016/j.cattod.2009.07.090.

[127] F. Gasc, S. Thiebaud-Roux, and Z. Mouloungui, "Methods for synthesizing diethyl carbonate from ethanol and supercritical carbon dioxide by one-pot or two-step reactions in the presence of potassium carbonate," *The Journal of Supercritical Fluids*, vol. 50, no. 1, pp. 46–53, Aug. 2009, ISSN: 08968446. DOI: 10.1016/j.supflu.2009.03.008.

[128] M. Décultot, A. Ledoux, M. C. Fournier-Salaün, and L. Estel, "Organic carbonates synthesis improved by pervaporation for CO_2 utilisation," *Green Processing and Synthesis*, vol. 8, no. 1, pp. 496–506, Jan. 28, 2019, Publisher: De Gruyter Open Ltd, ISSN: 21919550. DOI: 10.1515/GPS-2019-0018/MACHINEREADABLECITATION/RIS. Accessed: Apr. 8, 2024.

[129] M. Honda, M. Tamura, Y. Nakagawa, K. Nakao, K. Suzuki, and K. Tomishige, "Organic carbonate synthesis from CO_2 and alcohol over CeO_2 with 2-cyanopyridine: Scope and mechanistic studies," *Journal of Catalysis*, vol. 318, pp. 95–107, Oct. 2014, ISSN: 00219517. DOI: 10.1016/j.jcat.2014.07.022.

[130] W. S. Putro *et al.*, "Sustainable synthesis of diethyl carbonate from carbon dioxide and ethanol featuring acetals as regenerable dehydrating agents," *RSC Sustainability*, vol. 2, no. 5, pp. 1613–1620, 2024, ISSN: 2753-8125. DOI: 10.1039/D3SU00367A.

[131] T. Chang *et al.*, "An effective combination catalyst of CeO_2 and zeolite for the direct synthesis of diethyl carbonate from CO_2 and ethanol with 2,2-diethoxypropane as a dehydrating agent," *Green Chemistry*, vol. 22, no. 21, pp. 7321–7327, 2020, ISSN: 1463-9262, 1463-9270. DOI: 10.1039/D0GC02717K.

[132] M. F. O'Neill, M. Sankar, and U. Hintermair, "Sustainable synthesis of dimethyl- and diethyl carbonate from CO_2 in batch and continuous flow—lessons from thermodynamics and the importance of catalyst stability," *ACS Sustainable Chemistry & Engineering*, vol. 10, no. 16, pp. 5243–5257, Apr. 25, 2022, ISSN: 2168-0485, 2168-0485. DOI: 10.1021/acssuschemeng.2c00291.

[133] N. Asprion and M. Bortz, "Process modeling, simulation and optimization: From single solutions to a multitude of solutions to support decision making," *Chemie Ingenieur Technik*, vol. 90, no. 11, pp. 1727–1738, Nov. 1, 2018, Publisher: John Wiley & Sons, Ltd, ISSN: 1522-2640. DOI: 10.1002/CITE.201800051.

[134] A. D. Kamkeng, M. Wang, J. Hu, W. Du, and F. Qian, "Transformation technologies for CO_2 utilisation: Current status, challenges and future prospects," *Chemical Engineering Journal*, vol. 409, p. 128 138, Apr. 2021, ISSN: 13858947. DOI: 10.1016/j.cej.2020.128138.

[135] D. Chuquin-Vasco, F. Parra, N. Chuquin-Vasco, J. Chuquin-Vasco, and V. Lo-Iacono-Ferreira, "Prediction of methanol production in a carbon dioxide hydrogenation plant using neural networks," *Energies*, vol. 14, no. 13, p. 3965, Jan. 2021, Number: 13 Publisher: Multidisciplinary Digital Publishing Institute, ISSN: 1996-1073. DOI: 10.3390/en14133965.

[136] B. Varandas, M. Oliveira, C. Andrade, and A. Borges, "Thermodynamic equilibrium analysis of CO2 methanation through equilibrium constants: A comparative simulation study," *Physchem*, vol. 4, no. 3, pp. 258–271, Sep. 2024, Number: 3 Publisher: Multidisciplinary Digital Publishing Institute, ISSN: 2673-7167. DOI: 10.3390/physchem4030018.

[137] C. Otto and T. Kempka, "Synthesis gas composition prediction for underground coal gasification using a thermochemical equilibrium modeling approach," *Energies*, vol. 13, no. 5, p. 1171, Jan. 2020, Number: 5 Publisher: Multidisciplinary Digital Publishing Institute, ISSN: 1996-1073. DOI: 10.3390/en13051171.

[138] I. Vorrias, K. Atsonios, A. Nikolopoulos, N. Nikolopoulos, P. Grammelis, and E. Kakaras, "Calcium looping for CO2 capture from a lignite fired power plant," *Fuel*, vol. 113, pp. 826–836, Nov. 1, 2013, ISSN: 0016-2361. DOI: 10.1016/j.fuel.2012.12.087.

[139] Y. Tan, W. Nookuea, H. Li, E. Thorin, and J. Yan, "Property impacts on carbon capture and storage (CCS) processes: A review," *Energy Conversion and Management*, vol. 118, pp. 204–222, Jun. 2016, ISSN: 01968904. DOI: 10.1016/j.enconman.2016.03.079.

[140] H.-M. Wei, Q. Gao, W.-z. Jiao, and W. Wei, "Dynamic simulation and control of a triple column process for dimethyl carbonate-methanol separation," *Korean Journal of Chemical Engineering*, vol. 39, no. 12, pp. 3190–3203, Dec. 2022, ISSN: 0256-1115, 1975-7220. DOI: 10.1007/s11814-022-1259-0.

[141] M. Ni, "2d thermal modeling of a solid oxide electrolyzer cell (SOEC) for syngas production by h_2o/CO_2 co-electrolysis," *International Journal of Hydrogen Energy*, III Iberian Symposium on Hydrogen, Fuel Cells and Advanced Batteries, HYCELTEC-2011, vol. 37, no. 8, pp. 6389–6399, Apr. 1, 2012, ISSN: 0360-3199. DOI: 10.1016/j.ijhydene.2012.01.072.

[142] A. Zachopoulos and E. Heracleous, "Overcoming the equilibrium barriers of CO_2 hydrogenation to methanol via water sorption: A thermodynamic analysis," *Journal of CO2 Utilization*, vol. 21, pp. 360–367, Oct. 2017, Publisher: Elsevier BV, ISSN: 2212-9820. DOI: 10.1016/j.jcou.2017.06.007.

[143] K. Al-Ali, S. Kodama, and H. Sekiguchi, "Modeling and simulation of methane dry reforming in direct-contact bubble reactor," *Solar Energy*, vol. 102, pp. 45–55, Apr. 2014, ISSN: 0038092X. DOI: 10.1016/j.solener.2014.01.010.

[144] D. Zhang, E. A. D.-R. Chanona, V. S. Vassiliadis, and B. Tamburic, "Analysis of green algal growth via dynamic model simulation and process optimization," *Biotechnology and Bioengineering*, vol. 112, no. 10, pp. 2025–2039, Oct. 2015, Publisher: Wiley, ISSN: 0006-3592, 1097-0290. DOI: 10.1002/bit.25610.

[145] X. Hu, H. Cheng, X. Kang, L. Chen, X. Yuan, and Z. Qi, "Analysis of direct synthesis of dimethyl carbonate from methanol and CO_2 intensified by in-situ hydration-assisted reactive distillation with side reactor," *Chemical Engineering and Processing - Process Intensification*, vol. 129, pp. 109–117, Jul. 2018, Publisher: Elsevier BV, ISSN: 0255-2701. DOI: 10.1016/j.cep.2018.05.007.

[146] A. K. Verma, *Process Modelling and Simulation in Chemical, Biochemical and Environmental Engineering*. Boca Raton: CRC Press, Oct. 27, 2014, 424 pp., ISBN: 978-0-429-09069-1. DOI: 10.1201/b17595.

[147] Chantasiriwan Somchart, "Simulation and optimization of vapor absorption refrigeration system using dwsim," *Chemical Engineering Transactions*, vol. 100, pp. 613–618, Jun. 2023. DOI: 10.3303/CET23100103.

[148] M. Shalygin, S. Abramov, A. Netrusov, and V. Teplyakov, "Membrane recovery of hydrogen from gaseous mixtures of biogenic and technogenic origin," *International Journal of Hydrogen Energy*, vol. 40, no. 8, pp. 3438–3451, Mar. 2015, ISSN: 03603199. DOI: 10.1016/j.ijhydene.2014.12.078. Accessed: Aug. 7, 2024.

[149] I. C. A. Montoya, J. M. González, and A. L. Villa, "Liquid–liquid equilibrium for the water + diethyl carbonate + ethanol system at different temperatures," *Journal of Chemical & Engineering Data*, vol. 57, no. 6, pp. 1708–1712, Jun. 14, 2012, ISSN: 0021-9568, 1520-5134. DOI: 10.1021/je300094j.

[150] M. Fu, Y. Chen, and H. Jinghua. "Measurement of liquid–liquid equilibria for ternary mixtures with diethyl carbonate or methyl *tert*-butyl ether," Measurement of liquid–liquid equilibria for ternary mixtures with diethyl carbonate or methyl tert-butyl ether. Oct. 1, 2008 Vol.10 No.10 P.48 Copyright, Accessed: Nov. 4, 2024. [Online]. Available: https://www.mdpi.org/cji/cji/2008/10a048pe.htm.

[151] S. Raiguel, L. Gijsemans, A. Van Den Bossche, B. Onghena, and K. Binnemans, "Solvent extraction of gold(III) with diethyl carbonate," *Cite This: ACS Sustainable Chem. Eng*, vol. 8, pp. 13 713–13 723, 2020. DOI: 10.1021/acssuschemeng.0c04008. Accessed: Apr. 5, 2023.

[152] K. Aziaba, F. M. Mozina, M. Teufner-Kabas, F. Kabas, C. Jordan, and M. Harasek, "Stability of diethyl carbonate in the presence of acidic and basic solvents," *Chemical Engineering Transactions*, vol. 105, pp. 163–168, Nov. 30, 2023, ISSN: 2283-9216. DOI: 10.3303/CET23105028. Accessed: Aug. 7, 2024.

[153] K. Aziaba *et al.*, "Dehydration by pervaporation of an organic solution for the direct synthesis of diethyl carbonate," *Separations*, vol. 11, no. 10, p. 289, Oct. 10, 2024, ISSN: 2297-8739. DOI: 10.3390/separations11100289.

[154] K. Aziaba, C. Jordan, B. Haddadi, and M. Harasek, "Design of a gas permeation and pervaporation membrane model for an open source process simulation tool," *Membranes*, vol. 12, no. 12, p. 1186, Dec. 2022, Number: 12 Publisher: Multidisciplinary Digital Publishing Institute, ISSN: 2077-0375. DOI: 10.3390/membranes12121186. Accessed: Aug. 7, 2024.

[155] K. Aziaba, B. D. Weiss, V. Illyes, C. Jordan, M. Haider, and M. Harasek, "High purity hydrogen from liquid NH_3 - proposal and evaluation of a process chain," *Chemical Engineering Transactions*, vol. 96, pp. 169–174, Nov. 30, 2022, ISSN: 2283-9216. DOI: 10.3303/CET2296029. Accessed: Aug. 7, 2024.

[156] M. Teufner-Kabas *et al.*, "Verfahren zur herstellung organischer carbonate," pat. AT527086A1, Oct. 15, 2024.

CHEMICAL ENGINEERING TRANSACTIONS
VOL. 105, 2023
A publication of AIDIC
The Italian Association of Chemical Engineering
Online at www.cetjournal.it
Guest Editors: David Bogle, Flavio Manenti, Piero Salatino

ISBN 979-12-81206-04-5; **ISSN** 2283-9216
DOI: 10.3303/CET23105028

Stability of Diethyl Carbonate in the Presence of Acidic and Basic Solvents

Kouessan Aziaba[a,*], Florian M. Možina[a], Magdalena Teufner-Kabas[b], Florian Kabas[b], Christian Jordan[a], Michael Harasek[a]

[a] Thermal Process Engineering - Computational Fluid Dynamics, Institute of Chemical, Environmental & Bioscience Engineering, TU Wien, Getreidemarkt 9, 1060 Vienna, Austria
[b]kleinkraft OG, Turnergasse 27/5, 1150 Vienna, Austria
kouessan.aziaba@tuwien.ac.at

Reducing carbon dioxide (CO_2) emissions is an inevitable measure for fighting anthropogenic climate change. Carbon Capture and Utilization (CCU) technologies are gaining rising attention as an additional contributor to reaching the Paris Agreement goals. Giving CO_2 a value as a feedstock to be refined into chemicals to be used in industry is a crucial aspect of making these technologies interesting for vast industrial sectors. The synthesis of diethyl carbonate (DEC) is recognized as a promising prospect for the successful implementation of CCU. DEC is considered a fully biodegradable, low-toxic solvent, which can be synthesized from CO_2 and ethanol in the presence of a catalyst. DEC may be a non-toxic alternative to other solvents such as toluene or methyl isobutyl ketone (MIBK).
The optimization of DEC synthesis is one aspect that is under investigation today. For the exploration of DEC's applicability, an extensive amount of data is beneficial. Many applications of solvents involve the presence of acids and bases. Hence, an interest in DEC in various environments is reasonable. The decomposition of DEC after contact with water, different acids and bases at room temperature, and the boiling point was determined experimentally to characterize chemical stability. Further, the influence of sodium chloride and a cerium-based catalyst used in DEC synthesis was investigated.

1. Introduction

The application of CO_2-refinery processes is considered an essential contribution towards more sustainable strategies in the chemical industry. As a part of CO_2-refinery, CCU re-introduces carbon dioxide back into industrial cycles and is regarded as a promising tool in fighting anthropogenic climate change. The direct synthesis of DEC is considered to be a promising product of such an application which uses CO_2 as a feedstock. Another commonly positively perceived property of the reaction is the fact that the side product is water. The reaction of the direct synthesis of DEC is portrayed in equation 1.

$$C_2H_5OH + CO_2 \leftrightarrow C_5H_{10}O_3 + H_2O \quad (1)$$

DEC is currently used in lithium-ion batteries, organic synthesis and extraction procedures and has also been used in combustion engines, successfully reducing emissions.(Shukla and Srivastava, 2016) However, new applications for DEC must be further investigated to exploit its full potential as a green chemical. Many physical and chemical properties have already been described, but data about chemical stability is limited.(Huang *et al.*, 2015) One weakness of DEC is its susceptibility to hydrolysis under acid or alkaline conditions. An extraction process for phenol recovery from coal tar processing was developed. (Yang *et al.*, 2020) applying DEC to recover phenols from coal tar processing wastewater from an alkaline stripping solution. However, the stripping process is limited to about 8 minutes due to the imminent degradation of DEC in the organic phase. Experimental data on DEC decomposition after exposure to different aqueous phases of various acidities were reported by Raiguel et al. (Raiguel *et al.*, 2020). A "salting out"-effect was described. Dissolved inorganic salts like NaCl in an aqueous phase are observed to stabilize DEC. Due to the decrease in solubility, hydrolysis is slowed down.

Paper Received: 22 February 2023; Revised: 2 April 2023; Accepted: 27 April 2023
Please cite this article as: Aziaba K., Mozina F.M., Teufner-Kabas M., Kabas F., Jordan C., Harasek M., 2023, Stability of Diethyl Carbonate in the Presence of Acidic and Basic Solvents, Chemical Engineering Transactions, 105, 163-168 DOI:10.3303/CET23105028

The decomposition of DEC is mainly dominated by its acid- or base-catalyzed hydrolysis leading to the main reaction products carbon dioxide and ethanol. Other degradation mechanisms have also been observed since diethyl ether and chloroethane were detected as reaction products. Al-Shamary et al. (2017) investigated multiple dialkyl carbonates, observing an enhancement of the degradation in the presence of cationic micelles (Al-Shamary *et al.*, 2017). Anionic micelles are reported to reduce hydrolysis rates. To pave the way for further research about applications for DEC, this work focuses on the chemical stability of DEC after being in contact with various acidic and basic solutions. The presence of CeO_2, a catalyst, as well as the presence of NaCl shall also be monitored.

2. Materials and Methods

Different acids (HCl, H_2SO_4, H_3PO_4, formic acid, acetic acid) and bases (NaOH, KOH, Na_2CO_3) have been obtained for the investigations. DEC degradation has been calculated according to equation 2.

$$Degradation\ [\%] = \frac{m_{DEC,0} - m_{DEC}}{m_{DEC,0}} * 100 \quad (2)$$

The experimentally determined data shall be accompanied with theoretical ethanol (EtOH) formation and mass loss due to CO_2. The theoretical ethanol formation was calculated according to equation 3.

$$m_{EtOH,theoretical} = \frac{m_{DEC,0} - m_{DEC}}{M_{DEC}} * 2 * M_{EtOH} \quad (3)$$

CeO_2 which is used in the direct synthesis of DEC from CO_2 as a catalyst, is neither soluble in water nor DEC. However, no data about its interference with DEC degradation was available (Giram et al., 2018). 3ml of DEC were mixed with each of these solutions with a volume ratio of 1:1. When a two-phase system developed, phases were separated at the end of the experiment. Afterwards, DEC and EtOH were quantified with a GC-FID (gas chromatograph equipped with a flame ionization detector) as described in 2.2. It was assumed that DEC evaporation loss was negligible due to its high boiling point. For each substance, four experiments were carried out at ambient pressure, which differed in temperature and the presence or absence of 0,125 g of CeO_2. The influence of sodium chloride (NaCl) dissolved in the aqueous phase on chemical stability was investigated with the same solutions as above, except for HCOOH which was used as a pure compound. NaCl concentration in the aqueous phase was 250 g/l. The resulting phases were filtered before every analysis if a catalyst was applied. The net weight of the mixture before and after the experiment was documented. When the catalyst was present, it was assumed that it accumulated only in the aqueous phase. If a separation of the product into two phases was observed, it was necessary to collect three samples of each product containing a sample of the aqueous, organic and a mixture of both phases. Emulsions were drawn into a syringe to rest for 15 minutes until phase separation had taken place.

2.1 Materials

The experiments were carried out in three-neck round bottom flasks equipped with glass plugs and thermometers. The thermometers were inserted through a septum into the sample in the flask. The flasks were placed in an aluminum bowl filled with a sand bed to enable a homogeneous heat transfer. The samples were stirred with a magnetic stirrer for 24 (HCOOH for 64) hours and, if necessary, heated to boiling point through a sand bed. To prevent losses due to evaporation, a Liebig cooler was installed. A thermometer was connected, and the boiling temperature was read as soon as reflux occurred and the cooler's inner surface.
Diethyl carbonate (DEC, 99,9 %) was purchased from Carl Roth. Phosphoric acid (H_3PO_4, p.a., Lachema), fuming hydrochloric acid (HCl, 37 %, Sigma-Aldrich), potassium hydroxide (KOH, Neuber's Enkel), formic acid (HCOOH, >= 99 %, Merck), and acetic acid (HAc, 99,8 %, EMD Millipore) were obtained and solved in water to mix 0.5 M solutions of each compound. Potassium hydroxide (KOH, platelets), sodium carbonate (NaOH, beads), sodium chloride (NaCl, grains) and sulphuric acid (H_2SO_4) were obtained from the in-house laboratory stock and diluted in H_2O to form 0.5 molar solutions as well. HCOOH and HAc were also applied as pure compounds additionally.

2.2 Analytics

Gas chromatography coupled with a flame ionization detector (GC-FID) was used to analyze the samples. GC-FIDs are highly reliable analytic instruments for the purpose of detection and quantification of volatile organics. Samples were injected automatized from an autosampler (AOC 5000, Shimadzu), and 0,5 µl was set as the injection volume. Each sample was measured once. Dioxane was injected regularly before and between measurements to minimize carryover from the injector and column. Calibration curves for the quantification of DEC and ethanol were prepared by analyzing standards containing DEC and EtOH.

3. Results

3.1 Experiments

All chromatogram peaks have been checked manually and assigned to a substance by retention time for qualitative information about chemical stability. For quantitative information about chemical stability, the degradation of DEC was determined. The formation of EtOH as a decomposition product was considered unsuitable for the characterization of chemical stability because evaporation losses occurred during experiments. As documented in Figure 1, it can be seen that DEC may be involved in a reverse reaction with H_2O as described in the introduction.

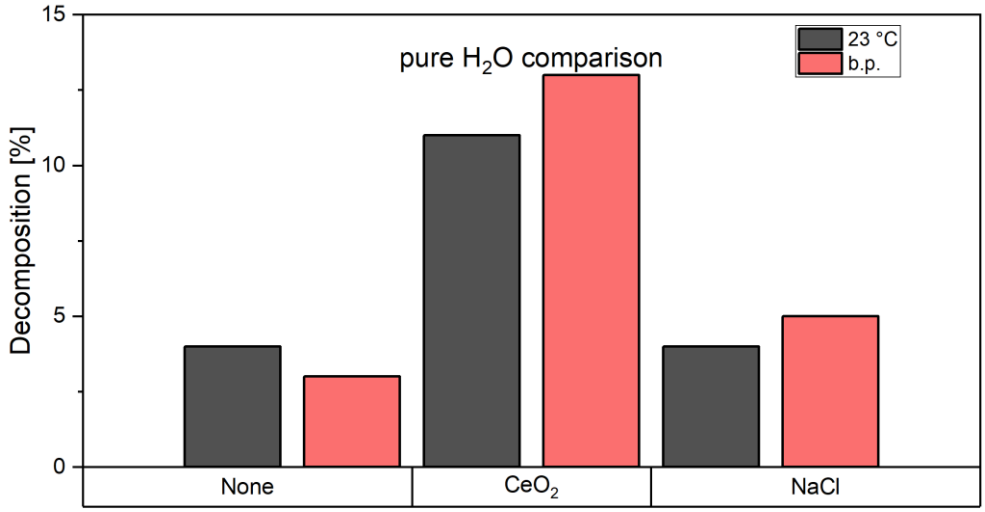

Figure 1: DEC degradation of a binary DEC-Water system in dependence on added CeO_2 or NaCl

Temperature does not seem to have a significant effect on the decomposition of DEC as long as there is no CeO_2 involved. Mentioning the catalyst CeO_2, the simultaneous presence of it and elevated temperatures seem to boost the degradation of DEC on a comparably low scale. Even though NaCl is added to prevent decomposition processes, it becomes lightly visible that this effect is observed to be inverse at elevated temperatures. It is not clear why the decomposition of DEC is enhanced in this case. This may be connected with the difference in the boiling points which also vary due to the different mixtures. Therefore, more experiments with varied amounts of salt would be required. The presence of acidic compounds in the solution reveals a different dynamic which is portrayed in Figure 2.

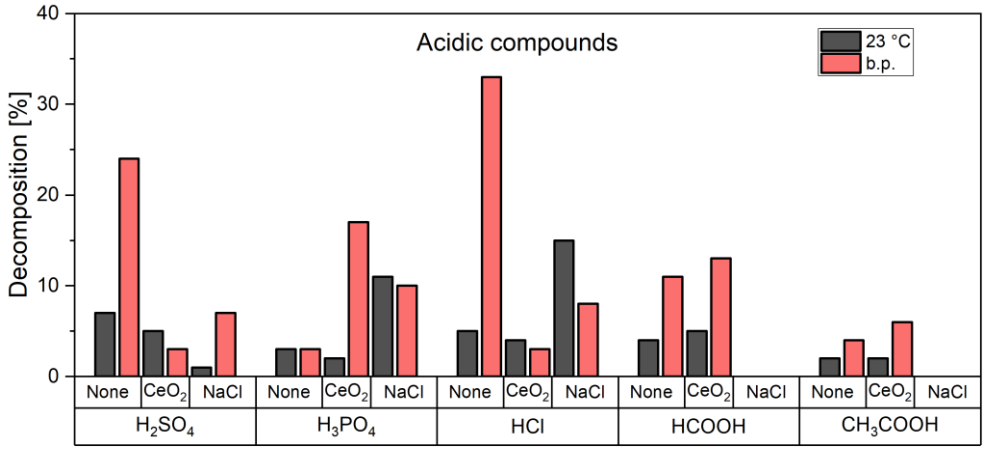

Figure 2: DEC degradation of a binary DEC-Acid (0.5 M) system in dependence of added CeO_2 or NaCl with H_2SO_4, H_3PO_4, HCl, HCOOH and HAc used as acids

The highest degradation is observed to occur in contact with HCl, followed H_2SO_4, H_3PO_4, HCOOH and HAc in a decreasing sequence. The values pK_A and pK_B (acid dissociation- and base dissociation constant) are

commonly accessed parameters to obtain an enhanced understanding of a solution's acidiy and basicity. Therefore, it is also consulted to observe DEC's degradation in the presence of acids and bases. Comparing DEC's degradation in contact with the acids mentioned earlier with the pK_A – values from the literature reveals that the degradation at higher temperatures follows the same trend as the pK_A – value (Trygg et al., 2016). The influence of CeO_2 and NaCl does not seem to follow any trends or patterns since it appears to be quite arbitrarily which reagent delivers the strongest decomposition in contact with DEC. Starting with H_3PO_4, which mainly shows the highest degradation of DEC in the presence of salt, increasing the temperature seems to improve the activity of the catalyst and increases the DEC degradation. Interestingly, the same effect is not seen in the same way with any of the other tested acidic compounds. The comparably weaker organic acids HCOOH and HAc deliver lightly higher degradations of both – ambient temperature and on the b.p. (boiling point) if CeO_2 is used. The application seems to avoid degradation completely. The general effect observed on the contact of DEC with acidic compounds is a comparably fair degradation where no presence of a catalyst is needed. The presence of salt, which shall incorporate an inhibitor's function as mentioned in 1.1., seems indifferent to the various acidic compounds. Similar to the presence of NaCl in binary DEC solutions with water it is unclear why no trend was observed. Therefore, further investigation with various acid concentrations and amounts of NaCl would be necessary. With many possible applications to be carried out in an alkaline environment the interest into the influence of basic compounds on DEC was present as well. Therefore, the recorded results are displayed in Figure 3.

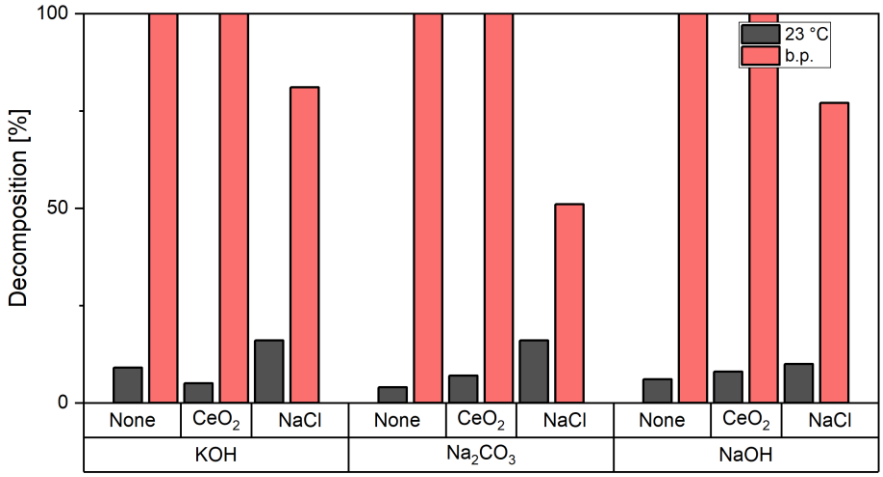

Figure 3: DEC degradation of a binary DEC-base (0.5 M) system in dependence of added CeO_2 or NaCl with KOH, NaOH and Na_2CO_3 used as acids

The decomposition of DEC already takes place at ambient temperatures. Even though the presence of CeO_2 and NaCl seems to have a moderate influence, it is not easily determined in which direction the trend of their effect leads. Temperature appears to be the most influential parameter for the decomposition of DEC. It can be stated that the exposure of DEC with all applied basic compounds leads to a complete decomposition that could be partially prevented with NaCl. The decomposition seems also to follow the trend following the pK_B-values of which KOH's and NaOH's pK_B-values are comparably low over the one of Na_2CO_3. NaCl usually dissolves in a fully solvated state in water. Comparably strong ions Na^+ and Cl^- may attract some of the water molecules, leaving fewer molecules behind. This results in limited availability of water to hydrolyze DEC. (Raiguel *et al.*, 2020)

3.2 Ethanol losses

The mass losses during the experiments were recorded and are displayed in Figure 4. Since the majority of the mass loss was associated with ethanol losses, the losses due to CO_2 were neglected.

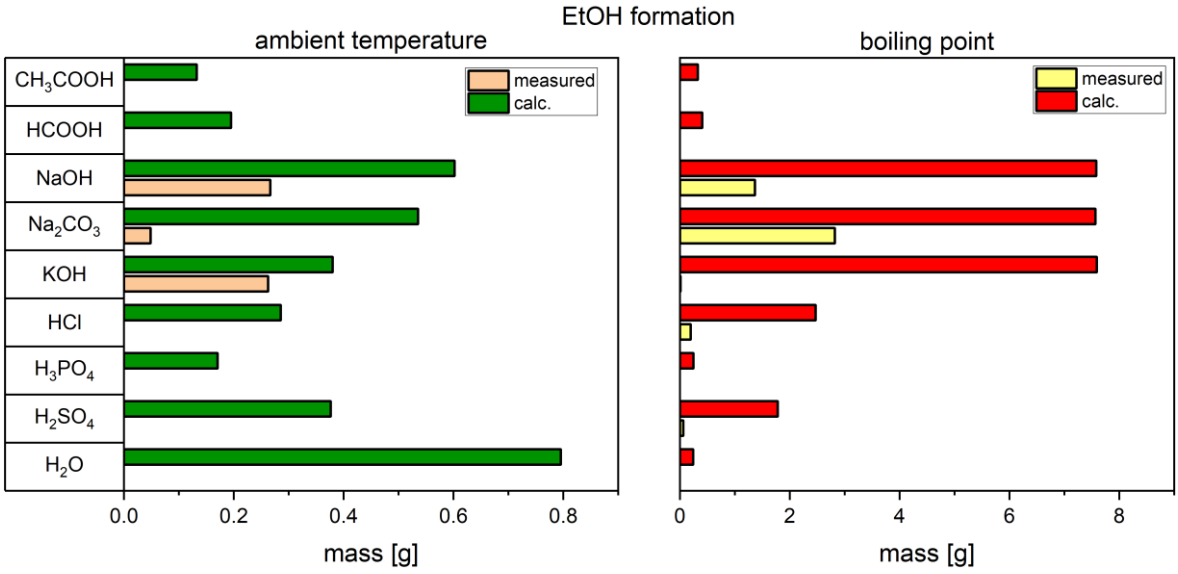

Figure 4: calculated theoretical and measured EtOH formation after experiments with various chemicals on ambient and elevated temperatures

The low boiling point of ethanol was estimated to be the reason for this. It was assumed for calculations that DEC loss was negligible since DEC has a higher boiling point than water and ethanol. However, this assumption is most likely not exact. Consequently, results are estimated to be influenced by an unknown error.

4. Conclusions

The experimental trial has clearly shown that decomposition of DEC can occur in various settings. At low temperatures degradation of DEC does not follow any obvious trends. However, the degradation mostly accelerated significantly at higher temperatures. The influence of catalyst was rather random and requires more experiments to be described in more detail. Enhanced chemical stability by adding NaCl was observed at high levels of DEC degradation, the influence of salt at lower degradation rates fluctuated. The expressiveness of the results for quantitative information about chemical stability are limited due to the rather facile setup and limited number of experiments. Exchanging the setup with a tightly sealed system which can also be exposed to elevated pressure, could have improved the expressiveness of the results but would also create the necessity for further possibly complex equipment such as a level sensor. Nevertheless, it was still possible to obtain information about DEC's behavior in acidic and basic solutions. DEC is apparently more susceptible to base-catalyzed than acid-catalyzed hydrolysis. The strength of the acid or base increased DEC degradation at boiling temperature. Nonetheless, since the decomposition products of DEC are mostly considered to be CO_2 and water, the effort which must be taken to cope with the resulting compounds is comparably low. Further, the idea of a reduction of the decomposition considering the limited availability of water for a reverse reaction fuels the idea that DEC may be a promising alternative to other electrolyte additives.

Nomenclature

b.p. – boiling point
FID – flame ionization detector
GC – gas chromatograph
pK_A – acid dissociation constant
pK_B – base dissociation constant
CeO_2 – cerium oxide
DEC – diethyl carbonate
HAc – acetic acid
HCl – hydrochloric acid
HCOOH – formic acid
H_2O – water
H_2SO_4 – sulfuric acid
H_3PO_4 – phosphoric acid
KOH – potassium hydroxide
NaCl – sodium chloride
Na_2CO_3 – sodium carbonate
NaOH – sodium hydroxide
$m_{EtOH,\ theoretical}$ – calculated mass EtOH, g
m_{DEC} – mass of DEC after experiment, g
$m_{DEC,\ 0}$ – mass of DEC fed to experiment, g
$m_{EtOH,\ theoretical}$ – ambient temperature, K
M_{EtOH} – molar mass of EtOH, g/mol
$m_{DEC,\ 0}$ – molar mass of DEC, g/mol

Acknowledgments

This research was subsidized by city of Vienna funds via the Vienna Business Agency (WAW), grant number 2761267. Further, the authors acknowledge the funding support of K1-MET GmbH, metallurgical competence center. The research program of the K1-MET competence center is supported by COMET (Competence Center for Excellent Technologies), the Austrian program for competence centers. COMET is funded by the Federal Ministry for Transport, Innovation, and Technology; the Federal Ministry for Digital and Economic Affairs; the provinces of Upper Austria, Tyrol, and Styria; and the Styrian Business Promotion Agency (SFG).

References

Al-Shamary, M.N. *et al.* (2017) 'Micellar effect upon the rate of alkaline hydrolysis of carboxylic and carbonate esters', *Journal of Saudi Chemical Society*, 21, pp. S193–S201. doi:10.1016/J.JSCS.2014.01.002.

Giram, G.G., Bokade, V. V. and Darbha, S. (2018) 'Direct synthesis of diethyl carbonate from ethanol and carbon dioxide over ceria catalysts', *New Journal of Chemistry*, 42(21), pp. 17546–17552. doi:10.1039/C8NJ04090G.

Huang, S. *et al.* (2015) 'Recent advances in dialkyl carbonates synthesis and applications', *Chemical Society Reviews*, 44(10), pp. 3079–3116. doi:10.1039/C4CS00374H.

Raiguel, S. *et al.* (2020) 'Solvent Extraction of Gold(III) with Diethyl Carbonate', *Cite This: ACS Sustainable Chem. Eng*, 8, pp. 13713–13723. doi:10.1021/acssuschemeng.0c04008.

Shukla, K. and Srivastava, V.C. (2016) 'Diethyl carbonate: Critical review of synthesis routes, catalysts used and engineering aspects', *RSC Advances*, 6(39), pp. 32624–32645. doi:10.1039/c6ra02518h.

Trygg, J., Trivedi, P. and Fardim, P. (2016) 'CONTROLLED DEPOLYMERISATION OF CELLULOSE TO A GIVEN DEGREE OF POLYMERISATION', *CELLULOSE CHEMISTRY AND TECHNOLOGY Cellulose Chem. Technol*, 50(6), pp. 557–567.

Yang, X. *et al.* (2020) 'Efficient recovery of phenol from coal tar processing wastewater with tributylphosphane/diethyl carbonate/cyclohexane: Extraction cycle and mechanism study', *Chemical Engineering Research and Design*, 157, pp. 104–113. doi:10.1016/J.CHERD.2020.03.005.

separations

MDPI

Article

Dehydration by Pervaporation of an Organic Solution for the Direct Synthesis of Diethyl Carbonate

Kouessan Aziaba [1,*], Marco Annerl [1], Gerhard Greilinger [1,2], Magdalena Teufner-Kabas [2], Florian Kabas [2], Christian Jordan [1] and Michael Harasek [1]

[1] Institute of Chemical, Environmental & Bioscience Engineering E166, Technische Universität Wien, 1060 Vienna, Austria
[2] kleinkraft OG, Turnergasse 27/5, 1150 Vienna, Austria
* Correspondence: kouessan.aziaba@tuwien.ac.at

Abstract: Pervaporation has been a central subject in the research community within the scope of the further development of energy- and cost-efficient alternatives to conventional liquid–liquid separation technologies. The potential eligibility of four commercial membranes (ZEBREX ZX0, PERVAP^{TM} 4155-80, PERVAP^{TM} 4100, PERVAP^{TM} 4101) for use in an integrated dehydration application of a diethyl carbonate/water/ethanol mixture by pervaporation was assessed experimentally. The impact of feed concentration, operating temperature, pressure, and sweep gas flow rate on membrane separation performance, including permeation flux, permeate quality, selectivity, and permeance, was thoroughly investigated. Applying the ZX0 membrane delivered the best qualities of all tested membranes of the permeate stream, with a water concentration of mostly >98%. In comparing the water flux, the ZX0 membrane remained reasonably competitive with the polymer membranes. Furthermore, the sweep gas volume flow rate and the operating temperature were identified as influencing the flux significantly but not the product composition. At the same time, the feed concentration of water also influenced the water purity within the permeate. The experiments were monitored with a partial least squares model, allowing a quick assessment of obtained samples while delivering accurate results.

Keywords: dehydration; ceramic; membrane; diethyl carbonate; DEC; PLS

Citation: Aziaba, K.; Annerl, M.; Greilinger, G.; Teufner-Kabas, M.; Kabas, F.; Jordan, C.; Harasek, M. Dehydration by Pervaporation of an Organic Solution for the Direct Synthesis of Diethyl Carbonate. *Separations* **2024**, *11*, 289. https://doi.org/10.3390/separations11100289

Academic Editor: Gavino Sanna

Received: 19 September 2024
Revised: 5 October 2024
Accepted: 8 October 2024
Published: 10 October 2024

1. Introduction

After several decades of comparatively high raw material security in industrialized countries, issues such as the procurement of raw materials are once again becoming the central focus of researchers and businesses. Significantly changed regulations in industry, natural disasters, and the shift in political interests result in a stronger emphasis on realignment towards a more sustainable raw material supply chain [1]. In the course of this, industrial residues are also being re-evaluated for further use, as are conventional technologies. In particular, separating liquid–liquid mixtures, often carried out by distillation, is considered energy-intensive. This can frequently be replaced entirely by pervaporation (PV) membrane technology. Pervaporation represents a separation technology in which a liquid mixture (feed) is brought into contact with one side of a membrane. The fraction that passes through the membrane (permeate) is withdrawn as a low-pressure vapor (vacuum) or with a gaseous compound (sweep gas), diluting the product on the permeate side. Major influencing parameters of the transport of permeating compounds are the chemical potential difference of the compounds on both sides of the membrane, as well as interactions between the permeate's and the membrane's selective layer, along with its mobility within the membrane matrix [2]. The comparatively low demands and increasing possibilities for a compact design of pervaporation open up new opportunities for recovering valuable liquid materials and new options for integrating the separation of product mixtures [3].

Further, pervaporation is more suitable for the separation of compounds that would be thermally decomposed if distilled [4]. This makes it potentially eligible to recover many organic compounds, such as organic carbonates, from various applications.

Organic carbonates are used in the chemical industry to produce resins, lithium-ion batteries, plastics, pharmaceuticals, and other materials. There is evidence of their use as a solvent and as a fuel additive. Their properties as hardly toxic aprotic substances with higher boiling points make them versatile substances for use in the chemical industry [5–7]. Among multiple current opportunities under which organic carbonates are synthesized, the most common ones rely on rather problematic conditions (toxicity, high energy demand). Recent years have brought about novel approaches to producing organic carbonates. Nevertheless, these synthesis routes still bear certain drawbacks (limited catalytic activity, adverse thermodynamics) before they become commercially attractive. Diethyl carbonate ($C_5H_{10}O_3$ or also DEC) is increasingly becoming of great interest among known organic carbonates since direct synthesis from sustainable raw materials (CO_2, bio-EtOH) is possible.

$$2C_2H_5OH + CO_2 \rightleftharpoons C_5H_{10}O_3 + H_2O \quad (1)$$

The reaction is carried out at elevated temperatures of 130–160 °C and pressures between 20–60 bar. The presence of water especially seems to drastically inhibit the reaction [8]. Membranes could potentially be considered a highly matching solution to remove water from the system and reduce the effect of water presence. Therefore, the dehydration of the reaction mixture is a promising and preferable approach. One of this work's primary interests is the assessment of the eligibility of membrane technology to dehydrate a ternary mixture consisting of DEC/water/EtOH. The suitability of FTIR-ATR measurements assessed with partial least squares regression (PLS) for fast process monitoring is also discussed.

1.1. Dehydration with Membranes—State of the Art

DEC forms an azeotrope with water at a molar ratio of 1:3 (DEC/water) [9]. Therefore, distillation is not the most efficient method to recover the desired purified product. Hinchliffe and Porter reported the potential eligibility of inorganic membranes to separate non-desired products of a reaction with a membrane back in 2000, while being competitive with distillation [10]. A novel zwitterionic polyamide membrane was developed by Zhang et al. [11] to dehydrate organic solvents mainly consisting of ethanol, with a relatively high flux of 4380 g/m^{2}h and selectivities of 3870 ($\alpha_{H_2O/EtOH}$) when fed with a water/ethanol mixture containing 90 wt% ethanol, yielding better qualities than 99.7% water purity. Increasing the temperature and feed water content likewise results in rising fluxes. No information, however, has been provided regarding the stability of elevated pressures and temperatures exceeding 76 °C [11]. Fujiki et al. [12] suspect limited levels of stability for organic membranes and, therefore, applied a microporous TiO_2–SiO_2–organic-chelating ligand composite membrane to dehydrate an IPA/water mixture containing 90 wt% IPA. Fluxes surpassing 1500 g/m^{2}h have been recorded for temperatures of 60 °C. As expected, a rising trend was observed for the flux with increasing temperature, while selectivities also rose alongside the rising flux until 70 °C [12].

As indicated in Section 1.2, the dehydration of the solution is preferred over the selective separation of ethanol or DEC for process enhancement reasons. Further, the availability of organic carbonate selective membranes is also limited compared to dehydrative membranes. One reason behind this could be a generic membrane selectivity design based on molecular sizes, resulting in lower diffusion of larger molecules, in which organic carbonates are generally compared to water. Wang et al. [13] engineered a nano-silica PDMS composite membrane to separate DMC from methanol in 2011. Even though a relatively high flux was achieved, yielding more than 700 g/m^{2}h of membrane flux, the selectivity ($\alpha_{MeOH/DMC}$) for this configuration remained comparably low, just under 4 [13]. Another approach was presented by Číhal et al. by deploying a polymer of intrinsic microporosity (PIM-1) membrane for MeOH/DMC separation, achieving slightly higher selectivities of 5

but with significantly higher permeances with values up to 1.82 mol/m^{2}h∗Pa than other solutions operated under sweep gas [14]. The earliest entry in the literature discussing the actual reactive conditions in which DEC would be formed was reported by Dibenedetto et al. [15] by testing several esterification-enhancing catalysts and a process loop including a pervaporation unit prior to the reaction. The consecutive dehydration of the reaction was identified as a central factor in boosting the reaction, which is why merging water separation and the catalyst into a single entity of a reactive membrane was proposed. Obstacles such as the DEC loss into the permeate for tested polymeric membranes have been reported. Additionally, the issue of a significant DEC loss due to the CO_2 content in the feed seems to be unsolved. However, it is advantageous that the operating temperatures of the membranes were comparably high and very close to the DEC formation temperature within the reactor [15]. Décultot et al. [16] also applied pervaporation to dehydrate the ternary DEC/water/EtOH mixture with a PERVAP^{TM} 4100 polymeric membrane, reducing the water content below 0.33% in the retentate. Further, it is stated that a DEC content of 0–15% seemingly has no effect on the water flux. The ideal selectivities $\alpha_{H_2O/DEC}$ and $\alpha_{H_2O/EtOH}$ have a range of 800–1630, which is tremendously high in comparison to other tested membranes. However, the total fluxes have a range of 8–14 g/m^{2}h and barely exceed purities of 80% for water in some cases. A temperature of 87 °C was the highest applied temperature, which is low compared to the synthesis conditions of DEC [16]. As already mentioned, the data on the dehydration of ternary systems and the separation of alcohol/organic–carbonate mixtures, including DEC, is very limited. However, DEC is expected to have similarities in terms of synthesis and separation methods like DMC. Thus, it is assumed to show a similar behavior to some pervaporation applications for DMC, of which further dehydration applications are reported in the literature [17–20].

1.2. Partial Least Squares Regression

In spectroscopy, partial least squares regression (PLS regression) is used to predict chemical or physical properties (e.g., concentration, viscosity, density, etc.) from spectra after calibration. Therefore, PLS has become a standard method in chemometrics and is primarily used in infrared, Raman, and fluorescence spectroscopy. Some recent example applications in ATR-FTIR spectroscopy for the quantification and qualification/authentication of chemical/biological substances or physical properties are as follows:

- Comparison of Raman and attenuated total reflectance (ATR) infrared spectroscopy for water quantification in a natural deep eutectic solvent [21];
- Application of ATR-FTIR spectroscopy along with regression modeling for the detection of adulteration of virgin coconut oil with paraffin oil [22];
- ATR-FTIR spectroscopy and chemometric techniques for the determination of polymer solution viscosity in the presence of SiO_2 nanoparticles and salinity [23];
- Further applications can be found in [24–30].

PLS can be described as an extension of principal component regression (PCR) or a combination of principal component analysis (PCA) and multiple regression. The main difference between PLS and other multivariate methods is the inclusion of the structure of the **Y**-data (variables to be predicted, e.g., concentrations) during the determination of the principal components for the **X**-data (predictor variables, e.g., spectra). This procedure increases the relation between the spectral data (**X**-data) and the analyte data (**Y**-data), resulting in slightly rotated principal components, termed PLS components. A good description of the mathematical background behind PLS can be found in [31].

2. Materials and Methods

2.1. Pervaporation System Setup

Figure 1 depicts a flow diagram of the membrane pervaporation system used. The specific components, valves, and sensors outlined in the flow diagram are listed in Table 1. For comprehensive details regarding the system's design, construction, and testing, please refer to the master's theses by G. Greilinger [32] and M. Annerl [33].

Table 1. List of applied sensors.

	Abbreviation	Measured Value	Measured Medium
pressure	PIC1	P	CO_2
	PIC2	P_S	sweep gas
	PR1	P_F	feed
temperature	TR1	T_F	feed
	TIR1	T	membrane module
volumetric flow	FR1	V_F	feed
	FRC1	V_S	sweep gas
relative humidity	MIR1/MIR2	φ	permeate
volumetric concentration of CO_2	QR1	v_{p,CO_2}	permeate

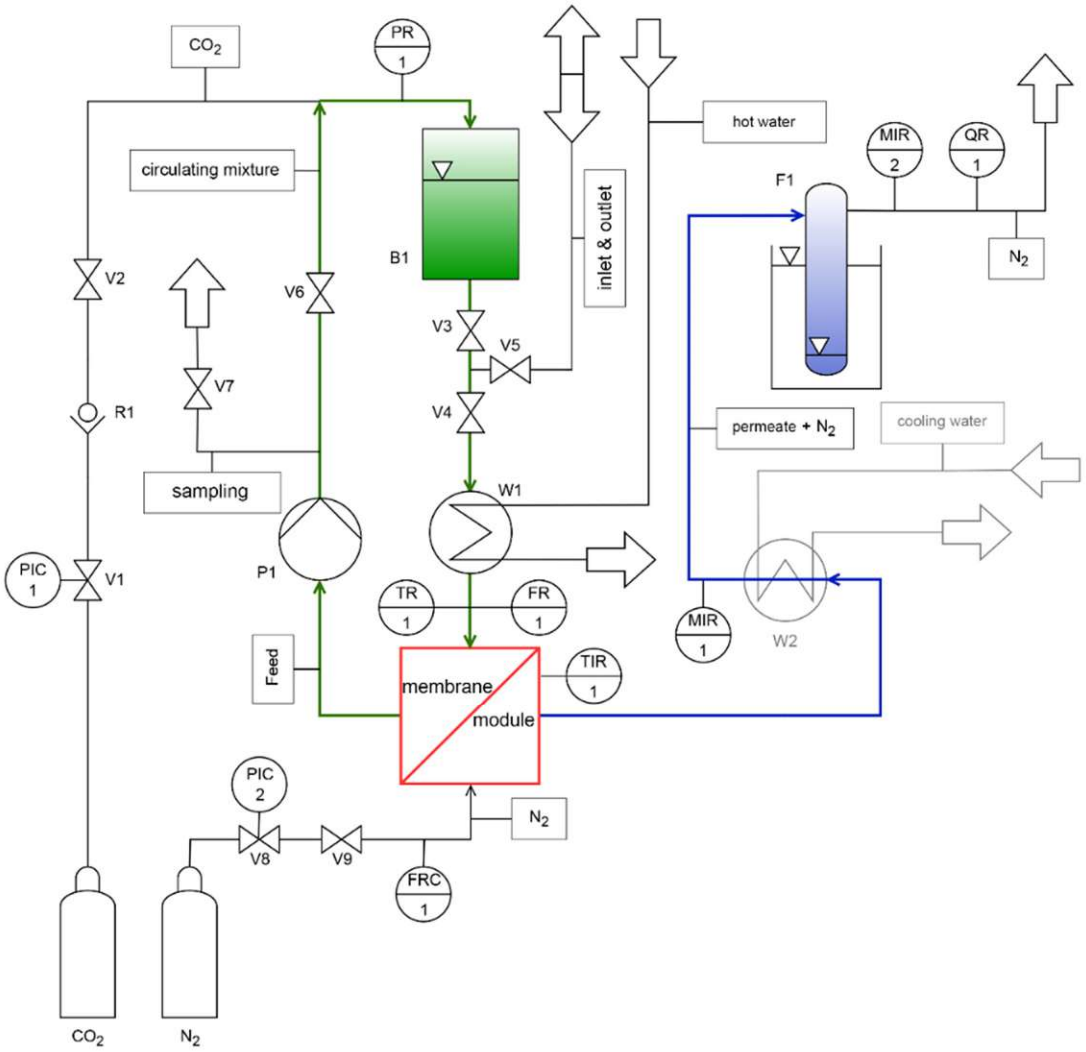

Figure 1. Flow diagram of the pervaporation equipment [33].

Several feed mixtures with various concentrations consisting of water (deionized), ethanol (99.9%, denatured with toluene, obtained from AustrAlco, Spillern, Austria), and DEC (99.9%, purchased from Carl Roth, Karlsruhe, Germany) were acquired and prepared for the experiments and standards. Preliminary tests were carried out to investigate the suitability of the design. The applied parameters are presented in Table 2. The data and parameters for the experimental campaign of the membranes are presented and discussed from Section 3.2.

Table 2. Overview of applied preliminary tests of the pervaporation setup using the ceramic ZEBREX ZX0 membrane.

Name	DEC	$w_{c,i}$ [$wt\%$] H_2O	EtOH	P_c [bar]	T_b [$°C$]	Duration [h]	N_2—Sweep Gas Flow [L/min]
PV1	0	0.00	100.00	3	80	2.00	1.5
PV2	0	6.20	93.80	3	80	1.53	1.5
PV3	0.79	0.99	98.22	7	80	5.33	0.5
PV4	1.21	0.00	98.79	6	85	4.30	0.7
PV5	1.12	0.24	98.64	6	85	4.80	0.7
PV6	0.13	1.15	99.58	6	85	5.00	0.7
PV7	1.14	0.00	98.86	6	85	5.60	0.7
PV8	0.25	3.78	99.46	6	65–85	7.50	0.7
PV9	0.88	3.70	95.42	3–6	75	7.50	0.7
PV10	3.37	0.89	95.74	5.7	75	7.50	0.35–1.4
PV11	1.31	0.00	98.69	3	85	6.75	0.7
PV12	0.18	1.06	98.76	3	85	5.50	0.7

Approximately 1 L of a defined mixture consisting of DEC, ethanol, and water (feed mixture) was filled into the tank (B1). Subsequently, the feed was pumped through a heat exchanger (W1) to reach the operating temperature. A water bath provided the operating temperature of the membrane module connected to a tube wrapped around the module. Tank B1 was pressurized through a feed line by introducing CO_2 after a consistent operating temperature was reached. Following this, a continuous carrier gas flow (N_2) on the permeate side of the membrane module was released under atmospheric pressure. The permeate was separated from the carrier gas flow by condensation with subsequent collection in a separator (F1), which maintained a temperature range between −15 °C and −20 °C due to a salted iced water mixture. This temperature range was selected because of the anticipation of a high water content in the permeate. It is sufficiently low to separate water without causing freezing or condensation in the pipes of the carrier gas. A Liebig condenser (W2) with a collecting flask was also used in high permeate flow cases. The volume flow of the circulating mixture was adjusted to a flow of 1.5–1.7 L/min.

Extraction of samples from the circulating mixture occurred by opening valve V7, and for the permeate by simultaneously emptying the separator F1 and (if present) collection of the content in the flask (W2) of the Liebig condenser. The retentate of the PV membrane process was recycled back to the feed tank, thus continuously changing the concentration actually fed to the membrane. It will be referred to as "circulate" in the following sections for better understanding.

Prior to each test, the system was rinsed with high-purity ethanol (99.9%) to remove residues. The predefined test mixture was then filled into the system and operated for at least half an hour. This was to free the system from local concentration differences caused by residues from dead volumes from preliminary tests and to achieve optimum homogenization. Furthermore, this procedure was used to test the system for the stability of the test parameters.

Figure 2a showcases the tubular module integrated into the membrane pervaporation system. The module consists of three main components, with the ZEBREX ZX0 (DeltaMem) tubular ceramic membrane featuring a module length of 20 cm and a non-disclosed selective layer measuring 0.00565 m^2. Alongside the heating hoses of the water bath (W1) wrapped around the casing, the module was also insulated with foam. Figure 2b displays the flat module integrated into the membrane pervaporation system. Again, assembled on a supporting structure, the most crucial element is the flat-sheet polymer membrane with an active membrane diameter of 9 cm, positioned between the upper and lower parts of the module. The feed inlet and outlet occur in the upper part, while the sweep gas inlet and the permeate-carrier gas mixture outlet occur in the lower part.

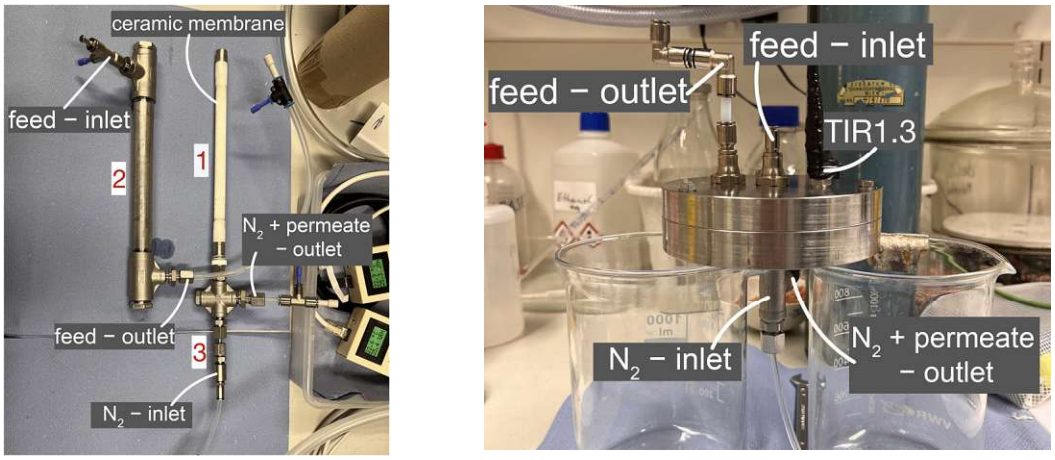

(**a**) (**b**)

Figure 2. Design of the tubular membrane module (**a**) and the flat-sheet module (**b**) (adapted from [33]).

Heating for the flat module was conducted similarly to that of the tube module, utilizing a water hose and insulation with foam. The polymer membranes (PERVAP^{TM} 4100, PERVAP^{TM} 4101, PERVAP^{TM} 4155-80) were purchased from DeltaMem (Allschwil, Switzerland). The membranes were each preserved in the feed mixture for 24 h prior to the installation to condition them appropriately.

2.2. Analytics

The permeate and circulating mixture were analyzed using a gas chromatograph (GC-2010, Shimadzu, Kyōto, Japan) equipped with an AOC-5000 autosampler, a flame ionization detector (GC-FID), and an RTX Volatiles capillary column (60 m length, 0.53 mm inner diameter, film thickness 2 µm). The sample compositions were evaluated based on standards (>100) consisting of water, ethanol, and DEC in varying concentrations. For the quantitative analysis of water in the feed and permeate samples, volumetric Karl Fischer titration (KFT, Karl Fischer titration) was employed. The double analyses were conducted using the Eco KF Titrator (Metrohm, Herisau, Switzerland). Additionally, all samples were analyzed using an FTIR-ATR spectrometer (Vertex 70, Bruker, Billerica, MA, USA) with PLS modeling.

2.3. PLS

In this work, PLS was used to create a calibration model for the prediction of the ethanol, diethyl carbonate, and water concentrations in a defined mixture (the feed), which was analyzed with an ATR-FTIR spectroscopy device. For this purpose, a MATLAB (2023b version) algorithm was created, which applies the plsregress function from the statistics and machine learning toolbox [34]. The algorithm behind the plsregress function provided by MATLAB is based on SIMPLS [35] and automatically performs a k-fold cross-validation [36].

To obtain the calibration model, a set of standard mixtures was created in the following concentration ranges: 0–100 wt% ethanol, 0–100 wt% DEC, and 0–1.5 wt% water. For each measurement, a wavenumber of 400–4000 cm^{-1} was taken into account, and 16 spectra were subsequently recorded and averaged, and the blank value was measured for every 4 measurements. The raw spectra (without smoothing, baseline correction, or derivation of the spectra) were used for further calibration.

The optimum number of PLS components was determined via mean squared error (MSE), which was calculated from models with a number of PLS components ranging 1–12. This step is necessary to prevent underfitting or overfitting [31]. Additionally, during the calculation of these models, ethanol and DEC were evaluated together, while water was evaluated separately to achieve a better predictive performance. The MSE was

determined for all models and applied to the number of PLS components (see Figure 3). If the concentration is predicted via PLS regression, the MSE is generally defined by

$$MSE = \frac{1}{n} \times \sum_{i=0}^{n} (y_i - \hat{y}_i)^2, \quad (2)$$

where n is the number of elements in the concentration matrix $\mathbf{Y}$, y_i is each element of $\mathbf{Y}$, and $\hat{y}_i$ is the predicted concentration by the PLS regression model [31].

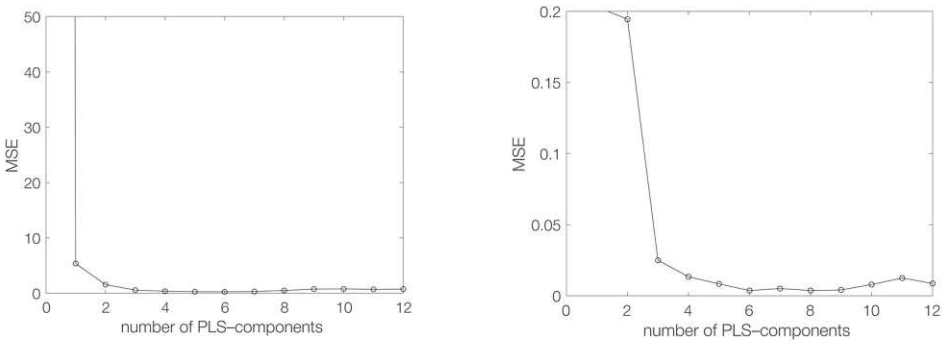

(**a**) (**b**)

Figure 3. Mean squared error against the number of partial least squares components. ((**a**) Model 1) Models for ethanol and diethyl carbonate. ((**b**) Model 2) Models for water.

For the PLS regression model of DEC and ethanol (model 1), a PLS component number of 3 was selected, and for water (model 2), a number of 7 was selected. The two actual calibration models were created using these numbers of PLS components.

The plsregress function provided by MATLAB was used to determine the regression coefficients for these two PLS regression models. The regression coefficients are essential for the prediction of an unknown sample. The MATLAB program of the PLS regression model of DEC and ethanol (model 1) can be found in the Supplementary Materials.

Furthermore, to examine the accuracy of the PLS regression models, the coefficients of determination R^2 and the standard error SE were calculated for each model. If the concentration is predicted via PLS regression, R^2 and SE are defined as follows:

$$R^2 = \frac{\sum_{i=0}^{n} (\hat{y}_i - \overline{y})^2}{\sum_{i=0}^{n} (y_i - \overline{y})^2} \quad (3)$$

$$SE = \sqrt{\frac{(y_i - \hat{y}_i - BIAS)}{n - 1}} \quad (4)$$

where n is the number of elements in the concentration matrix $\mathbf{Y}$, y_i is each element of $\mathbf{Y}$, $\overline{y}$ is the average of all elements from $\mathbf{Y}$, $\hat{y}_i$ is the predicted concentration by the PLS regression model, and $BIAS = \sum_{i=0}^{n} (y_i - \hat{y}_i)/n$ [31].

3. Results

3.1. PLS Model

The two PLS regression models are sufficiently accurate for the application since all R^2 values are >0.99, and the SE of the organic components (model 1) is <0.5 wt% and of water (model 2) is <0.05 wt% (see Table 3).

Table 3. Coefficient of determination and standard error.

Model	Analyte	R^2	SE [$wt\%$]
1	DEC	0.9999	±0.2379
	EtOH	0.9996	±0.4302
2	water	0.9945	±0.0330

Figure 4a,c illustrates the residuals of each standard mixture. These diagrams provide a good overview of the absolute deviations between the actual mass percentages of the standard mixtures and the mass percentages predicted by the PLS regression model. The standard error SE summarizes this observation in a single quantity.

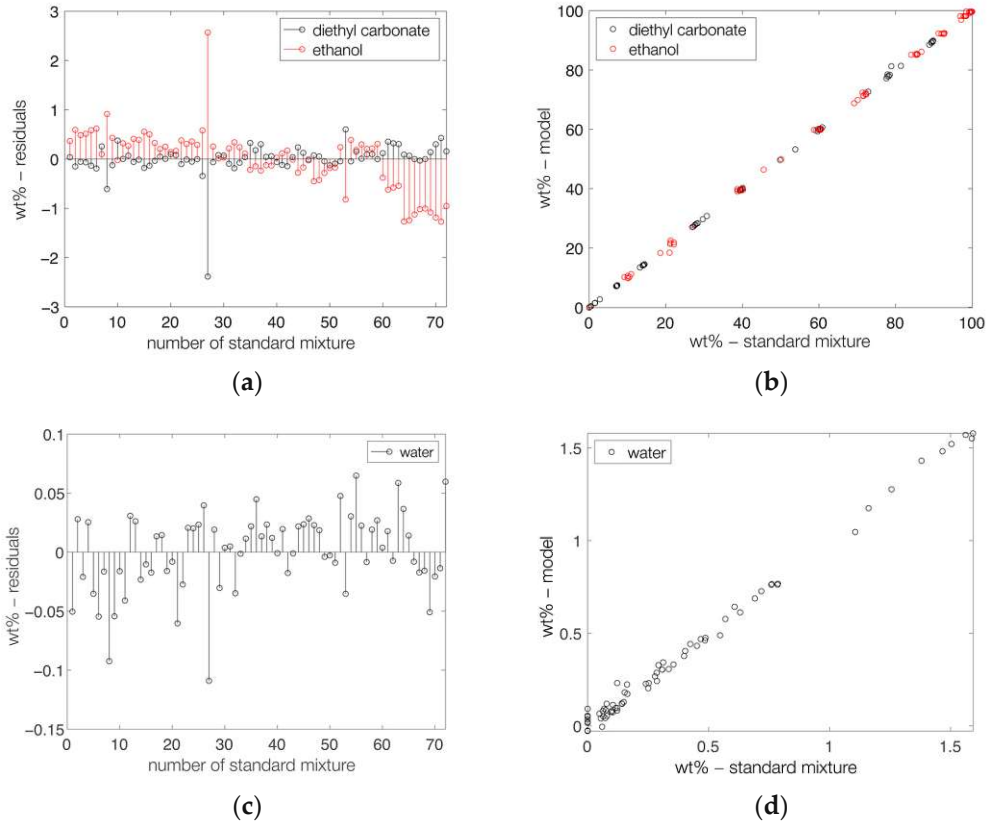

Figure 4. Residual and correlation plots for both PLS regression models: (**a**,**b**): model 1 and (**c**,**d**): model 2.

In Figure 4b,d, the actual mass percentages of the standard mixtures are plotted against the mass percentages predicted by the PLS regression model. It can be seen that there is a strong correlation between these two values for both models. This property is summarized by the coefficient of determination R^2.

3.2. Comparison of Tested Membranes

For a better understanding of the system, a more extensive concentration range of the components—water, ethanol, and minimally also DEC—was covered in the preliminary tests. Any minimal limitations concerning the applied methodology (leakage of the system, temperature drop at the measuring points used, pressure loss over the test period) were successfully corrected before the start of the test campaigns (V1–V17), which will be discussed in the following sections.

Four membranes were tested at different feed pressures to evaluate their eligibility for use in an integrated dehydration process for organic mixtures. In each experiment (V1–V16), mixtures consisting of 1% of each of H_2O and DEC, and 98% ethanol were

fed into the equipment and homogenized in the system. An overview of the resulting experimental data from these assessments is provided in Table 4.

Table 4. Experimental data of tested membranes at 98 °C.

Name	Membrane	P_c [*bar*]	$w_{c,i}$ [*wt*%]		$w_{p,i}$ [*wt*%]	J_i [g/m^2h]		α [−]	Q_{H_2O} [$mol/Pa*m^2*h$]
			DEC	H_2O	EtOH	H_2O	H_2O	Total		
V1	ZEBREX™ ZX0 at 85 °C	5	0.90	0.98	98.70	99.6	30.5	30.7	>13,000	3.39×10^{-6}
V2	PERVAP™ 4155-80	1	0.96	1.01	98.63	12.3	32.5	268.7	13–15	1.80×10^{-5}
V3		3	0.99	0.96	98.60	12	45.7	377.5	11–17	8.45×10^{-6}
V4	PERVAP™ 4100	1	1.04	0.95	98.55	5.1	30.6	599.1	5–6	1.70×10^{-5}
V5		3	1.07	0.94	98.52	4.7	24.4	523.3	5–6	4.52×10^{-6}
V6	PERVAP™ 4101	3	1.31	1.08	98.28	73.9	11.8	16.0	120–180	2.19×10^{-6}

First, it becomes apparent that the concentration of the circulate differs from the concentration fed to the system. This can be explained by the fact that, despite the preparation and rinsing processes, dead volumes remain in the system, marginally shifting the overall concentrations in the system after homogenizing the circulating mixture. This observation also applies to all subsequent experiments and is considered negligible.

While the tubular membrane module design allowed pressures up to 5 bar, the flat-sheet models were tested at 1 and 3 bar. The tubular membrane module's permeate stream had high water purity levels of >99%, while this quality remains unmatched by the polymer membranes. Only the PERVAP™ 4101 membrane delivers a permeate stream of mainly water, with more than 79%.

The water flux is almost the only constituent of total fluxes for the ceramic membrane experiments. The 4155-80 and 4100 polymer membranes deliver comparably high total fluxes of more than 250 g/m^{2}h, resulting in comparably large mass streams. Even though the permeance of water is within a similar magnitude for the two mentioned membranes, as for the ceramic one, it is already highly implied that both membranes are rather unsuitable for the desired application since large DEC and ethanol fluxes have also been observed, resulting in a comparably lower selectivity. Even though the water flux is the main constituent for the PERVAP™ 4101 membrane, it shares some drawbacks with the other tested polymeric membranes and is still not competitive enough regarding the selectivity compared to the ceramic membrane. Interestingly, the application by Décultot et al. [16] of the same membrane module (PERVAP™ 4100) delivers lower fluxes but higher selectivities for water, even though the mixtures submitted to the membrane are comparable. However, the experiments conducted by Décultot et al. were operated under a vacuum. The driving force of this work's setup was enhanced by the sweep gas of N_2 on the permeate side and pressurization with carbon dioxide in the circulating system. The comparatively poor quality of the permeate could also be potentially caused by effects such as membrane swelling due to the combined presence of CO_2 and relatively high temperature and pressure. Therefore, particular emphasis was placed on the ZEBREX ZX0 membrane.

3.3. Effect of Feed Water Content on Dehydration

Several experiments with the ZEBREX ZX0 membrane were carried out to assess the membrane's behavior on the water flux in dependency on the composition of the feed. The results of a long-term experiment carried out for 16 h with a water feed concentration of 0.7% are illustrated in Figure 5. The rest of the feed comprised about 1% DEC and >98% ethanol.

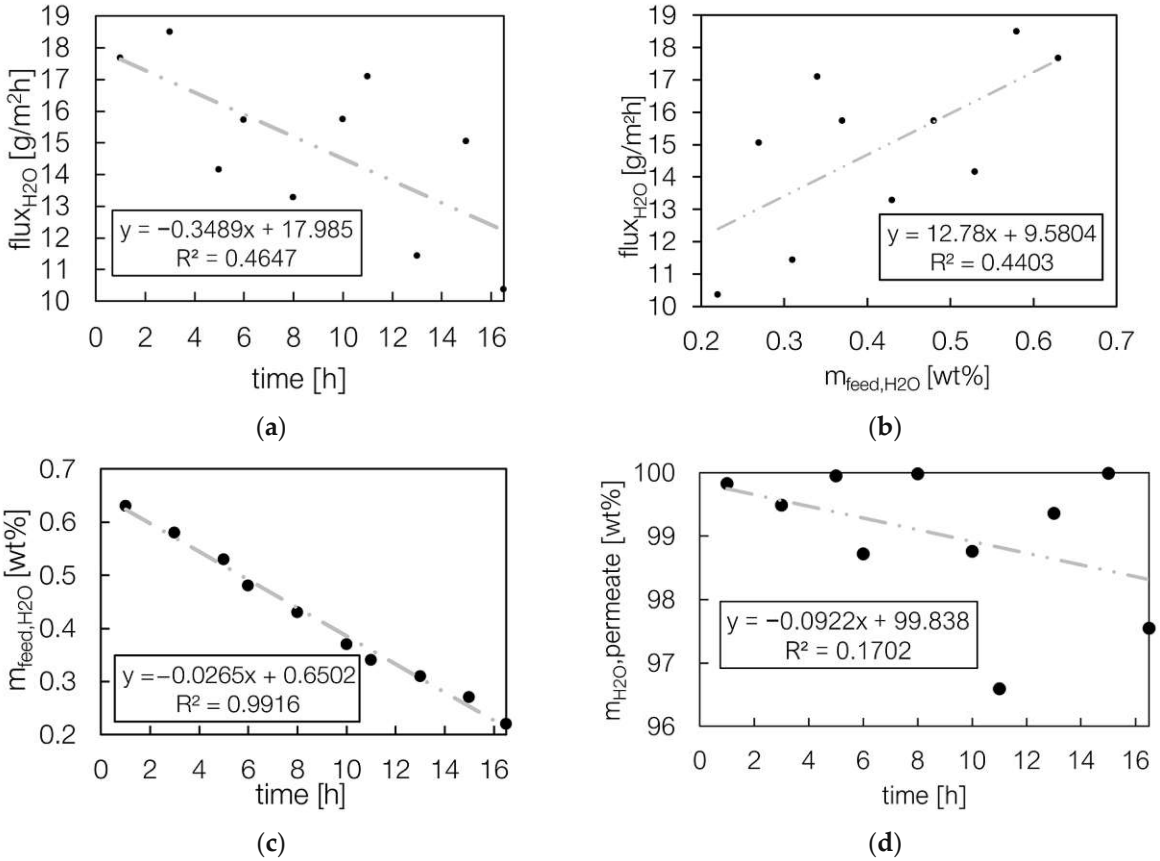

Figure 5. Illustration of the flux over time (**a**) and in dependency on the feed water content (**b**) as well as the circulates (**c**) and the permeates (**d**) water content using the ZEBREX ZX0 membrane.

The flux of water decreases on average, as Figure 5a portrays, throughout the test period. Furthermore, Figure 5b demonstrates a correlation between the permeate flow of water and the water content in the feed, illustrating that the water flux decreases as the water content in the feed decreases. A closer look at Figure 5c reveals an almost linear decrease in the circulating water concentration with passing time, depleting the water content in the circulate close to 0.2 wt% after 16.5 h of experimental running time. Further trend development was not assessed, but this data does not reveal a diminishment of the decreasing trend. The permeate was identified to be mainly water (Figure 5d) with a purity of mostly >98 wt%. Despite the trend, significant fluctuations in the measured values can be observed in Figure 5a,b,d. Due to the low sample mass of the permeate, slight fluctuations occurred in the measurements. These fluctuations increase by scaling up to the units shown (Figure 5), which makes the fluctuations appear large. Despite the comparatively poor R^2, a trend can nevertheless be recognized. This is particularly evident in the constant decrease in the water concentration of the circulating mixture, as shown in Figure 5c.

3.4. Effect of T_C on Dehydration

Since pressure and temperature are usual parameters that influence the flux, temperature variation experiments were performed, as shown in in Table 5.

Table 5. Overview of temperature variation experiments of the tubular ZEBREX ZX0 ceramic membrane at 3 bar.

Name	T_c [°C]	w_{c,H_2O} [wt%]	w_{p,H_2O} [wt%]	J_{H_2O} [g/m^2h]	J_{total} [g/m^2h]	α [−]	Q_{H_2O} [$mol/Pa*m^2*h$]
V7	65	0.67	98.38	16.3	16.5	9990	1.80×10^{-6}
V8	75	0.80	98.53	19.2	19.5	5068	2.13×10^{-6}
V9	85	0.72	98.39	30.5	31.0	3800	3.38×10^{-6}
V10	98	0.43	99.98	13.3	13.3	208,755	1.47×10^{-6}

A closer look at the H_2O fluxes and the permeate water content in Table 5 gives further insight into the behavior of the ceramic membrane. The flow of the organic part of the permeate rises while the percentage share of H_2O stays rather consistent. The total flux mainly consists of water. However, the absolute volume seems to level off somewhere between 98 and 99%. Considering the feed water content, a decreasing water flux with a reduced feed water amount is expected. The experiments carried out at 75 and 85 °C, however, debunk this theory by delivering consistently rising fluxes with rising temperature T_C. The last experiment carried out with even less H_2O in the feed and at a temperature of 98 °C, yields a purity of 99.98% of H_2O, delivering a comparatively tremendous ideal selectivity α of >200,000. This also marks the end of a seemingly decreasing α in dependence on rising temperature. Further elevation of the feed temperature is expected to result in even higher fluxes of H_2O but possibly slightly decreased selectivities due to the enhanced diffusion of the other components as well. Nevertheless, an assessment of the membrane's performance was conducted in the following section.

3.5. Effect of P_C on Dehydration

Several experiments were carried out to observe the influence of temperature on the PV separation using the tubular ceramic membrane. The results of these experiments are documented in Table 6.

Table 6. Overview of temperature variation experiments of the tubular ZEBREX ZX0 ceramic membrane at 75 °C.

Name	P_c [bar]	w_{c,H_2O} [wt%]	w_{p,H_2O} [wt%]	J_{H_2O} [g/m^2h]	J_{total} [g/m^2h]	α [−]	Q_{H_2O} [$mol/Pa*m^2*h$]
V11	1	0.80	94.48	10.9	11.5	8005	6.03×10^{-6}
V12	3	0.72	99.31	12.7	12.7	180,984	2.34×10^{-6}
V13	5	0.77	98.41	19.9	20.2	86,036	2.20×10^{-6}

The initial concentrations are not precisely the same but close enough for the purposes of the experiments. A positive correlation between the transmembrane flux and the increased pressure difference was observed. At first glance, no particular correlation could be observed for the purity of the permeate. The permeate quality is highest in the test conducted at 3 bar, with 99.31%. The test conducted at 1 bar showed the lowest value of the entire test campaign for the ceramic ZEBREX ZX0 membrane, at 94.48%. Considering the minimal sample quantity (<0.1 mL), an outlier favoring lower water purity cannot be ruled out.

3.6. Effect of V_s on Dehydration

The effect of the sweep gas flow rate on the separation was observed, and the data are summarized in Table 7.

Table 7. Overview of sweep gas variation experiments of the tubular ZEBREX ZX0 ceramic membrane at 5 bar.

Name	V_s [L/min]	w_{c,H_2O} [$wt\%$]	w_{p,H_2O} [$wt\%$]	J_{H_2O} [g/m^2h]	J_{total} [g/m^2h]	α [$-$]	Q_{H_2O} [$mol/Pa*m^2*h$]
V14	0.35	0.86	99.43	9.7	9.7	37,290	1.07×10^{-6}
V15	0.70	0.98	99.55	30.5	30.5	13,708	3.39×10^{-6}
V16	1.40	0.90	99.77	45.9	46.0	59,724	5.09×10^{-6}

It has to be mentioned that the feed concentrations of the experiments are not perfectly equivalent. Nonetheless, with rising sweep gas flow rates of N_2, a positive trend can be observed in the permeate concentrations and the flux. The purities of the permeates are consistently at least as high as 99%, while the flux for a sweep gas flow of 1.4 L/min delivered the highest flux of all experiments using the ceramic ZX0 membrane. While the permeate quality remained nearly unchanged, the flux decreased to less than one-third by cutting the sweep gas flow to half.

This indicates that dissolving water molecules on the selective layer of the membrane and diffusing through the membrane matrix is still faster than the desorption process on the permeate side. A high water concentration on the membrane permeate side surface could support this assumption. Conversely, doubling the sweep gas flow rate increased the flux by 50%.

3.7. Effect of Increased DEC Concentration in the Circulating Mixture on Dehydration

In order to gain an impression of the behavior of the membrane at a higher DEC concentration, the initial concentration of the circulating mixture was changed for experiment V17 (parameter). In this experiment, 8.89% DEC, 0.30% H_2O, and 90.81% ETOH were used and homogenized within the system, as in the other experiments (V1–V16). After the initial homogenization time, 8.92% DEC and 0.33% water were measured at the beginning of the experiment. Figure 6 shows the water concentration in the circulating mixture and in the permeate.

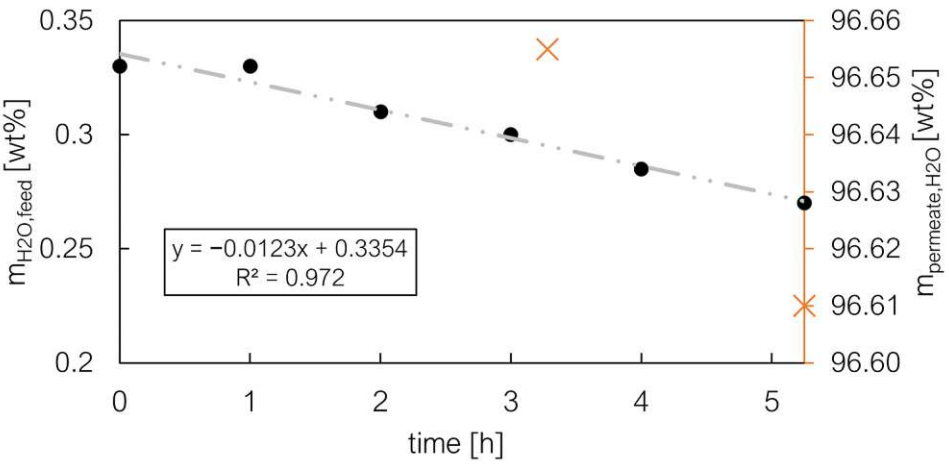

Figure 6. Experiment with increased DEC and decreased water concentration in the circulate of the tubular ZEBREX ZX0 ceramic membrane at 5 bar and 85 °C.

The water concentration in the circulating mixture decreases depending on the duration of the experiment. Despite the initially very low water concentration, the mixture was still dehydrated to 0.27% water concentration. Due to the very low permeate sample quantity, the water concentrations of only two samples could be determined, which, in both cases, matched the qualities of the other tests well, with >96%. The transmembrane flux was determined to be 10.6 g/m^{2}h after 3 h and 8.6 g/m^{2}h after a further 2 h and

15 min. Although the test time was somewhat shorter, it can still be observed that the continuously decreasing water concentration in the circulate also reduces the transmembrane flux. The determined permeance of 1.03×10^{-6} also fits into the overall context compared with the other experiments' results. In addition, this experiment shows that selective separation of water from the mixture ($\alpha = 5839$) is nevertheless possible with an increased DEC concentration.

4. Conclusions

Ternary DEC/water/EtOH mixtures were introduced into a pervaporation setup fordehydration. The removal of water is considered a crucial element in the direct synthesis of DEC, as water drastically slows down the reaction. The literature has reported challenges in the operation of pervaporation in combination with the direct synthesis due to stability issues of membranes regarding the applicable temperature, pressure, and CO_2 presence. The tubular ceramic membrane could be a possible solution for this demand, primarily since it operates close to DEC's synthesis temperature (>130 °C). Ceramic membranes typically do not suffer as frequently from swelling as polymeric membranes. Further, the presence of CO_2 was primarily below the detection limit in the permeate, while the circulating feed was saturated with CO_2. The polymeric membranes PERVAP^{TM} 4155-88 and 4100 provided the highest total fluxes and simultaneously the most significant losses in DEC and ethanol, resulting in comparatively low selectivities. Therefore, these membranes are not considered eligible for the initial separative instance of dehydration. The third polymeric membrane, PERVAP^{TM} 4101, showed superior dehydration characteristics ($\alpha > 120$) compared to those of the other tested polymeric membranes ($\alpha < 18$). Nevertheless, the losses of DEC and ethanol into the permeate were still too significant to be neglected. Therefore, all polymeric membranes are expected to perform insufficiently in terms of permeate quality within a direct synthesis process of DEC. However, the PERVAP^{TM} 4101 membrane could be considered in a possible second stage of permeate purification. Further tests would be necessary in this case. The tubular ZEBREX ZX0 membrane shows the best overall dehydration characteristics, with selectivities of at least 3800. The selectivity exceeded 10,000 in most cases, delivering permeate streams with mostly >98 wt% water. Parameters such as temperature, pressure, and sweep gas velocity significantly impacted the flux. Increasing the DEC content in the system had no noticeable effect on the permeate quality. Adapting the operating temperature to the proposed temperature for DEC synthesis may even enhance the flux of water but may also result in a reduced quality of the permeate. Nevertheless, increasing the pressure did not result in the same performance as altering the other parameters. The overall fluxes were observed to be comparatively low compared to other dehydration applications but higher than those with the ternary system composed of DEC/H_2O/EtOH. The ceramic membrane could be a suitable option to dehydrate the observed quaternary (DEC/H_2O/EtOH/CO_2) mixture. However, it has not been fully assessed whether the membrane could dehydrate the solution with sufficiently high flux. At the same time, monitoring the process using FTIR-ATR analyses is a time-saving approach, as using the PLS model provides relatively immediate and sufficiently accurate assessments of the samples. Accordingly, using the PLS model is preferable to using competing methods such as the KFT and GC.

Supplementary Materials: The following supporting information can be downloaded at: https://www.mdpi.com/article/10.3390/separations11100289/s1, The source code for the developed pls model is submitted with the manuscript.

Author Contributions: Conceptualization, M.T.-K., F.K., C.J. and M.H.; methodology, K.A., M.A., G.G. and C.J.; software, M.A. and G.G.; validation, K.A., M.A. and C.J.; formal analysis, K.A., M.A. and C.J.; investigation, K.A., M.A., G.G., M.T.-K., F.K., C.J. and M.H.; resources, M.T.-K., F.K., C.J. and M.H.; data curation, K.A., M.A. and G.G.; writing—original draft preparation, K.A. and M.A.; writing—review and editing, K.A., M.A., G.G., M.T.-K., F.K., C.J. and M.H.; visualization, K.A. and M.A.; supervision, K.A., M.T.-K., C.J. and M.H.; project administration, M.T.-K. and M.H.; funding

acquisition, M.T.-K., F.K. and M.H. All authors have read and agreed to the published version of the manuscript.

Funding: This research was funded by the Vienna Business Agency (2761267) and the Austrian Research Promotion Agency (891857). The APC was funded by the TU Wien Library.

Data Availability Statement: The data recorded in this study are available upon request from the corresponding author.

Acknowledgments: The authors are highly grateful for Markus Pekovits' technical support on the electrical installations.

Conflicts of Interest: Author Gerhard Greilinger, Magdalena Teufner-Kabas and Florian Kabas were employed by the company kleinkraft OG. The remaining authors declare that the research was conducted in the absence of any commercial or financial relationships that could be construed as a potential conflict of interest.

Abbreviations

ATR	attenuated total reflection
CCU	carbon capture and utilization
CeO_2	cerium oxide
CO_2	carbon dioxide
DEC	diethyl carbonate
DMC	dimethyl carbonate
EtOH	ethanol
FID	flame ionization detector
FTIR	Fourier-transform infrared spectroscopy
GC	gas chromatograph
GHG	greenhouse gas
H_2O	water
IPA	Isopropanol
KFT	Karl Fischer titration
MeOH	methanol
MSE	mean squared error
PLS	partial least squares
SE	standard error
V	experiment
J_i	flux of component i, g/m^2h
J_{total}	total flux, g/m^2h
n	number of elements in Y
m_i	mass of component i, g
M_i	molar mass of component i, g/mol
P_c	feed pressure, bar
Q_i	permeance of component i, $mol/(Pa*m^2h)$
R^2	coefficient of determination
T_c	feed temperature, $^\circ C$
V_s	volumetric sweep gas flow, L/min
$w_{c,i}$	$wt\%$ of component i in circulate
$w_{p,i}$	$wt\%$ of component i in permeate
y_i	element i of matrix Y
$\bar{y}_i$	average of all elements of Y
$\hat{y}_i$	prediction of element i in Y
Y	concentration matrix
α	ideal selectivity of H_2O over ethanol

References

1. Kanike, U.K. View of Factors Disrupting Supply Chain Management in Manufacturing Industries. *J. Supply Chain Manag. Sci.* **2023**, *4*, 1–24. [CrossRef]

2. Liu, G.; Jin, W. Pervaporation Membrane Materials: Recent Trends and Perspectives. *J. Membr. Sci.* **2021**, *636*, 119557. [CrossRef]
3. Norkobilov, A.; Gorri, D.; Ortiz, I. Comparative Study of Conventional, Reactive-Distillation and Pervaporation Integrated Hybrid Process for Ethyl Tert-Butyl Ether Production. *Chem. Eng. Process. Process Intensif.* **2017**, *122*, 434–446. [CrossRef]
4. Khoo, Y.S.; Tjong, T.C.; Chew, J.W.; Hu, X. Techniques for Recovery and Recycling of Ionic Liquids: A Review. *Sci. Total Environ.* **2024**, *922*, 171238. [CrossRef]
5. Zhang, H.; Liu, H.-B.; Yue, J.-M. Organic Carbonates from Natural Sources. *Chem. Rev.* **2014**, *114*, 883–898. [CrossRef]
6. Zou, B.; Hu, C. Halogen-Free Processes for Organic Carbonate Synthesis from CO_2. *Curr. Opin. Green Sustain. Chem.* **2017**, *3*, 11–16. [CrossRef]
7. Tabanelli, T.; Bonincontro, D.; Albonetti, S.; Cavani, F. Conversion of CO_2 to Valuable Chemicals: Organic Carbonate as Green Candidates for the Replacement of Noxious Reactants. In *Studies in Surface Science and Catalysis*; Elsevier: Amsterdam, The Netherlands, 2019; Volume 178, pp. 125–144. ISBN 978-0-444-64127-4.
8. Giram, G.G.; Bokade, V.V.; Darbha, S. Direct Synthesis of Diethyl Carbonate from Ethanol and Carbon Dioxide over Ceria Catalysts. *New J. Chem.* **2018**, *42*, 17546–17552. [CrossRef]
9. Ripoll, J.D.; Mejía, S.M.; Mills, M.J.L.; Villa, A.L. Understanding the Azeotropic Diethyl Carbonate-Water Mixture by Structural and Energetic Characterization of DEC(H_2O)(n) Heteroclusters. *J. Mol. Model.* **2015**, *21*, 93. [CrossRef]
10. Hinchliffe, A.B.; Porter, K.E. A Comparison of Membrane Separation and Distillation. *Chem. Eng. Res. Des.* **2000**, *78*, 255–268. [CrossRef]
11. Zhang, Y.; Liu, M.; Wu, Y.; Zhao, J.; Zhou, S.; Gu, P. Zwitterionic Polyamide Membranes via In-Situ Interfacial Polymerization Modification for Efficient Pervaporation Dehydration. *Sep. Purif. Technol.* **2024**, *333*, 125847. [CrossRef]
12. Fujiki, T.; Kaji, M.; Tamamizu, Y.; Yasunari, R.; Nakagawa, K.; Kitagawa, T.; Okamoto, Y.; Matsuoka, A.; Kamio, E.; Matsuyama, H.; et al. Pervaporation Dehydration of an Isopropanol Aqueous Solution Using Microporous TiO_2-SiO_2-OCL (Organic Chelating Ligand) Composite Membranes Prepared under Different Firing Conditions. *Sep. Purif. Technol.* **2024**, *337*, 126249. [CrossRef]
13. Wang, L.; Han, X.; Li, J.; Zhan, X.; Chen, J. Hydrophobic Nano-Silica/Polydimethylsiloxane Membrane for Dimethylcarbonate–Methanol Separation via Pervaporation. *Chem. Eng. J.* **2011**, *171*, 1035–1044. [CrossRef]
14. Číhal, P.; Vopička, O.; Durďáková, T.-M.; Budd, P.M.; Harrison, W.; Friess, K. Pervaporation and Vapour Permeation of Methanol-Dimethyl Carbonate Mixtures through PIM-1 Membranes. *Sep. Purif. Technol.* **2019**, *217*, 206–214. [CrossRef]
15. Dibenedetto, A.; Aresta, M.; Angelini, A.; Ethiraj, J.; Aresta, B.M. Synthesis, Characterization, and Use of Nb^{V}/Ce^{IV}-Mixed Oxides in the Direct Carboxylation of Ethanol by Using Pervaporation Membranes for Water Removal. *Chem. Eur. J.* **2012**, *18*, 10324–10334. [CrossRef]
16. Décultot, M.; Ledoux, A.; Fournier-Salaün, M.C.; Estel, L. Organic Carbonates Synthesis Improved by Pervaporation for CO_2 Utilisation. *Green Process. Synth.* **2019**, *8*, 496–506. [CrossRef]
17. Won, W.; Feng, X.; Lawless, D. Pervaporation with Chitosan Membranes: Separation of Dimethyl Carbonate/Methanol/Water Mixtures. *J. Membr. Sci.* **2002**, *209*, 493–508. [CrossRef]
18. Dong, G.; Nagasawa, H.; Yu, L.; Wang, Q.; Yamamoto, K.; Ohshita, J.; Kanezashi, M.; Tsuru, T. Pervaporation Removal of Methanol from Methanol/Organic Azeotropes Using Organosilica Membranes: Experimental and Modeling. *J. Membr. Sci.* **2020**, *610*, 118284. [CrossRef]
19. Xu, X.; Van Eygen, G.; Molina-Fernández, C.; Nikolaeva, D.; Depasse, Y.; Chergaoui, S.; Hartanto, Y.; Van der Bruggen, B.; Coutinho, J.A.P.; Buekenhoudt, A.; et al. Evaluation of Task-Specific Ionic Liquids Applied in Pervaporation Membranes: Experimental and COSMO-RS Studies. *J. Membr. Sci.* **2023**, *670*, 121350. [CrossRef]
20. Kim, D.; Lee, M.; Shin, Y.; Lee, J.; Lee, J.W. Direct Production of Diethyl Carbonate from Ethylene Carbonate and Ethanol by Energy-Efficient Intensification of Reaction and Separation. *Chem. Eng. Process. Process Intensif.* **2023**, *192*, 109519. [CrossRef]
21. Elderderi, S.; Wils, L.; Leman-Loubière, C.; Henry, S.; Byrne, H.J.; Chourpa, I.; Munnier, E.; Elbashir, A.A.; Boudesocque-Delaye, L.; Bonnier, F. Comparison of Raman and Attenuated Total Reflectance (ATR) Infrared Spectroscopy for Water Quantification in Natural Deep Eutectic Solvent. *Anal. Bioanal. Chem.* **2021**, *413*, 4785–4799. [CrossRef]
22. Amit; Jamwal, R.; Kumari, S.; Dhaulaniya, A.S.; Balan, B.; Singh, D.K. Application of ATR-FTIR Spectroscopy along with Regression Modelling for the Detection of Adulteration of Virgin Coconut Oil with Paraffin Oil. *LWT* **2020**, *118*, 108754. [CrossRef]
23. Mohammadi, M.; Khorrami, M.K.; Ghasemzadeh, H. ATR-FTIR Spectroscopy and Chemometric Techniques for Determination of Polymer Solution Viscosity in the Presence of SiO_2 Nanoparticle and Salinity. *Spectrochim. Acta A Mol. Biomol. Spectrosc.* **2019**, *220*, 117049. [CrossRef] [PubMed]
24. Anjos, O.; Santos, A.J.A.; Dias, T.; Estevinho, L.M. Application of FTIR-ATR Spectroscopy on the Bee Pollen Characterization. *J. Apic. Res.* **2017**, *56*, 210–218. [CrossRef]
25. Shi, H.; Yu, P. Comparison of Grating-Based near-Infrared (NIR) and Fourier Transform Mid-Infrared (ATR-FT/MIR) Spectroscopy Based on Spectral Preprocessing and Wavelength Selection for the Determination of Crude Protein and Moisture Content in Wheat. *Food Control* **2017**, *82*, 57–65. [CrossRef]
26. Oleszko, A.; Hartwich, J.; Wójtowicz, A.; Gąsior-Głogowska, M.; Huras, H.; Komorowska, M. Comparison of FTIR-ATR and Raman Spectroscopy in Determination of VLDL Triglycerides in Blood Serum with PLS Regression. *Spectrochim. Acta A Mol. Biomol. Spectrosc.* **2017**, *183*, 239–246. [CrossRef] [PubMed]

27. Mukherjee, S.; Martínez-González, J.A.; Dowling, D.P.; Gowen, A.A. Predictive Modelling of the Water Contact Angle of Surfaces Using Attenuated Total Reflection—Fourier Transform Infrared (ATR-FTIR) Chemical Imaging and Partial Least Squares Regression (PLSR). *Analyst* **2018**, *143*, 3729–3740. [CrossRef]
28. Madsen, R.B.; Anastasakis, K.; Biller, P.; Glasius, M. Rapid Determination of Water, Total Acid Number, and Phenolic Content in Bio-Crude from Hydrothermal Liquefaction of Biomass Using FT-IR. *Energy Fuels* **2018**, *32*, 7660–7669. [CrossRef]
29. Barmpalexis, P.; Karagianni, A.; Nikolakakis, I.; Kachrimanis, K. Artificial Neural Networks (ANNs) and Partial Least Squares (PLS) Regression in the Quantitative Analysis of Cocrystal Formulations by Raman and ATR-FTIR Spectroscopy. *J. Pharm. Biomed. Anal.* **2018**, *158*, 214–224. [CrossRef]
30. Nespeca, M.G.; Hatanaka, R.R.; Flumignan, D.L.; De Oliveira, J.E. Rapid and Simultaneous Prediction of Eight Diesel Quality Parameters through ATR-FTIR Analysis. *J. Anal. Methods Chem.* **2018**, *2018*, 1795624. [CrossRef]
31. Kessler, W. *Multivariate Datenanalyse für Die Pharma-, Bio- und Prozessanalytik: Ein Lehrbuch*; Wiley-VCH: Weinheim, Germany, 2006; ISBN 978-3-527-61003-7.
32. Greilinger, G. Construction of a Membrane Pervaporation Unit for the Dehydration of an Organic Reaction Mixture. Master's Thesis, Technische Universität Wien, Vienna, Austria, 2024.
33. Annerl, M. Optimierung Der Diethylcarbonatsynthese Aus CO_2 Und Ethanol Durch Pervaporation. Master's Thesis, Technische Universität Wien, Vienna, Austria, 2024. [CrossRef]
34. Partial Least-Squares (PLS) Regression—MATLAB Plsregress—MathWorks Deutschland. Available online: https://de.mathworks.com/help/stats/plsregress.html (accessed on 8 March 2024).
35. De Jong, S. SIMPLS: An Alternative Approach to Partial Least Squares Regression. *Chemom. Intell. Lab. Syst.* **1993**, *18*, 251–263. [CrossRef]
36. Xu, Q.S.; Liang, Y.Z. Monte Carlo Cross Validation. *Chemom. Intell. Lab. Syst.* **2001**, *56*, 1–11. [CrossRef]

membranes

MDPI

Article

Design of a Gas Permeation and Pervaporation Membrane Model for an Open Source Process Simulation Tool

Kouessan Aziaba, Christian Jordan, Bahram Haddadi * and Michael Harasek

Institute of Chemical, Environmental & Bioscience Engineering E166, Technische Universität Wien, 1060 Vienna, Austria

* Correspondence: bahram.haddadi@tuwien.ac.at

Abstract: Gas permeation and pervaporation are technologies that emerged several decades ago. Even though they have discovered increasing popularity for industrial separation processes, they are not represented equally within process simulation tools except for commercial systems. The availability of such a numerical solution shall be extended due to the design of a membrane model with Visual Basic based on the solution-diffusion model. Although this works approach is presented for a specific process simulator application, the algorithm can generally be transferred to any other programming language and process simulation solver, which allows custom implementations or modeling. Furthermore, the modular design of the model enables its further development by operators through the integration of physical effects. A comparison with experimental data of gas permeation and pervaporation applications as well as other published simulation data delivers either good accordance with the results or negligible deviations of less than 1% from other data.

Keywords: simulation; membranes; membrane model; DWSIM; gas permeation; pervaporation

Citation: Aziaba, K.; Jordan, C.; Haddadi, B.; Harasek, M. Design of a Gas Permeation and Pervaporation Membrane Model for an Open Source Process Simulation Tool. *Membranes* **2022**, *12*, 1186. https://doi.org/10.3390/membranes12121186

Academic Editors: Yuexiao Shen and Lianfa Song

Received: 30 September 2022
Accepted: 19 November 2022
Published: 25 November 2022

1. Introduction

Membranes are already widely considered an alternative separation route alongside conventional separation technologies, such as cryogenic and adsorptive technologies, delivering comparably sufficiently high purities for many subsequent applications. Particularly advantageous compared to the alternatives mentioned is the easy maintenance, facile operation, small size, and low energy consumption, while a separation of liquid–liquid, vapor–liquid, and also gaseous mixtures is possible [1–4].

Within the framework of the design of technical processes, process simulation (PS) takes over many relevant functions. PS is a comparably cost-efficient and decisive tool in a company with experimental and plant engineering data for the design, operation, and optimization fields of process engineering. It offers the opportunity to predict the behavior of single unit operations (UOs) and the results of full processes as long as the models are available. It provides the opportunity to apply sensitivity analyses (SA), multivariate optimization, and copes relatively rapidly with design-of-experiments compared to experimental work. In addition, didactic purposes can be pursued with the use of process simulation.

Nevertheless, drawbacks can arise from those with comparably weak capabilities limiting PS's expressive power. However, some UOs qualities may increase their predictive accuracy through further development and validation with test cases. Furthermore, convergence problems, the possible necessity of preconditions, occurring errors, and limited access to several PS software and its UOs are already adverse but improvable aspects. Yet, the predictions obtained by PS are increasingly indispensable in the technical industry [5].

Since the demands of PS users can vary significantly depending on the process that shall be designed or optimized, there is also a variable selection of UOs each PS software offers. The focus of this work lies within the development of membranes for an open-source tool. Several development approaches for designing and using membrane models in

process simulation tools have been discovered and explored. However, the proposed model combines object-oriented methods to directly introduce a numerical solution for multi-component and multi-stage membrane separation into an open-source process simulation tool, while laying the groundwork for further developments by providing the complete source code as Supplementary Information. This modularity offers extensive development opportunities for the simulation and membrane research community, which is considered a novel development.

1.1. State of the Art: Mathematic Solutions for Membrane Models

Even though several publications already report models and implementations of gas permeation of binary systems, there is far less information about simulations to separate multi-component systems with membranes. Even though some information about the modeling is available in the literature, it is still constrained [6–10].

Pan et al., delivered a comparably early approach for the mathematical modeling of gas permeation for the co-current- and counter-current flow configuration model based on the solution-diffusion model compared with experimental data from a field pilot-plant recovering Helium (He) from natural gas. Pan et al.'s work considered the residues concentrations as the parameter to be set, yielding the permeate pressure, composition, and required fiber length. Since many membrane manufacturers do not offer the opportunity to provide custom fiber lengths, the applicability of this specific result may be limited [11].

Kundu applied the solution-diffusion model to separate multi-component gaseous mixtures with polymeric membranes to calculate the enrichment of Methane (CH_4) from biogas. A mathematical model is proposed using ordinary differential equations (ODE) for co-current- and counter-current flow configurations. The numerical solving technique, which uses Gear's method, demands the feed composition and the ideal selectivity referenced to a single compound. It describes the flux, the permeates flow rate, the composition of both, the permeate and the retentate, and the pressure build-up within the fiber [12].

Rezakazemi et al., proposed a mathematical 2D model that was handled with CFD-solving technology based on the Navier-Stokes equations to model HFMC for natural gas sweetening. Validation with experimental data is described as in "good agreement" with the simulation results, indicating that the model could also be used as a predictive instance for process designs [13]. Farno et al., provided a 3D gas permeation PDMS membrane model derived from mass transport and momentum transfer equations, also considering the diffusivity for a ternary system. An artificial neural network's contribution to improving the prediction of the permeates composition, permeabilities, and solubilities was also discussed. The results were in good agreement with experimental findings [14]. Haddadi et al., introduced a CFD algorithm for gas permeation simulations based on a multi-compartment approach. Each region can be regarded as its standalone operation inheriting its turbulence models, and thermophysical properties. The algorithm was implemented in the open-source CFD environment OpenFOAM [15].

Katoh et al., proposed the tank-in-series method combined with the Runge–Katta integration method to solve the governing ODEs to handle the dynamic and non-ideal mixing behavior of the species across the membrane [16]. Elshof et al., described a mathematical model for the separation of water and organic solvents with a microporous silica membrane based on the Maxwell-Stefan model. The model relies on Maxwell-Stefan diffusion coefficients, which describe the transport through the microporous barrier, also considering the friction during this phenomenon [17]. Makaruk et al., developed a numerical approach for the calculation of co-current- counter current and cross-flow gas permeation membranes, which were also verified with experimental results [18].

Finally, it remains to mention the availability of further models to describe mass transfer across a membrane depending on the membrane type, such as the pore-flow model, which is occasionally applied for liquid binary mixtures and porous membranes. [19]

The following list shall highlight some advantages and drawbacks of the aforementioned modeling solutions:

- Solutions-Diffusion model Undoubtedly, the solution-diffusion model (SDM) is one of the most widely used and adapted models found in the literature and process simulators for gas permeation and pervaporation applications. The description of the product streams is usually possible depending on the feed concentration, permeance, and a set product value, such as the concentration of the permeate or the pressure difference. Theoretically, there is no limit to the number of compounds the model can handle. The limited accuracy of the model can be a drawback. However, its relative simplicity makes it more likely to be combined with customized solving routines. Most models to follow in Section 1.3 are based on further developments of the solution-diffusion model;
- Maxwell–Stefan Theory As a theory that also incorporates the migration in dependence of friction and influences of the interaction of components and membrane, the Maxwell-Stefan theory is comparably more complex than the SDM. Theoretically, the model can process multi-component gas permeation and pervaporation systems. An advantage of the Maxwell-Stefan theory is the opportunity to obtain comparably more accurate information about non-ideal multi-component systems from the results of single-component calculations and an estimation of the systems' selectivities [20];
- Pore flow Model This model is usually introduced as a theory for porous membranes separating liquid mixtures. In comparison, it is based on the migration of permeating components through theoretical pores on the membrane's surface through capillary. Several adaptions of the underlying mathematical relations are to be found in the literature, such as the equation of Ergun, Carman–Kozeny, or Darcy's law. While it is considered to perform roughly equivalently accurately, it shares the identical drawback as the SDM in that it majorly considers the pressure and concentration gradient. However, depending on the mathematical background, it may give information about the pressure drop due to the geometry of the membrane itself [19–21];
- Object-oriented Programming Even though modeling with object-oriented programming methods is not an actual calculation routine similar to the earlier mass transfer methods, it can be a powerful approach for modeling in general. While calculation routines and algorithms are the center of interest for developers, the product mainly displays the model itself and its handling. This may indicate an increased complexity since other routines must be implemented then the pure numeric solution. However, this also poses a huge potential since every method can communicate with each other [22].

1.2. State of the Art: Membrane Models in Process Simulators

Aspen Technology is a well-known provider of two proprietary process simulators, Aspen Plus and Aspen Hysys. The primary application fields are process design and optimization in chemical engineering industries [23]. Many PS tools have an interface for integrating custom models or licensed addons, as Aspen Technologies does. The Aspen Custom Modeler belongs to the Aspen software package and is a commonly used solution for integrating user-generated models [24,25]. Additional integration methods in the literature use Aspen technology products, such as FORTRAN or MATLAB [26].

Nonetheless, adverse effects are reported using Aspen Hysys in combination with MATLAB, Excel, Python, and C# [27]. According to custom modeling and membranes, several models have already emerged for Aspen Plus and Aspen Hysys. A flat sheet gas permeation membrane model was implemented into Aspen Plus with the Aspen custom modeler based on the fugacities and mixture diffusivities derived from Blanc's law. The predictive performance for the residuals molar fraction is described to be accurate [28].

ChemBrane is a custom membrane model developed by Graigner in 2007 which operates on Hysys based on a fourth-order Runga–Kutta method for the calculation of the flux. It is used to predict the flux for perfectly mixed, co-current, and counter-current flow configurations based on the permeabilities of each compound [29]. Cavalcanti et al., described a pervaporation membrane model based on the SDM integrated with the Aspen Custom

Modeler. It was applied to predict the purification of EtOH with a polyetherimide membrane [30]. A high-pressure hollow fiber membrane contactor for natural gas purification was modeled for the PS tool gPROMS in a counter-current flow configuration [31]. AVEVA's Pro/II is an equation-oriented steady-state PS tool that already inherits a membrane model developed based on a membrane reactor derived from Bishop et al. [32].

An overview of additional available PS tools which allow the development and integration of membrane models is available in the literature [33]. All described tools have in common that only proprietary PS tools are available today. This is an adverse and limiting precondition for multiple reasons. The accessibility for industry, researchers, and teachers is limited due to partially costly products. Further, the models are commonly provided as black box models. This excludes the opportunity to re-construct the algorithm to evaluate if the preliminarily determined preconditions are suitable for the model. In combination with the lost opportunity to modify or extend the model, many models' capabilities are limited in many ways. Therefore, the drive for the development of an initially facile but continuously extended open-source membrane model for an open-source software was given.

1.3. Mathematical Background of the Model

Currently, the solution-diffusion model is reportedly a popular approach to model membrane separation. It is suitable for various gas and liquid feeds in membrane permeation applications. [34] The idealized counter- and co-current flow patterns are illustrated in Figure 1.

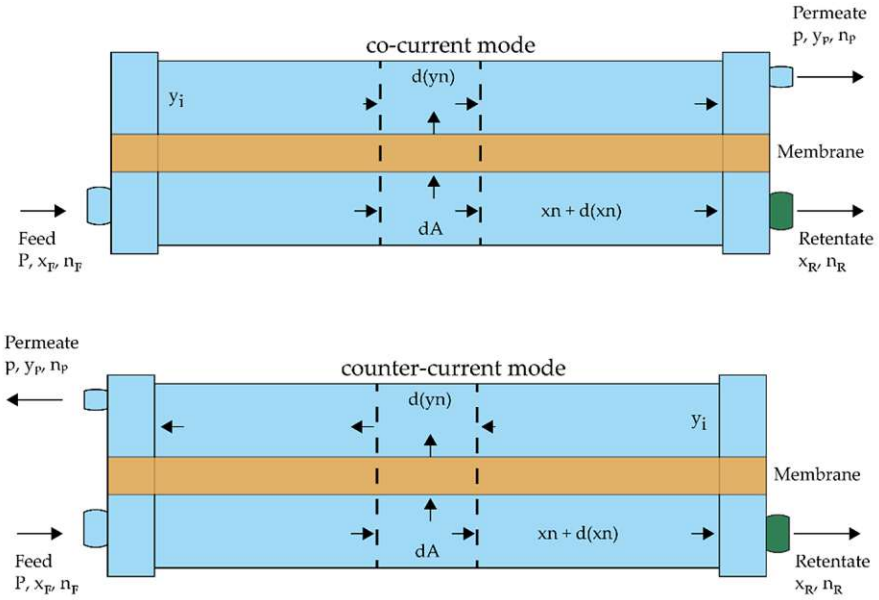

Figure 1. Illustrations of idealized co-current (top) and counter-current (bottom) flow patterns.

The local flux through the membrane is commonly described as follows Equation (1).

$$d(xn) = -Q \times A \times (xP - yp) \quad (1)$$

The molar flow, molar fraction, and permeance are abbreviated as n, x, and Q. The feed pressure P, permeate pressure p, A, and y as the surface area and the permeate composition of the operation also determine the flux. The subscripted variables F, p, and r represent the feed, permeate, and retentate side of the corresponding value. The membrane area A can be calculated from the number of fibers ϵ, the inner diameter of the fiber d_{fiber}, and the fiber length l_{fiber} as described in Equation (2).

$$A = \epsilon \times d_{fiber} \times \pi \times l_{fiber} \quad (2)$$

Considering the fact that process simulation tools will be obliged to set multiple preconditions, such as plug flow, perfect mixing on the permeate and the feed/retentate side Equation (1) shall be integrated and set in relation with its feed, which shall result in a relation between the flux and the stage-cut. The molar fractions x and y are to be chosen depending on the flow configuration.

$$\theta = \frac{yn_p}{x_F n_F} = \frac{AQ(xP - yp)}{x_F n_F} \tag{3}$$

Since the SDM is already well documented and published, this work will solely cover its implementation into the PS tool DWSIM, including its modifications and preconditions. However, the presented background is also well applicable to other PS tools. Alongside the solution-diffusion model itself, the following list of preconditions were also set:

- Negligible axial and radial pressure variation;
- Perfect mixing in every compartment;
- Negligible radial concentration variation
- Pure component permeances are independent of feed composition, temperature, and pressure variations;
- Negligible deformation of the hollow fiber under pressure.

Since not only the feed composition but also the permeate composition is decisive for the driving force, it must also be considered in the calculations. With the previously stated upper assumptions, the permeate composition y_i can be calculated as follows.

$$y_i n_p = AQ(x_r P - y_i p) \tag{4}$$

For multi-component fluid mixtures, the permeate molar fraction for counter-current flow is calculated by forming the ratio of the components' fluxes over the total flux [10]. The subscripts i, j, and k represent the ith, jth compound from a total number k of compounds.

$$\frac{y_i}{1 - y_i} = \frac{Q_i(x_{r,i}P - y_i p)}{\sum_{j \neq i}^{k} Q_j\{(1 - x_{r,j})P - (1 - y_j)p\}} \tag{5}$$

A distinction must be made on whether a counter-current or co-current membrane shall be modeled. The driving force of the membrane model configured as a counter-current model competes with the permeate side aside from the feed's end, which is indicated in Equation (6), which is a rearrangement from Equation (5).

$$y_i = \frac{Q_i x_{r,i} \alpha_i \sum_{j \neq i}^{k} y_j}{\sum_{i \neq j}^{k} Q_j(x_{r,i}\alpha_i - y_j) + Q_i \sum_{j \neq i}^{k} y_j} \tag{6}$$

The driving force for the co-current flow mode is slightly different since it is the retentate end of the feed that corresponds with the actual permeate, as indicated in Equation (6).

$$y_i = \frac{Q_i x_{F,i} \alpha_i \sum_{j \neq i}^{k} y_j}{\sum_{i \neq j}^{k} Q_j(x_{F,i}\alpha_i - y_j) + Q_i \sum_{j \neq i}^{k} y_j} \tag{7}$$

2. Materials and Methods

This section intends to provide an overview of the applied routines and methods to design and integrate the mathematical model into open-source PS software. Specific software was chosen to proceed with the approach, yet the presented procedures are applicable for any PS tool that can proceed or include numerical solvers.

2.1. Machine, Operating System and Software

Every applied software was operated on both a AsRock DeskMini A300 with a Ryzen 3 3400G and 32 GB of Ram and a Notebook Dell Inspiron 7415 with a Ryzen 5 5500U processor and 16 GB of RAM. All systems were operated with Windows 10. DWSIM was operated with version 8.0.3 on both systems. The Visual Basic(VB) code was scripted in Visual Studio 2017, its community distribution.

2.2. DWSIM

DWSIM is an open-source process simulation tool available on multiple platforms that was developed by Daniel Wagner Oliveira de Medeiros. It can be considered as a competitive alternative to other process simulators, such as Aspen Plus or PRO-II. It also operates its calculations as steady-state simulations. Since Version 6, dynamic simulations were introduced into DWSIM. With Version 7 DWSIM Pro was introduced, which offers various extensions, such as further Unit Operations (UO) and property packages. DWSIM provides the possibility to modify individual units as well as entire calculation routines of the flowsheet. Further, it already supports the opportunity to manipulate the communication between UOs and the flowsheet, and between UOs. The creation of whole UOs as custom plugins is an additional strength DWSIM offers. Yet, they must have been written in DWSIM's native coding language, Visual Basic and C# [35].

2.3. Steps to Follow

2.3.1. Work Environment

DWSIM was obtained from SourceForge [36]. The setup inherits Microsoft WebView 2 Runtime, ChemSep, CAPE-OPEN Type Libraries, Register Type Libraries, and DWSIM itself [35]. The initial step to set up the actual work environment is creating a VB Class project by configuring the project's name, location and aiming. NET Framework. Targeting the same. NET Framework as the DWSIM is running is recommended. A selection of DWSIM-related dynamic link library files (.dll) will offer the opportunity to run DWSIM-associated functions within VB if implemented in the reference section. Since not every library is needed for the developed functions, the complete list of DLL's is provided in Table A1.

2.3.2. Implementation of General Models Related Functions

Since DWSIM is an open-source tool, there are also open libraries that can be applied to various models. Functions and code structures, such as the opportunity to process several properties of incoming materials streams or even the cosmetic design of the model itself, are provided to a fair extent. Table A2 contains the applied libraries.

In order to ultimately start the code, a couple of initial properties must be defined. Since the model of interest is a UO, it must also inherit the data structure of it, while it should also include the opportunity to apply the typical functions of other UOs in DWSIM. The two following lines of code can realize these:

```
Inherits UnitOperations.UnitOpBaseClass
Implements DWSIM.Interfaces.IExternalUnitOperation
```

Following this, the first set of properties shall be declared here, such as the UO's name and description and the category to which the UO belongs. Whenever a UO is initialized, it also inherits default values for its parameters, which can also be provided as early as this step.

```
Public m_ResStageCut As Dictionary(Of String, Double)
Private Property UOName As String = "Membrane"
Private Property UODEscription As String = "Membrane Unit Operation"
Private _components As New List(Of String)
Private _componentsids As New List(Of String)
Private _components_re As New List(Of String)
```

```
Dim N0 As New Dictionary(Of String, Double)
Dim Colums, Rows As Integer
Public Overrides Property ComponentName As String = UOName
Public Overrides Property ComponentDescription As String = UODEscription
Public Overrides Property ObjectClass As SimulationObjectClass = SimulationObjectClass.Separators
Public Property Permeances As New Dictionary(Of String, Double)
Public Property AllPermeances As New Dictionary(Of String, Double)
Public Property PermeatePressure As Double = 100000.0
Public Property NumberFibers As Double = 100.0
Public Property InnerDiameterFibers As Double = 0.01
Public Property FiberLength As Double = 0.1
Public Property Chambers As Double = 1
Public Property StageCut As Double = 0.2
```

One primary motivation for creating this UO was the opportunity to design the property editor (PE) in a fully customized way. Therefore, the PE will take its own descriptive part within the Supplementary Information. However, the PE also has to be linked to the main UO model, which usually shall also occur in the initial part of the code.

```
Public Overrides Sub DisplayEditForm()
If editwindow Is Nothing Then
editwindow = New Editor() With {.HObject = Me}
editwindow.ShowHint = GlobalSettings.Settings.DefaultEditFormLocation
editwindow.Tag = "ObjectEditor"
Me.FlowSheet.DisplayForm(editwindow)
Else
If editwindow.IsDisposed Then
editwindow = New Editor() With {.HObject = Me}
editwindow.ShowHint = GlobalSettings.Settings.DefaultEditFormLocation
editwindow.Tag = "ObjectEditor"
Me.FlowSheet.DisplayForm(editwindow)
Else
editwindow.Activate()
End If
End If
FlowSheet.DisplayForm(editwindow)
End Sub
```

On a regular application of the UO on a flowsheet, the PE must be frequently closed and opened, resulting in the necessity of implementing these functions.

```
Public Overrides Sub UpdateEditForm()
If editwindow IsNot Nothing Then
If editwindow.InvokeRequired Then
editwindow.Invoke(Sub()
editwindow?.UpdateInfo()
End Sub)
Else
editwindow?.UpdateInfo()
End If
End If
End Sub
Public Overrides Sub CloseEditForm()
'editwindow?.Close()
If editwindow IsNot Nothing Then
If Not editwindow.IsDisposed Then
editwindow.Close()
```

```
editwindow = Nothing
End If
End If
End Sub
```

Further general model-specific functions, e.g., functions to manage and display the input and output connectors, a call function for the model image, and many more, are provided in the Supplementary Information.

2.3.3. Implementation of Membrane Specific Functions

With the general model-specific functions created, a suitable environment to implement membrane-specific properties and functions is finally available. The following section shall give an insight into the approach to implementing functions that shall provide specific properties for the membrane model, e.g., the membrane area, calculation mode, flow mode, and functions to calculate stream-related properties.

A selection of the most relevant functions is provided and explained in this section.

Creating an entity of a stream is necessary at some points of the calculations. Therefore, a method to do so is introduced

```
Public Function InitStream() As MaterialStream
Dim Value As MaterialStream
Value = New MaterialStream()
Me.FlowSheet.AddCompoundsToMaterialStream(Value)
Value.SetFlowsheet(FlowSheet)
Value.PropertyPackage = Me.PropertyPackage
Value.SpecType = StreamSpec.Temperature_and_Pressure
Value.ClearAllProps()
Return Value
End Function
```

This function is applied to introduce an intermediate stream different from all input and output streams. It offers the opportunity to use the DWSIM integrated calculation routine to find the physical properties of mixed streams without changing anything of the actual present streams on the flowsheet.

```
Public Function RefreshStream(Stream As MaterialStream, Temperature As Double, Pressure As
Double, MolarFraction As Double(), MolarFlow As Double()) As MaterialStream
Stream.ClearAllProps()
Stream.SetMolarFlow(SumY(MolarFlow))
Stream.SetOverallComposition(MolarFlow.ToArray)
Stream.SetTemperature(Temperature)
Stream.SetPressure(Pressure)
Stream.SetFlashSpec("PT")
Me.PropertyPackage.CurrentMaterialStream = Stream
Stream.Calculate()
Stream.Validate()
Return Stream
End Function
```

Especially the pervaporation process is highly dependent on the continuous calculation of the physical properties of the stream's compounds. The actual calculation routine utilizes quantization steps within a single model. This causes a change in concentration when the stream is submitted to the following chamber. The function "RefreshStream" recalculates all stream-specific properties again. The partial pressure is a crucial variable for calculating the driving force. The partial pressure calculation follows two different routes depending on whether a gas permeation or pervaporation is simulated. The algorithm for gas permeation implements the law of Dalton.

```
Public Function PartialPressure(MolFrac As Double(), Pressure As Double) As Double()
Dim Value(MolFrac.Length − 1) As Double
For I = 0 To MolFrac.Length − 1
Value(I) = Pressure * MolFrac(I)
Next
Return Value
End Function
```

Even though the partial pressures of the vapor flow could be calculated, DWSIM's internal functions were used to determine these values by getting the pressure of the feed stream.

```
Public Function PartialPressure(Stream As MaterialStream) As Double()
'get pressure and molarfrac from stream, apply Law of Dalton
Dim molarFraction As Double() = Stream.GetPhaseComposition(0)
Dim Pressure As Double = Stream.GetPressure()
Dim Value(molarFraction.Length − 1) As Double
For i = 0 To molarFraction.Length − 1
Value(i) = Pressure * molarFraction(i)
Next
Return Value
End Function
```

Having the relevant partial pressures available finally allows calculating the composition y_i of the permeate on the retentate end.

Public Function yiRetentateMultids2(RetMolFrac As Double(), MolFracLastIt As Double(), ratio As Double(), Perm As Double()) As Double()

```
Dim A(RetMolFrac.Length − 1), B(RetMolFrac.Length − 1), C(RetMolFrac.Length − 1), Value(RetMolFrac.Length − 1), ValueRaw(RetMolFrac.Length − 1) As Double
For I = 0 To RetMolFrac.Length − 1
A(I) = Perm(I) * RetMolFrac(I) * ratio(I) * (SumY(MolFracLastIt) - MolFracLastIt(I))
B(I) = 0
For J = 0 To RetMolFrac.Length − 1
If J = I Then
B(I) += 0
Else
B(I) += Perm(J) * ((RetMolFrac(J) * ratio(J)) − MolFracLastIt(J))
End If
Next
C(I) = Perm(I) * (SumY(MolFracLastIt) − MolFracLastIt(I))
ValueRaw(I) = A(I)/(B(I) + C(I))
Next
Dim SumRaw As Double = SumY(ValueRaw)
For I = 0 To RetMolFrac.Length − 1
Value(I) = ValueRaw(I)/SumRaw
Next
Return Value
End Function
```

The value y_i provides the opportunity to calculate the stage-cut θ and consequently the retentate composition x_r and the corresponding partial- and vapor pressures.

```
While (deviation >= 0.00001) And (count < 1000)
yi = yiRetentateMultids2(xr, yi, Ratio, Permeance)
pyi = PartialPressure(yi, pp)
For I = 0 To NumCompounds − 1
qi0(I) = qip(I)
```

```
Next
For I = 0 To NumCompounds − 1
sc(I) = (((Permeance(I) * (Area/Chambers))) * (((pxf(I) − pyp(I)) − (pxr(I) − pyi(I)))/(Log((pxf(I)
− pyp(I))/(pxr(I) − pyi(I))))))/NEff(I)
Next
For I = 0 To NumCompounds − 1
qip(I) = sc(I) * NEff(I)
Next
qtp = SumY(qip)
For I = 0 To NumCompounds − 1
yp(I) = qip(I)/qtp
Next
pyp = PartialPressure(yp, pp)
qtr = 0
For I = 0 To NumCompounds − 1
qir(I) = NEff(I) − qip(I)
Next
qtr = SumY(qir)
For I = 0 To NumCompounds − 1
xr(I) = qir(I)/qtr
pxr(I) = Pf * xr(I)
Next
deviation = 0
For I = 0 To NumCompounds − 1
deviation = deviation + Abs(qip(I) − qi0(I))
Next
count = count + 1
End While
```

This loop is the last instance of the actual calculations. It starts with an If- condition where the deviation of the stage-cut is compared. This error must fall below a tolerance of 10^{-6} to end the while loop, as long as the while-loop continues to run the calculations process with the determination of the permeate composition followed by its corresponding partial pressures. These calculations are followed by the determination of the stage-cut from y_i. x_r and the remaining total flows are calculated from the stage cut.

The exportation of the corresponding file delivered the model into the "unitop" folder of DWSIM as a .dll file.

2.4. Test Cases

As a performance benchmark, this subsection shall introduce applied test cases in this work. The first test case is a polyetherimide/γ-alumina composite membrane characterized and described by Park et al. It was used to separate HAc, EtOH, EtOAc, and H_2O. The initial model set-up was operated with a permeate pressure of 267 Pa. The fiber was further specified with an inner diameter of 7 mm and an arbitrarily large amount of fibers of 750,000 with 30 compartments. The length of the fibers was set to 1 m. An overview of the permeance of every compound and the feed, retentate, and permeate composition of the corresponding simulation of test case 1 is described in Section 4.1.

The model was also compared with other gas permeation and pervaporation solutions from the literature. These further test cases inherit both experimental results as well as simulated data. An overview of different investigated models is displayed in Table 1.

Table 1. An overview of compared gas permeation and pervaporation systems.

	Sada et al. [37] **Test Case 2**	**Chowdhury et al. [38]** **Test Case 3**	**Koch et al. [39]** **Test Case 4**
membrane	asymmetric cellulose triacetate hollow fiber (Sample 31)	simulated asymmetric cellulose acetate hollow fiber	Hydrophilic polymeric PERVAP^{TM} 1210
type	gas permeation	gas permeation	pervaporation
flow configuration	counter-current	counter-current	co-current
inner diameter [µm]	0.000125	80	
length [cm]	63	15	[1] membrane area 159.4 cm^2
no. of fibers [-]	270	70	
Temperature [K]	303	298	~333 K
feed pressure [bar]	Varied between 15.7–5.9	69.64	
feed composition	50.0% CO_2 10.5% O_2 39.5% N_2	51.78% H_2 24.69% N_2 19.57% CH_4 3.96% Ar	23.7 % ACE 65.1 % H_2 11.2 % IPA
permeate pressure [mbar]	1013.25	11230	
permeance [10^{-10} mol/s m^{2}Pa]	CO_2: 204.2 O_2: 60.2 N_2: 13.1	H_2: 284 N_2: 2.95 CH_4: 2.84 Ar: 70	variable permeances

[1] Values such as the inner diameter, number of fibers, and the fiber length are not provided by the source of the membrane.

The second test case can be described as a hollow-fiber gas permeation membrane module that was deployed to separate a three-component mixture consisting of CO_2, O_2 and N_2. Four different Modules were reported. However, only module 31 was compared in this study. The permeance of CO_2 in the membrane was determined experimentally at 30 °C and 24 bar [37].

Test case three is a membrane model for multi-component gas permeation developed for Aspen Plus as a FORTRAN calculation routine. The model was compared to multiple models and experimental data. The test case was created with a simulation separating H_2, N_2, CH_4, and Ar with an upstream pressure of approximately 69 bar and a permeate pressure slightly above 11 bar. The permeances were taken from another publication specified in the work of Chowdhury et al. [38].

The final and fourth test case was derived from the work of Koch et al., who managed to separate EtOH, IPA, and ACE with a polymeric PERVAP^{TM} 1210 membrane with an active layer of polyvinyl alcohol receiving high purities of water in the permeate stream. The feed pressure was kept atmospheric, while the permeate pressure was adjusted to approximately 3000 Pa.

3. The Model

Staring DWSIM also initiates results in the usual loading screen, which is terminated with the initial menu, where a new file can be either set up or an existing one can be loaded. For this investigation, a new empty file was created. A random number of compounds can be chosen all of which shall have the same state. If the compounds are in a liquid form, the availability of interaction parameters must be considered. Nevertheless, the properties of test case 1 were chosen for this specific set-up. The membrane model can be found on the Separator/Tanks tab of the UO's menu. The implementation of the flowsheet does not differ from the other UOs. The model offers the opportunity to attach two inlets, one of which is an energy inlet, and two outlet streams. The flow direction happens to be the configuration of a co-current model. The model is portrayed in Figure 2.

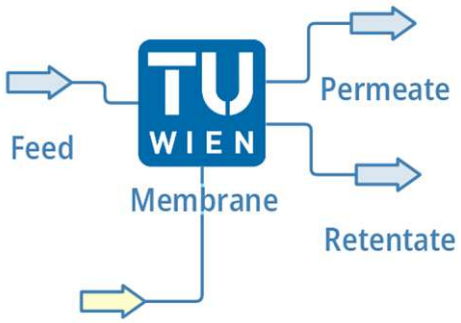

Figure 2. An actual impression of the unit operation on DWSIM's flowsheet.

Property Editor

The property's editor was designed to improve the operability of the whole model itself. The editor of the model occurs just analogously to the other model's editors by clicking on the model itself. Alongside the general information and the group of connections, there is also a box element with three tabs. Another box with only two tabs follows this box. The property table is portrayed in Figure 3.

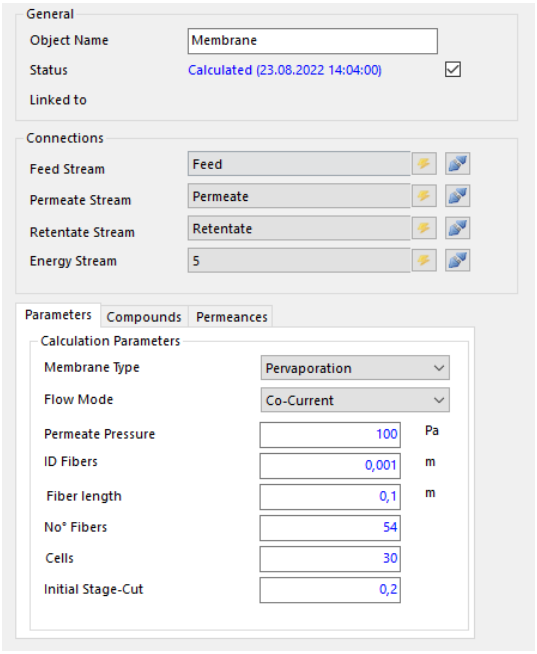

Figure 3. The property table with the first tab and its calculation parameters.

The major calculation parameters are to be found on the first Table 2 drop-down menus with three entries each that are followed by the six fields with values that can be set here. The permeate pressure as well as three further fields with fiber-related properties are revealed on this part of the editor. Fiber is the primary area determining property. Further, the number of compartments is to be specified on the 5th field.

Toggling through the tabs by clicking delivers a list of compounds handled by the membrane and a table with the corresponding permeances.

The only function of the compounds tab is the opportunity to check specific compounds of the simulation. If a particular compound is checked, it will be considered in the separation process. Figure 4b is derived from the compounds checked in the tab before and only displayed the compounds and the lists which have been checked. The initial values for the permeances of the displayed compounds are 0 mol/m^2sPa.

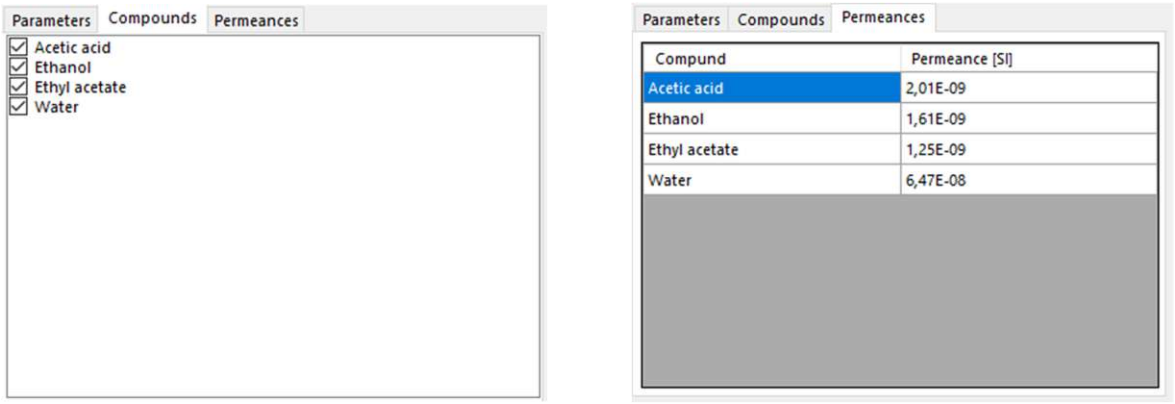

(**a**) (**b**)

Figure 4. This figure portrays the compound (**a**) and the permeances (**b**) tabs of the membrane model.

4. Results and Discussion

The following section shall give an insight into the behavior of the developed UOs in dependence on various parameters. Further, the accuracy and reliability of the results shall also be investigated.

4.1. Influence of Parameters

As mentioned in Section 1, the permeance of a compound through a specific membrane is a highly influential parameter for the flux of a compound through a membrane. Therefore, the behavior of the model, which uses the solution-diffusion model as a calculative background, is of interest. The permeance must be a highly influential parameter for the calculative background. The results of the test case one simulations are listed in Table 2.

Table 2. An overview of the permeance of every compound and the feed, retentate, and permeate composition of the corresponding simulation of test case 1. Permeance data obtained from [40].

Compound	Permeances [mol/m^{2}sbar]	Feed mol%	Permeate mol%	Retentate mol%
HAc	0.000201	14	1.07	14.98
EtOH	0.000161	14	1.25	14.97
EtOAc	0.000125	36	3.01	38.51
H_2O	0.00647	36	94.68	31.54

The permeance of H_2O is seen to be at least ten times higher than the permeance of any other compound. Alongside this, it can also be observed that the composition of the permeate consists of almost 95% water, followed by EtOAc with 3%. HAc and EtOH share approximately 1% of the permeate composition. The composition of the retentate is quite similar to the feedstock. All compounds seem to be enriched with the exception of H_2O, which dropped to a composition of 31.54%. The stage-cut was calculated to be 0.071.

4.1.1. Area

Alongside the permeance of each compound, the available area of the membrane is decisive for the flux and composition of the product streams. Sensitivity analyses with the number of fibers as a variable were carried out to obtain an overview of the influence of the area on the simulation. The compositions of the permeate and retentate are displayed in dependence on the stage cut in Figure 5.

The initial behavior regarding the permeate reoccurs again, showing that the H_2O content in the permeate is the highest at any stage-cut, followed by EtOAc with a very long distance. EtOH and HAc almost share the same compositions, close to 1% for all stage

cuts < 0.3. While the behavior of the initial simulation in 3.2.1 was basically reproduced for the counter-current configuration, slight differences can be observed if the simulation was run in co-current mode. However, even though every compound permeates concentrations are still deficient compared to H_2O, two compounds switch their positions in the rankings of the permeate molar fraction. EtOH surpasses HAc on the co-current simulations.

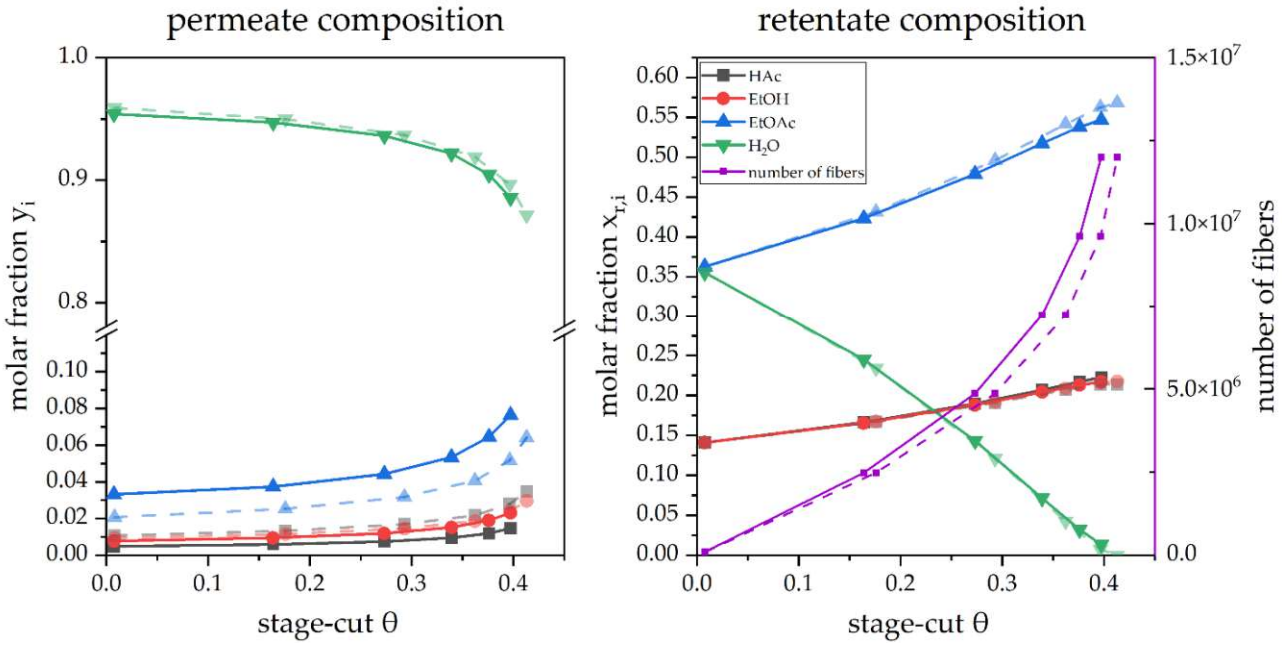

Figure 5. A simulated pervaporation operation in counter-current (—■—) and co-current (- -■- -) mode in dependence on the stage cut θ.

Further information about the model's behavior is displayed by the decrease of H_2O in the permeate and the corresponding increase of the other compounds. It can be observed that the trends shown are clearly non-linear in dependence on the stage cut. Since the permeate composition does not portray a complete picture of the system, the retentate composition is also displayed in Figure 5.

Two interesting trends are revealed in Figure 5. The trend for the H_2O content in the retentate is driven down to a value very close to 0 at a stage cut of 0.4. The second information in this plot is revealed as the initial rise of other compounds concentrations up to a stage cut of approximately 0.4.

Another notable behavior is the fact that the simulations do not converge after a further increase in the number of fibers. This behavior may also be related to the low residual water content in the feed/retentate, resulting in a deficient driving force.

4.1.2. Feed

The performance of the same membrane was also investigated numerically in dependence on the feed by increasing the EtOH content of the feed from 0.1 to approximately 0.7 wt%. A comparison of y_p and x_r for the counter-current and co-current is displayed for the permeate and the retentate streams in Figure 6.

The share of fast permeating H_2O is the largest, starting with above 95 mol%. However, the rising share of EtOH in the feed leads to reduced water content in the permeate. While the composition of EtOAc and HAc stay almost constant in the permeate stream, a comparably strong rise of EtOH is revealed with rising $x_{F,\,EtOH}$. Figure 6 also reveals a seemingly linear depletion of all compounds in the retentate stream with the exception of EtOH which is displayed with a strong rise to a similar scale as $x_{F,\,EtOH}$. Further, also the stage cut is revealed to decline in both flow configurations with increasing $x_{F,\,EtOH}$.

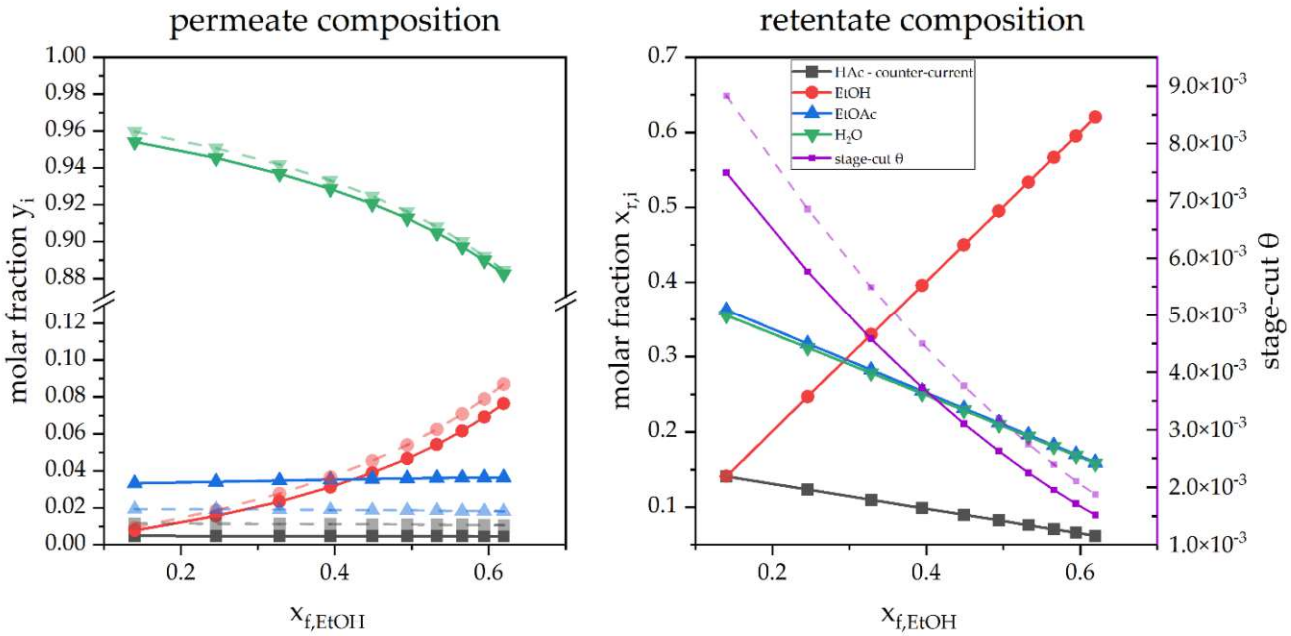

Figure 6. A simulated pervaporation operation in counter-current (—■—) and co-current (- - ■ - -) mode depending on $x_{F,\,EtOH}$.

4.1.3. Cells

Many models follow the approach to calculate the membrane as a single unit. Since the retentate and also the permeate composition is highly dependent on the change of the feed composition proceeding through the membrane, it can be assumed that a model could be tuned by a separation into multiple compartments. These compartments were realized as cells. The influence of the number of cells is displayed in Figure 7.

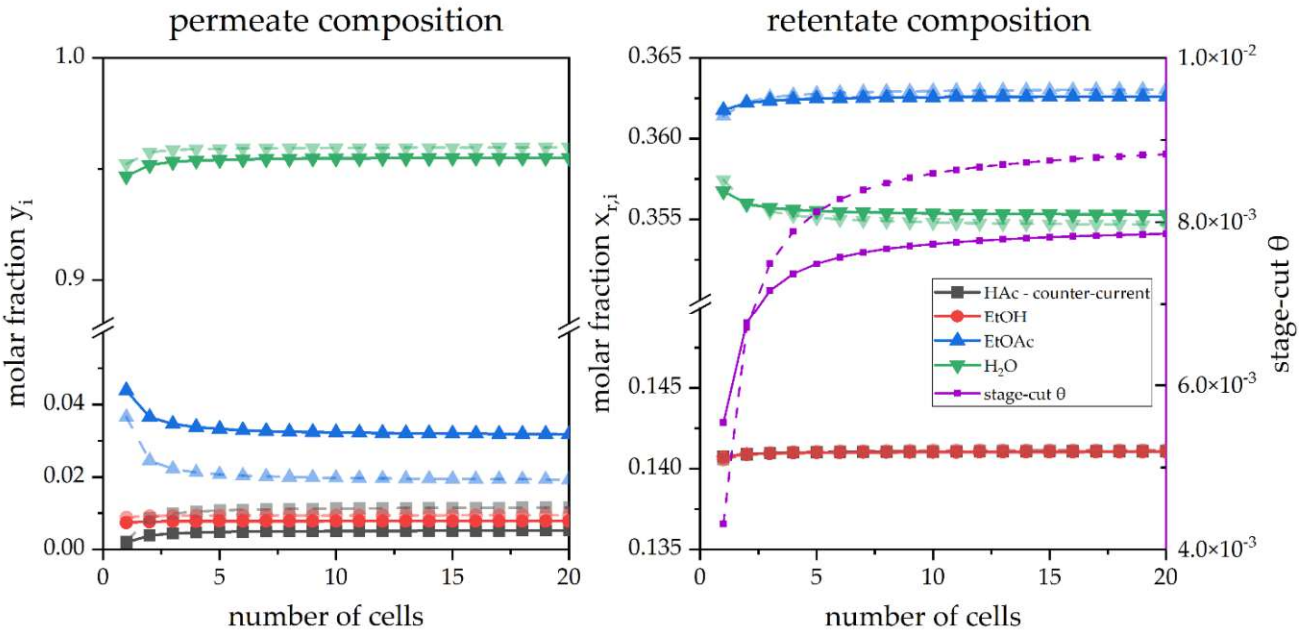

Figure 7. A simulated pervaporation operation in dependence on the number of compartments in counter-current (—■—) and co-current (- - ■ - -) mode.

Specifying here what is visible in the images, the trends display a significant deviation for the compositions in the permeate for less than five cells. Whenever the amount of five cells is surpassed; the concentrations stay constant with comparably low deviations.

4.2. Comparisons

Three other test cases, cases 2, 3 and 4, were prepared and simulated. The test cases are covered and described in Section 2.4 and Table 1.

4.2.1. Gas Permeation

Two test cases were carried out as gas permeation simulations. Test case 2 was simulated, resulting in a comparison between the experimental data obtained by Sada et al., and the DWSIM simulation is displayed in Figure 8.

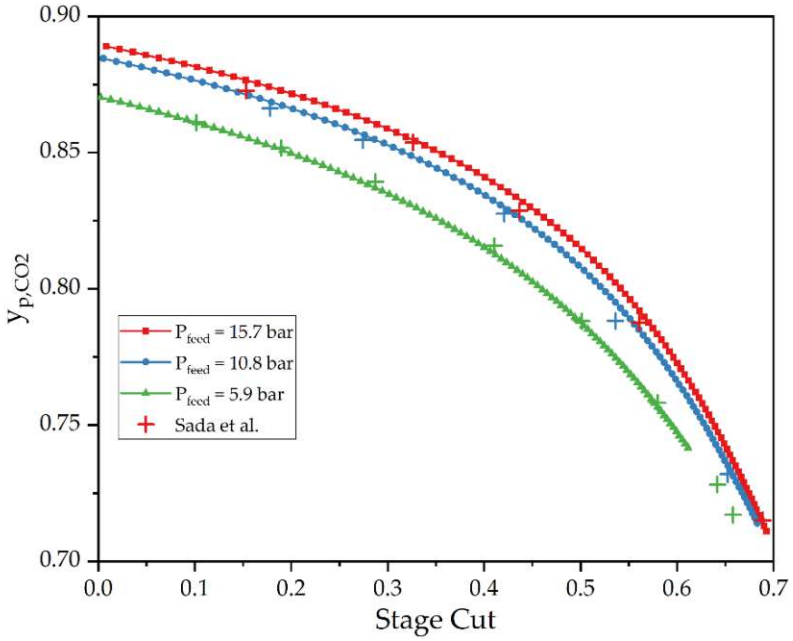

Figure 8. A comparison of an experimental gas permeation operation by Seda et al. [37]. (test case 2) and a DWSIM simulation in dependence of θ.

As a first impression, it can be seen that the trends of the experimental data are in accordance with the trends of the simulations, while the actual CO_2 concentrations also range in the same scale. The CO_2 content of the permeate decreases with the rising stage cut. The deviation between the simulated data and experimental values is <0.84% for all simulations.

Test case three is another comparison for gas permeation. A comparison between the DWSIM model and the work of Chowdhury et al., is portrayed in Figure 9.

For practical reasons, the scale of the *y*-axis was cut into two segments giving better visibility of the plots. As indicated by the permeances of the available components, the composition of the permeate mainly consists of H_2. It starts at approximately 97.5% for a stage cut of 0.3 and proceeds to decrease the more the flux increases. Correspondingly, the composition of the other compounds starts at just approximately 1% each and increases with the N_2, CH_4, and Ar in decreasing order. The most exciting information in Figure 9 is the seemingly good agreement between the data delivered by DWSIM and the simulated results of Chowdhury et al. [38].

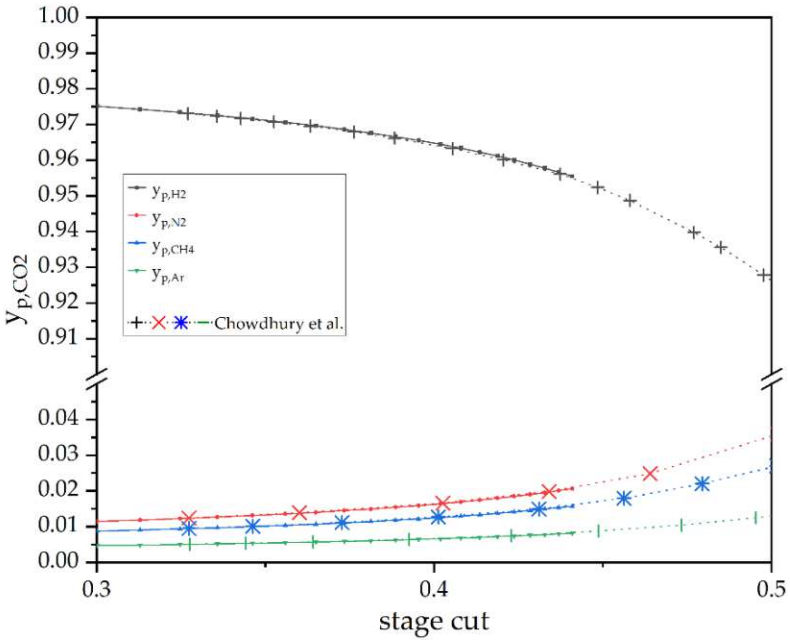

Figure 9. A comparison of an experimental gas permeation operation by Chowdhury et al. [38]. (test case 3) and a DWSIM simulation in dependence of θ.

4.2.2. Pervaporation

The separation of liquid–liquid mixtures received less attention in simulation tools, as already mentioned at the beginning of the work. Yet, a test case for the pervaporation was set up for comparison purposes with this model with test case 4, which is based on the work of Koch et al. A comparison of the water composition of the permeate depending on the water fraction in the feed is displayed in Figure 10 [39].

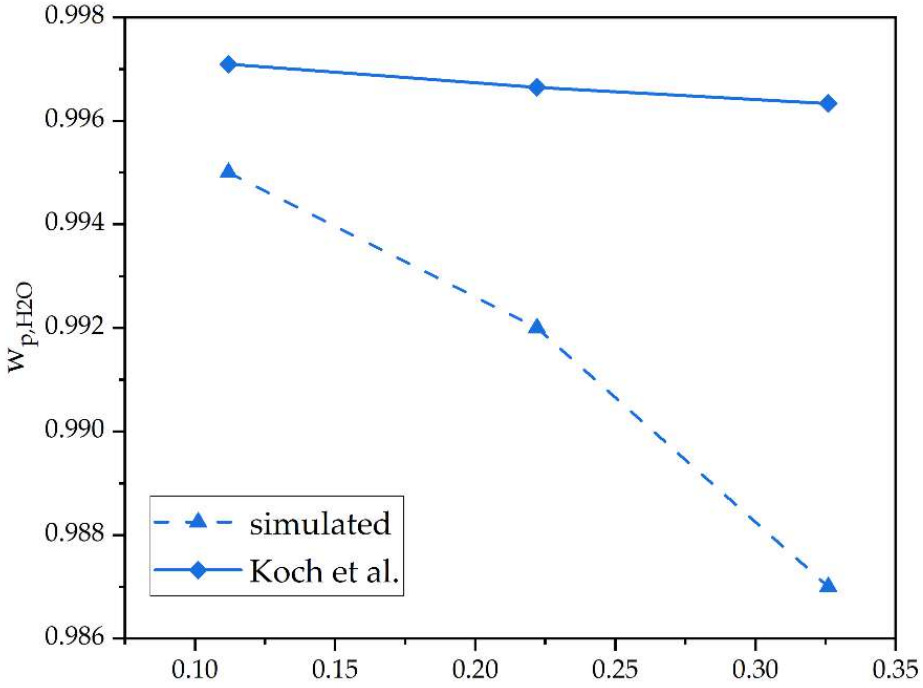

Figure 10. A comparison of an experimental pervaporation operation by Koch et al. [39] and a DWSIM simulation in dependence of $w_{F, H2O}$.

Both curves show the same trend declining from considerably high purities of 99 wt% of water in the permeate. The experimental values' slope is comparably low compared to the simulated. The maximum error between the experimental and the simulated results for $w_{p,H2O}$ is still <1%.

5. Conclusions

This article has given a substantial description of the design and operation of a membrane model, which can simulate the separation of gaseous and liquid mixtures. The design enables comparably easy implementation of the model into DWSIM, including its property editor. However, due to the object-oriented design and general approach to the proceeding, the model may be integrated into every PS tool that can interact with custom solvers. In particular, this model based on open-source software is not just limited to prominent players in the field of the process engineering industry. Further, due to its convenient applicability, the model may also be considered suitable for didactic purposes, including subsequent development. The model's performance reveals consistent and credible trends according to the significant influences of its primary mode.

Further, comparisons with experimental data unveil a comparably adequate predictive performance of the model for gas permeation operations. The accuracy of the pervaporation simulations is distinctly lower, which may be attributed to the more extensive influence of physical effects, such as the effects of friction and other impacts due to its more significant dependence on temperature. Yet, the major objective of a design of an integrated and modular membrane model with counter- and co-current flow configuration has been achieved. The basic algorithm of the code still allows enhancements and upgrades.

A proposal for such an upgrade would be the implementation of a fourth tab for the property editor, which shall inherit check-boxes for additional physical effects, e.g., the equation of Hagen–Poiseuille, an opportunity to provide the Reynolds number and the permeance as a function of temperature. Another perspective could be the implementation of estimates along the lines of an artificial neural network. Integrating more complex solvers or membrane types would also result in an increased simulation duration, which accurate predictions could mitigate.

Supplementary Materials: The following supporting information can be downloaded at: https://www.mdpi.com/article/10.3390/membranes12121186/s1. The source code for the developed model is submitted with the manuscript.

Author Contributions: Conceptualization, K.A., C.J. and B.H.; methodology, K.A.; software, K.A.; validation, K.A.; formal analysis, K.A.; investigation, K.A. and C.J.; resources, K.A. and M.H.; data curation, K.A.; writing—original draft preparation, K.A., C.J. and B.H.; writing—review and editing, K.A., C.J., B.H. and M.H.; visualization, K.A.; supervision, B.H., C.J. and M.H.; project administration, C.J. and M.H.; funding acquisition, C.J. and M.H. All authors have read and agreed to the published version of the manuscript.

Funding: This research was subsidized by city of Vienna funds via the Vienna Business Agency (WAW), grant number 2761267. Further, the authors acknowledge the funding support of K1-MET GmbH, metallurgical competence center. The research program of the K1-MET competence center is supported by COMET (Competence Center for Excellent Technologies), the Austrian program for competence centers. COMET is funded by the Federal Ministry for Transport, Innovation, and Technology; the Federal Ministry for Digital and Economic Affairs; the provinces of Upper Austria, Tyrol, and Styria; and the Styrian Business Promotion Agency (SFG).

Institutional Review Board Statement: Not applicable.

Informed Consent Statement: Not applicable.

Data Availability Statement: Not applicable.

Acknowledgments: The authors are especially grateful for the administrative and financial support of kleinkraft OG.

Conflicts of Interest: The authors declare no conflict of interest.

Abbreviations

CFD	computational fluid dynamics
DLL	dynamic link library
HFMC	hollow fiber membrane contactor
ODE	ordinary differential equation
PDMS	Polydimethylsiloxane
PE	property editor
PS	process simulation/process simulator
SDM	solution-diffusion model
UO	Unit Operation
VB	Visual Basic
Substances:	
ACE	Acetone
Ar	Argon
CH_4	Methane
CO_2	Carbon dioxide
EtOAc	Ethyl acetate
EtOH	Ethanol
H_2	Hydrogen
H_2O	Water
HAc	Acetic acid
He	Helium
IPA	Isopropyl alcohol
N_2	Nitrogen
O_2	Oxygen

List of Symbols:

A	membrane area	[m^2]
d_{fiber}	inner diameter of fiber	[µm]
i, j as subscripts	the ith/jth compound of the mixture	[-]
k	number of compounds	[-]
l_{fiber}	fiber length	[cm]
n	molar flow	[mol/s]
P, p	feed pressure, permeate pressure	[bar]
n_F, n_p	feed molar flow, permeate molar flow	[mol/s]
$w_{F,H2O}$, $w_{p,H2O}$	feed/permeate weight fraction of H_2O	[-]
x, y	molar fraction	[-]
x_F, x_r	feed molar fraction, retentate molar fraction	[-]
y_i	permeate molar fraction closed end	[-]
y_p	permeate molar fraction	[-]
Q	permeance	[mol/(m^2*s*Pa)]
α_i	ideal selectivity for the i^{th} compound	[-]
ϵ	number of fibers	[-]
θ	stage-cut	[-]

Appendix A

Table A1. List of used DLL's.

dll
CapeOpen
DWSIM.Drawing.SkiaSharp
DWSIM.DrawingTools.Point
DWSIM.ExtensionMethods
DWSIM.ExtensionMethods.Eto
DWSIM.FlowsheetBase
DWSIM.GlobalSetting
DWSIM.Interfaces
DWSIM.SharedClasses
DWSIM.Thermodynamics
DWSIM.UnitOperations
DWSIM.XMLSerializer
Eto
Newtonsoft.Json
RichTextBoxExtended
Skiasharp
Skiasharp.Extended
Skiahsarp.Views.Desktop.Common
Skiasharp.Views.WindowsForms
System
System.Core
System.Data
System.Data.DataSet.Extensions
System.Drawing
System.Net.Http
System.Windows
System.Windows.Forms
System.Xml
System.Xml.Linq
WeifenLuo.WinFormsUI.Docking

Table A2. A list of all applied Libraries.

Functions
System.Math
DWSIM.Thermodynamics
DWSIM.Thermodynamics.BaseClasses
DWSIM.Thermodynamics.Streams
DWSIM.Thermodynamics.PropertyPackages
DWSIM.Interfaces
DWSIM.Interfaces.Enums
DWSIM.Interfaces.Enums.GraphicObjects
DWSIM.FlowsheetBase
SkiaSharp.Views.Desktop.Extensions
DWSIM.Drawing.SkiaSharp.GraphicObjects
DWSIM.ExtensionMethods
DWSIM.UnitOperations.UnitOperations.Auxiliary
DWSIM.UnitOperations.UnitOperations
DWSIM.SharedClasses
DWSIM.Thermodynamics.PropertyPackages.PropertyPackage

References

1. Rom, A.; Friedl, A. Investigation of pervaporation performance of POMS membrane during separation of butanol from water and the effect of added acetone and ethanol. *Sep. Purif. Technol.* **2016**, *170*, 40–48. [CrossRef]
2. Liemberger, W.; Groß, M.; Miltner, M.; Harasek, M. Experimental analysis of membrane and pressure swing adsorption (PSA) for the hydrogen separation from natural gas. *J. Clean. Prod.* **2017**, *167*, 896–907. [CrossRef]
3. Bernardo, G.; Araújo, T.; Lopes, T.d.; Sousa, J.; Mendes, A. Recent advances in membrane technologies for hydrogen purification. *Int. J. Hydrogen Energy.* **2020**, *45*, 7313–7338. [CrossRef]
4. Lee, A.; Elam, J.W.; Darling, S.B. Membrane materials for water purification: Design, development, and application. *Environ. Sci. Water Res. Technol.* **2016**, *2*, 17–42. [CrossRef]
5. Asprion, N.; Bortz, M. Process Modeling, Simulation and Optimization: From Single Solutions to a Multitude of Solutions to Support Decision Making. *Chem. Ing. Tech.* **2018**, *90*, 1727–1738. [CrossRef]
6. Coker, D.T.; Freeman, B.D.; Fleming, G.K. Modeling multi-component gas separation using hollow-fiber membrane contactors. *AIChE J.* **1998**, *44*, 1289–1302. [CrossRef]
7. Szwast, M. Modelling the gas flow in permeate channel in membrane gas separation process. *Chem. Process Eng.* **2018**, *39*, 271–280. [CrossRef]
8. Giglia, S.; Bikson, B.; Perrin, J.E.; Donatelli, A.A. Mathematical and Experimental Analysis of Gas Separation by Hollow Fiber Membranes. *Ind. Eng. Chem. Res.* **1991**, *30*, 1239–1248. [CrossRef]
9. Khalilpour, R.; Abbas, A.; Lai, Z.; Pinnau, I. Analysis of hollow fibre membrane systems for multi-component gas separation. *Chem. Eng. Res. Des.* **2013**, *91*, 332–347. [CrossRef]
10. Davis, R.A. Simple gas permeation and pervaporation membrane unit operation models for process simulators. *Chem. Eng. Technol.* **2002**, *25*, 717–722. [CrossRef]
11. Pan, C.Y. Gas separation by high-flux, asymmetric hollow-fiber membrane. *AIChE J.* **1986**, *32*, 2020–2027. [CrossRef]
12. Kundu, P.K. Process Analysis of Asymmetric Hollow Fiber Permeators, Unsteady State Permeation and Membrane-Amine Hybrid Systems for Gas Separations. Ph.D. Thesis, University of Waterloo, Waterloo, ON, Canada, 2013.
13. Rezakazemi, M.; Niazi, Z.; Mirfendereski, M.; Shirazian, S.; Mohammadi, T.; Pak, A. CFD simulation of natural gas sweetening in a gas–liquid hollow-fiber membrane contactor. *Chem. Eng. J.* **2011**, *168*, 1217–1226. [CrossRef]
14. Farno, E.; Rezakazemi, M.; Mohammadi, T.; Kasiri, N. Ternary Gas Permeation Through Synthesized PDMS Membranes: Experimental and CFD Simulation Based on Sorption-Dependent System Using Neural Network Model. *Polym. Eng. Sci.* **2014**, *54*, 215–226. [CrossRef]
15. Haddadi, B.; Jordan, C.; Miltner, M.; Harasek, M. Membrane modeling using CFD: Combined evaluation of mass transfer and geometrical influences in 1D and 3D. *J. Memb. Sci.* **2018**, *563*, 199–209. [CrossRef]
16. Katoh, T.; Tokumura, M.; Yoshikawa, H.; Kawase, Y. Dynamic simulation of multi-component gas separation by hollow-fiber membrane module: Nonideal mixing flows in permeate and residue sides using the tanks-in-series model. *Sep. Purif. Technol.* **2011**, *76*, 362–372. [CrossRef]
17. Elshof, J.E.t.; Abadal, C.R.; Sekulić, J.; Chowdhury, S.R.; Blank, D.H.A. Transport mechanisms of water and organic solvents through microporous silica in the pervaporation of binary liquids. *Microporous Mesoporous Mater.* **2003**, *65*, 197–208. [CrossRef]
18. Makaruk, A.; Harasek, M. Numerical algorithm for modelling multi-component multipermeator systems. *J. Memb. Sci.* **2009**, *344*, 258–265. [CrossRef]
19. Luis, P.; van der Bruggen, B. Pervaporation modeling. In *Pervaporation, Vapour Permeation and Membrane Distillation*; Elsevier: Amsterdam, The Netherlands, 2015; pp. 87–106. [CrossRef]
20. Azimi, H.; Thibault, J.; Tezel, F.H. Separation of Butanol Using Pervaporation: A Review of Mass Transfer Models. *J. Fluid Flow Heat Mass Transf.* **2019**, *5*, 53–82. [CrossRef]
21. Frikha, S.; Frikha, N.; Gabsi, S. Modeling of the flow inside a pore in vacuum membrane distillation. *Euro-Mediterr. J. Environ. Integr.* **2021**, *6*, 66. [CrossRef]
22. Fontoura, T.B.; de Sá, M.C.C.; de Menezes, D.Q.F.; Oechsler, B.F.; Melo, A.; Luiz, L.F.; Anzai, T.K.; Diehl, F.C.; Thompson, P.H.; Pinto, J.C. Modeling of spiral wound membranes for gas separations. Part III: A nonisothermal 2D permeation model. *Chem. Eng. Res. Des.* **2022**, *177*, 376–393. [CrossRef]
23. Evans, L.B.; Boston, J.F.; Britt, H.I.; Gallier, P.W.; Gupta, P.K.; Joseph, B.; Mahalec, V.; Ng, E.; Seider, W.D.; Yagi, H. ASPEN: An Advanced System for Process Engineering. *Comput. Chem. Eng.* **1979**, *3*, 319–327. [CrossRef]
24. Shen, M.T.; Chen, Y.H.; Chang, H. Simulation of the Dynamics and Control Responses of the Carbon Dioxide Chemical Absorption Process using Aspen Custom Modeler. *Energy Procedia.* **2019**, *158*, 4915–4920. [CrossRef]
25. Sánchez, M.; Amores, E.; Abad, D.; Rodríguez, L.; Clemente-Jul, C. Aspen Plus model of an alkaline electrolysis system for hydrogen production. *Int. J. Hydrogen Energy* **2020**, *45*, 3916–3929. [CrossRef]
26. Kombe, E.Y.; Lang'at, N.; Njogu, P.; Malessa, R.; Weber, C.T.; Njoka, F.; Krause, U. Process modeling and evaluation of optimal operating conditions for production of hydrogen-rich syngas from air gasification of rice husks using aspen plus and response surface methodology. *Bioresour. Technol.* **2022**, *361*, 127734. [CrossRef] [PubMed]
27. Bartolome, P.S.; van Gerven, T. A comparative study on Aspen Hysys interconnection methodologies. *Comput. Chem. Eng.* **2022**, *162*, 107785. [CrossRef]

28. Brinkmann, T.; Pohlmann, J.; Withalm, U.; Wind, J.; Wolff, T. Theoretical and experimental investigations of flat sheet membrane module types for high capacity gas separation applications. *Chem. Ing. Tech.* **2013**, *85*, 1210–1220. [CrossRef]
29. Grainger, D. Development of Carbon Membranes for Hydrogen Recovery. Ph.D. Thesis, Norwegian University of Science and Technology, Trondheim, Norway, 2007.
30. Cavalcanti, C.; Ramos, W.; Brito, R.; Britoa, K. Detailed evaluation of pervaporation modeling to obtaining anhydrous ethanol. *Quim. Nova* **2022**, *45*, 374–382. [CrossRef]
31. Quek, V.C.; Shah, N.; Chachuat, B. Modeling for design and operation of high-pressure membrane contactors in natural gas sweetening. *Chem. Eng. Res. Des.* **2018**, *132*, 1005–1019. [CrossRef]
32. Bishop, B.A.; Lima, F.V. Modeling, Simulation, and Operability Analysis of a Nonisothermal, Countercurrent, Polymer Membrane Reactor. *Processes* **2020**, *8*, 78. [CrossRef]
33. Kancherla, R.; Nazia, S.; Kalyani, S.; Sridhar, S. Modeling and simulation for design and analysis of membrane-based separation processes. *Comput. Chem. Eng.* **2021**, *148*, 107258. [CrossRef]
34. Wijmans, J.G.; Baker, R.W. The solution-diffusion model: A review. *J. Membr. Sci.* **1995**, *107*, 1–21. [CrossRef]
35. de Medeiros, D.W.O. DWSIM–The Open Source Chemical Process Simulator, (Version 8.0.3.). Available online: https://dwsim.org/index.php/about/ (accessed on 7 June 2022).
36. DWSIM-Open Source Process Simulator-Browse Files at SourceForge.net. Available online: https://sourceforge.net/projects/dwsim/files/ (accessed on 29 September 2022).
37. Sada, E.; Kumazawa, H.; Wang, J.-S.; Koizumi, M. Separation of carbon dioxide by asymmetric hollow fiber membrane of cellulose triacetate. *J. Appl. Polym. Sci.* **1992**, *45*, 2181–2186. [CrossRef]
38. Chowdhury, M.H.M.; Feng, X.; Douglas, P.; Croiset, E. A New Numerical Approach for a Detailed Multicomponent Gas Separation Membrane Model and AspenPlus Simulation. *Chem. Eng. Technol.* **2005**, *28*, 773–782. [CrossRef]
39. Koch, K.; Górak, A. Pervaporation of binary and ternary mixtures of acetone, isopropyl alcohol and water using polymeric membranes: Experimental characterisation and modelling. *Chem. Eng. Sci.* **2014**, *115*, 95–114. [CrossRef]
40. Park, B.G. Pervaporation characteristics of polyetherimide/γalumina composite membrane for a quaternary equilibrium mixture of acetic acid-ethanol-ethyl acetate-water. *Korean J. Chem. Eng.* **2004**, *21*, 882–889. [CrossRef]

CHEMICAL ENGINEERING TRANSACTIONS
VOL. 96, 2022
A publication of AIDIC
The Italian Association of Chemical Engineering
Online at www.cetjournal.it
Guest Editors: David Bogle, Flavio Manenti, Piero Salatino

ISBN 978-88-95608-95-2; **ISSN** 2283-9216
DOI: 10.3303/CET2296029

High Purity Hydrogen from Liquid NH_3 – Proposal and Evaluation of a Process Chain

Kouessan Aziaba[a,*], Barbara D. Weiß[a,*], Viktoria Illyés[b,*], Christian Jordan[a], Markus Haider[b], Michael Harasek[a]

[a]Thermal Process Engineering - Computational Fluid Dynamics, Institute of Chemical, Environmental & Bioscience Engineering, TU Wien, Getreidemarkt 9, 1060 Vienna, Austria
[b]Thermodynamics and Heat Technology, Institute for Energy Systems and Thermodynamics, TU Wien, Getreidemarkt 9, 1060 Vienna, Austria
kouessan.aziaba@tuwien.ac.at, viktoria.illyes@tuwien.ac.at, barbara.weiss@tuwien.ac.at

This study proposes a process chain to gain high purity hydrogen from liquid ammonia. The utilization of the stored hydrogen requires the endothermic decomposition of ammonia

$$2\ NH_3 \leftrightarrow N_2 + 3\ H_2 \quad (1)$$

and the subsequent purification of H_2. A process model from liquid NH_3 to high purity hydrogen was developed. The process model includes the reaction kinetics for the catalytic decomposition of NH_3 using a catalyst, such as Ni-Pt/Al_2O_3, and the necessary purification steps. Based on the simulation, a final process chain is proposed. Finally, heat integration calculations were performed to optimize the energy efficiency of the process.
The application of a polyimide membrane system is proposed. The performed calculations show that using membrane separation, a H_2 purity of around 97 wt% can be achieved. For a final NH_3 content of < 1 ppm, the study found acidic or adsorptive removal of remaining NH_3 necessary even for high decomposition conversion rates. To achieve even higher H_2 purity, the application of an additional pressure swing absorption separation is proposed. This application can ensure H_2 purities of > 99 wt% suitable for PEM fuel cells.

1. Introduction

Energy storage has been the focus of research and industries as global energy demand is rising and zero-carbon and renewable systems are of interest. In this scenario, the hydrogen economy has undeniable potential (Oliveira et al. 2021). Nevertheless, the handling of H_2 still poses substantial hazards and difficulties such as high flammability, complex storability, and a high specific volume (Tashie-Lewis and Nnabuife 2021). Therefore, ammonia, methane, and methanol are options for indirect storage. Among these, ammonia has been (well-)investigated and utilized globally on an industrial scale with established infrastructure. Due to its high volumetric hydrogen density (higher than hydrogen itself) and moderate conditions to liquefy (-33.4 °C at atmospheric pressure or 20 °C at 0.8 MPa), liquid ammonia allows (cost-)efficient storage of hydrogen.
Despite the knowledge in ammonia handling, recovering high purity hydrogen is still under investigation - separation and purification of hydrogen being the main challenge(Makhloufi and Kezibri 2021). The required purity of hydrogen for proton exchange membrane (PEM) fuel cells is a minimum mole fraction of 99.97 %, according to (DIN EN 17124), with limits for individual contaminants, some of which are reported in Table 1.
Many researchers focus on enabling green ammonia production, making the whole process sustainable and carbon-free. Ammonia from fossil fuels (brown ammonia) contains impurities such as CH_4 and hydrocarbons, which are not present in green ammonia. However, the shift from brown to green ammonia will be continuous. Therefore, the authors propose an process chain from low purity brown ammonia to high purity hydrogen: (1) pre-treatment, (2) catalytic NH_3 decomposition, (3) pre-separation purification, (4) H_2 separation via membranes and (5) post-separation purification. As the impurities decrease with the share of green ammonia in the mix, some pre-treatment and purification steps will grow unnecessary. Since Membranes are considered to serve as

Paper Received: 8 December 2021; Revised: 6 August 2022; Accepted: 8 July 2022
Please cite this article as: Aziaba K., Weiss B.D., Illyes V., Jordan C., Haider M., Harasek M., 2022, High Purity Hydrogen from Liquid NH_3 - Proposal and Evaluation of a Process Chain, Chemical Engineering Transactions, 96, 169-174 DOI:10.3303/CET2296029

a separation unit with a comparably low complexity and energy demand, they have also been implemented into the product purification chain.

Table 1: Maximum allowable content of individual contaminants in hydrogen for an application in PEM FC

Contaminant	Max. content (µmol/mol)
Water H_2O	5
Hydrocarbons (excluding methane)	2
Methane CH_4	100
Nitrogen N_2	300
Argon Ar	300
Carbon dioxide CO_2	2
Ammonia NH_3	0.1

2. Methods

The foundation of the proposed process chain is a comprehensive literature study of applicable technologies as well as a process simulation of the individual process steps and a final flowsheet calculation for the proposed process chain. The calculations were performed using the sequential modular simulation tool Aspen Plus® V10 and the open source simulation environment DWSIM Version 6.6. The following chapters describes the methods used for every process step in detail.

2.1 NH_3 feed and pressure input

The input feed is liquid ammonia. Liquid ammonia comes with impurities, which must be considered when designing a process chain to produce highly purified hydrogen. According to experts, the following impurities are present in ammonia coming from hydrogen produced from natural gas reforming:

- H_2O: 0.15 mass%
- Oil: 10 mg/kgNH_3
- Dissolved gas containing H_2, CH_4, N_2, and Ar: max. 450 ml/100gNH_3

The oil was calculated as $C_{15}H_{23}$ in the process simulation. The liquid ammonia was assumed to be stored at 10 bar and 15 °C. The expansion was calculated at 1.4 bar and 15 °C. From the expansion until the compressor before the membrane, a total pressure loss of 0.4 bar was assumed, leading to a final pressure of 1 bar at the scrubber outlet. The flowsheet (see figure 1) was designed for a hydrogen output of around 45 kg/h.

2.2 Pretreatment

As water and oil in the feed stream can influence the catalyst performance and harm the process, pre-treatment is necessary to reduce their content before entering the catalytic reactor. The effect of cooling the feed stream for purification was assessed by calculating the thermodynamic equilibrium using a flash calculation in AspenPlus.

2.3 Catalytic decomposition reaction

The performance of the decomposition is highly dependent on the catalyst choice. Following Wang et al. (2017) the catalyst Ni-Pt/Al_2O_3 was chosen to model the decomposition due to its high activity. The catalytic reactor was calculated as a kinetic reactor in AspenPlus. The reaction kinetics for the catalyst Ni-Pt/Al_2O_3 are given by Chellappa et al. (2002). The reaction rate was implemented according to the power-law expression on a partial pressure basis:

$$r = k_0 * e^{-\frac{E}{RT}} * p_{NH_3} \quad (2)$$

According to Chellappa et al. (2002) the activation energy E is 46.9 kcal/mol and the reaction rate constant is $3.639*10^{11}$ kmol/(h*kg*bar). The decomposition of NH_3 is an endothermic reaction and produces an increased number of molecules. Following Le Châtelier's principle, high temperature and low pressures are required for the reaction to proceed. The decomposition reactor was calculated at a reaction temperature of 600 °C. The conversion rate is strongly dependent on the catalyst loading of the reactor. When designing the reactor, the catalyst loading choice is a trade-off between conversion rate and catalyst costs. In this work, two scenarios were calculated: One with a catalyst loading of 5 g/(mol/h) NH_3 and one with 40 g/(mol/h) NH_3.

2.4 NH_3 removal

Since the reactor does not achieve complete conversion of NH_3, NH_3 in the outlet gas needs to be removed. NH_3 can cause hydrolysing effects at the membrane. Therefore, it needs to be removed before separating N_2 and H_2 via a membrane. Lamb et al. (2019) reviewed several purification steps. This work investigates the removal of NH_3 by water or acidic scrubbing with subsequent cool drying. To calculate the NH_3 theoretical removal potential by water scrubbing and subsequent cool drying, flash calculations were performed in AspenPlus. For the scrubbing, a liquid/gas ratio of 3.9 l/m^3(std) was considered.

2.5 Membrane separation

Various available publications lay the groundwork for a multi-stage membrane model that can separate gaseous mixtures with multiple components (Coker et al. 1998).

Membrane characteristics

The purification of H_2 with a membrane demands a comparably high selectivity of H_2 over any other compound and good industrial applicability.
Both of these requirements are fulfilled by the Polyimide Membrane Matrimid 5218. Shalygin et al. (2015) reports a high H_2/N_2 selectivity of > 800 as well as a relatively high H_2 permeability of > 100 Barrer. The permeances of CO, CH_4, C_2H_4, C_2H_6 and CO_2 are also documented. Table 2 gives an insight into the permeances of the most relevant compounds of the membrane separation step.

Table 2: Membrane permeance

Compound	Permeance Nm^3/m^{2}sPa	Reference
H_2	5,87E-10	(Shalygin et al. 2015)
N_2	7,07E-13	

Liemberger et al. (2017) separated H_2/CH_4 gas mixtures using a polyimide membrane while achieving a stage cut of 0.7 and an H_2 permeate purity of > 95 % when applying a feed with 70 % H_2 and a pressure of 21 bar. The selectivity of H_2/CH_4 is > 100 and consequently lower than the selectivity of H_2/N_2 (> 800) (Shalygin et al. 2015). Based on these studies found in literature, it is expected that that the polyimide membrane performs very well when separating H_2 and N_2 is therefore chosen for the calculations.

Membrane calculation

Alongside the illustrative model for the mass transfer through the membrane, which was chosen to be the solution diffusion model, further preliminary assumptions must be specified:

- Negligible radial pressure variation.
- Minor pressure loss from the feed to the retentate side.
- Perfect mixing of the feed, permeate and retentate streams.
- Negligible radial concentration variation.
- The difference between components' permeance in a mixture or as a pure compound through a membrane is negligible.
- The permeance of a compound is independent of temperature and pressure.

The calculation routine is derived from the solution diffusion model. The mass transfer is driven by the logarithmic mean pressure difference and must overcome the resistance consisting of a series of adsorption, diffusion, and desorption (Davis 2002). The molar flux J_i of each component i is calculated over the product of its permeance Pm_i, the total area of the membrane A and the logarithmic-mean trans-membrane partial pressure for counter current flow, where p_{xf} and p_{xr} describe the partial pressure of the feed and retentate components and p_{yp} the partial pressure of the permeate components:

$$J_i = Pm_i * A \frac{(p_{xf_i} - p_{yp_i}) - (p_{xr_i} - p_{yi_i})}{\ln \frac{p_{xf_i} - p_{yi_i}}{p_{xr_i} - p_{ye_i}}} \quad (3)$$

3. Results and discussion

Figure 1 shows the proposed process chain to gain high purity H_2 from liquid NH_3.

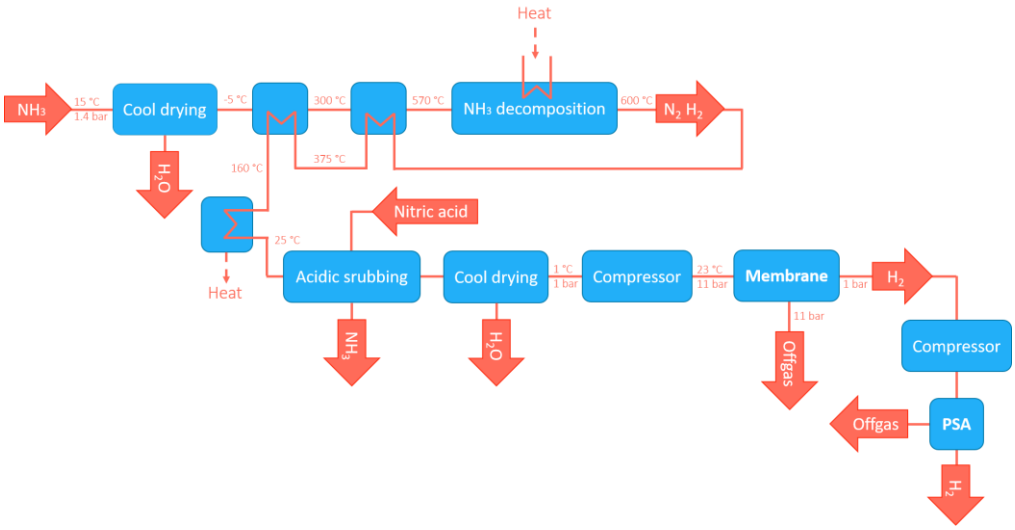

Figure 1: Proposed flowsheet for high purity H_2 production from liquid NH_3

The following summarizes and discusses the single process steps in detail.

3.1 Pretreatment

Finding the right cooling temperature is a trade-off between H_2O removal, NH_3 losses in the condensate, and energy demand. With the considered pressure of 1.3 bar at the cool dryer, cooling down to -5 °C can reduce the water content to around 290 ppm and leads to an NH_3 loss of 0.16 mass%. Lowering the temperature reduces the water content even more: Cooling down to –20 °C results in a water content of 16 ppm in the gas and leads to an NH_3 loss of 0.45 mass%. However, the technical demand for such low-temperature drying is excessive. The technical demand could be lowered by utilizing the cooling effect of the expansion of the gas after exiting the liquid tank. This work suggests cool drying to -5 °C. The necessity of more extensive drying depends on the water content of the used ammonia and the applied catalyst in the reactor. If lower water concentrations are required, a drying adsorbent can be used (Chiang et al. 2005).

3.2 Catalytic decomposition

The calculations revealed that a catalyst loading of 40 g/(mol/h) achieves a conversion of over 97.1 % NH_3 and a catalyst loading of 5 g/(mol/h) achieves a conversion of over 80.9 % NH_3. Table 3 summarizes the streams after decomposition for both catalyst loadings.

Table 3: Gas stream before and after catalytic reactor

Catalyst loading		40 g/(mol/h)		5 g/(mol/h)	
		in	out	in	out
Volume flow	Nm^3/h	390	770	431	778
Mass flow	kg/h	298	298	328	328
NH_3	mol-%	99.75	1.61	99.75	10.72
H_2	mol-%	0.01	73.71	0.01	66.87
N_2	mol-%	0.03	24.58	0.03	22.30
H_2O	mol-%	0.03	0.01	0.03	0.02
CH_4	mol-%	0.14	0.07	0.14	0.08
Ar	mol-%	0.03	0.02	0.03	0.02
$C_{15}H_{32}$	mol-%	0.00	0.00	0.00	0.00
External heat demand	kW	262		242	
	MJ/kg H_2	18.5		18.6	

The heat demand for the reactor can be minimized by heat integration: The input stream can be preheated with the hot output stream to 570 °C by using two heat exchangers. The first heat exchanger is used to preheat the stream from – 5 to 300 °C, the second to preheat to 570 °C. After heat integration, the reaction requires an external heat of around 18.5 MJ per kg H_2. The residual external heat can be provided by electrical heat.

3.3 NH_3 removal

The results show that with water scrubbing and subsequent cool drying at 1 °C, the NH_3 content can be reduced from 1.61 mol% to 800 ppm when applying a catalyst loading of 40 g/(mol/h). Water scrubbing and subsequent drying do not sufficiently remove the NH_3 from the gas. A higher catalyst loading n the reactor leads to a higher NH_3 conversion and therefore can minimize the need of subsequent NH_3 removal. However, even with higher catalyst loading, it is expected that an acid scrubbing or adsorptive NH_3 removal operation is necessary to reach the required NH_3 content of < 1 ppm. To show the limitations of water scrubbing, the flowsheet was calculated with the Gibbs reactor. Assuming a GIBBS Equilibrium leads to an NH_3 concentration of 18 ppm after water scrubbing and drying. A commonly applied scrubber fluid for acid scrubbing contains sulfuric acid or nitric acid. When applying nitric acid, the scrubber liquid can be utilized as a product for agricultural use afterwards. Acidic scrubbing towers are expected to reduce the NH3 concentration with an optimized design down to < 1 ppm. Due to the high removal efficiency, acid ammonia scrubbing is a widely applied method to remove ammonia from gas. Many industrial companies offering ammonia scrubbing towers guarantee removal efficiencies of 99.9 %.

3.4 Membrane separation

Table 4 and 5 present the results of the membrane calculation for the permeate and the retentate.

Table 4: Product permeate streams after membrane separation

Catalyst loading		40 g/(mol/h)	5 g/(mol/h)
Volume flow	Nm^3/h	763	501
Mass flow	Kg/h	47.68	44.16
H_2	mol-%	99.34	99.29
N_2	mol-%	0.12	0.16
H_2O	mol-%	0.53	0.54

Table 5: Product retentate streams after membrane separation

Catalyst loading		40 g/(mol/h)	5 g/(mol/h)
H_2	mol-%	27.04	16.03
N_2	mol-%	71.86	82.97
H_2O	mol-%	0.85	0.63
CH_4	mol-%	0.20	0.30
Ar	mol-%	0.05	0.06

Since the processes did not come with a diverse inlet stream composition, also the permeate streams show some similarities. In both calculated cases (high and low catalyst loading) the H_2 concentrations of the permeate streams have a maximum amount of approximately 99.3 %. Impurities that remain in the permeate stream are N_2 with 0.16 % and Ar and CH_4 with below 0.01 %. The retentate stream mainly consists of N_2 and H_2 with a H_2 content of up to 27.04 %.

4. Conclusion

The design of the reactor and the resulting reactor conversion decide over the necessary NH_3 removal steps after the reactor. For NH_3-residues of < 1 ppm, an ammonia-removal step is necessary even for high conversion reactors. If acid scrubbing is chosen for NH_3 removal, subsequent drying is also required. Alternatively, adsorptive removal is an option.

A separation of N_2 and H_2 is necessary after NH_3 removal. In this work, the separation of N_2 and H_2 using membrane technology was calculated. Using a polyimide membrane, a high H_2 purity of around 99.3 mol% can be met while an off-gas stream containing the rest of the H_2 is produced. PSA separation as subsequent separation step after membrane separation is necessary to reach higher H_2 purity.

Future work will investigate the purification steps in more detail to assess the applicability of membranes in specific situations in comparison to other separation technology. An economic analysis will be needed.

Furthermore, we will analyse possible utilization of the off-gas and optimize the membranes and their interconnection to utilize the by-product.

References

Chellappa, A.S; Fischer, C.M; Thomson, W.J (2002): Ammonia decomposition kinetics over Ni-Pt/Al2O3 for PEM fuel cell applications. In Applied Catalysis A: General 227 (1-2), pp. 231–240. DOI: 10.1016/S0926-860X(01)00941-3.

Chiang, Robert Ling; Whitley, Roger Dean; Wu, Dingiun; Dong, Chun Christine, Rao; Bhaskara, Madhukar (2005): Process for removing water from ammonia. App. no. 10/730,505. Patent no. US 6,892,473 B1.

Coker, D.; Freeman, B.; Fleming, G. K. (1998): Modeling multicomponent gas separation using hollow-fiber membrane contactors. In undefined. Available online at https://www.semanticscholar.org/paper/Modeling-multicomponent-gas-separation-using-Coker-Freeman/b334787ed2aabd0f9e53232144efa3d82d2d0ee5.

Davis, R. A. (2002): Simple Gas Permeation and Pervaporation Membrane Unit Operation Models for Process Simulators. In Chem. Eng. Technol. 25 (7), p. 717. DOI: 10.1002/1521-4125(20020709)25:7<717::AID-CEAT717>3.0.CO;2-N.

DIN EN 17124: DIN EN 17124:2019-07, Wasserstoff als Kraftstoff_- Produktfestlegung und Qualitätssicherung_- Protonenaustauschmembran (PEM)-Brennstoffzellenanwendungen für Straßenfahrzeuge; Deutsche Fassung EN_17124:2018 (DIN EN 17124).

Lamb, Krystina E.; Dolan, Michael D.; Kennedy, Danielle F. (2019): Ammonia for hydrogen storage; A review of catalytic ammonia decomposition and hydrogen separation and purification. In International Journal of Hydrogen Energy 44 (7), pp. 3580–3593. DOI: 10.1016/j.ijhydene.2018.12.024.

Liemberger, Werner; Groß, Markus; Miltner, Martin; Harasek, Michael (2017): Experimental analysis of membrane and pressure swing adsorption (PSA) for the hydrogen separation from natural gas. In Journal of Cleaner Production 167, pp. 896–907. DOI: 10.1016/j.jclepro.2017.08.012.

Makhloufi, Camel; Kezibri, Nouaamane (2021): Large-scale decomposition of green ammonia for pure hydrogen production. In International Journal of Hydrogen Energy 46 (70), pp. 34777–34787. DOI: 10.1016/j.ijhydene.2021.07.188.

Oliveira, Alexandra M.; Beswick, Rebecca R.; Yan, Yushan (2021): A green hydrogen economy for a renewable energy society. In Current Opinion in Chemical Engineering 33, p. 100701. DOI: 10.1016/j.coche.2021.100701.

Shalygin, M. G.; Abramov, S. M.; Netrusov, A. I.; Teplyakov, V. V. (2015): Membrane recovery of hydrogen from gaseous mixtures of biogenic and technogenic origin. In International Journal of Hydrogen Energy 40 (8), pp. 3438–3451. DOI: 10.1016/j.ijhydene.2014.12.078.

Tashie-Lewis, Bernard Chukwudi; Nnabuife, Somtochukwu Godfrey (2021): Hydrogen Production, Distribution, Storage and Power Conversion in a Hydrogen Economy - A Technology Review. In Chemical Engineering Journal Advances 8, p. 100172. DOI: 10.1016/j.ceja.2021.100172.

Wang, Ganzhou; Mitsos, Alexander; Marquardt, Wolfgang (2017): Conceptual design of ammonia-based energy storage system: System design and time-invariant performance. In AIChE J. 63 (5), pp. 1620–1637. DOI: 10.1002/aic.15660.

(12) NACH DEM VERTRAG ÜBER DIE INTERNATIONALE ZUSAMMENARBEIT AUF DEM GEBIET DES PATENTWESENS (PCT) VERÖFFENTLICHTE INTERNATIONALE ANMELDUNG

(19) Weltorganisation für geistiges Eigentum
Internationales Büro

(43) Internationales Veröffentlichungsdatum
03. Oktober 2024 (03.10.2024)

WIPO | PCT

(10) Internationale Veröffentlichungsnummer
WO 2024/197329 A1

(51) Internationale Patentklassifikation:
C07C 68/04 (2006.01) *C07C 69/96* (2006.01)

(21) Internationales Aktenzeichen: PCT/AT2024/060114

(22) Internationales Anmeldedatum:
02. April 2024 (02.04.2024)

(25) Einreichungssprache: Deutsch

(26) Veröffentlichungssprache: Deutsch

(30) Angaben zur Priorität:
A 50231/2023 31. März 2023 (31.03.2023) AT

(71) Anmelder: **KLEINKRAFT OG** [AT/AT]; Turnergasse 27/5, 1150 WIEN (AT).

(72) Erfinder: **GREILINGER, Gerhard**; [redacted] **JORDAN, Christian**; [redacted] **KABAS, Florian**; [redacted] **AZIABA, Kouessan**; [redacted] **GENOV, Miroslav**; [redacted] **TEUFNER-KABAS, Magdalena**; [redacted] **HARASEK, Michael**; [redacted]

(74) Anwalt: **BABELUK PATENTANWÄLTE GMBH**; Florianigasse 26/3, 1080 WIEN (AT).

(81) Bestimmungsstaaten *(soweit nicht anders angegeben, für jede verfügbare nationale Schutzrechtsart)*: AE, AG, AL, AM, AO, AT, AU, AZ, BA, BB, BG, BH, BN, BR, BW, BY, BZ, CA, CH, CL, CN, CO, CR, CU, CV, CZ, DE, DJ, DK, DM, DO, DZ, EC, EE, EG, ES, FI, GB, GD, GE, GH, GM, GT, HN, HR, HU, ID, IL, IN, IQ, IR, IS, IT, JM, JO, JP, KE, KG, KH, KN, KP, KR, KW, KZ, LA, LC, LK, LR, LS, LU, LY, MA, MD, MG, MK, MN, MU, MW, MX, MY, MZ, NA, NG, NI, NO, NZ, OM, PA, PE, PG, PH, PL, PT,

(54) **Title:** PROCESS FOR THE PREPARATION OF ORGANIC CARBONATES

(54) **Bezeichnung:** VERFAHREN ZUR HERSTELLUNG ORGANISCHER CARBONATE

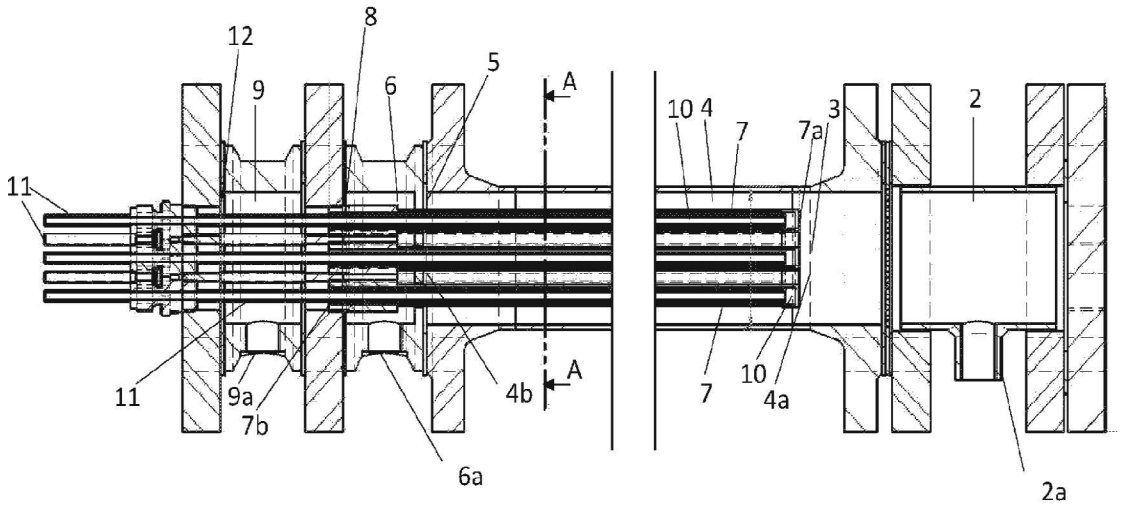

Fig. 1a

(57) **Abstract:** The invention relates to a process for the preparation of organic carbonates, in particular diethyl carbonate, comprising a catalytic reaction of corresponding alcohols (ROH) with carbon dioxide, wherein R is a straight-chain or branched-chain alkyl group having 1-6 carbon atoms, preferably an ethyl group, and wherein water formed during the catalytic reaction is separated off via at least one inorganic membrane (21) and/or at least one hybrid membrane (21), characterised in that the catalyst comprises cerium oxide (CeO_2) and in that the catalytic reaction is carried out at a temperature of at least 80°C and at a pressure of at least 5 bar.

(57) **Zusammenfassung:** Die Erfindung betrifft ein Verfahren zur Herstellung organischer Carbonate, insbesondere von Diethylcarbonat, umfassend eine katalytische Reaktion von entsprechenden Alkoholen (ROH) mit Kohlendioxid, wobei R ein gerad- oder verzweigt-kettiger Alkylrest mit 1-6 Kohlenstoffatomen, vorzugsweise ein Ethylrest, ist, und wobei während der katalytischen Reaktion entstehendes Wasser über zumindest eine anorganische Membran (21) und/oder zumindest eine Hybridmembran (21) abgetrennt wird, dadurch gekennzeichnet, dass der Katalysator Ceroxid (CeO_2) umfasst und dass die katalytische Reaktion bei einer Temperatur von mindestens 80°C und bei einem Druck von mindestens 5 bar durchgeführt wird.

[Fortsetzung auf der nächsten Seite]

QA, RO, RS, RU, RW, SA, SC, SD, SE, SG, SK, SL, ST, SV, SY, TH, TJ, TM, TN, TR, TT, TZ, UA, UG, US, UZ, VC, VN, WS, ZA, ZM, ZW.

(84) **Bestimmungsstaaten** *(soweit nicht anders angegeben, für jede verfügbare regionale Schutzrechtsart)*: ARIPO (BW, CV, GH, GM, KE, LR, LS, MW, MZ, NA, RW, SC, SD, SL, ST, SZ, TZ, UG, ZM, ZW), eurasisches (AM, AZ, BY, KG, KZ, RU, TJ, TM), europäisches (AL, AT, BE, BG, CH, CY, CZ, DE, DK, EE, ES, FI, FR, GB, GR, HR, HU, IE, IS, IT, LT, LU, LV, MC, ME, MK, MT, NL, NO, PL, PT, RO, RS, SE, SI, SK, SM, TR), OAPI (BF, BJ, CF, CG, CI, CM, GA, GN, GQ, GW, KM, ML, MR, NE, SN, TD, TG).

Veröffentlicht:

— *mit internationalem Recherchenbericht (Artikel 21 Absatz 3)*

— *vor Ablauf der für Änderungen der Ansprüche geltenden Frist; Veröffentlichung wird wiederholt, falls Änderungen eingehen (Regel 48 Absatz 2 Buchstabe h)*

Verfahren zur Herstellung organischer Carbonate

Die Erfindung betrifft ein Verfahren zur Herstellung organischer Carbonate, insbesondere von Diethylcarbonat, umfassend eine katalytische Reaktion von entsprechenden Alkoholen (ROH) mit Kohlendioxid, wobei R ein gerad- oder verzweigtkettiger Alkylrest mit 1-6 Kohlenstoffatomen, vorzugsweise ein Ethylrest, ist, und wobei während der katalytischen Reaktion entstehendes Wasser über zumindest eine anorganische Membran und/oder zumindest eine Hybridmembran abgetrennt wird.

Die Erfindung betrifft einen Reaktor zur Herstellung organischer Carbonate, insbesondere von Diethylcarbonat, wobei der Reaktor zumindest ein Reaktormodul aufweist, und das Reaktormodul einen Reaktionsraum aufweist, wobei der Reaktionsraum durch zumindest eine anorganische Membran und/oder zumindest eine Hybridmembran von einem Abführraum zum Abführen von Wasser aus dem Reaktionsraum abgetrennt ist.

Organische Carbonate werden unter anderem als Ausgangsmaterial für die Synthese von Kunststoffen, Medikamenten, Veterinärwirkstoffen, Pflanzenschutzmitteln, Farbstoffen, Fotochemikalien sowie als Elektrolyt in Li-Ionen Batterien verwendet. Obwohl sie derzeit hauptsächlich als Rohstoff in der chemischen Industrie verwendet werden, eignen sie sich als Treibstoff oder Treibstoffzusatz, um Abgasemissionen zu reduzieren. Insbesondere Diethylcarbonat hat sich besonders vorteilhaft als Treibstoffzusatz herausgestellt. Bei Beimischung werden weniger Kohlenmonoxid (CO), Partikel und Rauch emittiert. Wenn DEC aus erneuerbaren Quellen produziert wird, werden auch die fossilen CO_2 Emissionen reduziert. Insbesondere die Möglichkeit der Beimischung zu Diesel im Vergleich zum Ausgangsprodukt Ethanol hat großes ökologisches und ökonomisches Potential.

Die Synthese von organischen Carbonaten erfolgt mit CO_2 und entsprechenden Alkoholen als Ausgangsstoff, wobei im Zuge der katalytischen Reaktion das organische Carbonat und Wasser entsteht. Die Reaktionsgleichung für diese katalytische Reaktion ist also allgemein:

Beispielsweise kann bei der Verwendung von Ethanol als Alkohol Diethylcarbonat hergestellt werden:

Als Endprodukt von Verbrennungsprozessen ist CO_2 thermodynamisch stabil und nur mit hohem Energieeinsatz reaktiv. Die Bildung von organischen Carbonaten aus CO_2 und Alkohol ist exotherm und läuft nicht spontan bei Raumtemperatur ab. Es hat sich gezeigt, dass die Entfernung des bei der katalytischen Reaktion entstehenden Wassers die Reaktion stark begünstigt. Daher wurden wasserbindende Substanzen (chemische Wasserfänger) verwendet, um das Wasser zu entfernen.

Dies ist bei der Herstellung von größeren Mengen aber wenig praktisch, da entweder der Wasserfänger aus dem Reaktionsgemisch entfernt und regeneriert oder gar verworfen werden muss. Darüber hinaus kann es zu einer Verunreinigung des Endprodukts kommen. Daher sind diese Verfahren im größeren, industriellen Maßstab nicht zur Herstellung von organischen Carbonaten geeignet.

In Wang et al., 2017[1] wird ein Verfahren und ein Reaktor offenbart, welcher unter Umgebungsdruck und unter Verwendung eines $Ce_{0,8}Zr_{0,2}O_2$-Katalysators Diethylcarbonat herstellt. Dabei wird das Wasser über eine anorganische Membran während der Reaktion laufend abgeführt. Dies ermöglicht jedoch nur eine sehr geringe Ausbeute, laut dem Dokument von etwa 0,06%.

In der CN 112657434 A wird ein weiteres Verfahren und ein Reaktor zur elektrochemischen Synthese offenbart, der bei etwas höherem Druck im Bereich und Temperatur arbeitet. Als Katalysator wird ein Übergangsmetall wie Cu, Fe, Ni, Co, oder Zn verwendet. Das Metall wird auf einem Träger aus CeO_2 getragen, der die mechanische Unterstützung darstellt. Das entstehende Wasser wird durch eine Polyimidmembran abgeschieden. Damit die Reaktion stattfindet, muss über Elektroden Strom zugeführt werden. Dies bedingt einen höheren Energieeinsatz und komplexeren Aufbau des Reaktors. Es hat sich außerdem herausgestellt, dass auch diese Ausführungsform unzureichende Ergebnisse erzielt.

In Kuenen et al, 2016[2], wird vorgeschlagen, einen Ceroxid-Katalysator in Kombination mit einer PEEK-Chitosan-Membran - eine Polymer -Membran - zu verwenden. Dies weist eine ungenügende Ausbeute auf. Das Dokument beschreibe die

[1] Wang, J., Hao, Z., Wohlrab, S., 2017. Continuous CO2 esterification to diethyl carbonate (DEC) at atmospheric pressure: application of porous membranes for in situ H2O removal. Green Chem. 19, 3595–3600. https://doi.org/10.1039/C7GC00916J

[2] Kuenen, H. J., Mengers, H. J., van der Ham, A. G. J., & Kiss, A. A. (2016). Novel Process for Conversion of CO2 to Dimethyl Carbonate using Catalytic Membrane Reactors. In 26 European Symposium on Computer Aided Process Engineering, 2016 (Vol. 38, pp. 991-996). (Computer Aided Chemical Engineering; Vol. 38). Elsevier. https://doi.org/10.1016/B978-0-444-63428-3.50170-3

direkte Synthese von Dimethylcarbonat aus Methanol und CO_2 in einem Membranreaktor mit der in-situ Abtrennung von Wasser. Außerdem wurden die Daten mittels einer Simulation gewonnen, wodurch keine Aussage darüber getroffen werden kann, ob die präsentierte Membran die angegebene Selektivität auch bei erhöhten Temperaturen in der Praxis halten kann.

Aufgabe der Erfindung ist, ein Verfahren und einen Reaktor bereitzustellen, mit Hilfe dessen in größeren Mengen organische Carbonate hergestellt werden können und eine höhere Ausbeute erzielt wird.

Diese Aufgabe wird erfindungsgemäß dadurch gelöst, dass die katalytische Reaktion bei einer Temperatur von mindestens 80°C und bei einem Druck von mindestens 5 bar durchgeführt wird und dass der Katalysator zumindest eines der genannten Substanzen umfasst: Ceroxid (CeO_2), ZrO_2, CrO_2, Fe, Cu, Mg, Ni, SiO_2, Al_2O_3, TiO, MoO, BiO, ZnO, Ta_2O_5, Nb_2O_5 oder eine Legierung umfassend Kupfer und Nickel.

Sie wird auch dadurch gelöst, dass im Reaktionsraum ein Katalysator angeordnet ist und dass der Katalysator zumindest eines der genannten Substanzen umfasst: Ceroxid (CeO_2), ZrO_2, CrO_2, Fe, Cu, Mg, Ni, SiO_2, Al_2O_3, TiO, MoO, BiO, ZnO, Ta_2O_5, Nb_2O_5 oder eine Legierung umfassend Kupfer und Nickel.

Die angegebenen Metalle Eisen, Kupfer, Magnesium und/oder Nickel (Fe, Cu, Mg und/oder Ni) sind vorzugsweise in metallischer Form Teil des Katalysators, sie können aber auch in anderer Form, beispielsweise in Form eines Salzes, Oxids oder einer organischen Verbindung vorliegen.

Vorzugsweise ist der Katalysator zumindest teilweise auf einem Trägermaterial immobilisiert. Dieses kann beispielsweise Aktivkohle sein. Insbesondere wenn der Katalysator Metalle wie Fe, Cu, Mg und/oder Ni umfasst ist dies vorteilhaft. Es kann vorgesehen sein, dass das Trägermaterial mit der Membran verbunden ist und/oder Teil der Membran ist. Beispielsweise kann auf der Membran zumindest eine Schicht umfassend Trägermaterial und Katalysator angeordnet sein, wobei diese Membran vorzugsweise wasserdurchlässig und/oder porös ist. So wird erreicht, dass die Reaktion in unmittelbarer Nähe zur Membran stattfindet.

Es hat sich gezeigt, dass anorganische Membranen und Hybridmembranen besonders gut geeignet sind, bei höheren Drücken und Temperaturen verwendet zu werden. Denn auch unter diesen Bedingungen weisen sie eine hohe Selektivität für Wasser auf und können größere Mengen Wasser aus dem Reaktionsraum abscheiden. Organische Membranen können unter Umständen quellen und dabei zunehmend undurchlässig für Wasser werden. Durch die Verwendung von anorganischen Membranen oder Hybridmembranen wird dies vermieden.

Die Membran ist dabei durchlässig für Wasser. Vorzugsweise ist sie im Wesentlichen undurchlässig oder zumindest im Vergleich zu ihrer Durchlässigkeit für Wasser undurchlässiger für die Ausgangsstoffe, also CO_2 und/oder den Alkohol und/oder im Wesentlichen undurchlässig oder zumindest im Vergleich zu ihrer Durchlässigkeit für Wasser undurchlässiger für das Endprodukt, also das organische Carbonat. So kann das entstehende Wasser selektiv aus dem Raum, in dem die Reaktion statt findet, abgeführt werden und so das Reaktionsgleichgewicht auf die Seite des organischen Carbonats verschoben werden.

Die Membran kann dabei mehrere Schichten aufweisen, welche unterschiedliche Materialien oder Eigenschaften aufweisen. Es können mehrere Membranen parallel zueinander Wasser abscheiden, oder mehrere Membranen parallel zueinander zwischen dem Reaktionsraum und dem Abscheideraum angeordnet sein. Mit "parallel zueinander" ist dabei nicht die räumliche Ausrichtung der Membranflächen zueinander gemeint, sondern dass beide Membranen nicht hintereinander zwischen Reaktionsraum und Abscheideraum angeordnet sind, sondern die Wasserabscheidung auf den Membranen parallel zueinander erfolgt.

Im Allgemeinen können Membranen drei verschiedener Materialien unterschieden werden: organisch, anorganisch, eine Verbindung der beiden (hybrid).

Organische Polymermembranen sind in der Membrantechnologie im Allgemeinen weit verbreitet, da sie vergleichsweise günstig sind und durch die Auswahl an Polymeren bzw. die gut kontrollierbare Herstellung die Membranspezifikationen einfacher an die Kundenbedürfnisse angepasst werden können. Jedoch tendieren Polymermembranen bei erhöhten Temperaturen, welche bei unserem Prozess notwendig sind dazu zu quellen, wodurch die Selektivität signifikant herabgesetzt wird. In der Literatur vorgestellte Pervaporations-Membranen auf Polymer-Basis werden bei Temperaturen bis zu 60°C beschrieben. Da im erfindungsgemäßen Verfahren jedoch Temperaturen >100°C erforderlich sind, wird von diesen Membranen bei erhöhten Temperaturen keine ausreichende Selektivität mehr erreicht. Von einzelnen Herstellern werden experimentelle Spezialmembranen für bis 110°C vorgestellt, die jedoch deutlich schlechtere Eigenschaften aufweisen. Andere, klassische Hochtemperaturmembranmaterialien wie Polyimid weisen keine ausreichend gute Performance (Selektivität) auf.

Anorganische Membranen werden im Allgemeinen aus einem keramischen oder zeolithischen Material gefertigt, wodurch diese Membranen auch für höhere Temperaturen oder aggressivere Medien geeignet sind. Im Vergleich zu Polymer-Membranen ist die Herstellung aufwendiger und auch die Möglichkeiten zur Anpassung der Spezifikationen an Kundenanforderungen ist weniger ausgeprägt. Außerdem

sind anorganische Membranen teurer und anfälliger gegenüber mechanischen Belastungen.

Es sind auch sogenannte Hybridmembranen bekannt, welche sowohl organische als auch anorganische Werkstoffe umfassen.

Vorzugsweise weist eine Membran, besonders vorzugsweise eine Hybridmembran, zumindest eine zumindest überwiegend anorganische und/oder zumindest eine zumindest überwiegend organische Schicht auf. Die zumindest überwiegend anorganische Schicht kann Materialien oder Werkstoffe wie zumindest eine Keramik (beispielsweise oxidische Keramik, und/oder auf Aluminium-, Zirkonoxid- und/oder Siliziumoxidbasis), Carbid und/oder Zeolith umfassen. Die zumindest überwiegend organische Schicht kann Materialien oder Werkstoffe wie PVA (Polyvinylalkohol) umfassen

Es kann vorgesehen sein, dass die Membran, vorzugsweise eine Hybridmembran zumindest eine zumindest überwiegend anorganische Trägerschicht, vorzugsweise umfassend zumindest eine Keramik aufweist und/oder dass die Membran zumindest eine weitere Schicht, vorzugsweise umfassend zumindest einen organischen Werkstoff, besonders vorzugsweise einen Polymer-Werkstoff, aufweist. Vorzugsweise weist die weitere Schicht eine höhere Selektivität gegenüber Wasser auf als die Trägerschicht.

Durch die Verbindung aus dem anorganischen Träger und der organischen Schicht wird das Quellen des organischen Werkstoffs minimiert, wodurch auch bei erhöhten Temperaturen gute Selektivitäts-Ergebnisse zu erwarten sind.

Besonders vorzugsweise umfasst die Membran zumindest eine Polymer-Metall-Carbide-Membran. Diese Membranen weisen eine besonders gute Temperaturstabilität auf.

Es kann vorgesehen sein, dass die Hybridmembran zumindest eine Einzelschicht aufweist, die organische und anorganische Materialien aufweist. Mit Einzelschicht ist eine Schicht gemeint, die sich nicht in unterschiedliche Subschichten abhängig von ihren Materialien unterteilen lässt. Es kann vorgesehen sein, dass das organische und das anorganische Material miteinander vermischt ist. Solche Membranen werden manchmal auch Mixed Matrix Membranen genannt.

Es kann vorgesehen sein, dass die Hybridmembran zumindest eine Schicht aufweist, welche eine organische Matrix umfasst, in der anorganisches Material angeordnet ist, vorzugsweise Partikel und/oder vorzugsweise der Katalysator und/oder Adsorbens.

Weitere Beispiele für Membranmaterialien finden sich in Vane et.al[3].

Es hat sich überraschenderweise herausgestellt, dass besonders hohe Ausbeuten erzielt werden können, wenn als Katalysator die angegebenen Substanzen verwendet und eine höhere Temperatur und Druck eingestellt wird. Es kann auf eine Stromzufuhr - wie bei der elektrochemischen Reduktion von CO_2 unter Verwendung von Übergangsmetallen notwendig – verzichtet werden. Als ganz besonders effizient hat sich dabei ein Katalysator herausgestellt, der Ceroxid (CeO_2) umfasst. Mit einem solchen Katalysator haben sich besonders hohe Ausbeuten ergeben.

Überraschender Weise hat sich gezeigt, dass sich eine höhere Temperatur von mindestens 80°C positiv auf die Ausbeute und Reaktionsgeschwindigkeit auswirkt, obwohl die Reaktion exotherm ist, also Wärme freisetzt.

Der Reaktionsraum des Reaktormoduls ist jener Raum, in dem der Katalysator angeordnet ist und dem die Ausgangsstoffe zugeführt werden, damit eine katalytische Reaktion stattfindet. Dabei ist wesentlich, dass der Druck und die Temperatur in diesem Reaktionsraum den vorgegebenen Werten entsprechen, damit die Reaktion effizient und möglichst vollständig abläuft.

Der Abführraum ist vorzugsweise frei von Katalysator und dient zum Abführen des Wassers, das aus dem Reaktionsraum über die Membran in den Abführraum abgeführt wird. Das durch die Reaktion entstehende Wasser durchdringt die Membran und scheidet sich in den Abführraum ab, wo es abgeführt werden kann, beispielsweise über einen Wasserauslass oder gespeichert in einem Wassertank.

Vorzugsweise ist vorgesehen, dass der die Membran den Reaktionsraum an zumindest einer Seite begrenzt. Es kann also vorgesehen sein, dass der Katalysator und die Membran nebeneinander angeordnet sind. So kann das entstehende Wasser direkt nach der Entstehung über die Membran entfernt werden. Dies gilt sowohl für das erfindungsgemäße Verfahren als auch für den erfindungsgemäßen Reaktor.

Vorzugsweise herrscht im Abführraum ein Druck, der sich von dem Druck im Reaktionsraum um weniger als 6 bar unterscheidet. So wird eine zu starke Druckbelastung der Membran verhindert.

Die katalytische Reaktion kann dabei kontinuierlich oder diskontinuierlich durchgeführt werden.

[3] Vane LM. Review: Membrane Materials for the Removal of Water from Industrial Solvents by Pervaporation and Vapor Permeation. J Chem Technol Biotechnol. 2019;94(2):343-365. doi: 10.1002/jctb.5839. PMID: 30930521; PMCID: PMC6436640.

Es kann auch ein Reaktor zur Herstellung organischer Carbonate, insbesondere von Diethylcarbonat, vorteilhaft sein, wobei der Reaktor zumindest ein Reaktormodul aufweist, und das Reaktormodul einen Reaktionsraum aufweist, der durch zumindest eine organische, anorganische Membran und/oder Hybridmembran von einem Abführraum zum Abführen von Wasser aus dem Reaktionsraum abgetrennt ist, wobei im Reaktionsraum ein Katalysator, vorzugsweise immobilisiert auf einem Molsieb oder ähnliche Trägermaterialien, wie beispielsweise zumindest ein Polymer angeordnet ist und dass der Katalysator zumindest eines der genannten Substanzen umfasst: Ceroxid (CeO_2), ZrO_2, CrO_2, Fe, Cu, Mg, Ni, SiO_2, Al_2O_3, TiO, MoO, BiO, ZnO, Ta_2O_5, Nb_2O_5 oder eine Legierung umfassend Kupfer und Nickel.

Dem entsprechend kann auch ein Verfahren zur Herstellung organischer Carbonate, insbesondere von Diethylcarbonat, vorteilhaft sein, umfassend eine katalytische Reaktion von entsprechenden Alkoholen (ROH) mit Kohlendioxid, wobei R ein gerad- oder verzweigtkettiger Alkylrest mit 1-6 Kohlenstoffatomen, vorzugsweise Ethylalkohol, ist, wobei während der katalytischen Reaktion entstehendes Wasser über zumindest eine organische oder anorganische Membran und/oder Hybridmembran abgetrennt wird, und wobei der Katalysator umfasst, welcher vor der Durchführung der katalytischen Reaktion auf einem Molsieb oder ähnliche Trägermaterialien immobilisiert wurde, und dass die katalytische Reaktion bei einer Temperatur von mindestens 80°C und bei einem Druck von mindestens 5 bar durchgeführt wird und dass der Katalysator zumindest eines der genannten Substanzen umfasst: Ceroxid (CeO_2), ZrO_2, CrO_2, Activated Carbon(Fe,Cu,Mg,Ni), SiO_2, Al_2O_3, TiO, MoO, BiO, ZnO, Ta_2O_5, Nb_2O_5 oder eine Legierung umfassend Kupfer und Nickel.

Ausführungsformen gemäß der letzten beiden Absätze sind besonders vorteilhaft, da sie auf besonders einfache Art und Weise eine effektive Umsetzung ermöglichen. Sie können mit sämtlichen besonderen Merkmalen und Ausführungsformen, die in dieser Beschreibung oder den Ansprüchen beschrieben sind, kombiniert werden. Durch die Anordnung des Katalysators auf einem Molsieb, also einem Molekularsieb, oder ähnliche Trägermaterialien wird eine besonders große Oberfläche erreicht, die für die katalytische Beschleunigung des Verfahrens besonders sinnvoll ist. Die Anordnung auf einem Molsieb ist in Kombination mit der Membran besonders vorteilhaft, da so komplex aufgebaute Membranformen, welche möglichst viel Membranoberfläche zur Ableitung des Wassers bieten und den Reaktionsräumen eine räumlich verwinkelte Form geben, besonders gut mit möglichst viel Katalysator kombiniert werden können. Denn trotz der komplexen und verwinkelten räumlichen Struktur des Reaktionsraums kann dieser einfach und dicht mit dem Molsieb gefüllt werden, der durch seine stückige Form den Raum trotzdem gut ausfüllen kann. Molsiebe liegen nämlich üblicherweise in rieselfähiger stückiger

Form vor, als Granulat- oder Pelletform beispielsweise. So kann eine besonders große Membranoberfläche mit einer besonders großen Katalysatoroberfläche auf engem Raum kombiniert werden, was zu einer synergistischen Verbesserung der Ausbeute führt. Daneben hat das Aufbringen auf dem Trägermaterial den Vorteil, dass nicht lose im Reaktionsraum vorliegt, was zu Verstopfungen führen kann.

Besonders vorteilhaft ist, wenn die Reaktion bei mindestens 100°C, vorzugsweise mindestens 120°C und besonders vorzugsweise zwischen 110°C und 150°C durchgeführt wird, und/oder wenn die Reaktion bei mindestens 10 bar, vorzugsweise bei einem Druck über 12 bar und/oder über 15 bar und besonders vorzugsweise zwischen 20 bar und 40 bar durchgeführt wird. Wie oben erläutert ermöglichen diese Temperatur- und Druckbereiche besonders hohe Ausbeuten, obwohl dies aufgrund der exothermen Reaktion zuerst paradox erscheint. Insbesondere bei einer Temperatur zwischen 110°C und 150°C und/oder einem Druck über 12 bar, ganz besonders aber bei einem Druck zwischen 20 bar bis 40 bar, konnte eine besonders hohe Ausbeute erzielt werden.

In einer bevorzugten Ausführungsform ist vorgesehen, dass die Abtrennung über die Membran mittels Membranpervaporation und/oder Dampfpermeation erfolgt. Insbesondere bei höheren Drücken und Temperaturen kann so eine besonders effiziente Abscheidung des Wassers erfolgen. Dem entsprechend kann auch vorgesehen sein, dass die Membran dazu ausgelegt ist, Wasser mittels Membranpervaporation und/oder Dampfpermeation abzuscheiden.

Besonders vorteilhaft ist, wenn die Abtrennung über zumindest eine Carbon-Membran und/oder zumindest eine keramische Membran, besonders vorzugsweise zumindest eine Zeolith-Membran erfolgt. Es hat sich gezeigt, dass solche Membranen, insbesondere Zeolith-Membranen trotz des hohen Drucks und der hohen Temperaturen eine gute Selektivität für Wasser aufweisen und über weite Zeiträume stabil bleiben. Entsprechendes gilt auch, wenn vorgesehen ist, dass die Membran eine Carbon-Membran und/oder eine keramische Membran, besonders vorzugsweise eine Zeolith-Membran umfasst.

Weiters ist vorteilhaft, wenn die katalytische Reaktion in zumindest einem Reaktormodul durchgeführt wird, in dem der Katalysator angeordnet ist. Dies ermöglicht einen kompakten und kontrollierten Reaktionsablauf im Reaktormodul. Das Reaktormodul kann einen oder mehrere Reaktionsräume aufweisen, in dem der Katalysator angeordnet ist und in dem die katalytische Reaktion ablaufen kann. Besonders vorteilhaft ist, wenn dabei der Reaktionsraum durch zumindest eine anorganische Membran und/oder Hybridmembran von einem Abführraum zum Abführen von Wasser aus dem Reaktionsraum abgetrennt ist. So kann das Wasser

sofort nach dem Entstehen bei der katalytischen Reaktion abgetrennt werden. Somit wird die Verweildauer des Wassers beim Katalysator minimiert.

In diesem Sinne ist auch vorteilhaft, wenn der Reaktor zumindest eine Kohlendioxidquelle und zumindest eine Alkoholquelle (ROH) aufweist, wobei R ein gerad- oder verzweigtkettiger Alkylrest mit 1-6 Kohlenstoffatomen, vorzugsweise Ethylalkohol, ist. Diese Quellen können beispielsweise Speichermedien für die Substanzen sein, also eine CO_2-Flasche oder ein Container mit Alkohol. Es kann auch sein, dass die Quelle selbst die Substanz direkt herstellt, beispielsweise kann die Kohlendioxidquelle also eine Brennkraftmaschine sein, die Kohlendioxid durch die Verbrennung von Treibstoff erzeugt. Weitere Kohlendioxidquellen könnten Anlagen sein, die Kohlendioxid auf biologischem Wege freisetzen, beispielsweise durch Fermentation, oder auch chemische Anlagen. Auch eine Anlage zur Gewinnung von Kohlenstoffdioxid direkt aus der Umgebungsluft (direct air capture) ist möglich.

Besonders vorteilhaft ist, wenn während der katalytischen Reaktion das Reaktionsgemisch im Kreislauf durch das Reaktormodul geführt wird. So wird das Gemisch aus Ausgangsstoffen und Endprodukt ständig durchmischt und der Katalysator stets mit Ausgangsstoffen und die Membran stets mit Wasser versorgt, um einen effizienten Reaktionsablauf zu erreichen. In diesem Sinne ist auch vorteilhaft, wenn vorgesehen ist, dass der Reaktor zumindest einen Kreislauf mit zumindest einer Förderpumpe zum Transport eines flüssigen und/oder gasförmigen Gemisches entlang des Kreislaufes aufweist, dass das Reaktormodul Teil des Kreislaufes ist und dass vorzugsweise die Kohlendioxidquelle und die Alkoholquelle mit dem Kreislauf strömungsverbunden sind.

Um eine besonders effiziente Umsetzung zu erreichen kann vorgesehen sein, dass während der katalytischen Reaktion das Reaktionsgemisch im Kreislauf durch mehrere parallel geschaltete Reaktormodule geführt wird. Durch die parallele Schaltung der Reaktormodule kann die Menge an umgesetzten Ausgangssubstanzen weiter erhöht werden. Insbesondere bei einem diskontinuierlichen Verfahrensablauf ist dies vorteilhaft. Entsprechendes gilt auch, wenn der Kreislauf mehrere Reaktormodule aufweist, die parallel zueinander geschaltet sind. Alternativ können auch mehrere Reaktormodule seriell zueinander geschaltet sein. So kann eine höhere Konzentration erreicht werden.

Es kann auch vorgesehen sein, dass mehrere Kreisläufe seriell hintereinandergeschaltet sind, wobei zumindest ein erster und zweiter Kreislauf jeweils zumindest ein Reaktormodul aufweist. Mit anderen Worten kann also vorgesehen sein, dass das Reaktionsgemisch nach der Führung in einem ersten Kreislauf zumindest teilweise in einem zweiten Kreislauf geführt wird, wobei das Reaktionsgemisch im

Zuge der Führung durch den zweiten Kreislauf durch zumindest ein weiteres Reaktormodul geführt wird. Dabei kann vorgesehen sein, dass in den Kreisläufen unterschiedliche Reaktionsgleichgewichte eingestellt werden. Dies kann insbesondere bei einer kontinuierlichen Verfahrensdurchführung zweckdienlich sein.

Vorzugsweise ist vorgesehen, dass die katalytische Reaktion so lange durchgeführt wird, bis das Reaktionsgemisch einen Schwellengewichtsanteil an Endprodukt, vorzugsweise zumindest 80%-wt aufweist, und dass bei oder nach Erreichen des Schwellengewichtsanteils das Reaktionsgemisch aus dem Reaktormodul abgeleitet wird und dass nach der Ableitung vorzugsweise Kohlendioxid, der Alkohol oder zumindest eine andere Substanz von dem organischen Carbonat als Endprodukt abgeschieden wird. Durch eine derartige diskontinuierliche Reaktionsführung wird schnell ein hoher Umsetzungsgrad erreicht. Dabei kann bis zum Erreichen des Schwellengewichtsanteils das Reaktionsgemisch im Kreislauf geführt werden. Es kann in diesem Sinne auch vorteilhaft sein, wenn nach oder bei der Ableitung Kohlendioxid, vorzugsweise über einen Tropfenabscheider, aus dem Reaktionsgemisch abgeschieden wird und/oder dass der Alkohol und/oder andere Substanzen aus dem Reaktionsgemisch abgeschieden werden, besonders vorzugsweise über Destillation und/oder über zumindest eine Membran. Dem entsprechend ist es auch vorteilhaft, wenn vorgesehen ist, dass der Kreislauf zumindest einen aus dem Kreislauf führenden Abführkanal zum Abführen von Endprodukt aufweist und dass der Abführkanal vorzugsweise zumindest einen Kondensator und/oder zumindest einen Tropfenabscheider und besonders vorzugsweise einen Kohlendioxidrückführkanal zur Rückführung von Kohlendioxid aus dem Tropfenabscheider in den Kreislauf umfasst.

Die abgeschiedene Substanz oder Substanzen können dabei wieder in den Kreislauf rückgeführt werden. Es kann also vorgesehen sein, dass zumindest ein Rückführkanal für die jeweilige Substanz zur Rückführung in den Kreislauf vorgesehen ist. Dabei kann die Substanz, also Kohlendioxid oder der Alkohol, vor der Rückführung vorbehandelt werden, beispielsweise verdichtet, erhitzt oder abgekühlt oder gereinigt werden.

Weiters ist vorteilhaft, wenn nach der Ableitung Kohlendioxid und Alkohol in den Reaktor geleitet werden und eine weitere katalytische Reaktion durchgeführt wird. Es kann damit eine neue Reaktion gestartet werden.

Um eine zu starke Belastung der Membran zu verhindern kann vorgesehen sein, dass während der katalytischen Reaktion auf der dem Reaktionsgemisch abgewandten Seite der Membran ein Druck eingestellt wird, der vom Druck des Reaktionsgemisches um weniger als 10 bar, vorzugsweise weniger als 6 bar abweicht.

Weiters ist vorteilhaft, wenn an der dem Reaktionsgemisch abgewandten Seite der Membran ein Sweepgas vorbeiströmt, wobei das Sweepgas vorzugsweise Kohlendioxid ist. Das Sweepgas treibt durch seine Strömung das Wasser, dass aus der Membran austritt und von der Membranoberfläche weg, was die Wasserabscheidung verbessert. Über das Sweepgas kann der Druck auf dieser Seite der Membran eingestellt werden. Alternativ kann als Sweepgas auch Stickstoff (N_2), Ethanoldampf oder Gasgemische, vorzugsweise Gasgemische der genannten Gase wie ein beispielsweise CO_2-Ethanoldampfgemisch verwendet werden.

Besonders vorteilhaft ist, wenn vor der katalytischen Reaktion der Katalysator auf einem Molsieb immobilisiert wird und vorzugsweise dabei ein Cer-Salz, besonders vorzugsweise ein Cer-Halogen-Salz wie Cerchlorid und/oder Cer(III)Nitrat, auf das Molsieb aufgebracht wird und das Molsieb anschließend kalziniert wird. So wird wie oben beschrieben eine besonders große Katalysatoroberfläche erreicht. Entsprechendes gilt auch, wenn vorgesehen ist, dass der Reaktionsraum im Wesentlichen mit einem Molsieb und dem darauf immobilisierten Katalysator gefüllt ist.

Vorzugsweise ist die Membran als zumindest ein Membranrohr ausgeführt, in dessen Inneren sich zumindest ein Teil des Abführraums befindet. Durch die Ausführung als Rohr kann auf effiziente Weise mittels Sweepgas der Wasserabtransport verbessert werden. Dem entsprechend kann auch vorgesehen sein, dass während der katalytischen Reaktion entstehendes Wasser über zumindest eine als zumindest ein Membranrohr ausgeführte Membran abgetrennt wird.

Besonders vorteilhaft ist, wenn die Membran eine Selektivität α auf Wasser von mindestens 100 bei einer Temperatur von 80°C und einem Druck von 5 bar aufweist und/oder eine Selektivität α auf Wasser von mindestens 100 bei einer Temperatur von 100°C und einem Druck von 10 bar aufweist. So kann eine möglichst reine Abtrennung des Wassers erfolgen. Eine Selektivität auf Wasser von 100 bedeutet, dass die Membran bei 100 Teilen Wasser nur 1 Teil Ethanol hindurchlässt.

Weiters kann zur Einstellung der Temperatur für die katalytische Reaktion vorgesehen sein, dass der Kreislauf zumindest eine Temperierquelle zur Einstellung der Temperatur des Gemisches im Kreislauf aufweist und/oder die Temperatur des Gemisches im Kreislauf über zumindest eine Temperierquelle eingestellt wird.

In einer bevorzugten Ausführungsform ist vorgesehen, dass das Reaktormodul einen mit dem Reaktionsraum strömungsverbundenen Einlass aufweist, der mit einem Feedkanal des Kreislaufs verbunden ist, und einen, vorzugsweise am gegenüberliegenden Ende des Reaktionsraums angeordneten Auslass aufweist, der

mit einem Retentatkanal des Kreislaufs verbunden ist. Der Feedkanal und der Retentatkanal sind dabei – neben der Verbindung über das Reaktormodul - ebenso direkt oder indirekt miteinander verbunden, sodass ein Kreislauf entsteht.

Besonders vorteilhaft ist, wenn in den Reaktionsraum zumindest ein Membranrohr hineinragt und sich vorzugsweise von einem Ende des Reaktionsraums bis zum anderen Ende des Reaktionsraums erstreckt. So kann über die gesamte Länge des Reaktionsraums Wasser aus dem Reaktionsraum entfernt werden und im gesamten Reaktionsraum wird durch die geringe Wassermenge eine besonders große Menge von Ausgangssubstanzen zu organischem Carbonat umgesetzt.

Vorteilhaft ist weiters, wenn das Membranrohr im Bereich eines ersten Endes mit einer Sweepgasquelle strömungsverbunden ist und das Membranrohr im Bereich eines zweiten Endes mit einem Wasserabführkanal zum Abführen des Wassers strömungsverbunden ist. So wird ein besonders effizienter Wasserabtransport erreicht.

In diesem Sinne kann vorgesehen sein, dass das erste Ende geschlossen ist und die Strömungsverbindung zur Sweepgasquelle über ein Tauchrohr erfolgt, das über das zweite Ende in das Membranrohr hineinragt. Dies ermöglicht die Anordnung der Anschlüsse für das Sweepgas an einer Seite des Reaktionsraums. Darüber hinaus wird so ermöglicht, solche Membranrohre zu verwenden, die bereits industriell an einer Seite geschlossen hergestellt werden.

Zur effizienten Abscheidung des Wassers kann vorgesehen sein, dass der Wasserabführkanal einen Tropfenabscheider zum Abscheiden von Sweepgas, vorzugsweise ein dem Tropfenabscheider vorgeschaltetem Kondensator und/oder eine Sweepgasrückführleitung zur Rückleitung von gewonnenem Sweepgas in das Membranrohr aufweist.

Das Sweepgas kann beispielsweise Kohlendioxid sein. Selbst wenn etwas davon über die Membran in den Reaktionsraum eintreten sollte, so würde es das Gemisch dort so nicht verunreinigen. Alternativ kann ein anderes Gas, beispielsweise Stickstoff (N_2), Ethanoldampf oder Gasgemische, vorzugsweise Gasgemische der genannten Gase wie ein beispielsweise CO_2-Ethanoldampfgemisch verwendet werden.

Die Abscheidung des Wassers wird weiter verbessert, wenn zumindest fünf, vorzugsweise sechs oder sieben Membranrohre in dem Reaktormodul angeordnet sind.

In weiterer Folge wird die Erfindung anhand nicht einschränkender, erfindungsgemäßer Ausführungsformen in den Figuren beschrieben. Es zeigen:

Fig. 1a ein erfindungsgemäßes Reaktormodul zum Einbau in einen erfindungsgemäßen Reaktor und zur Durchführung eines erfindungsgemäßen Verfahrens in einem Längsschnitt;

Fig. 1b einen Schnitt durch das Reaktormodul aus Fig. 1a entlang der Linie A-A;

Fig. 2 ein Fließschema eines erfindungsgemäßen Reaktors, der ein erfindungsgemäßes Verfahren verwendet, in einer ersten Ausführungsform.

Das in Fig. 1a und Fig. 1b gezeigte Reaktormodul 1 weist eine längliche, im Wesentlichen zylindrische Form auf. An einem Ende ist ein Einlassbereich 2 angeordnet, der einen Anschluss 2a zur Verbindung mit einem Feedkanal aufweist. So wird das Reaktormodul mit Kohlendioxid und Alkohol versorgt. Der Einlassbereich 2 ist über einen Einlass 3 mit einem ersten Ende 4a des Reaktionsraums 4 verbunden, der mit Molsieb (nicht dargestellt) in Pelletform und dem darauf kalzinierten Katalysator gefüllt ist, sodass die Ausgangsstoffe durch den Katalysator im Reaktionsraum 4 zu organischem Carbonat umgesetzt werden können. Der Reaktionsraum 4 erstreckt sich über den Großteil des Reaktormoduls 1, zur besseren Ansicht ist das Reaktormodul 1 im Bereich des Reaktionsraums 4 unterbrochen dargestellt.

Der Reaktionsraum 4 ist an seinem gegenüberliegenden zweiten Ende 4b über einen Auslass 5 mit einem Auslassbereich 6 strömungsverbunden. Der Auslassbereich 6 weist einen Anschluss 6a zur Verbindung mit einem Retentatkanal auf. So kann das Retentat, das das Endprodukt, gegebenenfalls gemischt mit den Ausgangssubstanzen, die nicht umgesetzt wurden, umfasst, aus dem Reaktionsraum 4 herausgeführt werden.

Entlang der Längserstreckung des Reaktionsraums 4 erstrecken sich im Reaktionsraum 4 insgesamt sieben Membranrohre 7, welche sich durch eine Stirnwand 8 des Auslassbereichs 6 hindurch in den Auslassbereich 6 und weiter in den Reaktionsraum 4 bis zum ersten Ende 4a erstrecken. Die Stirnwand 8 ist dabei dicht mit den Membranrohren 7 verbunden. Die Membranrohre 7 enden in einen Wassersammelbereich 9, der hinter der Stirnwand 9 angeordnet ist. Die Außenwände der Membranrohre 7 zeigen also zum Reaktionsraum 4, die Innenwände der Membranrohre 7 hingegen zeigen zu einem Abführraum 10, der sich aus den Innenräumen der Membranrohre 7 bildet und der frei von Katalysator ist.

An einem zweiten Ende 7b der Membranrohre 7 sind diese offen und in Strömungsverbindung mit dem Wassersammelbereich 9. Wasser, das so über die Membranrohre 7 aus dem Reaktionsraum 4 in den Abführraum 10 eindringt, kann so in dem

Wassersammelbereich 9 gesammelt werden und über einen Anschluss 9a des Wassersammelbereichs 9 in einen Abführkanal abgeführt werden.

An einem ersten Ende 7a, das ist das Ende, das zum ersten Ende 4a des Reaktionsraums 4 zeigt, sind die Membranrohre 7 verschlossen. Über das zweite Ende 7b sind Tauchrohre 11 in die Membranrohre 7 eingeführt, welche sich bis zum ersten Ende 7a erstrecken und dort offen sind. So kann Sweepgas über die Tauchrohre 11 in den Bereich des ersten Endes 7a in den Abführraum 10 gebracht werden. Die Tauchrohre 11 begrenzen den Abführraum 10 auf den engen Bereich zwischen der Außenseite der Tauchrohre 11 und der Innenseite der Membranrohre 7.

Die Tauchrohre 11 erstrecken sich vom zweiten Ende 7b weiter durch den Wassersammelbereich 9 und durch eine weitere Stirnwand 12 des Reaktormoduls 1, wobei diese Stirnwand 12 ebenso dicht mit den Tauchrohren 11 verbunden ist. Jenseits der Stirnwand 12 sind die Tauchrohre 11 mit einer Sweepgasquelle strömungsverbindbar.

In Fig. 2 wird eine erfindungsgemäße Ausführungsform eines Reaktors anhand eines Fließschemas näher erläutert. Dabei weist der Reaktor ein Reaktormodul 20 auf, das eine Membran 21 aufweist, die einen Reaktionsraum 4 von einem Abführraum 10 trennt. Der Reaktionsraum 4 ist Teil eines Kreislaufes 22, der eine Kreislauf-Pumpe 23 aufweist, die dessen Fluid in eine Richtung bewegt. Der Kreislauf 22 kann zur Führung des Fluids Kanäle wie beispielsweise Rohrleitungen aufweisen. Die Membran 21 umfasst zumindest eine anorganische Membran und/oder zumindest eine Hybridmembran.

Der Reaktionsraum ist über einen Einlass mit einem Feedkanal 29 des Kreislaufs 22 stromabwärts der Kreislauf-Pumpe 23 verbunden und über einen Auslass mit einem Retentatkanal 30 stromaufwärts der Kreislauf-Pumpe 23 verbunden. Mit verbunden ist in diesem Sinne, sind Strömungsverbindungen gemeint. Die Kreislauf-Pumpe 23 wirkt damit als Förderpumpe.

In Fig. 2 ist nur ein Reaktormodul 20 dargestellt. Es kann wie bereits ausgeführt jedoch auch vorgesehen sein, dass sich der Feedkanal 29 stromaufwärts des Reaktormoduls verzweigt und mehrere Rekatormodule 20 parallel versorgt. Dem entsprechend würde dann auch der Retantatkanal 30 entsprechend verzweigt das Reaktionsgemisch aus den Reaktormodulen sammeln und stromaufwärts der Kreislaufpumpe 23 zu einem einzelnen Kanal zusammenführen.

Mit dem Kreislauf 22 ist des Weiteren eine Zuführleitung 24 für Ethanol verbunden, über die Ethanol aus einem Ethanoltank 25 und durch eine Feed-Pumpe in den Kreislauf eingespeist wird. Vorzugsweise ist die Zuführleitung 24 – so wie in dieser

Ausführungsform gezeigt – stromabwärts der Kreislauf-Pumpe 23 und stromaufwärts des Reaktormoduls 20 angeordnet.

Mit dem Kreislauf 22 ist des Weiteren eine Zuführleitung 26 für Kohlendioxid (CO_2) verbunden, über die CO_2 aus einem Kohlendioxidtank 27 und gegebenenfalls eine weitere Feed-Pumpe in den Kreislauf eingespeist wird. Vorzugsweise ist die Zuführleitung 26 – so wie in dieser Ausführungsform gezeigt – stromabwärts der Kreislauf-Pumpe 23 und stromaufwärts des Reaktormoduls 20 angeordnet.

Der Kreislauf 22 ist auch mit einer Abführkanal 28 zwischen Reaktionsraum 4 und der Kreislauf-Pumpe 23 verbunden, über die Retentat in einen Retentattank 31 abgeführt werden kann.

Der Abführraum 10 ist mit über eine weitere Zuführleitung 35 mit einer Kohlendioxidquelle, vorzugsweise dem gleichen Kohlendioxidtank 27 verbunden. Somit wirkt das CO_2 im Abführraum 10 als Sweepgas und führt das Wasser von der Membran 21 weg.

Der Abführraum 10 ist mit einem Wasserabführkanal 32 verbunden, über den Wasser aus dem Abführraum 10 herausgeführt und in einen Wassertank 34 geleitet werden kann. Dabei weist der Wasserabführkanal 32 vorzugsweise einen Kondensator 33 auf, über den das Wasser vor dem Einführen in den Wassertank 34 kondensiert wird.

Das Reaktormodul 20 ist vorzugsweise temperiert, besonders vorzugsweise über ein Temperierfluid wie ein Öl, das über Temperierkanäle 36 zu und von dem Reaktormodul 20 geführt wird.

PATENTANSPRÜCHE

1. Verfahren zur Herstellung organischer Carbonate, insbesondere von Diethylcarbonat, umfassend eine katalytische Reaktion von entsprechenden Alkoholen (ROH) mit Kohlendioxid, wobei R ein gerad- oder verzweigtkettiger Alkylrest mit 1-6 Kohlenstoffatomen, vorzugsweise ein Ethylrest, ist, und wobei während der katalytischen Reaktion entstehendes Wasser über zumindest eine anorganische Membran (21) und/oder zumindest eine Hybridmembran (21) abgetrennt wird, **dadurch gekennzeichnet**, dass die katalytische Reaktion bei einer Temperatur von mindestens 80 °C und bei einem Druck von mindestens 5 bar durchgeführt wird und dass der Katalysator zumindest eines der genannten Substanzen umfasst: Ceroxid (CeO_2), ZrO_2, CrO_2, Fe, Cu, Mg, Ni, SiO_2, Al_2O_3, TiO, MoO, BiO, ZnO, Ta_2O_5, Nb_2O_5 oder eine Legierung umfassend Kupfer und Nickel.

2. Verfahren nach Anspruch 1, **dadurch gekennzeichnet**, dass die Reaktion bei mindestens 100°C, vorzugsweise mindestens 120°C und besonders vorzugsweise zwischen 110°C und 150°C durchgeführt wird, und/oder dass die Reaktion bei mindestes 10 bar, vorzugsweise bei einem Druck zwischen 20 bar und 40 bar durchgeführt wird.

3. Verfahren nach Anspruch 1 oder 2, **dadurch gekennzeichnet**, dass die Abtrennung über die Membran (31) mittels Membranpervaporation und/oder Dampfpermeation erfolgt.

4. Verfahren nach einem der Ansprüche 1 bis 3, **dadurch gekennzeichnet**, dass die Abtrennung über zumindest eine Carbon-Membran und/oder zumindest eine keramische Membran, besonders vorzugsweise zumindest eine Zeolith-Membran erfolgt und/oder, dass die die Abtrennung über zumindest eine Membran erfolgt, die zumindest eine zumindest überwiegend anorganische und/oder zumindest eine zumindest überwiegend organische Schicht aufweist.

5. Verfahren nach einem der Ansprüche 1 bis 4, **dadurch gekennzeichnet**, dass die katalytische Reaktion in zumindest einem Reaktormodul (20) durchgeführt wird, in dem der Katalysator angeordnet ist und dass vorzugsweise der Reaktionsraum (4) durch zumindest eine anorganische Membran (21) und/oder zumindest eine Hybridmembran (21) von einem Abführraum (10) zum Abführen von Wasser aus dem Reaktionsraum (4) abgetrennt ist.

6. Verfahren nach Anspruch 5, **dadurch gekennzeichnet**, dass während der katalytischen Reaktion das Reaktionsgemisch im Kreislauf (22) durch das Reaktormodul (20) geführt wird.

7. Verfahren nach Anspruch 6, **dadurch gekennzeichnet**, dass während der katalytischen Reaktion das Reaktionsgemisch im Kreislauf (22) durch mehrere parallel geschaltete Reaktormodule (20) geführt wird.

8. Verfahren nach einem der Ansprüche 1 bis 7, **dadurch gekennzeichnet**, dass die katalytische Reaktion so lange durchgeführt wird, bis das Reaktionsgemisch einen Schwellengewichtsanteil an Endprodukt, vorzugsweise zumindest 80%-wt aufweist, und dass bei oder nach Erreichen des Schwellengewichtsanteils das Reaktionsgemisch aus dem Reaktormodul (20) abgeleitet wird und dass nach der Ableitung vorzugsweise Kohlendioxid, der Alkohol oder zumindest eine andere Substanz von dem organischen Carbonat als Endprodukt abgeschieden wird.

9. Verfahren nach Anspruch 8, **dadurch gekennzeichnet**, dass nach oder bei der Ableitung Kohlendioxid aus dem Reaktionsgemisch abgeschieden wird und/oder dass der Alkohol und/oder andere Substanzen aus dem Reaktionsgemisch abgeschieden werden, besonders vorzugsweise über Destillation und/oder über zumindest eine Membran.

10. Verfahren nach Anspruch 8 oder 9, **dadurch gekennzeichnet**, dass nach der Ableitung Kohlendioxid und Alkohol in den Reaktor geleitet werden und eine weitere katalytische Reaktion durchgeführt wird.

11. Verfahren nach einem der Ansprüche 1 bis 10, **dadurch gekennzeichnet**, dass während der katalytischen Reaktion auf der dem Reaktionsgemisch abgewandten Seite der Membran (21) ein Druck eingestellt wird, der vom Druck des Reaktionsgemisches um weniger als 10 bar, vorzugsweise weniger als 6 bar abweicht.

12. Verfahren nach einem der Ansprüche 1 bis 11, **dadurch gekennzeichnet**, dass an der dem Reaktionsgemisch abgewandten Seite der Membran (21) ein Sweepgas vorbeiströmt, wobei das Sweepgas vorzugsweise Kohlendioxid ist.

13. Verfahren nach einem der Ansprüche 1 bis 12, **dadurch gekennzeichnet**, dass vor der katalytischen Reaktion der Katalysator auf einem Molsieb immobilisiert wird und vorzugsweise dabei ein Cer-Salz, besonders vorzugsweise ein Cer-Halogen-Salz wie Cerchlorid und/oder Cer(III)Nitrat, auf das Molsieb aufgebracht wird und das Molsieb anschließend kalziniert wird.

14. Verfahren nach einem der Ansprüche 1 bis 13, **dadurch gekennzeichnet**, dass das Wasser direkt nach der Entstehung bei der katalytischen Reaktion über die Membran (21) abgetrennt wird.

15. Reaktor zur Herstellung organischer Carbonate, insbesondere von Diethylcarbonat, wobei der Reaktor zumindest ein Reaktormodul (20) aufweist, und das Reaktormodul (20) einen Reaktionsraum (4) aufweist, wobei der Reaktionsraum (4) durch zumindest eine anorganische Membran (21) und/oder zumindest eine Hybridmembran (21) von einem Abführraum (10) zum Abführen von Wasser aus dem Reaktionsraum (4) abgetrennt ist, **dadurch gekennzeichnet**, dass im Reaktionsraum (4) ein Katalysator angeordnet ist und dass der Katalysator zumindest eines der genannten Substanzen umfasst: Ceroxid (CeO_2), ZrO_2, CrO_2, Fe, Cu, Mg, Ni, SiO_2, Al_2O_3, TiO, MoO, BiO, ZnO, Ta_2O_5, Nb_2O_5 oder eine Legierung umfassend Kupfer und Nickel.

16. Reaktor nach Anspruch 15, **dadurch gekennzeichnet**, dass die Membran (20) eine Carbon-Membran und/oder eine keramische Membran, besonders vorzugsweise eine Zeolith-Membran umfasst und/oder dass die Membran zumindest eine zumindest überwiegend anorganische und/oder zumindest eine zumindest überwiegend organische Schicht aufweist.

17. Reaktor nach Anspruch 15 oder 16, **dadurch gekennzeichnet**, dass der Reaktor zumindest eine Kohlendioxidquelle und zumindest eine Alkoholquelle (ROH) aufweist, wobei R ein gerade- oder verzweigtkettiger Alkylrest mit 1-6 Kohlenstoffatomen, vorzugsweise Ethylalkohol, ist.

18. Reaktor nach einem der Ansprüche 15 bis 17, **dadurch gekennzeichnet**, dass der Reaktor zumindest einen Kreislauf (22) mit zumindest einer Förderpumpe zum Transport eines flüssigen und/oder gasförmigen Gemisches entlang des Kreislaufs (22) aufweist, dass das Reaktormodul (20) Teil des Kreislaufs (22) ist und dass vorzugsweise die Kohlendioxidquelle und die Alkoholquelle mit dem Kreislauf (22) strömungsverbunden sind.

19. Reaktor nach Anspruch 18, **dadurch gekennzeichnet**, dass der Kreislauf (22) mehrere Reaktormodule (20) aufweist, die parallel zueinander geschaltet sind.

20. Reaktor nach einem der Ansprüche 15 bis 19, **dadurch gekennzeichnet**, dass die Membran (21) als zumindest ein Membranrohr (7) ausgeführt ist, in dessen Inneren sich zumindest ein Teil des Abführraums befindet.

21. Reaktor nach einem der Ansprüche 15 bis 20, **dadurch gekennzeichnet**, dass die Membran (21) eine Selektivität α auf Wasser von mindestens 100 bei einer Temperatur von 80°C und einem Druck von 5 bar aufweist und/oder eine Selektivität α auf Wasser von mindestens 100 bei einer Temperatur von 100°C und einem Druck von 10 bar aufweist.

22. Reaktor nach einem der Ansprüche 18 bis 21, **dadurch gekennzeichnet**, dass der Kreislauf (22) zumindest eine Temperierquelle zur Einstellung der Temperatur des Gemisches im Kreislauf (22) aufweist.

23. Reaktor nach einem der Ansprüche 18 bis 22, **dadurch gekennzeichnet**, dass der Kreislauf (22) zumindest einen aus dem Kreislauf (22) führende Abführkanal (28) zum Abführen von Endprodukt aufweist.

24. Reaktor nach einem der Ansprüche 15 bis 23, **dadurch gekennzeichnet**, dass das Reaktormodul (20) einen mit dem Reaktionsraum (4) strömungsverbundenen Einlass (3) aufweist, der mit einem Feedkanal (29) des Kreislaufs (22) verbunden ist, und einen, vorzugsweise am gegenüberliegenden Ende des Reaktionsraums (4) angeordneten Auslass (5) aufweist, der mit einem Retentatkanal (30) des Kreislaufs (22) verbunden ist.

25. Reaktor nach einem der Ansprüche 15 bis 24, **dadurch gekennzeichnet**, dass im Reaktionsraum (4) zumindest ein Membranrohr (7) hineinragt und sich vorzugsweise von einem Ende des Reaktionsraums (4) bis zum anderen Ende des Reaktionsraums (4) erstreckt.

26. Reaktor nach Anspruch 25, **dadurch gekennzeichnet**, dass das Membranrohr (7) im Bereich eines ersten Endes (7a) mit einer Sweepgasquelle strömungsverbunden ist und das Membranrohr (7) im Bereich eines zweiten Endes (7b) mit einem Wasserabführkanal (32) zum Abführen des Wassers strömungsverbunden ist.

27. Reaktor nach Anspruch 26, **dadurch gekennzeichnet**, dass das erste Ende (7a) geschlossen ist und die Strömungsverbindung zur Sweepgasquelle über ein Tauchrohr (11) erfolgt, das über das zweite Ende (7b) in das Membranrohr (7) hineinragt.

28. Reaktor nach einem der Ansprüche 25 bis 27, **dadurch gekennzeichnet**, dass zumindest fünf, vorzugsweise sechs Membranrohre (7) in dem Reaktormodul (20) angeordnet sind.

29. Reaktor nach einem der Ansprüche 15 bis 28, **dadurch gekennzeichnet**, dass der Reaktionsraum (4) im Wesentlichen mit einem Molsieb und dem darauf immobilisierten Katalysator gefüllt ist.

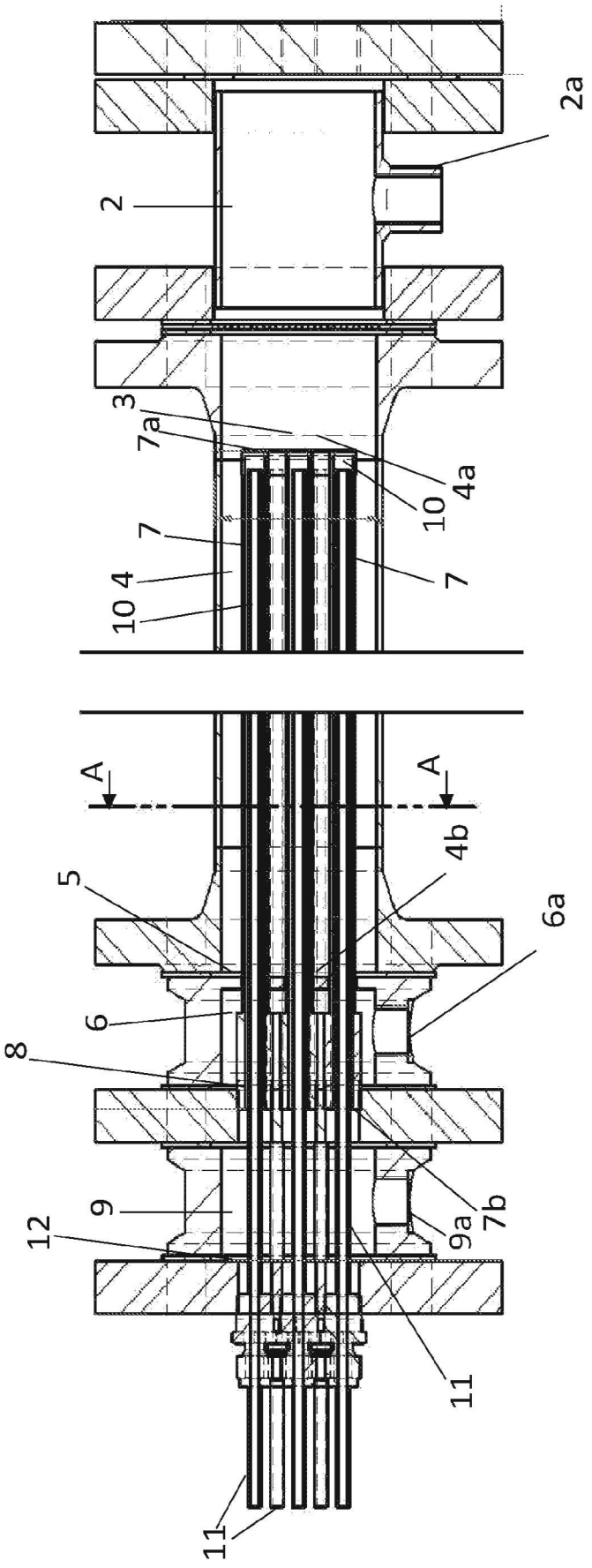

Fig. 1a

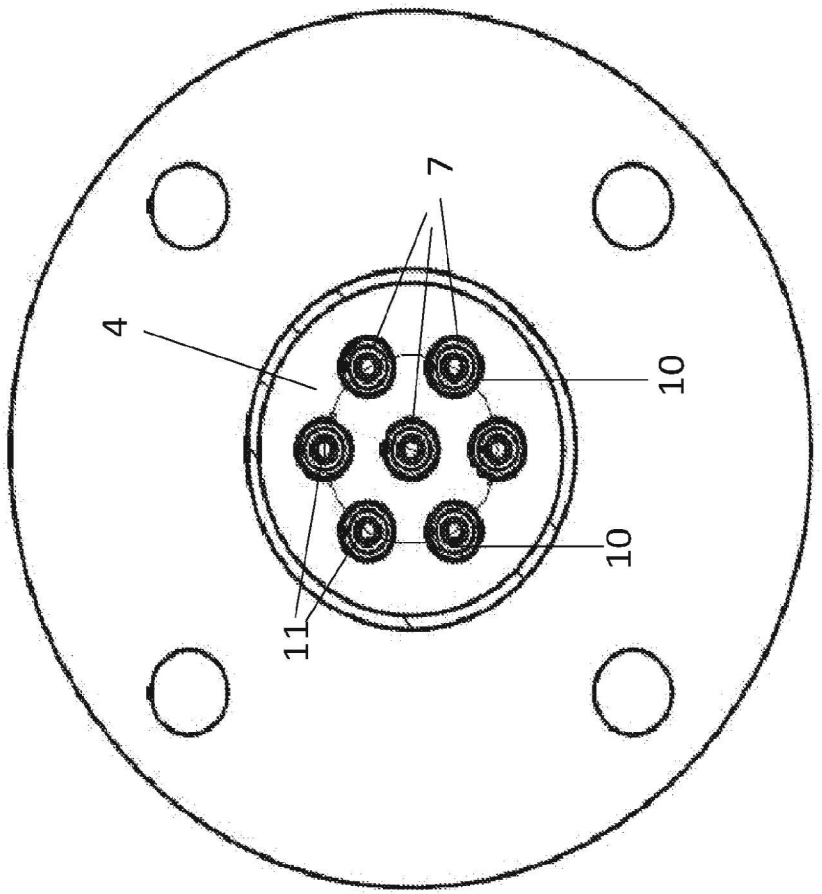

Fig. 1b

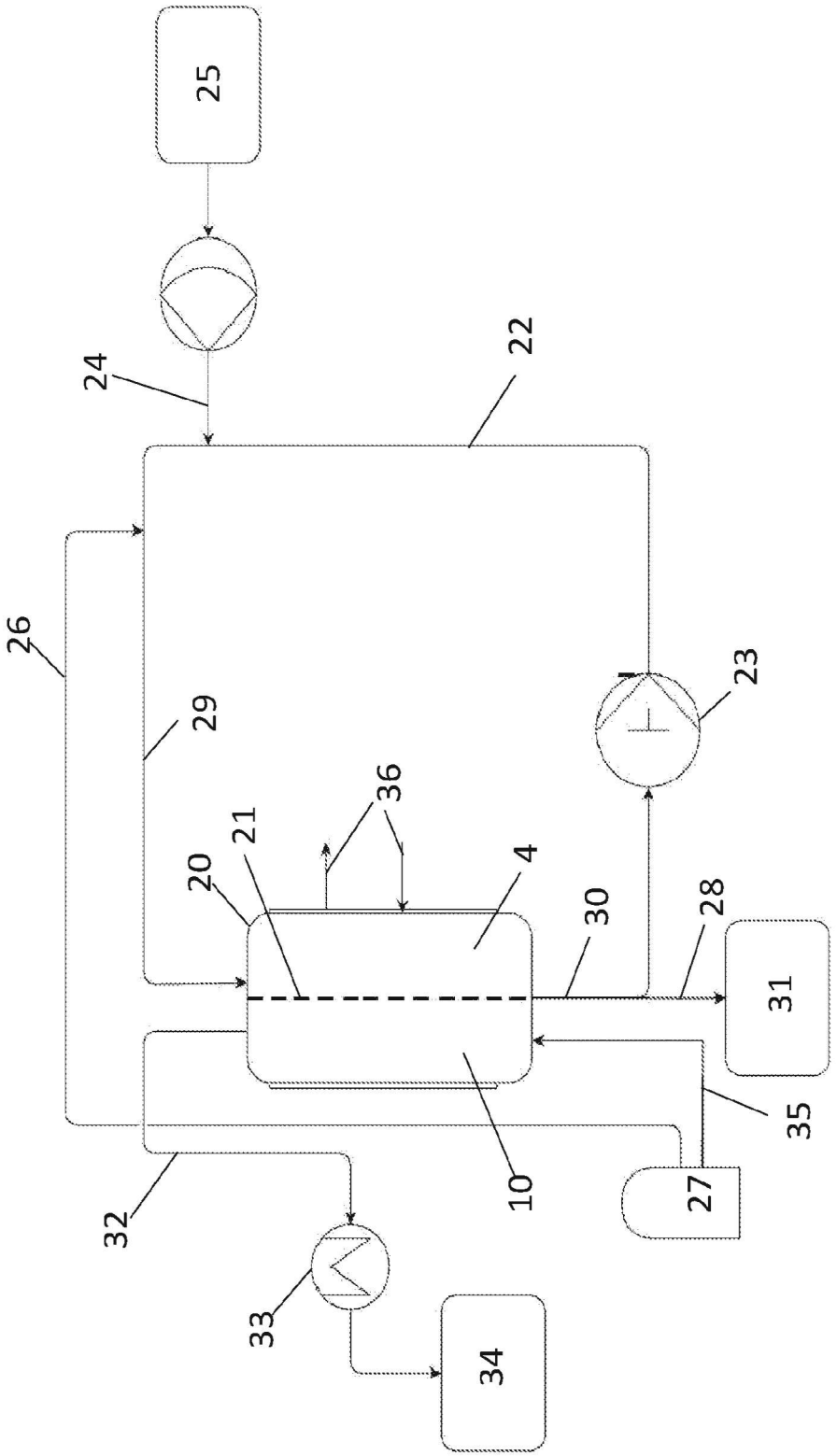

Fig. 2

INTERNATIONAL SEARCH REPORT

International application No.
PCT/AT2024/060114

A. CLASSIFICATION OF SUBJECT MATTER

C07C 68/04(2006.01)i; ***C07C 69/96***(2006.01)i

According to International Patent Classification (IPC) or to both national classification and IPC

B. FIELDS SEARCHED

Minimum documentation searched (classification system followed by classification symbols)

C07C

Documentation searched other than minimum documentation to the extent that such documents are included in the fields searched

Electronic data base consulted during the international search (name of data base and, where practicable, search terms used)

EPO-Internal

C. DOCUMENTS CONSIDERED TO BE RELEVANT

Category*	Citation of document, with indication, where appropriate, of the relevant passages	Relevant to claim No.
X	CN 115282887 A (INST PROCESS ENG CAS) 04 November 2022 (2022-11-04) paragraphs [0014], [0102]; claims 3, 5, 9; figure 1	1-25,27-29
X	LI CHUAN-FENG ET AL. "Study on application of membrane reactor in direct synthesis DMC from CO2 and CH3OH over Cu-KF/MgSiO catalyst" *CATALYSIS TODAY*, AMSTERDAM, NL, Vol. 82, No. 1-4, July 2003 (2003-07), pages 83-90 DOI: 10.1016/S0920-5861(03)00205-0 ISSN: 0920-5861, XP093184465 Summary figures 1-2; tables 3-4	15-17,20,25,26

☐ Further documents are listed in the continuation of Box C. ☑ See patent family annex.

* Special categories of cited documents:
"A" document defining the general state of the art which is not considered to be of particular relevance
"E" earlier application or patent but published on or after the international filing date
"L" document which may throw doubts on priority claim(s) or which is cited to establish the publication date of another citation or other special reason (as specified)
"O" document referring to an oral disclosure, use, exhibition or other means
"P" document published prior to the international filing date but later than the priority date claimed
"T" later document published after the international filing date or priority date and not in conflict with the application but cited to understand the principle or theory underlying the invention
"X" document of particular relevance; the claimed invention cannot be considered novel or cannot be considered to involve an inventive step when the document is taken alone
"Y" document of particular relevance; the claimed invention cannot be considered to involve an inventive step when the document is combined with one or more other such documents, such combination being obvious to a person skilled in the art
"&" document member of the same patent family

Date of the actual completion of the international search	Date of mailing of the international search report
12 July 2024	**23 July 2024**

Name and mailing address of the ISA/EP	Authorized officer
European Patent Office **p.b. 5818, Patentlaan 2, 2280 HV Rijswijk** **Netherlands (Kingdom of the)** Telephone No. **(+31-70)340-2040** Facsimile No. **(+31-70)340-3016**	**Seitner, Irmgard** Telephone No.

INTERNATIONAL SEARCH REPORT
Information on patent family members

International application No.
PCT/AT2024/060114

Patent document cited in search report	Publication date (day/month/year)	Patent family member(s)	Publication date (day/month/year)
CN 115282887 A	04 November 2022	NONE	

INTERNATIONALER RECHERCHENBERICHT

Internationales Aktenzeichen
PCT/AT2024/060114

A. KLASSIFIZIERUNG DES ANMELDUNGSGEGENSTANDES
INV. C07C68/04 C07C69/96
ADD.

Nach der Internationalen Patentklassifikation (IPC) oder nach der nationalen Klassifikation und der IPC

B. RECHERCHIERTE GEBIETE

Recherchierter Mindestprüfstoff (Klassifikationssystem und Klassifikationssymbole)
C07C

Recherchierte, aber nicht zum Mindestprüfstoff gehörende Veröffentlichungen, soweit diese unter die recherchierten Gebiete fallen

Während der internationalen Recherche konsultierte elektronische Datenbank (Name der Datenbank und evtl. verwendete Suchbegriffe)
EPO-Internal

C. ALS WESENTLICH ANGESEHENE UNTERLAGEN

Kategorie*	Bezeichnung der Veröffentlichung, soweit erforderlich unter Angabe der in Betracht kommenden Teile	Betr. Anspruch Nr.
X	CN 115 282 887 A (INST PROCESS ENG CAS) 4. November 2022 (2022-11-04) Absätze [0014], [0102]; Ansprüche 3, 5, 9; Abbildung 1 -----	1-25, 27-29
X	LI CHUAN-FENG ET AL: "Study on application of membrane reactor in direct synthesis DMC from CO2 and CH3OH over Cu-KF/MgSiO catalyst", CATALYSIS TODAY, Bd. 82, Nr. 1-4, Juli 2003 (2003-07), Seiten 83-90, XP093184465, AMSTERDAM, NL ISSN: 0920-5861, DOI: 10.1016/S0920-5861(03)00205-0 Zusammenfassung Abbildungen 1-2; Tabellen 3-4 -----	15-17, 20,25,26

☐ Weitere Veröffentlichungen sind der Fortsetzung von Feld C zu entnehmen ☒ Siehe Anhang Patentfamilie

* Besondere Kategorien von angegebenen Veröffentlichungen :
"A" Veröffentlichung, die den allgemeinen Stand der Technik definiert, aber nicht als besonders bedeutsam anzusehen ist
"E" frühere Anmeldung oder Patent, die bzw. das jedoch erst am oder nach dem internationalen Anmeldedatum veröffentlicht worden ist
"L" Veröffentlichung, die geeignet ist, einen Prioritätsanspruch zweifelhaft erscheinen zu lassen, oder durch die das Veröffentlichungsdatum einer anderen im Recherchenbericht genannten Veröffentlichung belegt werden soll oder die aus einem anderen besonderen Grund angegeben ist (wie ausgeführt)
"O" Veröffentlichung, die sich auf eine mündliche Offenbarung, eine Benutzung, eine Ausstellung oder andere Maßnahmen bezieht
"P" Veröffentlichung, die vor dem internationalen Anmeldedatum, aber nach dem beanspruchten Prioritätsdatum veröffentlicht worden ist
"T" Spätere Veröffentlichung, die nach dem internationalen Anmeldedatum oder dem Prioritätsdatum veröffentlicht worden ist und mit der Anmeldung nicht kollidiert, sondern nur zum Verständnis des der Erfindung zugrundeliegenden Prinzips oder der ihr zugrundeliegenden Theorie angegeben ist
"X" Veröffentlichung von besonderer Bedeutung;; die beanspruchte Erfindung kann allein aufgrund dieser Veröffentlichung nicht als neu oder auf erfinderischer Tätigkeit beruhend betrachtet werden
"Y" Veröffentlichung von besonderer Bedeutung;; die beanspruchte Erfindung kann nicht als auf erfinderischer Tätigkeit beruhend betrachtet werden, wenn die Veröffentlichung mit einer oder mehreren Veröffentlichungen dieser Kategorie in Verbindung gebracht wird und diese Verbindung für einen Fachmann naheliegend ist
"&" Veröffentlichung, die Mitglied derselben Patentfamilie ist

Datum des Abschlusses der internationalen Recherche	Absendedatum des internationalen Recherchenberichts
12. Juli 2024	23/07/2024

Name und Postanschrift der Internationalen Recherchenbehörde	Bevollmächtigter Bediensteter
Europäisches Patentamt, P.B. 5818 Patentlaan 2 NL - 2280 HV Rijswijk Tel. (+31-70) 340-2040, Fax: (+31-70) 340-3016	Seitner, Irmgard

Formblatt PCT/ISA/210 (Blatt 2) (April 2005)

INTERNATIONALER RECHERCHENBERICHT

Angaben zu Veröffentlichungen, die zur selben Patentfamilie gehören

Internationales Aktenzeichen
PCT/AT2024/060114

Im Recherchenbericht angeführtes Patentdokument	Datum der Veröffentlichung	Mitglied(er) der Patentfamilie	Datum der Veröffentlichung
CN 115282887 A	04-11-2022	KEINE	